EFFECT OF ELECTRONIC AND NUCLEAR FACTORS ON THE DYNAMICS OF DYE-TO-SEMICONDUCTOR ELECTRON TRANSFER

THÈSE N^O 3447 (2006)

PRÉSENTÉE À LA FACULTÉ SCIENCES DE BASE

Institut des sciences et ingénierie chimiques

SECTION DE CHIMIE ET GÉNIE CHIMIQUE

ÉCOLE POLYTECHNIQUE FÉDÉRALE DE LAUSANNE

POUR L'OBTENTION DU GRADE DE DOCTEUR ÈS SCIENCES

PAR

Bernard WENGER

ingénieur chimiste diplômé EPF
de nationalité suisse et originaire de Rüschegg (BE)

acceptée sur proposition du jury:

Prof. M. Grätzel, directeur de thèse
Prof. C. Bressler, rapporteur
Prof. S. Haacke, rapporteur
Prof. J.-E. Moser, rapporteur
Prof. E. Vauthey, rapporteur

Lausanne, EPFL
2006

Effect of Electronic and Nuclear Factors on the Dynamics of Dye-to-Semiconductor Electron Transfer

PhD Thesis
Bernard Wenger

January 18, 2006

Thèse présentée à la faculté des sciences de base pour l'obtention du grade de docteur ès sciences.

Prof. Michael Grätzel
Directeur de Thèse

Prof. Jacques-E. Moser
Rapporteur

Prof. Stefan Haacke
Rapporteur

Prof. Eric Vauthey
Rapporteur

Prof. Christian Bressler
Rapporteur

Résumé

Le transfert d'électron d'un colorant excité électroniquement vers un semi-conducteur est l'étape initiale dans de nombreux procédés utilisant la lumière comme vecteur d'information (par exemple en photographie argentique), ou dans la conversion d'énergie lumineuse en électricité comme c'est le cas pour les cellules solaires à colorant. Dans ce cas particulier, l'injection de charge a lieu dans un temps variant de quelques dizaines de femtosecondes (10^{-15} s) à plusieurs picosecondes (10^{-12} s) avec une efficacité proche de 100 %. Les modèles théoriques standard classent les paramètres contrôlant la cinétique du transfert d'électron en deux catégories: a) les facteurs électroniques, qui dépendent essentiellement du recouvrement des fonctions d'onde électroniques du donneur et de l'accepteur, et b) les facteurs nucléaires qui comportent notamment les énergies de réorganisation aussi bien des réactifs que des molécules de solvant les environnant. En raison des temps d'injection ultracourts observés pour des couples colorant/semiconducteur utilisés pour des applications photovoltaïques, les limites des hypothèses fondamentales conduisant à ces modèles sont atteintes. Dans ce travail, nous étudions l'influence de paramètres électroniques et nucléaires sur la cinétique de l'injection de charge dans des semi-conducteurs par des techniques de spectroscopie laser résolues en temps.

En préambule, nous nous sommes intéressés à la réaction de photo-réduction par l'iodure de complexes polypyridyl de Ru(II) adsorbés sur du TiO$_2$ nano-cristallin. Nos expériences montrent que le rendement de cette réaction, en compétition avec l'injection de charge, dépend fortement de la concentration en iodure, mais aussi de la préparation et de la maturation des échantillons. De ces observations, nous déduisons qu'une fraction des molécules n'est pas adsorbée directement sur le semiconducteur mais plutôt sous une forme agrégée. A la lumière de ces résultats, nous avons reconsidéré le problème de l'injection de charge dans le TiO$_2$ à partir des colorants standard utilisés dans la conception de cellules solaires. En effet, plusieurs études ont révélé un mécanisme biphasique pour ces systèmes, caractérisé par une partie rapide (< 100 fs), suivie d'une composante plus lente (1-100 ps) dont l'amplitude varie considérablement selon les auteurs. Nos mesures montrent que la partie lente est liée aux molécules qui ne sont pas directement

5

en contact avec la surface. Lorsque la formation d'agrégats est minimisée, nous observons une cinétique monophasique ($\tau < 20$ fs). Ce résultat suggère que ce processus ne peut être décrit de manière satisfaisante par des modèles théoriques basés sur la réorganisation nucléaire des réactifs et des produits.

Nous avons ensuite examiné l'effet de la distance sur laquelle le transfert de charge a lieu au moyen de deux approches distinctes. Dans un premier temps, nous étudions la cinétique de l'injection de charge ainsi que celle du transfert en retour, pour des colorants dont le chromophore est séparé du groupe d'ancrage par plusieurs unités p-phénylène. Pour les deux réactions, la vitesse diminue de façon exponentielle avec la distance. Toutefois cet effet, caractérisé par le facteur d'atténuation β, est sensiblement supérieur pour la recombinaison ($\beta = 0.5$ Å^{-1}) que pour l'injection ($\beta = 0.19$ Å^{-1}). Nous expliquons cette différence par l'influence de la réorganisation nucléaire pour la recombinaison. La deuxième approche consiste à insérer une fine couche isolante d'Al_2O_3 entre le colorant et le TiO_2. Ici, le paramètre β est similaire pour les deux réactions, indiquant un processus dominé par les facteurs électroniques. La faible valeur estimée ($\beta = 0.15$ Å^{-1}) suggère que l'oxyde d'aluminium déposé est nettement moins isolant que l'alumine cristalline pure et que le transfert a lieu par effet tunnel relayé par des niveaux d'énergie inoccupés de la couche mince.

Finalement nous étudions l'influence de la densité d'états accepteurs en utilisant un couple formé d'un complexe de ruthénium et d'un film nanocristallin de Nb_2O_5. En faisant varier la longueur d'onde d'excitation nous parvenons à sonder le bas de la bande de conduction où la densité d'état décroît de manière exponentielle. Bien que la largeur de spectre de l'impulsion d'excitation s'avère trop importante pour ce type d'expériences, un faible ralentissement de l'injection (2-3 fois) est observé.

Globalement, nos expériences montrent que les facteurs électroniques, en particulier la diminution du couplage électronique avec la distance, contrôlent largement la cinétique du transfert d'électron interfacial. En révélant le rôle de l'adsorption imparfaite de certains sensibilisateurs sur la surface du semiconducteur, ces résultats ont des conséquences directes pour le développement des cellules solaires à colorant. Finalement, dans le cas d'un processus de transfert d'électron prenant place à une échelle de temps si courte qu'aucun mouvement nucléaire n'est possible, il semble que le transfert d'électron est contrôlé par le déphasage et la relaxation de l'électron dans le continuum d'états accepteurs du semiconducteur.

Mots-clés: Dynamique de transfert d'électron interfacial, spectroscopie laser ultra-rapide, sensibilisation, semiconducteurs, TiO_2, Nb_2O_5, couplage électronique.

Abstract

Dye-to-semiconductor electron transfer is the initial step in many processes where light is used for the storage of information (e. g. color photography) or converted into electricity as in dye-sensitized solar cells. In the latter, interfacial charge injection occurs on a timescale spanning from tens of femtoseconds (10^{-15} s) to several picoseconds (10^{-12} s), with an efficiency approaching 100 %. In standard electron transfer theory, the parameters controlling charge transfer dynamics are divided into two categories: a) electronic factors, depending essentially upon the overlap between the electronic wavefunctions of the donor and the acceptor, and b) nuclear factors, characterized by the reorganization energies of both the reactants and the surrounding solvent molecules. Because of the ultrafast injection rates observed for dye/semiconductors couples typically used in photovoltaic applications, the hypotheses leading to these models are likely to be invalid. In this work, we make use of time-resolved spectroscopic techniques to study the influence of some electronic and nuclear parameters influencing charge injection dynamics into wide bandgap semiconductors.

As a preliminary study, we investigated reductive quenching of excited dyes by iodide at the surface of nanocrystalline TiO_2. Our experiments show that the quantum yield of this reaction, that is in competition with electron injection, depends strongly upon the I^- concentration, but also upon the preparation and aging of the samples. We deduce that a fraction of the dye molecules are not adsorbed directly onto the surface of the semiconductor, but rather aggregated in a second adsorption layer. In the light of these results we reconsidered the issue of charge injection from the standard N3 dye into TiO_2. This reaction, largely studied due to its importance for dye-sensitized solar cells, has previously been reported to take place with a fast (< 100 fs) phase, followed by a slower (1-100 ps) component. Our measurements show that the slow part is actually related to the presence of weakly adsorbed dye molecules. When aggregation is minimized, we observe monophasic injection dynamics (τ < 20 fs). This result suggests the process is beyond the scope of vibration-mediated electron transfer models and is controlled by electron dephasing in the solid.

Next, we applied two different approaches to investigate the influence of the distance over which charge transfer takes place. First, forward and back electron transfer kinetics were measured for a series of bridged-sensitizers containing p-phenylene spacer groups. For both reactions the rate decays exponentially with distance. However, the damping factor is much larger for the back transfer ($\beta = 0.5$ Å^{-1}) than for injection ($\beta = 0.19$ Å^{-1}), suggesting that nuclear reorganization plays an important role for the former reaction. In the second approach, a thin layer of Al$_2$O$_3$ of controlled thickness is inserted between the sensitizer and TiO$_2$. In this case the distance parameter β is similar for both reactions. The weak estimated value ($\beta = 0.15$ Å^{-1}) indicates that thin layers of aluminum oxide is much less insulating that pure, crystalline Al$_2$O$_3$, and that electron tunneling is mediated by empty states in the thin layer according to the superexchange mechanism.

Finally, the influence of the density of acceptor states has been examined by using a ruthenium complex adsorbed on Nb$_2$O$_5$ films. Varying the excitation wavelength made it possible to probe the bottom of the conduction band where the density of states decays exponentially. Despite the spectral width of the pump laser pulses, a weak retardation (2-3 times) of electron injection was observed.

In summary, our experiments show that electronic factors, in particular variations of electronic coupling with distance, mainly control electron injection dynamics at dye/semiconductor interfaces. By revealing the role of aggregation for standard dyes adsorbed on TiO$_2$, these results have important consequences for the development of dye-sensitized solar cells. Finally, in the case of ultrafast monophasic kinetics, standard electron transfer models are not obeyed, and the dynamics is rather controlled by electron dephasing and relaxation in the continuum of acceptor states in the solid.

Keywords: Interfacial electron transfer dynamics, ultrafast laser spectroscopy, dye sensitization, wide bandgap semiconductors, TiO$_2$, Nb$_2$O$_5$, electronic coupling.

Contents

Contents   v

CHAPTER 1

Introduction

When the ancient Phenicians extracted the Tyre purple dye from a shellfish, they certainly ignored the underlying mechanisms responsible for its coloring properties. However, the control of color was already recognized as an important cultural and economic factor in these early times. Much later, the success of the first chemical syntheses of dyes, such as alizarin or indigo, induced the development of chemical industry in the second half of the 19th century. In 1837, Daguerre made the first photographic images, introducing at the same time the idea to use light for the storage of information. With the following development of color photography, the importance of the control of energetic and spectral properties of dyes became evident. In the same time, the role of chlorophyll in photosynthesis demonstrated the potential of dyes for the conversion of light into energy. The dream to capture the energy that is freely available from sunlight by the intermediate of dyes to produce electricity or chemical fuels (such as hydrogen), has therefore been a driving force in this field for many decades.

Photoinduced electron transfer from an excited dye is the primary step in many systems capable of converting light into information (color photog-

raphy, electrophotography, vision) or into energy (photosynthesis, water cleavage by visible light, dye-sensitized solar cells). Most of the artificial realizations are based on the dye sensitization of semiconductors, that can be defined as the process by which the excitation of a chromophore is followed by interfacial electron transfer, or electron injection, into the semiconductor. Although it was earlier recognized that dyes could increase the action spectrum in photographic or photoelectrochemical processes, it is only in the 1960s and 1970s that the accepted mechanism was developed. At that time most of the studies involved electrochemical measurements of sensitized photocurrents at single-crystal wide-bandgap semiconductor electrodes.[1] While these early studies set the theoretical framework, the real breakthrough was achieved by O'Regan et al. in 1990,[2] by using nanocrystalline TiO_2 electrodes. With such mesoporous films the effective surface for sensitizer adsorption was roughly 1000 times that of a planar electrode. Soon, dye-sensitized solar cells based on this concept yielded promising solar-to-electricity conversion efficiencies.[3]
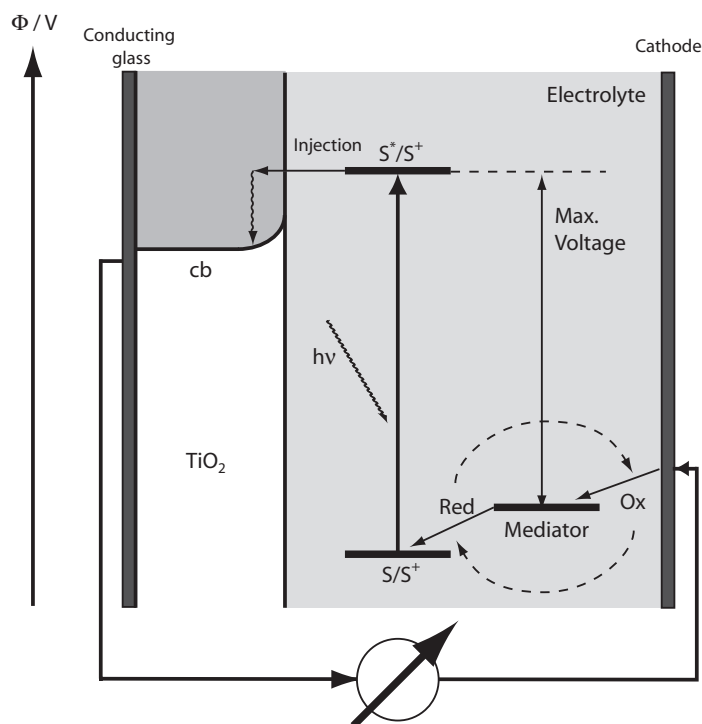
**Figure 1.1 —** Operational principle of a dye-sensitized solar cell.

The working principle of a dye-sensitized solar cell is depicted in figure 1.1. At the heart of the device is a mesoscopic semiconductor oxide film on which surface a dye sensitizer layer is adsorbed. Upon illumination, an electron is transferred from the excited dye to the semiconductor. This electron

then diffuses through the interconnected network formed by the sintered nanoparticles towards the conductive glass electrode where it is collected by the external circuit. To prevent recombination of the injected electron with the oxidized dye, the latter is quickly intercepted by electron donation from the electrolyte, usually an organic solvent containing a redox system such as the I^-/I_3^- couple. The oxidized mediator is in turn regenerated at the counter electrode. The overall conversion efficiencies of the best devices made of mesopourous TiO_2 films sensitized by ruthenium polypyridyl complexes have now reached 11 %. In such devices, more than 80 % of the incident photons are converted into electricity in the range 500-600 nm with only 10 μm-thick films.[4]

The astounding performance of dye-sensitized solar cells (DSCs) can be understood in regard of the kinetic competition of the various redox processes involved in the conversion of light into electricity. Ultrafast electron injection has been observed in the femtosecond-picosecond (10^{-15}-10^{-12} s) time domain.[5] Regeneration of the oxidized dye is typically characterized by rate constants of 10^5-10^7 s^{-1}.[4] This is more than 100 times faster than recombination of injected electrons with the oxidized redox species (e.g. triiodide) and orders of magnitude faster than back transfer to the dye cation in the absence or a redox mediator. As electron transport in the semiconductor electrode is generally one order of magnitude faster than recombination, the charge collection efficiency is near unit for optimized cells.[6]
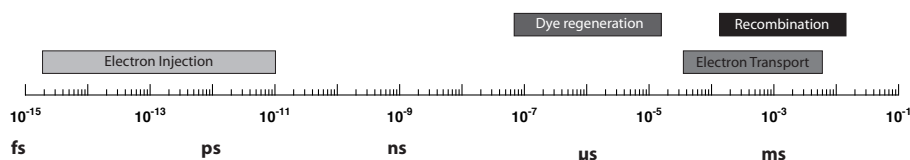
Figure 1.2 — Dynamics of the processes involved in the conversion of light into electricity in a dye-sensitized solar cell.

Because of the prevailing role of electron transfer dynamics in DSCs, the various processes have been widely studied in the last decade.[5] While photoelectrochemical techniques have proved to be most adequate for the study of electron transport,[6] time-resolved optical spectroscopy remains the leading tool for the study of interfacial electron transfer. Dye regeneration and back transfer reactions have been intensely studied by nanosecond laser spectroscopy.[1,7] Because of its astonishing rate, the forward electron transfer reaction remained unresolved for several years. The advent of femtosecond laser spectroscopy opened the door to enter the domain of ultrafast chemical processes.[8,9] The first direct observation of electron injection into nanocrystalline TiO_2 films was achieved in 1996 by Rehm and co-workers.[8]

They found that the surface-attached dye (coumarin 343) transferred an electron to the conduction band of titania with a time constant of ca. 200 fs. Since then, numerous studies have been reported featuring dyes of various families (Ru complexes, phtalocyanines, anthraquinones, xanthenes, ...)[1,5,10,11,12,13] adsorbed on nanocrystalline films of metal oxides (TiO_2, ZnO, SnO_2, ...).[5]

Since the injection rate was found to be orders of magnitude faster than the other processes relevant to efficient light-to-electricity conversion, this reaction has usually been considered as non-critical for device improvement. Recently, it was even argued that optimal device efficiency is obtained when the injection rate is just fast enough to compete successfully with the dye excited-state decay, thereby minimizing "kinetic redundancy".[14] As will be shown in this work, this might not be true when high concentrations of iodide are present in the electrolyte.

In fact, the main motivation for this work is the insight given by model systems such as dye/semiconductor interfaces, on the elemental mechanisms governing electron transfer reactions. In contrast to electron transfer between chemical species in solution, or even intramolecular ET[a], charge injection into a quasi-continuum of acceptor states is characterized by efficient tunneling processes. As a consequence, the dynamics of electron injection is mainly controlled by electronic factors, i.e. the overlap between the electronic wavefunctions of the donor and the acceptor states. Subtle variations of parameters such as the distance separating the chromophore from the surface, are expected to yield significant changes in the injection dynamics.

In this work, we take advantage of the considerable knowledge acquired in the group of Prof. Grätzel during the last 15 years in the production of efficient dye-sensitized solar cells, in order to investigate some of the intimate mechanisms underlying electron transfer at dye/semiconductor interfaces. Our results are confronted with the standard models of ET theory, and significance to DSC performance is discussed when relevant. The structure of the work is outlined below.

Chapter 2 contains an introduction to the theoretical concepts relevant to dye sensitization of semiconductors. It is essentially meant to present the terminology which will be used in the following sections. In the chapter following, we present a detailed description of the experimental tools used in this study. Emphasis is given on the improvement of the femtosecond spectrometer which was an essential part of the thesis work.

---

[a]ET = electron transfer

In Chapter 4, the discovery of reductive quenching as an alternative mechanism for dye deactivation on the semiconductor is reported. Although this issue is not obviously related to the objectives of this thesis, it provides indications of dye aggregation that will have major repercussions on the interpretation of the following results.

Sensitization of TiO$_2$ by the N3 dye is probably the most studied dye/semiconductor couple in the field of dye-sensitized solar cells. Most of the recent studies have reported injection dynamics to take place with a fast ($<$ 100 fs) phase, followed by a slower (0.7-100 ps) component. In chapter 5, we show that when dye aggregation on the surface is avoided, monophasic electron injection is observed ($\tau < 20$ fs). This result suggests that the process is beyond the scope of vibration-mediated ET models and is controlled by electron dephasing in the solid.

In Chapter 6, two different approaches are adopted to study the dependence of the ET dynamics upon the distance separating the chromophore from the semiconductor. First, forward and back ET kinetics is investigated on TiO$_2$ films sensitized by a series of bridged sensitizers. In the second part, an insulating Al$_2$O$_3$ layer of controlled thickness is deposited on TiO$_2$ before dye adsorption. In most cases, an exponential dependence on the distance is found in agreement with an electronic tunneling mechanism. The magnitude and the variations of the damping factor β are discussed.

Then, in chapter 7, we investigate the influence of the density of states. Based on the observation that electron transfer occurs prior to thermal relaxation of the excited dye, we propose to vary the excitation wavelength so as to probe the bottom of the conduction band edge of the semiconductor where the density is expected to fall off exponentially. Because of the higher energy of its conduction band edge, Nb$_2$O$_5$ nanocrystalline films are here preferred to titania. Surprisingly, weak effects are measured. Our analysis suggest that the weak spectral resolution inherent to femtosecond laser pulses prevents detailed exploration of the density of states.

Eventually, the results are summarized and global conclusions are presented in chapter 8.

1.1 References

1. Watson, D.; Meyer, G. "Electron injection at dye-sensitized semiconductor electrodes", *Annu. Rev. Phys. Chem.* **2005,** *56,* 119–156.

2. O'Regan, B.; Moser, J.; Anderson, M.; Grätzel, M. "Vectorial Electron Injection into Transparent Semiconductor Membranes and Electric-Field Effects on the Dynamics of Light-Induced Charge Separation", *J. Phys. Chem.* **1990,** *94,* 8720-8726.

3. O'Regan, B.; Grätzel, M. "A Low-Cost, High-Efficiency Solar-Cell Based on Dye-Sensitized Colloidal TiO$_2$ Films", *Nature* **1991,** *353,* 737-740.

4. Grätzel, M. "Solar energy conversion by dye-sensitized photovoltaic cells", *Inorg. Chem.* **2005,** *44,* 6841–6851.

5. Anderson, N.; Lian, T. "Ultrafast electron transfer at the molecule-semiconductor nanoparticle interface", *Annu. Rev. Phys. Chem.* **2005,** *56,* 491–519.

6. Frank, A. J.; Kopidakis, N.; van de Lagemaat, J. "Electrons in nanostructured TiO$_2$ solar cells: transport, recombination and photovoltaic properties", *Coord. Chem. Rev.* **2004,** *248,* 1165-1179.

7. Durrant, J. R.; Haque, S. A.; Palomares, E. "Towards optimisation of electron transfer processes in dye sensitised solar cells", *Coord. Chem. Rev.* **2004,** *248,* 1247-1257.

8. Chergui, M. "Femtochemistry and Femtobiology: The New Age", *ChemPhysChem* **2002,** *8,* 713-717.

9. Zewail, A. "Nobel Lecture", *http://nobelprize.org* .

10. Grätzel, M.; Moser, J. E. Electron Transfer in Chemistry. In , Vol. 5; Balzani, V., Ed.; Wiley-VCH: 2001; Chapter "Solar Energy Conversion", pages 589–641.

11. He, J. J.; Benkö, G.; Korodi, F.; Polivka, T.; Lomoth, R.; Akermark, B.; Sun, L. C.; Hagfeldt, A.; Sundström, V. "Modified phthalocyanines for efficient near-IR sensitization of nanostructured TiO$_2$ electrode", *J. Am. Chem. Soc.* **2002,** *124,* 4922-4932.

12. Pelet, S.; Grätzel, M.; Moser, J. E. "Femtosecond dynamics of interfacial and intermolecular electron transfer at eosin-sensitized metal oxide nanoparticles", *J. Phys. Chem. B* **2003,** *107,* 3215-3224.

13. Huber, R.; Moser, J. E.; Grätzel, M.; Wachtveitl, J. "Real-time observation of photoinduced adiabatic electron transfer in strongly coupled dye/semiconductor colloidal systems with a 6 fs time constant", *J. Phys. Chem. B* **2002,** *106,* 6494-6499.

14. Haque, S.; Palomares, E.; Cho, B.; Green, A.; Hirata, N.; Klug, D.; Durrant, J. "Charge separation versus recombination in dye-sensitized nanocrystalline solar cells: the minimization of kinetic redundancy", *J. Am. Chem. Soc.* **2005,** *127,* 3456–3462.

Theoretical considerations

Summary

In this chapter some basic theoretical considerations about the different topics relevant to this work will be given. The idea here is mainly to define the framework for the discussion of the results that will be presented in the following chapters. First, the attention will be drawn to the photochemistry relevant to dyes made of transition metal complexes. Then, the semiconductor phase will be described, and we will put our focus on the electrochemical behavior of large bandgap metal oxides. The process of dye sensitization will then be introduced, and finally electron transfer theories in solution and at interfaces will be reviewed.

2.1   Dyes, Photophysics and Photochemistry

All electron transfer processes studied in this work involve molecular dyes either as donors or acceptors. Therefore a good understanding of the basic principles governing light absorption and deactivation of excited states is required before discussing electron transfer theories.

2.1.1   Absorption of light

The photon may be viewed as a quantum of energy capable of promoting an electron from an occupied orbital to a higher empty state thereby creating an electronic isomer of the initial chemical species. This electronic transition can occur only if the energy of the photon equals the difference between the initial and the final state of the absorber:

$$h\nu = E_{\text{final}} - E_{\text{initial}} \tag{2.1}$$

Light absorption is proportional to the effective *cross section*, the apparent area of the absorbing molecule. The extinction coefficient (units: cm^{-1}/M) for absorption is given by:

$$\varepsilon = \frac{1}{\ln 10} N_A \sigma \tag{2.2}$$

where σ is the effective area or cross section of the molecule in cm^2 and N_A is Avogadro's number. An ε value of $\sim 10^5$ $mol^{-1} \cdot L \cdot cm^{-1}$ would therefore correspond to an area of ~ 4 Å^2.

The intensity of a transition is best viewed considering the electron perturbed by an electromagnetic wave. If an electron bound to a nuclear framework possesses perfect oscillating properties, it has an excitation probability, or an *oscillator strength f*, of unity. This quantity can be estimated experimentally and is essential due to the relationship between this classical concept and quantum mechanics. The oscillator strength is proportional to the induced dipole μ_i produced by a light wave on an electron. This μ_i is an observable quantity related to the quantum mechanical transition dipole moment integral μ. The final expression is given by:

$$\text{Classical} \rightarrow f = \frac{8\pi m_e \bar{\nu}}{3he^2} \mu^2 \leftarrow \text{Quantum mechanical} \tag{2.3}$$

where m_e is the mass of an electron and $\bar{\nu}$ the energy of the transition given in wavenumber units. The transition dipole moment μ is the expectation value of the dipole moment operator. When we evaluate the transition dipole matrix element for molecular wavefunctions one arrives at the well-known *selection rules* for spectroscopic transitions.

Selection rules

Relation 2.3 shows that a non-zero transition dipole moment is needed for a transition to occur. The expression of μ can be simplified by separating the molecular wavefunction into the electronic spatial wavefunction and two overlap integrals related to the electron spin and nuclear wavefunction making use of the Born-Oppenheimer approximation:

$$\mu = \langle \Psi_1 | \hat{\mu} | \Psi_0 \rangle = \langle \phi_1 | \hat{\mu} | \phi_0 \rangle \langle S_1 | S_0 \rangle \langle N_1 | N_0 \rangle \tag{2.4}$$

All three components have to be non-zero and the selection rules arise from their analysis.

To evaluate if the $\langle \phi_1 | \hat{\mu} | \phi_0 \rangle$ component is non-zero we can make use of the symmetry properties of the molecule. If the symmetry of one of the components of the electronic transition dipole moment is transformed following the same symmetry as the overall symmetry of the molecule, the transition is said to be *symmetry-allowed*. For octahedral transition metal complexes for example the symmetry selection rule forbids d-d transitions whereas d-π^* or π-d transitions are added to the π-π^* usually encountered in the ligands.

The nuclear overlap integral $\langle N_1 | N_0 \rangle$ is usually non-zero, but the intensity of the transition is highly dependent on the square of the integral known as *Franck-Condon factor*. Depending on the relative nuclear configuration of the fundamental and excited states, the most intense transition may not be the $0 \rightarrow 0$ as depicted in figure 2.1. This principle is of course only valid in the Born-Oppenheimer approximation since the nuclear positions must be frozen during the transition.

Spin is another important factor determining the transition probability. The spin overlap integral will be zero if the total spin is modified and equal to 1 if it is conserved. The transition will therefore occur only if the *total spin is conserved*. This means that singlet-singlet transitions are allowed whereas singlet-triplet or triplet-singlet are forbidden.

These selection rules have been established using great simplifications and therefore must not be considered as absolute laws but rather as indicators for the intensities of the considered transitions. A "forbidden" transition is always weak compared to an "allowed" one but there are possibilities to circumvent these rules. Within the assumptions used so far the molecule remains in its particular point group upon excitation. If the electronic and nuclear motion are somehow related, the symmetry selection rule can be overcome. This effect is known as *vibronic coupling* and the transition is said to be *vibronically allowed*.
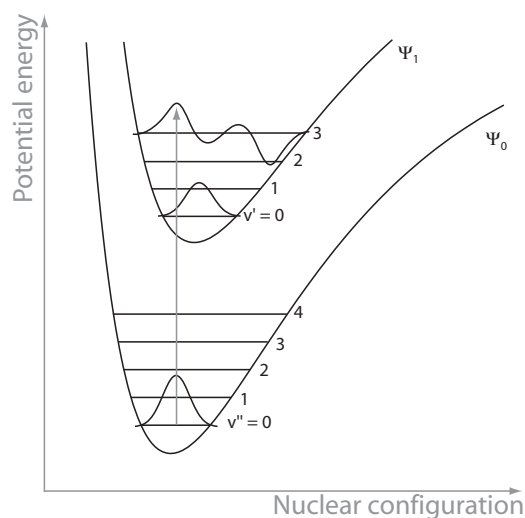
Figure 2.1 — $0 \rightarrow 3$ transition favoured by the Franck-Condon factors

The spin conservation selection rule can also be bypassed according to the coupling effect. The electronic spin can be influenced by the magnetic angular momentum of the electrons moving in their orbitals. This *spin-orbit coupling* is dependent upon the number of neighboring electrons, the size and the angular momentum of their orbitals. Therefore it is proportional to Z^4 where Z is the atomic number. This effect is very important for atoms like Br or I, but also for Ru and Os compounds.

2.1.2   Excited State evolution

The fate of an excited species is usually depicted in a Jablonski diagram (fig. 2.2). The kinetics of the different transitions illustrated in this picture are of major importance since any photochemical reaction must enter into competition with these processes to occur. The time for absorption is similar to the optical cycle of the incident light and is thus very short (few fs). The timescales for the different processes are given in a separate table (table 2.1). The values vary over several orders of magnitude and these differences tell a lot about the photochemical behavior of the compounds.

The photo-excited state has usually the same total spin as the ground state. Yet, exceptions are found when heavy atoms are present. Excited state de-activation can take place in a radiative or non-radiative way. In the latter case, vibrational relaxation depends upon the neighboring atoms but also upon the surrounding media (solvent, solid matrix,...), and ranges over a
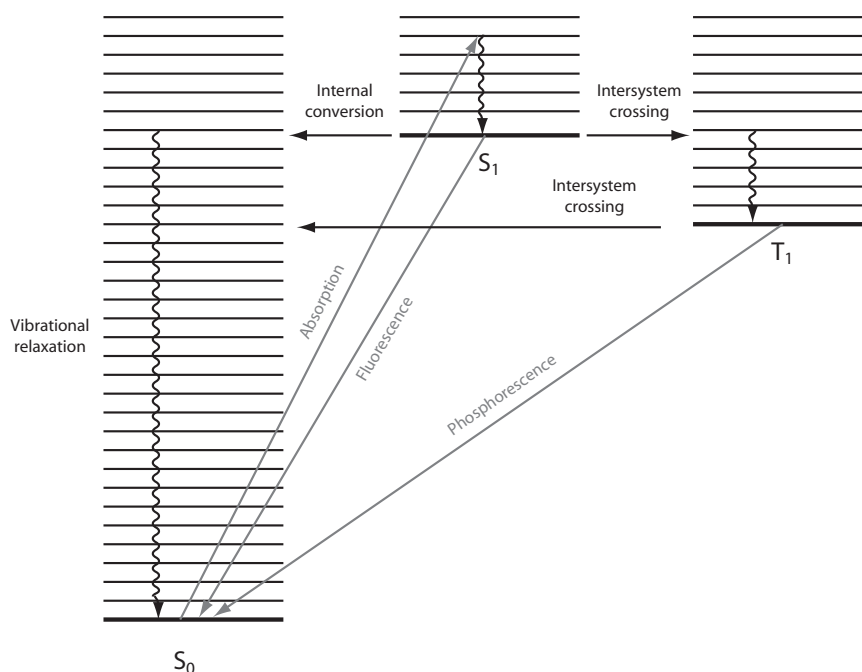
Figure 2.2 — The Jablonski diagram

Transition	Timescale [s]
Absorption	10^{-15}
Vibrational relaxation	10^{-2} - 10^{-12}
Internal conversion	10^{-8} - 10^{-12}
Intersystem crossing $S_1 \rightarrow T_1$	10^{-6} - 10^{-14}
Intersystem crossing $T_1 \rightarrow S_0$	10^{3} - 10^{-3}
Fluorescence	10^{-6} - 10^{-9}
Phosphorescence	10^{4} - 10^{-2}

Table 2.1 — Timescales for excited state deactivation

wide timescale. Radiative deactivation (fluorescence and phosphorescence) takes usually place from the lowest vibrational level (Kasha's rule). The fluorescence spectrum is approximately the mirror image of the absorption spectrum. However, the absorption and emission peaks are usually shifted because of the vibrational cooling in the singlet excited state (*Stokes shift*). The triplet state is normally energetically stabilized due to spin correlation and may be readily populated for systems where high spin-orbit coupling is present.

2.1.3 Charge transfer in transition metal complexes

Most of the experiments carried out in this work feature ruthenium poly-pyridyl complexes. These are octahedral complexes of Ru(II) that possess a center of symmetry. The symmetry selection rule tells that it is a necessary condition for a transition to be "allowed" that the electron moves from an orbital that is even with respect to inversion through the center of symmetry, to an orbital that is uneven with respect to inversion (or vice versa). Since all d orbitals in an octahedral complex are even with respect to inversion d-d transitions are "forbidden". Under visible irradiation these complexes undergo strong *metal-to-ligand charge transfer transitions (MLCT)*. What is called a *charge transfer* is nothing but a transition with a very large transition dipole moment. In the case of transition metal complexes in addition to ligand-based transitions, electron density can be transferred from d or n orbitals localized on the metal ion to a π^* orbital on the ligand. If the lowest unoccupied molecular orbital (LUMO) is located on the metal ion, the opposite charge transfer (LMCT) is observed.
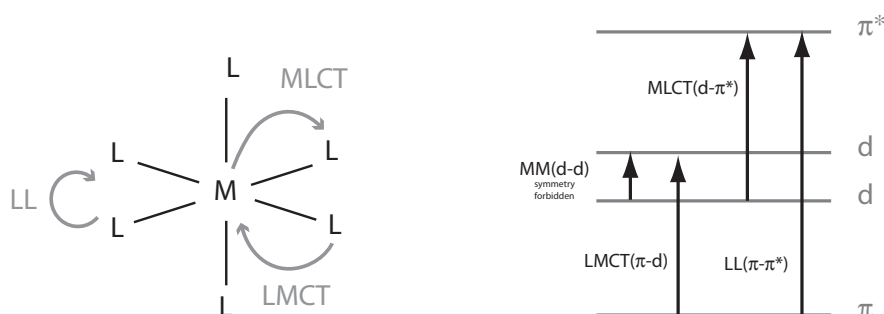
Figure 2.3 — Charge transfers in a transition metal complex

2.2 Semiconductors

To build up an overall picture of interfacial electron transfer it is essential to give an introduction to semiconductor physics. In this section we shall focus on the behavior of semiconductors under light illumination, in the presence of a solvent containing a redox electrolyte and in contact with adsorbed species. A description of the sensitization process will also be given.

2.2.1   Band structure of solids

Unlike in molecular systems, the energy levels of semiconductors are so dense that they form broad energy bands instead of discrete molecular orbitals energy levels. There are two ways to understand how these bands are formed. In the first approximation, derived from Sommerfeld's free electron theory, electrons in a crystalline solid experience a periodic potential that has the periodicity of the lattice. The one-electron wavefunctions (Bloch functions) have the form of plane waves with a propagation vector $\mathbf{k}$. The solution of Schrödinger's equation for this system yields ranges of electron energies that are alternatively allowed or forbidden depending on whether $\mathbf{k}$ is real or complex. An important consequence of this model is that an electron in the crystal responds to the same Newtonian laws of motion as an electron in an external electric field except that the electrical force is now equal to the time derivative of the crystal momentum $p = \hbar\mathbf{k}$. This leads to the concept of the effective mass m_e^*.

$$m_e^* = \frac{\hbar^2}{d^2 E/d\mathbf{k}^2} \tag{2.5}$$

The other approach is more intuitive for a chemist and also more accurate for systems with large band gaps where the atoms in the lattice retain more atomic character. In this approximation, the *tight-binding model*, the band structure is closely related to the atomic wavefunctions. Let us start with the atomic electronic configurations of n identical atoms. When the interatomic distance decreases the atomic orbitals mix together and, similar to the case of molecules formed from atoms, the equal energy levels are split into a new set of discrete energy levels. Since the number of interacting wavefunctions in a solid is huge ($> 10^{22}$ atoms/cm^3) these energy levels form a quasi-continuum of states with forbidden energy gaps (see fig. 2.4).

The lowest band containing empty states is known as the *conduction band*. It is partially filled for metallic compounds, while it is empty for semiconductors and insulators, the difference between the latter cases lying in the width of the band gap energy.

2.2.2   The semiconductor/electrolyte interface

The semiconductor/electrolyte interface is characterized by the different electronic potentials depicted in figure 2.5. Similar to metal/solution interfaces, the potential drop on the electrolyte side is determined by the adsorption of solvent molecules or ions at the surface of the solid. This
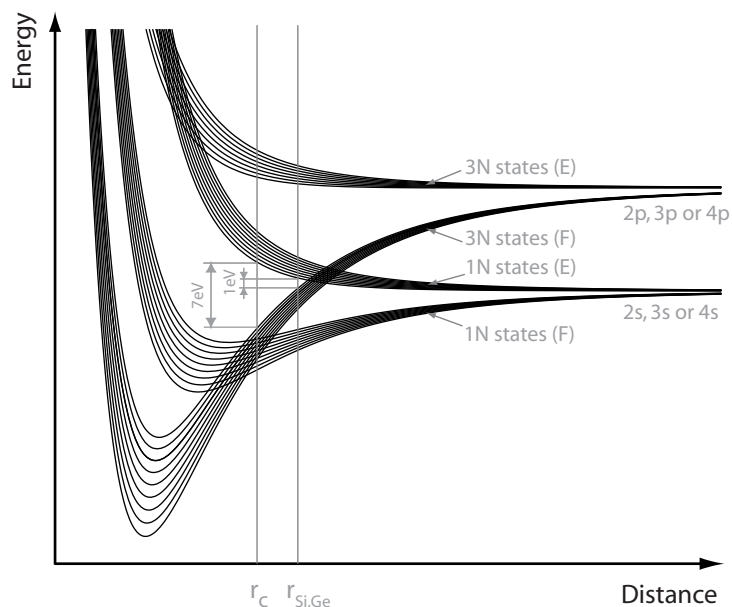
Figure 2.4 — Schematic view of the formation of the band structure in the tight-binding approximation for carbon, silicon and germanium. E=empty, F=filled. The values in eV correspond to the bandgap energy

linear potential falloff corresponds to the Helmholtz layer and d_H is typically the thickness of a monolayer. A further decrease is observed in the Goüy-Chapman layer where the solvated ion concentration variation causes the potential to decrease exponentially following Poisson's law.

On the semiconductor's side, the potential of the electron in the bulk is called the Fermi potential (ϕ_F) and at equilibrium is equal to ϕ_{sol}. Since the density of the free carriers in a semiconductor is much smaller than in a metal, the part of the interfacial potential change located in the solid extends much deeper into the material. The thickness of this layer is given by d_{SC} which corresponds to a space charge layer which can be a depletion or an accumulation layer depending on the Fermi level and the doping of the semiconductor.

The positions of the different potentials has a strong influence on the efficiency and the dynamics of interfacial electron transfer. The flatband potential corresponds to the conduction band edge potential, which corresponds to the energy needed to put the first electron in the electrode if we except surface trap states. This potential is determined by the adsorption of chemical species at the surface of the solid, and by surface states. The latter states correspond to metal ions with incomplete coordination and are of re-
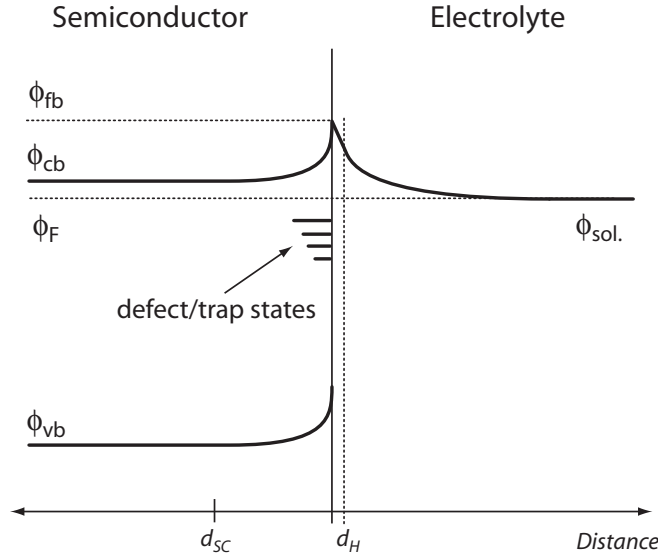
Figure 2.5 — Electronic structure of a semiconductor/electrolyte interface. ϕ_F: Fermi potential, ϕ_{cb}: conduction band potential, ϕ_{fb}: flatband potential, ϕ_{vb}: valence band potential, ϕ_{sol}: solution potential, d_{SC}: space charge layer thickness, d_H: Helmholtz layer thickness

markable importance for nanoparticles where the surface-to-volume ratio is exceptionnally high. In addition, for sintered nanocrystalline films, defect states are found at grain boundaries.

The thickness and the bending of the space charge layer depends on the material and the size of the semiconductor particles. For small particles (with a radius r similar to d_{SC}) the potential drop can be estimated by:

$$\Delta\phi_{SC} = \frac{k_B T}{6e}\left(\frac{r}{L_D}\right)^2 \qquad (2.6)$$

where e is the charge of an electron and L_D is the Debye length given by:

$$L_D = \sqrt{\frac{\epsilon_0 \epsilon k_B T}{2e^2 n_d}} \qquad (2.7)$$

where ϵ_0 is the permittivity of free space, ϵ is the dielectric constant of the material and n_d is the carrier density in the semiconductor. These equation show that nanometer-sized semiconductor particles cannot allow for the buildup of space charge layers. As an example, for 25-nm TiO_2 particles ($\epsilon=130$ and $n_d=10^{17}$ cm^{-3})[1] the band bending is only 0.7 meV and is small compared to kT. Therefore it is usually neglected in the discussion of conduction band energetics for metal oxide nanoparticles.

Electronic energy levels under illumination

In thermal equilibrium, the probability of finding an occupied energy level at an energy E is given by the Fermi-Dirac function:

$$f(E) = \left[1 + \exp\left(\frac{E - E_F}{kT} \right) \right]^{-1} \tag{2.8}$$

where E_F is the Fermi energy or Fermi level. When a semiconductor is not at thermal equilibrium (i. e. under illumination for instance), it is very likely that the electron population is in equilibrium with the conduction band energy levels and the holes in equilibrium with the valence band energy levels. In these conditions, the *quasi-Fermi level* has to be defined separately for electrons and holes. For electrons:

$$E_{F,n}^* = E_{cb} + k_B T \ln\left(\frac{n^* + n_d}{N_{cb}} \right) \tag{2.9}$$

where n^* is the outer-equilibrium concentration of electrons in the conduction band under illumination, n_d is the concentration of donor impurities, and N_{cb} is the apparent density of states in this band.

2.3 Dye sensitization of semiconductor electrodes

At the heart of a dye-sensitized solar cell (DSC) lies the process of sensitization of colloidal semiconductor electrodes. In this approach electrons are transferred to the conduction band of wide bandgap semiconductors by means of organic or inorganic compounds, producing usable current or voltage responses. This technique allows to reach high optical densities over a broad range of wavelengths by using thoroughly engineered chemical dyes. As an example, TiO_2 with a bandgap of 3.2 eV, is able to absorb most of the UV light below 380 nm. Sensitization of nanocrystalline electrodes of this material by ruthenium polypyridyl compounds extends the optical response up to ca. 800 nm with a high efficiency due to the appreciable extinction coefficient of these compounds over all the visible spectrum.

Dye sensitization is not restrained to solar energy conversion and has been successfully applied for more than a century to photographic techniques, xerography and photoelectrochemistry.

The traditional picture of the sensitization mechanism has been given by Gerischer during the 70's. If one assumes that the electron transfer occurs
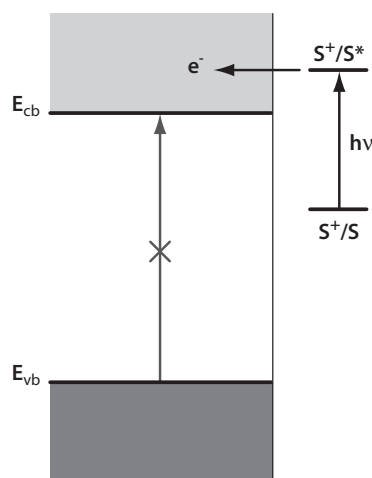
Figure 2.6 — Dye sensitization mechanism. E_{cb} and E_{vb} are the energy of the conduction and valence bands, respectively. S refers to the sensitizer.

on a much shorter timescale than nuclear motion (Franck-Condon principle), the energy terms for electron transfer are different from those obtained from the formal reduction potentials of the chemical compounds. Gerischer derived a distribution of energy levels when the sensitizer behaves as an electron donor or as an electron acceptor, $W_{don}(E)$ and $W_{acc}(E)$, respectively. Assuming harmonic thermal fluctuations with polarization changes in the solvent and equal potential energy surfaces for the donor and the acceptor, the distribution is given by a Gaussian function:

$$W_{don}(E) \;=\; \frac{1}{\sqrt{4\pi\lambda_{ox}kT}}\exp\left[-\frac{(E-(E^0-\lambda_{ox}))^2}{4kT\lambda_{ox}}\right] \qquad (2.10)$$

$$W_{acc}(E) \;=\; \frac{1}{\sqrt{4\pi\lambda_{red}kT}}\exp\left[-\frac{(E-(E^0+\lambda_{red}))^2}{4kT\lambda_{red}}\right] \qquad (2.11)$$

where λ_{ox} is the total reorganization energy for oxidizing the donor, λ_{red} is total reorganization energy for reducing the acceptor (see 2.4.3), and E^0 is the energy corresponding to the formal reduction potential. Graphically the model can be represented as in figure 2.7. The rate constant for electron transfer can be estimated by the overlap between the density of donor occupied states (D_{don} = concentration $\cdot W_{don}$) and the density of acceptor states in the electrode (D_{acc}):

$$k_{ET} = \int \kappa(G)D_{don}(G)D_{acc}(G)dG \qquad (2.12)$$

where $\kappa(G)$ is the transfer frequency reflecting the probability that electron transfer will occur at the transition state and G is the free energy.
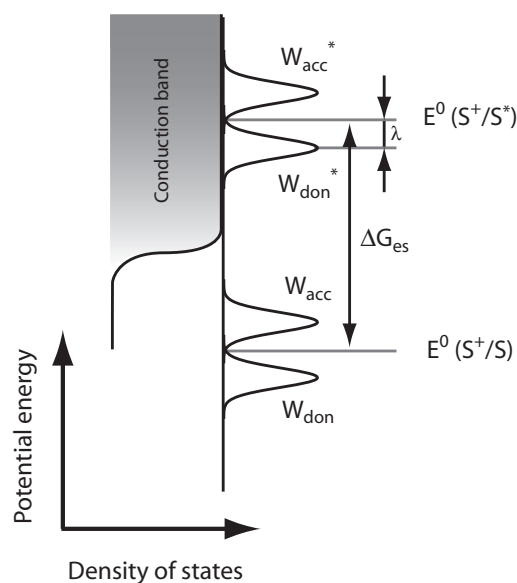
Figure 2.7 — Gerischer's model for a sensitizer (S) and its excited state

Due to the difficulty of systematically varying the energies of the donor and the acceptor, Gerischer's theory has been applied only to a small number of studies. Nevertheless, the theoretical picture is widely used to discuss electron injection kinetics even if the values of the energy levels relevant to the electrode conduction band and the reorganization energies for the sensitizer are usually not known with enough accuracy.

2.4 Theory of electron transfer kinetics

2.4.1 Classical electron transfer in solution

The simplest kinetic scheme describing activated electron transfer (ET) reactions is given by:

$$R \quad \underset{k_{-act}}{\overset{k_{act}}{\rightleftarrows}} \quad R^{\ddagger} \quad \overset{k^{\ddagger}}{\rightarrow} \quad P \tag{2.13}$$
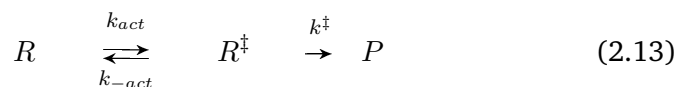
where the reactants (R) are activated into the transition state ($R^{\ddagger}$) and generate the products (P). Two cases can be distinguished:

- $k^{\ddagger} >> k_{act}$: the reaction is controlled by the activation of the precursor complex

- $k^{\ddagger} << k_{act}$: the ratio of R and $R^{\ddagger}$ is maintained at equilibrium and transition state theory (TST) can be employed.

For the particular case of a donor D and an acceptor A in solution the picture can be detailed as follows:

$$D + A \quad \underset{k_{-12}}{\overset{k_{12}}{\rightleftarrows}} \quad D|A \quad \underset{k_{-n}}{\overset{k_{n}}{\rightleftarrows}} \quad [D|A]^{\ddagger} \quad \underset{\nu_{-e}}{\overset{\nu_e}{\rightleftarrows}} \quad [D^+|A^-]^{\ddagger} \quad \overset{k_{-n}}{\longrightarrow} \quad D^+ + A^-$$

(2.14)

The first step represents the diffusion of the two reactants to form the precursor complex. The second step is the reorganization of the complex to a configuration appropriate for electron transfer. Then, the transfer occurs with an effective electron-hop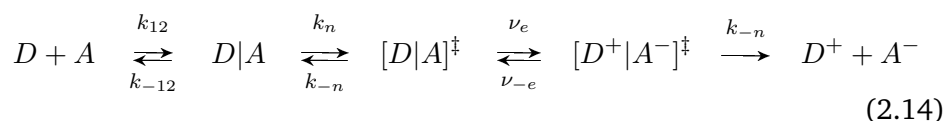ping frequency ν_e, and finally the vibrational relaxation and diffusion yields the separated products. In the ensuing discussion the rate constant k_{ET} is not taking into account the diffusion of reacting species and the formation of the encounter complex.

2.4.2   Adiabatic vs non-adiabatic behavior

An electron transfer process can be considered as a transition between an initial electronic state ψ_i where the electron is localized on the donor (D), to a final state ψ_f in which the electron has been transferred to a spatially distinct acceptor region (A). These states give rise to the *diabatic* energy profiles depicted in figure 2.8(a). The interaction between these states is described by the electronic coupling matrix element $H_{DA} \equiv \langle \psi_i | H_{el} | \psi_f \rangle$ where H_{el} is the system electronic Hamiltonian.

(a) Diabatic   (b) Adiabatic
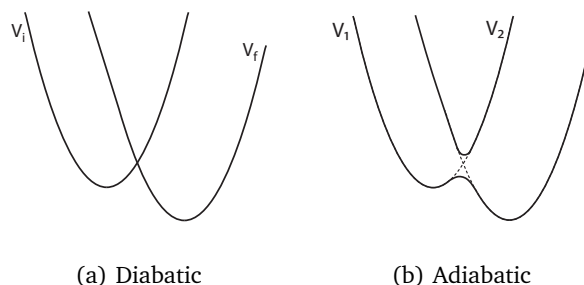
Figure 2.8 — Diabatic and adiabatic energy profiles for ψ_i (V_i) and ψ_f (V_f), and for ψ_1 (V_1) and ψ_2 (V_2), respectively.

Under the Born-Oppenheimer approximation, an electron transfer is said to be *adiabatic* when it is occurring on a potential energy surface associated with a *single* electronic state. This situation is best viewed in the *adiabatic* basis (ψ_1, ψ_2) obtained from the diabatic states by a unitary transformation. In these conditions, the electron transfer occurs gradually with progress along the reaction coordinate (figure 2.9), and the rate is governed by the frequency of motion on the potential curve.

Since the electrons and the atoms participating in the transfer are not free, the previous approximation is not always true. Therefore, for weakly interacting systems, the non-adiabatic coupling terms (i. e. electronic matrix elements associated with nuclear operators) can no more be neglected. As depicted in figure 2.9, the system can now acquire some energy from the environment and cross the reaction zone several times while staying on the same potential curve (V_i in the diabatic representation). The splitting between the upper and lower adiabatic potential curves corresponds to twice the coupling strength calculated in the diabatic basis. Obviously, the crossing is much easier for weakly interacting systems. This situation corresponds to the so-called *non-adiabatic* or weak coupling limit, and is valid for most electron transfer processes in condensed phase.
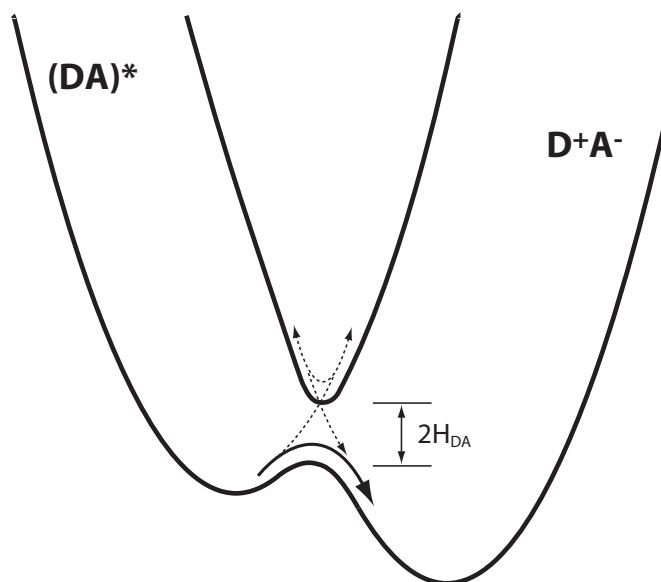
Figure 2.9 — Adiabatic vs. non-adiabatic electron transfer. H_{DA} is the electronic coupling matrix element. The adiabatic pathway is represented by the filled arrow and the non-adiabatic pathway by the dashed arrows

2.4.3 Fermi's Golden Rule

In the non-adiabatic limit, the coupling elements can be treated as perturbations in the diabatic basis. Using time-dependent perturbation theory the resulting rate constant is known as Fermi's Golden Rule:

$$k_{ET} = \frac{2\pi}{\hbar} |\langle \psi_i |H_{el}| \psi_f \rangle|^2 |\langle d_{vib} | a_{vib} \rangle|^2 \rho(E_A) \qquad (2.15)$$

$$k_{ET} = \frac{2\pi}{\hbar} |H_{DA}|^2 (FCWD) \qquad (2.16)$$

H_{DA} is the electronic coupling matrix element. $\rho(E_A)$ is the density of acceptor states in the product. The nuclear overlap is given by the interaction of the vibrational states of the donor and the acceptor, $|d_{vib}\rangle$ and $|a_{vib}\rangle$. The two latter parameters are usually expressed in terms of the Franck-Condon weighted density of states (FCWD). This factor reflects the influence of all nuclear modes of the system. Here, different approximation of the FCWD lead to the equations used in practice.

High-temperature classical limit

In the high-temperature limit (where all the nuclear frequencies ω obey the relation $\hbar\omega << k_B T$) the classical limit for the FCWD is given by:

$$FCWD = \frac{1}{\sqrt{4\pi k_B T \lambda}} \exp(-\Delta G^{\ddagger}/k_B T) \qquad (2.17)$$

$$\text{where} \quad \Delta G^{\ddagger} = \frac{(\Delta G^0 + \lambda)^2}{4\lambda} \qquad (2.18)$$

This is equivalent to the result of the classical Marcus theory. The different parameters are depicted in figure 2.10. This important result arises from a TST model and provides an Arrhenius type relation. More important is the concept of the reorganization energy introduced here. This quantity reflects the nuclear rearrangement needed to prepare the reactant in a configuration appropriate to the electron transfer. λ is usually divided into two components λ_s and λ_v which corresponds to the reorganization of the solvent molecules around the reactants, and to the inner-shell vibrational rearrangement, respectively. Another important feature is the remarkable relation between the driving force $-\Delta G^0$, which is a thermodynamic quantity, and the rate constant, a kinetic quantity.

A detailed examination of the reaction profile shown in figure 2.10 gives more information about the course of the overall process. Starting from
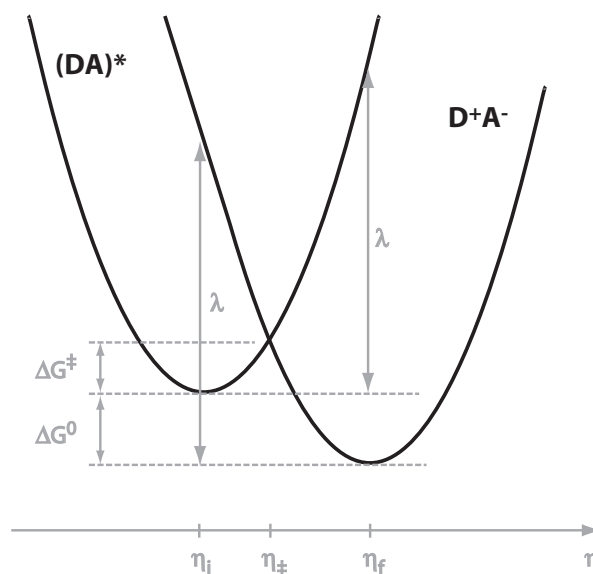
Figure 2.10 — Energy profiles along the reaction coordinate η. λ is the reorganization energy, $-\Delta G^0$ the reaction driving force and $\Delta G^{\ddagger}$ the activation free energy.

a D/A excited complex oscillating around the η_i equilibrium position, the complex has to reach the crossing point ($\eta_{\ddagger}$) where the electron transfer occurs by a tunnelling process. The probability of electron tunnelling derives from the electronic coupling and when this coupling is weak the system can proceed across the transition state several times before hopping to the products potential energy surface. The reorganization energy λ is found twice in this scheme. It can be interpreted as the displacement along the energy potential needed for the reactants to reach the equilibrium configuration of the products. Symmetrically, the same energy is required for the products to reach the configuration corresponding to η_i. Of course this is only valid when quadratic potential curves are assumed as it is in Marcus theory.

When the driving force, $-\Delta G^0$, is increased we can see that the potential curves are shifted vertically (see figure 2.11). This results in the decrease of the activation energy needed to reach the transition state until the products curve intercepts the reactants potential at the bottom of the parabola. At this particular point $\Delta G^{\ddagger}$ is zero and the rate is maximal. If we further increase the driving force the activation energy gets larger again and the rate constant is reduced. This leads to the definition of the *normal region* and the *inverted region* for electron transfer where counter-intuitively the rate decreases whith increasing driving force.

(a) Normal region   (b) $\Delta G^{\ddagger} = 0$ (c) Inverted region
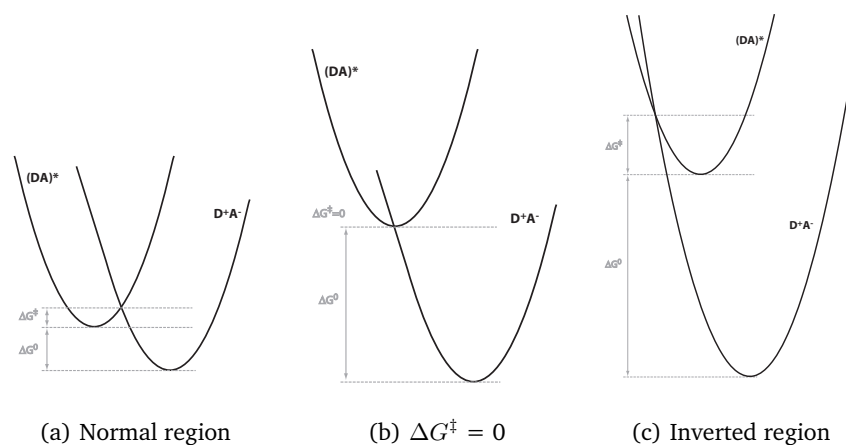
Figure 2.11 — Reaction regimes with increasing driving force $-\Delta G^0$

Semi-classical approach

In the high-temperature classical limit, nuclear tunnelling effects are completely neglected. This can lead to significant errors when high frequency vibrational modes are present ($\hbar\omega_i >> k_BT$) or for cases where the temperature is very low. In the semiclassical approach these high frequency modes are treated quantum mechanically whereas low frequency modes are still treated classically. The Hamiltonian used here derives from the spin-boson model or polaron model consisting of two electronic states interacting with a large number of vibrational levels. The resulting FCWD is given by:

$$FCWD = (4\pi\lambda_s k_B T)^{-1/2} \exp(-S) \sum_{n=0}^{\infty} \frac{S^n}{n!} \exp\left[\frac{-(\Delta G^0 + n\hbar\omega + \lambda_s)^2}{4\lambda_s k_B T}\right]$$

$$where \quad S = \frac{\lambda_v}{\hbar\omega} \tag{2.19}$$

Here λ_s, the solvent reorganization energy, is treated classically and λ_v is the vibrational reorganization energy associated with the harmonic frequencies ω corresponding to the quantized modes.

The importance of the overlap of nuclear wavefunctions is depicted in figure 2.12. In the normal region, significant overlap is only observed for higher vibrational states. In contrast, in the inverted region, where the potential curve of the reactants is inscribed into the products parabola, strong interaction is found even for the lowest vibrational states.

As a consequence, nuclear tunneling effects are very important in the Marcus inverted region while they are generally negligible in the normal region.
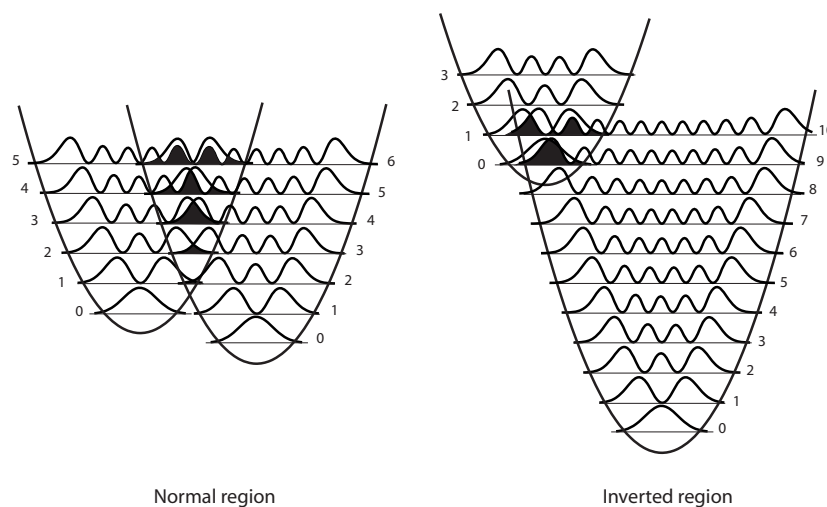
Figure 2.12 — Overlap of the nuclear wavefunctions. In the normal regime, the overlap between the v=0 vibrational level of the reactant state with the levels of the product state is negligible. In contrast, strong overlap with the v'=9 level is found in the inverted region.

The difference between the classical and the semiclassical treatment is illustrated in figure 2.13. In the classical approach, the evolution of the logarithm of the rate constant with respect to the driving force is described by an inverted parabola. The maximum is found when $-\Delta G^0$ is equal to the total reorganization energy λ. In the semiclassical treatment, the rate constant follows the same trend in the normal region, while the decrease is much slower in the inverted region because of the influence of nuclear tunneling.

2.4.4 Electronic coupling

The electronic coupling matrix element ($|H_{DA}|^2 = |\langle D|H_{el}|A|^2\rangle$) is predicted to decline exponentially with distance because of the exponential radial character of the electronic wave functions of the donor and acceptor. It is given by:

$$|H_{DA}|^2 = |H_{DA}^0|^2 \exp\left[-\beta(r - r_0)\right] \tag{2.20}$$

where β is the damping factor usually given in Å^{-1}, and $(r - r_0)$ is the displacement from van der Waals contact distance. If the FCWD variation with increasing distance is negligible, the rate constant can be approximated as:

$$k_{ET} \cong k_0 \exp\left[-\beta(r - r_0)\right] \tag{2.21}$$
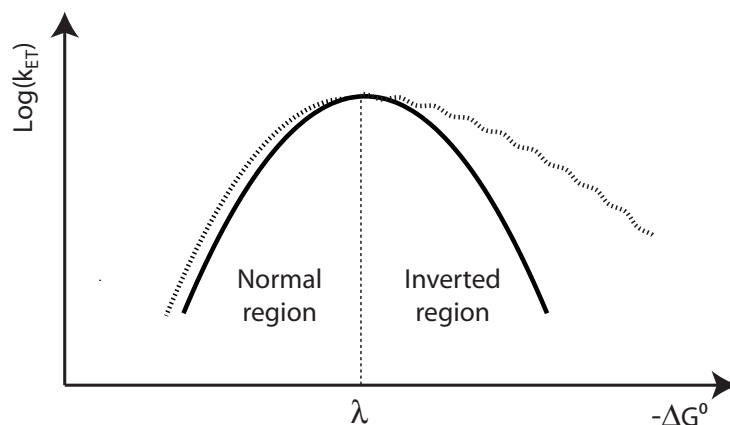
Figure 2.13 — Electron transfer rate constants vs. driving force obtained from the classical (filled line) and semiclassical (dotted line) approaches.

For large systems, the reorganization energy might change significantly with distance and the latter relation might be misleading. Numerous studies have been published where the focus was put on the influence of the bridging media between the donor and the acceptor. Typical β values are found experimentally between 0.2 and 1.2 Å^{-1}, the lower values corresponding to conjugated bridges. In general, two models are invoked to interpret the distance dependence in donor-bridge-acceptor systems: the *sequential model* and the *superexchange model*. In the latter representation, the role of the bridge is simply to mediate the coupling between the donor and the acceptor. The electron tunnels between them and the bridge population is negligible at all times. In the sequential model the population is no more neglected and the electron is considered to be hopping between adjacent sites. This model has been applied for example to doped polymers and electron transfer along DNA chains.

2.4.5 Heterogeneous electron transfer

The specific case of electron transfer between a molecular species and a metal or a semiconducting electrode has first been addressed from an electrochemical point of view. Gerischer's approach (see section 2.3) leads to the same quantitative expression for $\Delta G^{\ddagger} = f(\lambda, \Delta G^0)$ as Marcus theory. This result can be applied to the emission of an electron from a semiconductor electrode or to electron injection with the assumption of weak electronic coupling and in the absence of tunneling effects. In this framework the nuclear activation barrier for electronic resonance dominates the reaction kinetics.

For electron emission, electronic coupling between the molecular potential and the periodic lattice potential is a key issue. In the adiabatic limit (strong coupling), the electron transfer can proceed on the same timescale as the fluctuations in nuclear coordinates leading to charge stabilization in the molecular acceptor. The characteristic bath mode frequency is on the order of 10^{12}-10^{13} s^{-1} for many molecular systems.

In the case of electron injection from a molecular donor into a semiconductor the situation is different because of the huge density of acceptor states. Nuclear tunneling is now expected to be extremely efficient. The vibrational overlap integrals given by the Franck-Condon factors (FC = $|\langle d_{vib}|a_{vib}\rangle|^2$ see eq. 2.15) approach unity. Hence, the nuclear factor can be approximated by the "density of states" in the molecular species, given by the level spacing for the harmonic oscillator ($\rho(E_A) = 1/\hbar\omega$). The physical origin of this harmonic oscillator can be intramolecular vibrations in the adsorbed molecule or a collective mode in the medium surrounding the molecule. The rate constant is given by:

$$k_{ET} = \frac{2\pi}{\hbar}|H_{DA}|^2 \frac{1}{\hbar\omega}(FC) \tag{2.22}$$

and the maximum rate is attained when FC $\rightarrow$ 1:

$$k_{ET}^{max} = \frac{2\pi}{\hbar}|H_{DA}|^2 \frac{1}{\hbar\omega} \tag{2.23}$$

In the model developed by Lanzafame et al.[2,3] the large number of states in the semiconductor creates the possibility of localizing the charge in the accepting phase without any need to invoke nuclear relaxation. When the molecular species is excited the electron resonantly tunnels across the interface to a single electronic state of the semiconductor which is mixed with the entire quasi-continuum of states in the conduction band. If no relaxation occurs, the wave function propagation remains coherent, but if some electron dephasing and/or carrier thermalization occurs, the electron is localized in the accepting phase. The timescale for electron injection is now dependent upon the tunneling time across the interface and the relaxation into the conduction band. The first parameter is directly proportional to the electronic coupling between the donor and the acceptor phase and the second one depends on the material and can be as fast as 10 fs. In this model no bath mode is needed to describe the transfer and the upper limit of ca. 100 fs, corresponding to nuclear relaxation of the molecular species in the case of electron emission, can be overpassed for significant electronic coupling. The formal derivation of this model[2] leads to a relation analogous to Fermi's Golden Rule, depending only on the electronic coupling and the density of electronic states in the conduction band $\rho(cb)$.

$$k_{ET} = \frac{2\pi}{\hbar}|H_{DA}|^2\rho(cb) \tag{2.24}$$

More recently, ET at dye-semiconductor interfaces has been addressed by several research groups. Prezdho et al.[4,5,6,7,8] performed *ab initio* non-adiabatic molecular dynamics simulations, using time-dependent density functional theory (TD-DFT). In a series of papers Ramakrishna et al.[9,10,11,12] studied the effects of electronic-vibrational coupling employing Anderson-Newns type Hamiltonians. These simulations have been realized in a framework valid for weak coupling, but Thoss et al.[13] extended the study over this limit using different methods such as the self-consistent hybrid method. A detailed discussion of the results of these studies is beyond the scope of this introduction but it can be noticed that most of them agree with very fast reaction rates characterized by time constants of less than a few tens of femtoseconds. The importance of the electronic coupling but also the coupling to the different vibrational degrees of freedom has been highlighted especially in cases where the injection level lies near the bottom of the conduction band.

2.5   References

The discussion presented in this chapter is based on the following books and reviews:

Balzani, V., Ed.; *Electron Transfer in Chemistry;* volume 1-5 Wiley-VCH: 2001.

Barbara, P. F.; Meyer, T. J.; Ratner, M. A. "Contemporary issues in electron transfer research", *J. Phys. Chem.* **1996,** *100,* 13148-13168.

Gilbert, A.; Baggott, J. *Essentials of Molecular Photochemistry;* Blackwell Scientific Publications: 1991.

Dwayne Miller, R.; McLendon, G.; Nozik, A. J.; Schmickler, W.; Willig, F. *Surface Electron Transfer Processes;* VCH Publishers, Inc: 1995.

Moser, J. E. *Processus Photochimiques, Lectures Notes;* EPFL: 1998-1999.

Newton, M. D.; Sutin, N. "Electron-Transfer Reactions In Condensed Phases", *Annu. Rev. Phys. Chem.* **1984,** *35,* 437-480.

Newton, M. D. "Quantum Chemical Probes of Electron-Transfer Kinetics - the Nature of Donor-Acceptor Interactions", *Chem. Rev.* **1991,** *91,* 767-792.

Rizzo, T. *Quantum Chemistry, Lectures Notes;* EPFL: 2003-2004.

Turro, N. J. *Modern Molecular Photochemistry;* University Science Books, Sausalito, CA: 1991.

Other references cited in this chapter:

1. O'Regan, B.; Moser, J.; Anderson, M.; Grätzel, M. "Vectorial Electron Injection into Transparent Semiconductor Membranes and Electric-Field Effects on the Dynamics of Light-Induced Charge Separation", *J. Phys. Chem.* **1990,** *94,* 8720-8726.

2. Lanzafame, J. M.; Miller, R. J. D.; Muenter, A. A.; Parkinson, B. A. "Ultrafast Charge-Transfer Dynamics at SnS_2 Surfaces", *J. Phys. Chem.* **1992,** *96,* 2820-2826.

3. Lanzafame, J. M.; Palese, S.; Wang, D.; Miller, R. J. D.; Muenter, A. A. "Ultrafast Nonlinear-Optical Studies of Surface-Reaction Dynamics - Mapping the Electron Trajectory", *J. Phys. Chem.* **1994,** *98,* 11020-11033.

4. Duncan, W. R.; Prezhdo, O. V. "Electronic structure and spectra of catechol and alizarin in the gas phase and attached to titanium", *J. Phys. Chem. B* **2005,** *109,* 365-373.

5. Duncan, W. R.; Stier, W. M.; Prezhdo, O. V. "Ab initio nonadiabatic molecular dynamics of the ultrafast electron injection across the alizarin-TiO_2 interface", *J. Am. Chem. Soc.* **2005,** *127,* 7941-7951.

6. Stier, W.; Prezhdo, O. V. "Nonadiabatic molecular dynamics simulation of light-induced, electron transfer from an anchored molecular electron donor to a semiconductor acceptor", *J. Phys. Chem. B* **2002,** *106,* 8047-8054.

7. Stier, W.; Prezhdo, O. V. "Thermal effects in the ultrafast photoinduced electron transfer from a molecular donor anchored to a semiconductor acceptor", *Isr. J. Chem.* **2002,** *42,* 213-224.

8. Stier, W.; Duncan, W. R.; Prezhdo, O. V. "Thermally assisted sub-10 fs electron transfer in dye-sensitized nanocrystalline TiO_2 solar cells", *Adv. Mater* **2004,** *16,* 240-+.

9. Ramakrishna, S.; Willig, F.; May, V. "Photoinduced ultrafast electron injection from a surface attached molecule: Control of electronic and vibronic distributions via vibrational wave packets", *Phys. Rev. B* **2000,** *62,* R16330-R16333.

10. Ramakrishna, S.; Willig, F.; May, V. "Theory of ultrafast photoinduced heterogeneous electron transfer: Decay of vibrational coherence into a finite electronic-vibrational quasicontinuum", *J. Chem. Phys.* **2001,** *115,* 2743-2756.

11. Ramakrishna, S.; Willig, F.; May, V. "Bridge mediated ultrafast heterogeneous electron transfer", *Chem. Phys. Letters* **2002,** *351,* 242-250.

12. Ramakrishna, S.; Willig, F.; May, V.; Knorr, A. "Femtosecond spectroscopy of heterogeneous electron transfer: Extraction of excited-state population dynamics from pump-probe signals", *J. Phys. Chem. B* **2003,** *107,* 607-611.

13. Thoss, M.; Kondov, I.; Wang, H. B. "Theoretical study of ultrafast heterogeneous electron transfer reactions at dye-semiconductor interfaces", *Chem. Phys.* **2004,** *304,* 169-181.

CHAPTER 3

Experimental Setup

Summary

Getting direct information about ultrafast processes is nowadays mostly accessible with laser-based techniques. Electron injection processes at dye/semiconductor interfaces have been observed with time constants lower than 100 fs. Therefore the principal requirement for the experimental tool is a time resolution of 10-100 fs. The early processes following excitation of dye-sensitized electrodes involve several transient species. In order to separate the contributions from the different protagonists, spectral resolution is also a necessity. Slower processes, such as recombination of an electron from the conduction band of a semiconductor with the oxidized dye, demand an experimental setup working in the ns to ms time domain. Hereafter a detailed description of the two experimental setup used in this work and their typical performances is given. Ultrafast phenomena were studied by means of a femtosecond spectrometer and slower processes were observed with a nanosecond laser flash photolysis system.

29

3.1 Femtosecond Spectrometer

The femtosecond spectrometer described in this section was mainly built during the thesis work of S. Pelet.[1] In order to get information about the ultrafast kinetics of the system studied, two-color pump-probe spectroscopy (fig. 3.1) was usually performed. In this configuration a narrow band excitation pulse triggers the photochemical processes, and another narrow band pulse analyses the absorption changes after some time delay. More information can be obtained in the pump-supercontinuum probe scheme. In this case, the sample is probed by means of a white light short pulse adding spectral information to the kinetic data.

A very detailed description of this experimental system has been previously published.[1,2] Therefore in this section I will only present a general overview of the different components of the setup and give some more details about the improvements done in the course of the present work.
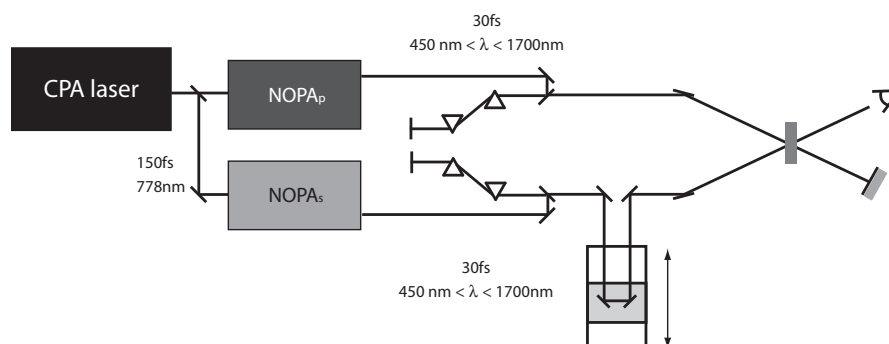
Figure 3.1 — General scheme of the femtosecond spectrometer in the two-color pump-probe configuration.

CPA laser

The fundamental laser pulses are generated in a commercial CPA-2001 laser source from Clark-MXR. This laser consists of a mode-locked oscillator and a regenerative amplifier delivering pulses with a duration of less than 150 fs centered around 778 nm at a 1 kHz frequency. The originality of this system lies in the compactness, the stability and the ease of use. Indeed all the components fit into a single closed box and almost no tweaking is necessary in a day-to-day operation.

The oscillator is made of a self-mode-locked Erbium doped fiber pumped by a telecom diode laser. The fiber delivers pulses at a 25.8 MHz frequency with a remarkable stability. A frequency doubler converts the NIR light (1550 nm) into red light (775 nm).

The amplification is realized in a chirped-pulse amplification (CPA) scheme. This technique allows to avoid crystal damage while obtaining high intensities of ultrashort pulses by stretching the pulses with a pair of dispersing diffraction gratings. The amplification is carried out in a Ti:Sapphire rod pumped by a Nd:YAG laser whose output frequency is doubled to 532 nm (8 W). The pulses are picked out of the amplifying cavity with a frequency of 1 kHz determining the repetition rate of the final pulse train. Another diffraction grating is used to compress the pulses down to 150 fs. The output energy is 1 mJ per pulse (1 W).
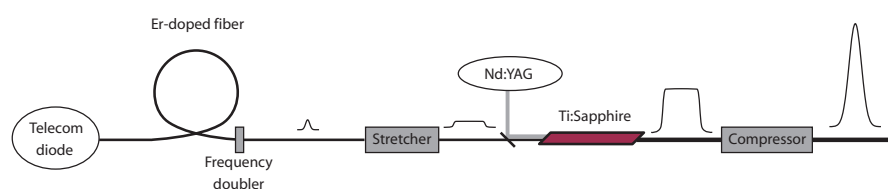

Figure 3.2 — Principle of the CPA-2001 laser source

Wavelength conversion

NOPA   In the pump-probe technique (see page 34) short pulses with defined wavelengths are needed in order to get kinetic knowledge about the different transient species involved in the physical and chemical processes. In the case of dye sensitization of semiconductor particles one may wish to excite the dye complex at a wavelength close to its absorption maximum and analyze the presence of the excited state at an other wavelength specific to that species. Since the laser provides narrowband pulses in the near-infrared domain we have to be able to convert the wavelength without deteriorating the temporal behavior of the pulses. In our setup this is achieved by using two-stages noncollinearly phase-matched optical parametric amplifiers (NOPAs).

The two NOPAs involved are based on a scheme (fig. 3.3) developed by the group of Prof. Riedle at Ludwig-Maximilians University in München.[3]. A part of the output of the CPA laser (200 μJ) is sent to each of the amplifiers. A beamsplitter samples a fraction of the input beam (< 10%) to generate a white-light continuum by focusing it tightly into a 3-mm sapphire plate.
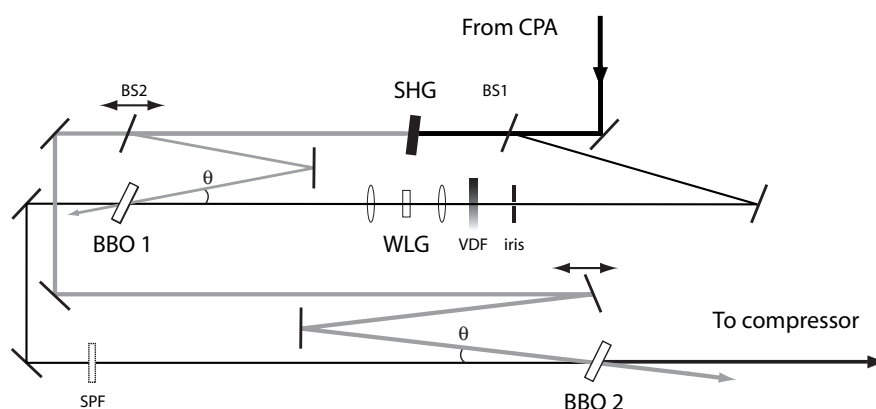
Figure 3.3 — Scheme of the double-stage NOPA. BS: beamsplitter, SHG: second harmonic generation, VDF: variable density filter, WLG: white light continuum generation, BBO: β-barium borate, θ: non-collinear angle ($\sim 6°$), SPF: short-pass filter.

This broadband pulse, collimated by an achromatic lens, is strongly chirped[a] due to the group velocity dispersion (GVD) introduced by the sapphire and the lens. The remaining part of the input beam is frequency-doubled in a 0.5 mm thick β-barium borate (BBO) crystal and the resulting blue light is divided with an 80/20 beamsplitter. The smaller part pumps a 1-mm BBO crystal (34°, type I) used to amplify a portion of the white-light. The control of the delay between the blue pump and the WLC[b], and the angle of the crystal enables the selection of a defined amplified wavelength. The signal obtained is further amplified in a 2-mm BBO crystal with the remaining part of the blue beam. This double-stage configuration allows generation of pulses within the range 450-1700 nm with a gap between 700 and 900 nm due to the instability of the WLC around the fundamental wavelength. For wavelengths between 600 and 700 nm the use of an additional short-pass filter (Calflex X, Balzers) is recommended to cut the residual part of the 778 nm fundamental beam since it can potentially be amplified in the second BBO crystal. The energy of the outcoming pulses is commonly 6-10 μJ depending on the central wavelength.

To generate pulses in the gap between 700 and 900 nm an additional white-light generation unit can be inserted after the first amplification stage. In this configuration (NOPA-plus), the first stage is optimized for pulses in the near-infrared (say 1100 nm). This output is used to generate a second WLC now centered around 1100 nm. The resulting continuum is much more

---

[a]The chirp corresponds to temporal dispersion of frequencies
[b]WLC: white-light continuum

stable in the gap region, and is amplified in the second BBO crystal used now in a single-stage way. The output energy is usually smaller but 3-5 μJ is commonly attained.

The pulses are further compressed with a pair of SF10 glass prisms down to $\sim$30 fs. The spectral widths of the output is usually of 20 to 40 nm depending on the wavelength. Typical performances are given in figure 3.4.

(a) Pulse bandwidth

(b) Pulse duration
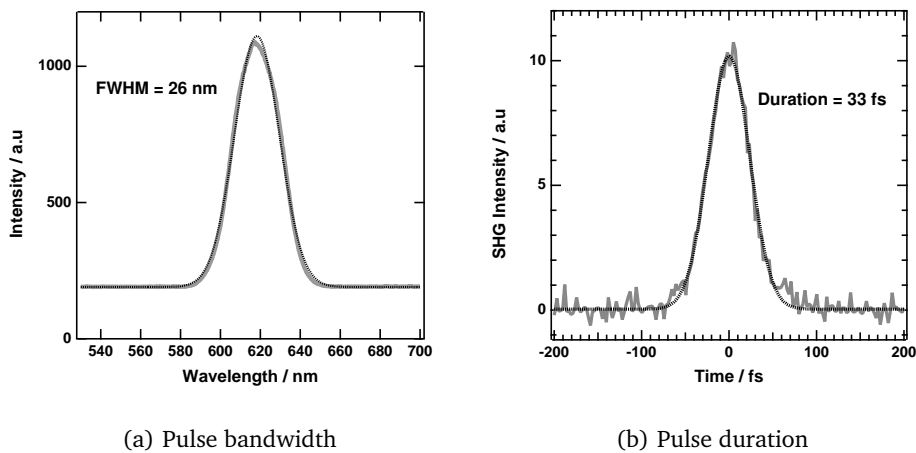
Figure 3.4 — Characteristics of a 620 nm laser pulse tuned in the NOPA.

Supercontinuum probe   If simultaneous temporal and spectral information is desired, the setup is used in the pump-supercontinuum probe scheme. In this configuration, a white-light supercontinuum pulse is generated in a sapphire plate. Careful control of the quality and the intensity of the incident beam is essential to get stable broadband pulses. This is achieved
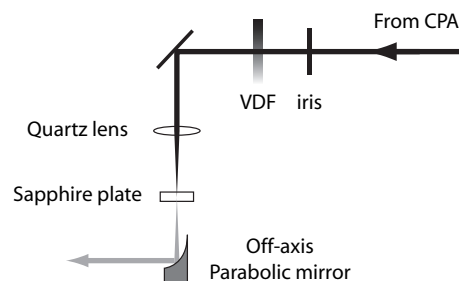
Figure 3.5 — Generation of a supercontinuum probe. VDF: variable density filter.

by reducing the intensity between 1 to 3 μJ with the help of an iris and a variable density filter (see figure 3.5). To avoid unwanted chirp of the generated continuum, the attenuated 778 nm beam is focused into a 2 mm-thick sapphire plate with a 100 mm focal length plano-convex quartz lens and re-collimation of the resulting white light is realized by a 90° off-axis uncoated aluminum parabolic mirror (EFL[c] = 50 mm, Coherent). The supercontinuum probe produced by this technique is stable in the range extending from 460 to 700 nm. The wavelength range can be extended towards shorter wavelengths if the continuum is generated into a CaF$_2$ window. In that case the window has to be constantly rotated due to the lower damage threshold of this material. Another way to control the wavelength range of the continuum would be to use the output of the NOPA tuned at a judicious center wavelength.

Pulse diagnostics In day-to-day operation the pulses are regularly characterized in order to optimize their temporal and spectral characteristics. The spectral profile is measured with a dual-channel spectrometer (S2000, Ocean Optics) coupled with an optical fiber. The pulse duration is obtained from an intensity autocorrelator (AC150, Clark-MXR). In the initial setup the duration was derived from the intensity of the SHG[d] resulting from the recombination of the beams coming from the two arms of the autocorrelator in a BBO crystal. For some wavelengths it is difficult to get a good signal-to-noise ratio with this technique. Therefore the system was improved by using a SiC UV-photodiode (JEC 0.1, Laser Components GmbH) measuring two-photon absorption.[4]

3.1.1   Two colors pump-probe setup

In the pump-probe technique, the transient response of a sample to a short excitation pulse (the pump) is monitored by a second short pulse (the probe) hitting the sample after a controlled time delay. The probe monitors the transmission or the reflective properties of the excited sample. In our case only transient absorption was measured. Time evolution of the transient chemical species is achieved by changing the relative path length of the two beams. Since light travels through air at a limited velocity, increasing the path length will induce a time delay. A 3 μm extension of the distance corresponds approximately to 10 fs. The dynamic response of the sample
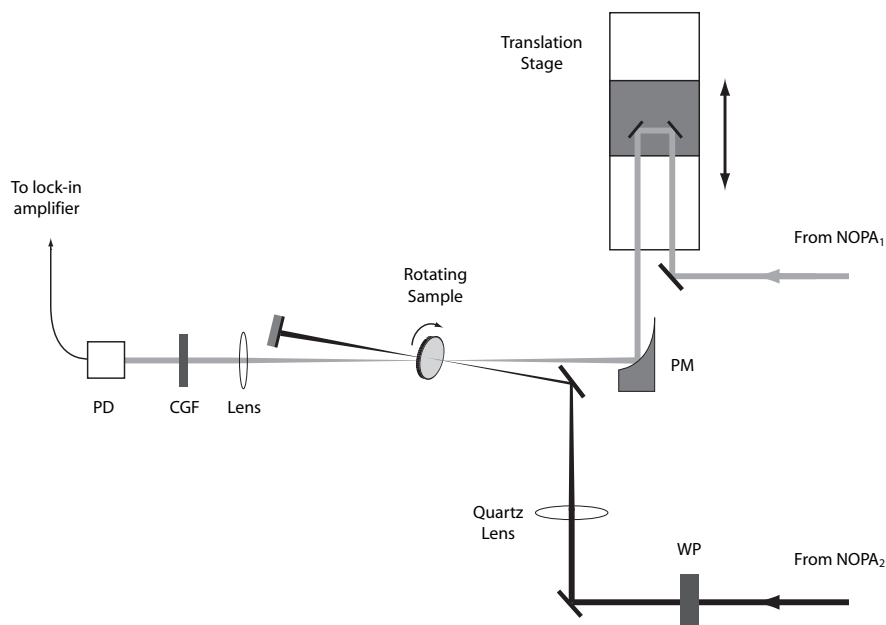
---

[c]EFL = effective focal length
[d]SHG: second harmonic generation

is therefore acquired by moving a translation stage over a distance corresponding to the desired time range.

Figure 3.6 — Scheme of the pump-probe setup. PD: photodiode, CGF: color glass filters, PM: off-axis parabolic mirror, WP: $\lambda/2$ waveplate.

In the setup used for the present work, the pump and probe pulses are provided by the two NOPAs (see page 31) tuned at different center wavelengths. Two independent translation stages make it possible to delay the pump or the probe pulse. On the probe path, a 306 mm long translation stage (M-531.PD, Physik Instrumente) allows for delays up to 2 ns. A shorter translation stage (102 mm, 0-700 ps, M-511.DD, Physik Instrumente) is also available on the pump line. Both stages are driven by the same controller (C-844, Physik Instrumente) interfaced to the computer through the GPIB bus. To avoid artifacts, the relative polarization of the two beams is set at the magic angle ($54.7°$) with the help of a $\lambda/2$ waveplate. The probe pulse is reduced with an iris to less than 1 μJ/pulse before being focused on the sample with an $90°$ off-axis aluminum parabolic mirror (EFL = 200 mm, Janos). The spot diameter at the sample position is typically less than 300 μm. On the other path, the pump beam is also weakened by an iris, and optionally, a broadband pellicle beamsplitter (40:40, Coherent). It is focused on the sample with a movable fused silica lens (f = 250 mm). The spot size is adjusted in order to cover the probe spot entirely. Additionally, the spot diameter can be increased to reduce the fluence on the sample. To avoid degradation of the dye due to high pump intensities, the sample is rotated

constantly with a home-built rotator whose speed can be adjusted from 0.1 to 1 turn per second. After passing through the sample the pump beam is blocked and color glass filters or edgepass interference filters are used in the probe path in order to remove scattered light from the pump.

The intensity of the probe light is measured by a photodiode. The first experiments featured a 1 cm^2 silicon photodiode (DET110, Thorlabs) but the use of an autobalanced photoreceiver (Nirvana 2007, New Focus) used as a single detector allows for better results.[e] The signal is then amplified and filtered by a lock-in amplifier (SR830, Stanford Research Systems). The lock-in is synchronized to the frequency of a chopper wheel (MC1000A, Thorlabs) itself triggered at half the frequency of the CPA. This means that the chopper wheel blocks exactly 1 pulse over 2 (500 Hz). The lock-in was set with a time constant of at least 1 s, a slope of 24 dB/octet and a high reserve sensitivity.

The amplitude of the absorption change is calculated from the response of the lock-in amplifier. The phase is manually adjusted to minimize Y and the difference between the transmitted light intensity when the pump is on or not, is given by the X value. The Y component should remain stable during the experiment. If some slow unwanted process occurs (for example a misalignment of the translation stage changing the spatial overlap on the sample) the Y value may change. The value read by the lock-in is only a relative absorption change. To calculate the absolute absorption change one has to measure the amplitude of the probe pulse. This is simply achieved by switching the chopper off and synchronizing the lock-in to the frequency of the CPA (1 kHz). The final absorption change is given by:

$$\Delta A = log\left(\frac{I_t - I_0}{I_0}\right) = log\left(\frac{X_{500Hz}}{X_{1kHz}}\right) \tag{3.1}$$

where I_t is the intensity at time t with pump, I_0 the intensity without pump, X_{500Hz} is the value read on the lock-in with the chopper wheel set at 500 Hz and X_{1kHz} the value when triggered at the CPA frequency. To determine if the signal is positive or negative one has to measure the phase for a known sample when the Y value is minimized. A signal with opposite sign will give a phase shifted by $\sim$180°.

---

[e]The photoreceiver could not be used in the autobalanced mode due to the repetition rate of the laser (see discussion in Pelet's dissertation[1])

Instrument response   The cross-correlation time between the pump and
the probe pulses in the sample corresponds to the instrument response. Usu-
ally this time is significantly longer than the single pulse autocorrelations
due to the angle between them and retardation while traveling through the
sample. A Kerr gating technique is used to measure precisely the temporal
overlap of the pulses. In this approach the polarization of the pump is set to
$45°$ relative to the probe's polarization plane. A Glan-Thompson polarizer
is placed after the Kerr medium (0.3 mm SFS1 window or Menzel-Gläser,
0.13-0.16 mm-thick glass cover slip), in order to entirely reject the probe.
When the pump hits the Kerr medium, the birefringence induced by the op-
tical pulse (Kerr effect) slightly rotates the polarization of the probe, hence
allowing one part of the beam to travel across the polarizer. The lifetime of
the induced birefringence (Kerr effect) is short enough to enable the probe
pulse to be rotated ("open the gate") only when both pulses temporally and
spatially overlap. A typical cross-correlation experiment in a thin glass sub-
strate is given in figure 3.7.
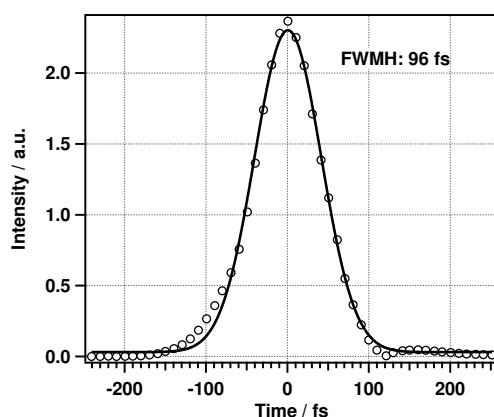
Figure 3.7 — Cross-correlation obtained by the Kerr gating technique in a thin
glass substrate. The line represents a Gaussian fit of the measured data

3.1.2   Pump-supercontinuum probe scheme

In order to acquire time-resolved spectral information, a pump-superconti-
nuum probe scheme was used. The white-light supercontinuum generation
has been described on page 33. After the sapphire plate, reflective optics
are used to minimize the chirp. The broadband pulse is first cleaned by an
iris so as to remove the red circle around the white central part. It is then
divided into a signal and reference by a home-made aluminum beamsplit-
ter (30:50). This beamsplitter was simply made by evaporating a thin layer

of aluminum (few nm) on a thin glass cover slip (0.13-0.16 mm, Menzel-Gläser) in an evaporator (Auto 500, Edwards). This was required because the reflection/transmission ratio of a dielectric pellicle beamsplitter is not constant over the spectrum of the probe pulse and the thickness of commercial metallic beamsplitters add to much chirp. To lead the pump and probe pulses to the sample, the same configuration as for the two colors pump-probe scheme is used except that the translation stage has now to be in the pump path.
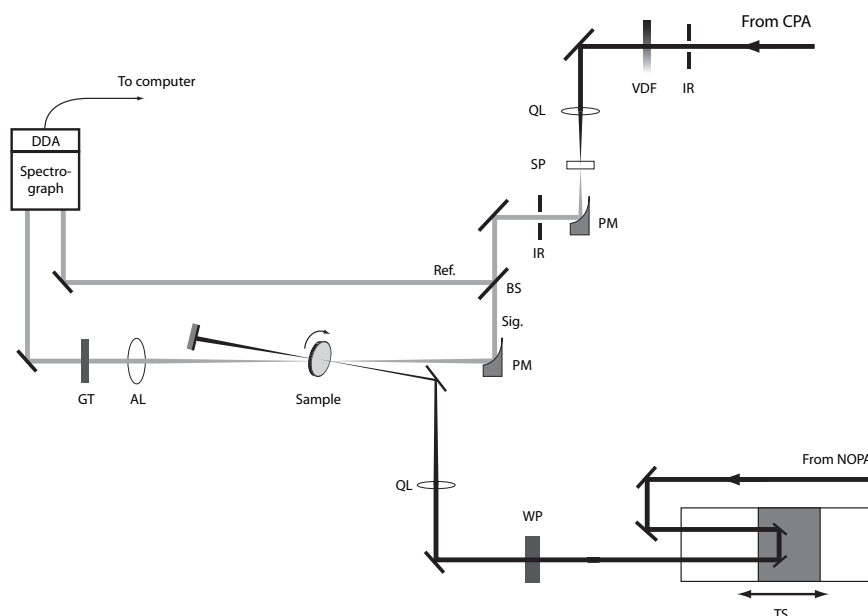
Figure 3.8 — Scheme of pump-supercontinuum probe setup. DDA: double diode array, GT: Glan-Thompson polarizer, AL: Achromatic lens, QL: quartz lens, IR: iris, PM: off-axis parabolic mirror, BS: metallic beamsplitter, SP: sapphire plate, VDF: variable density filter, WP: $\lambda/2$ waveplate, TS: translation stage.

After the sample, that can be optionally rotated, the beam is recollimated in an achromatic lens (f = 100 mm) and filtered by a Glan-Thompson calcite polarizer (Newport) turned at 90° with respect to the polarization plane of the pump. The signal and the reference beams are then sent into a Czerny-Turner spectrograph (Triax 320, Jobin-Yvon) through a slit opened to 1.5 mm. The detection is performed by a double photodiode array consisting of two separate rows of each 1024 pixel diodes (ST-116, Princeton Instruments). To remove dark noise the arrays are cooled down to -40°C by means of a thermoelectric cooler. The diode arrays are exposed for 100 ms and scanned 5 times. To measure the absorption difference, the pump is then blocked by a home-built fast pneumatic shutter and the arrays are again

scanned. This pair of measurements (with and without pump) is repeated up to 20 times. In these conditions the spectra are averaged 10'000 times.

It has been found that the way data is averaged may lead to different signal-to-noise ratios. If the number of scans is increased (up to 50 times), an offset is building up. This is probably related to saturation of the diodes. It is therefore much more efficient to raise the number of cycles with the pneumatic shutter. Special care must also be taken for the alignment of the beams entering the spectrograph. Both beams must be perfectly parallel and the vertical separation should correspond to the spacing between the two photodiode arrays. Small deviations lead to considerable errors. The final absorption change is calculated by the following equation:

$$\Delta A = log \left(\frac{I_t^* - I_0^*}{I_0^*} \right) \tag{3.2}$$

where

$$I_i^* = \frac{I_{i,sig}(\lambda)}{I_{i,ref}(\lambda)} \tag{3.3}$$

Instrument response   To characterize the instrument response the Kerr gating technique described above is applied. The gating pulse is still the pump pulse and the fraction of the continuum that temporally overlaps with the pump is transmitted through the polarizer. This experiment gives both the chirp of the broadband pulse and the cross-correlation for each individual wavelength. Every wavelength in the raw data (figure 3.10) is fitted with a gaussian to yield the FWHM [f]. Then the maxima of these gaussians are plotted with respect to the wavelengths to evaluate the temporal distribution of the frequencies.

The linear fit shown in figure 3.9b gives a slope of 1.1 fs/nm. The quality of this fit is obviously not good enough for data correction. Therefore an exponential fit was performed and used to make the rectification of the raw data as shown in figure 3.11. This correction is also applied to the transient absorption measurement when high time resolution is needed.

The cross-correlations for the individual wavelength are found between 45 and 65 fs. This provides a satisfactorily time resolution allowing for identification of time constant as low as 20 fs.

---

[f]FWHM: Full-width at half maximum
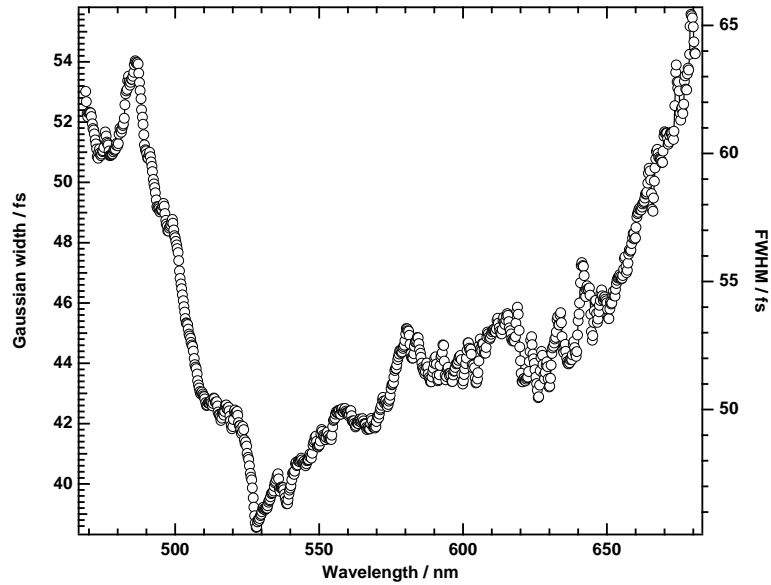
(a) FWHM obtained by fitting the individual wavelengths in figure 3.10 with a Gaussian function.
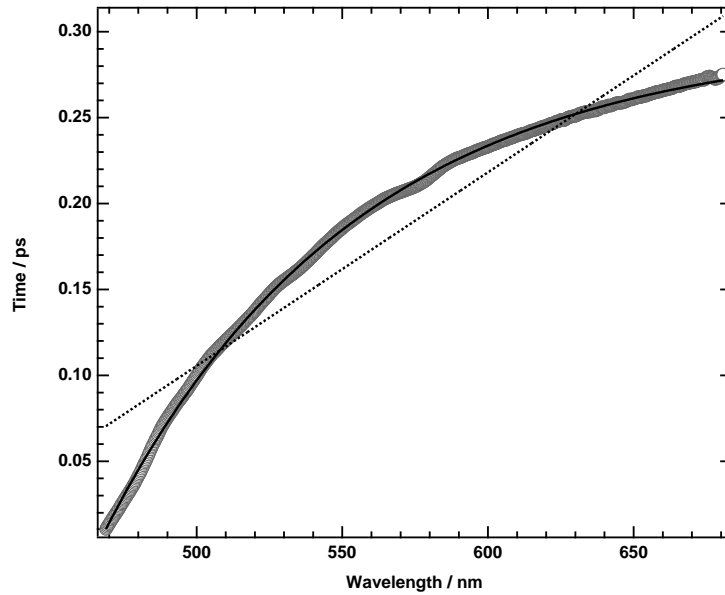
(b) Locations of the gaussians (see a) for each wavelength. The chirp is fitted with an exponential (solid line) and a linear function (dotted line).

Figure 3.9 — Analysis of the chirp of the supercontinuum.
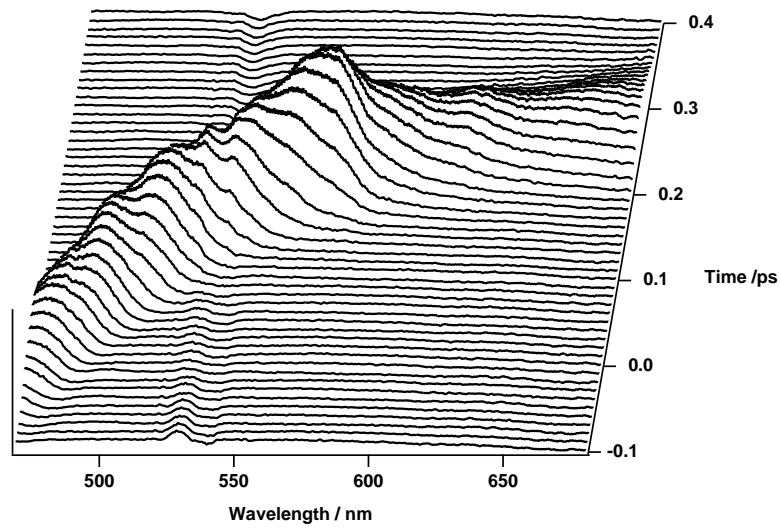
Figure 3.10 — Chirp of the supercontinuum probe measured by the Kerr gating technique. Pump wavelength: 530 nm.
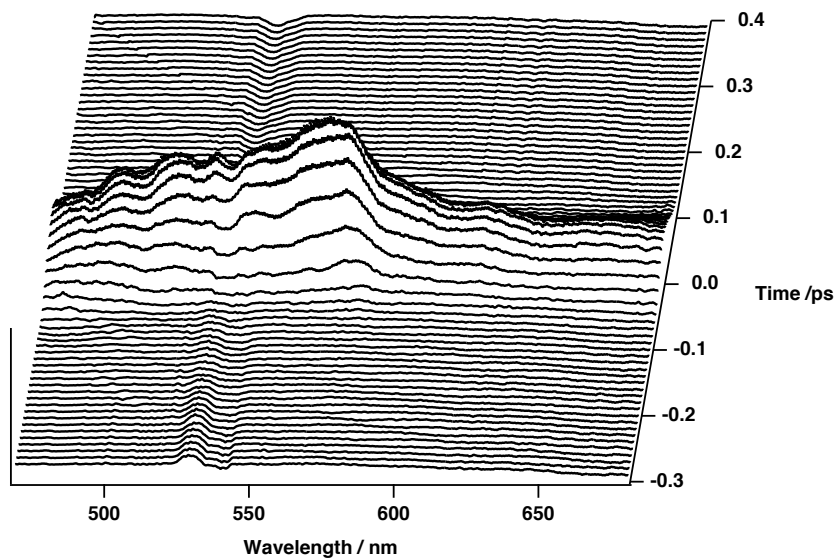
Figure 3.11 — Kerr gating data of figure 3.10 after chirp correction.

3.1.3 Computer procedures

All instruments are controlled by a personal computer through a GPIB PCI card and Labview virtual instruments (National Instruments). The time steps for the translation stages can be equally spaced or follow a logarithmic progression in order to have more points around time zero where fast processes are expected. Data are preanalyzed directly using Labview programs but further analysis is carried out in Matlab (Mathworks) or Igor Pro (Wavemetrics Inc.) software packages.

Transient traces at particular wavelengths are usually fitted with an analytical convolution of a Gaussian instrument response and up to n exponential decays:

$$\Delta A(t) = \sum_{i=0}^{n} \frac{a_i}{2} \exp\left(k_i(\mu - t) + \frac{(k_i\sigma)^2}{2}\right) \left\{1 + \text{erf}\left(\frac{t - (\mu + k_i\sigma^2)}{\sqrt{2}\sigma}\right)\right\}$$
(3.4)

where k_i is the constant rate, a_i the amplitude of decay i, μ the location of the gaussian and σ its width. In our case μ is equal to time zero and σ is related to the full width at half-maximum by:

$$\text{FWHM} = 2\sigma\sqrt{2\ln 2}$$
(3.5)

Hence the fit provides an estimation for the time zero, the cross-correlation time, the amplitudes and the time constants for the exponential decays. The parameters characterizing the instrument response (μ and σ) are usually compared to the bare measurement in the Kerr medium (see page 36).

3.2 Nanosecond Spectrometer

In the case of the nanosecond spectrometer, the experimental scheme is considerably simplified since the sample can be analyzed by continuous light. In this configuration the time resolution is fulfilled by the electronic part of the setup.

The excitation source is provided by a Nd:YAG Q-switched laser (Continuum Powerlite-7030) with a frequency-tripled output (355 nm). The UV beam (FWHM = 7 ns, power = 2.8 W, repetition rate = 30 Hz) is used to pump a broadband optical parametric oscillator (OPO, GWU-Lasertechnik) so as to tune the excitation pulse to the desired wavelength. An OPO is basically an OPA (see previous section) where the nonlinear crystal is enclosed in an

oscillator cavity. This configuration allows for a better conversion efficiency due to the multipass character of the device. The output wavelength (from 410 to 2500 nm) is simply chosen by rotation of the crystal and selection of appropriate cavity mirrors. The pulses are subsequently attenuated by neutral density filters before excitation of the sample with a fluence inferior to 40 μJ/cm^2 per pulse. The sample is kept at a 45° angle with respect to the pump and probe beams.

The sample is probed by continuous light provided by a CW 450W Xe arc lamp. The beam is passed through a first Fabry-Pérot monochromator, focused on the sample and finally driven through a second monochromator before detection.

A fast photomultiplier tube (PMT) is used to convert photons into electrons (Hamamatsu R910). A voltage of 750-900 V is applied to the detector by a Stanford Research Systems PS310 high voltage source. The current resulting from the PMT is measured by a Tektronix DSA 602A digital signal analyzer. The device is triggered by a small fraction of the excitation beam driven into a fast photodiode. Absorbance changes following laser excitation are monitored over the chosen time window and a satisfactory signal-to-noise ratio is obtained by averaging over 1000 shots.

When measuring events faster than 1 μs the time constant of the DSA is no more negligible when it's operated with a 1 MΩ entrance impedance. The impedance is then switched to 50 Ω and a home-built filter/divider is added to separate the difference signal (ΔI) from the background intensity (I) still measured with a high impedance.

This versatile setup makes it possible to measure easily transient absorbance changes in a time domain ranging from about 10 ns to several ms. The stability of the system is good enough to measure transient spectra by accumulation of traces at selected wavelengths.

Further data treatment is done using routine procedures written in Igor Pro's software programming language (Wavemetrics Inc.).
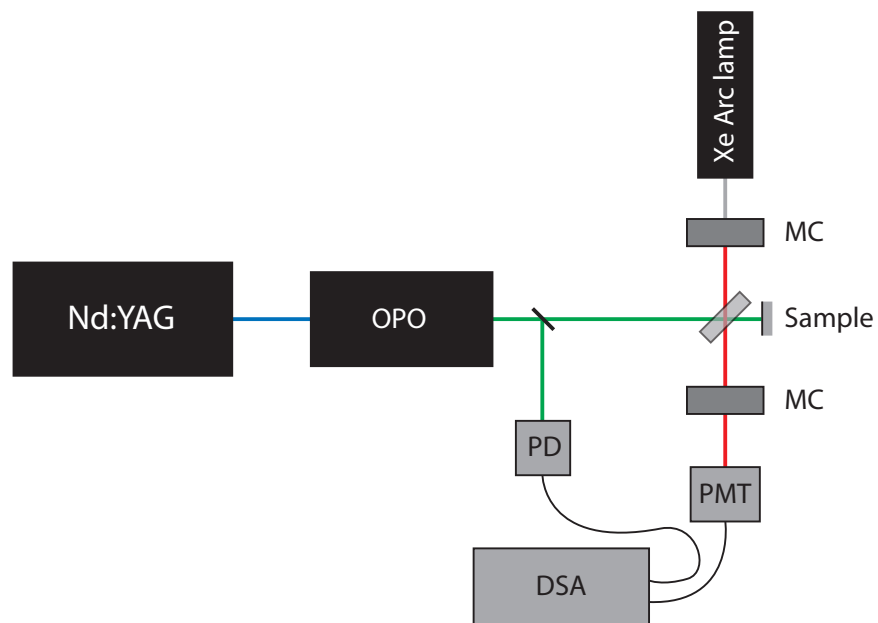
Figure 3.12 — Nanosecond spectrometer. (MC: monochromator, PD: photo-diode, PMT: photomultiplier tube, DSA: digital signal analyzer, OPO: optical parametric oscillator)

3.3   References

1. Pelet, S. *Femtosecond Dynamics of Electron Transfer in the Photosensitization of Wide Band Gap Semiconductors,* Thesis, Ecole Polytechnique Fédérale de Lausanne, 2002.

2. Pelet, S.; Grätzel, M.; Moser, J. E. "Femtosecond dynamics of interfacial and inter-molecular electron transfer at eosin-sensitized metal oxide nanoparticles", *J. Phys. Chem. B* **2003,** *107,* 3215-3224.

3. Riedle, E.; Beutter, M.; Lochbrunner, S.; Piel, J.; Schenkl, S.; Sporlein, S.; Zinth, W. "Generation of 10 to 50 fs pulses tunable through all of the visible and the NIR", *Appl. Phys. B* **2000,** *71,* 457-465.

4. Lochbrunner, S.; Huppmann, P.; Riedle, E. "Crosscorrelation measurements of ultra-short visible pulses: comparison between nonlinear crystals and SiC photdiodes", *Opt. Commun.* **2000,** *184,* 321-328.

Reductive Quenching: an alternative deactivation pathway

Summary

To investigate the influence of ionic liquids containing high iodide concentrations on the charge transfers at dye/semiconductor interfaces, we applied time-resolved spectroscopic techniques to TiO$_2$ nanocrystalline films sensitized by Ru(II) polypyridyl complex dyes. Our experiments show that when $[I^-] >$ 0.3 M reductive quenching of the excited states by iodide competes efficiently with direct injection into the conduction band of the semiconductor. The quantum yield for reductive quenching exceeds 17 % and is found to be dependent upon the sample preparation. From these observations, we conclude that dye aggregates are present in the mesoporous network. The implications of aggregation on the properties of dye-sensitized solar cells are discussed. In the framework of this PhD dissertation the conclusions of this chapter form the basis of the forthcoming interpretation of the kinetic heterogeneity of ultrafast electron injection in dye-sensitized TiO$_2$.

4.1   Introduction

Several electron transfers follow excitation of a dye adsorbed at the surface of nanocrystalline TiO_2 in a dye-sensitized solar cell. After injection, the desired pathway is diffusion of the electron across the semiconductor film to reach the doped tin oxide layer on the glass electrode in order to be used in an external circuit. This diffusion is in competition with back electron transfer from the electron located in the semiconductor to the oxidized dye or to redox species present in the electrolyte. Additionally, electron transfer can also occur from the doped tin oxide layer to the electrolyte. All of these reactions are thermodynamically very favorable and the reason why such high efficiencies are attained in DSCs[a] lies in the kinetic control of these electron transfer processes.

The aim of this PhD thesis is mainly the characterization of the electron injection process. Since this process was reported to occur in the fs/ps time domain and the quantum yields for injection were found to be near unity for thermodynamically allowed reactions, the importance of other pathways has been usually neglected in the discussion. Accidentally, we found that when using high quantities of iodide in the electrolyte, reductive quenching could compete with electron injection. This chapter will deal with the characteristics of this alternative deactivation pathway and its consequences on the electron injection kinetics.

4.1.1   Reaction schemes for a dye-sensitized solar cell

As mentioned above a cascade of electron transfer reactions follow excitation of the dye in a DSC. The complete diagram is depicted in figure 4.1. The direct injection scheme (fig. 4.1(a)) shows the possible reactions upon excitation of the dye sensitizer (1). First, electron injection takes place and relaxation in the semiconductor leads to a delocalized conduction band state or more likely to a localized trapped state (2). This electron can now diffuse through the mesoporous film and be transferred to the fluorine or indium doped tin oxide layer of the conductive glass electrode (3). The unwanted reactions can take place from the TiO_2 or the SnO_2 electrodes. The most relevant to solar cell efficiency is certainly the back reaction to the oxidized dye (4). To avoid this reaction a redox donor from the electrolyte re-reduces the sensitizer with a reaction rate faster than the back transfer (5). Unfortu-

---

[a]DSC = dye-sensitized solar cell

nately the oxidized donor becomes now an acceptor for the electrons located in the nanocrystalline electrode (6) or in the conductive glass electrode (7).

(a) Direct injection pathway   (b) Reductive quenching pathway
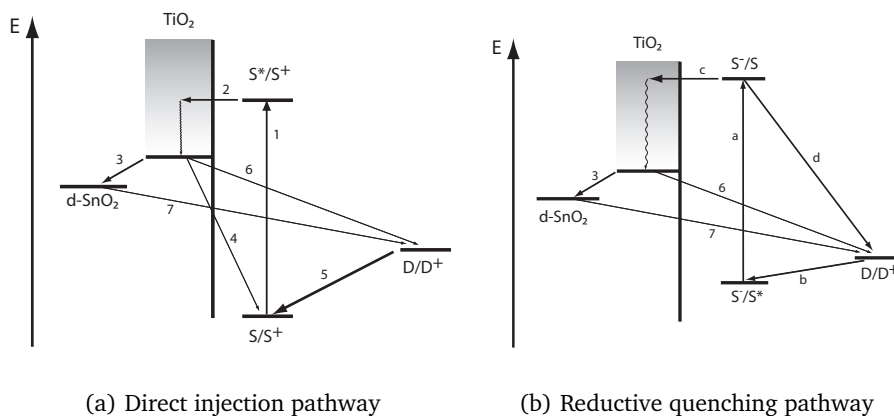
Figure 4.1 — Reaction scheme upon excitation of a sensitizer (S) in a dye-sensitized solar cell in the presence of a redox donor (D). Bold arrows: desired reactions, thin arrows: unwanted reactions (See text).

$$S|SC + h\nu \quad \rightarrow \quad S^*|SC \tag{1}$$
$$S^*|SC \quad \rightarrow \quad S^+|SC + e_{cb}^- \tag{2}$$
$$e_{cb}^- \quad \rightarrow \quad e_{tco}^- \,^{\text{b}} \tag{3}$$

$$e_{cb}^- + S^+|SC \quad \rightarrow \quad S|SC \tag{4}$$
$$S^+|SC + D \quad \rightarrow \quad S|SC + D^+ \tag{5}$$

$$e_{cb}^- + D^+ \quad \rightarrow \quad D \tag{6}$$
$$e_{tco}^- + D^+ \quad \rightarrow \quad D \tag{7}$$
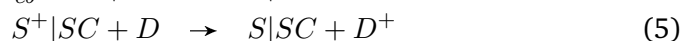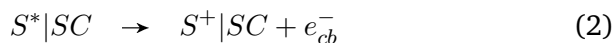
An alternative mechanism will be presented in this section. In this scheme the excited dye (a) is directly reduced by the donor (b). The reduced sensitizer may be able to inject an electron in the conduction band of TiO_2 (c) or recombine with the oxidized donor in the electrolyte (d). After electron injection, the back transfer from the electrodes to the donor are still possible (6 and 7). The chemical equations relevant to the reductive quenching pathway are given by:

---

[b]tco = transparent conductive oxide

$$
\begin{aligned}
S|SC + h\nu &\rightarrow S^*|SC & \text{(a)} \\
S^*|SC + D &\rightarrow S^-|SC + D^+ & \text{(b)} \\
S^-|SC &\rightarrow S|SC + e_{cb}^- & \text{(c)} \\
S^-|SC + D^+ &\rightarrow S|SC + D & \text{(d)}
\end{aligned}
$$
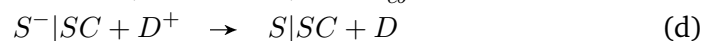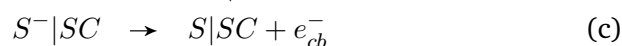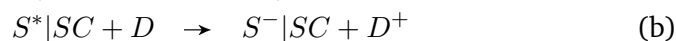
4.1.2   Ionic liquids

The reductive quenching pathway introduced above has been observed only when iodide, used as a redox donor, was present in high concentrations. This was made possible by the use of ionic liquids as hosts for the redox species. Ionic liquids (formerly also called molten salts) are, as their name indicate, liquids containing only ionic species. Most of them are obtained at high temperature (hence the "molten salt" appellation) but exceptionally some compounds are found in the liquid phase at room temperature. These RTILs[c] have attracted much attention in the last decade because of their remarkable properties. These include negligible vapor pressure, high electrical conductivity, chemical inertia, polarity and a large electrochemical window. They are now widely used in electrochemical applications (batteries, DSCs) but the absence of evaporation in conjunction with their tunable solvent action has promoted them as candidates to replace organic solvents in large-scale chemical synthesis.[d][1]

The amazing properties of ionic liquids are imputed to a special combination of short- and long-range interactions. It seems that the coulombic forces experienced by the ions centers are strong enough to avoid evaporation, while the short-range Van der Waals interactions are maintained weak so as to facilitate local rearrangements preventing the formation of a solid phase.[2] Most of the known RTILs make use of large cations with important charge delocalization. These include the 1,3-dialkylimidazolium, pyridinium or tetralkylammonium cations (figure 4.2). The less viscous liquids are obtained also with large delocalized anions (like the successful imide ion[e]), but use of smaller ions like I$^-$ leads to satisfying results.[3,4]

---

[c]RTIL = room-temperature ionic liquid
[d]This application is a major issue in the "green chemistry" approach
[e]$(CF_3SO_2)_2N^-$

1,3-dialkylimidazolium   N-alkylpyridinium   tetraalkylammonium

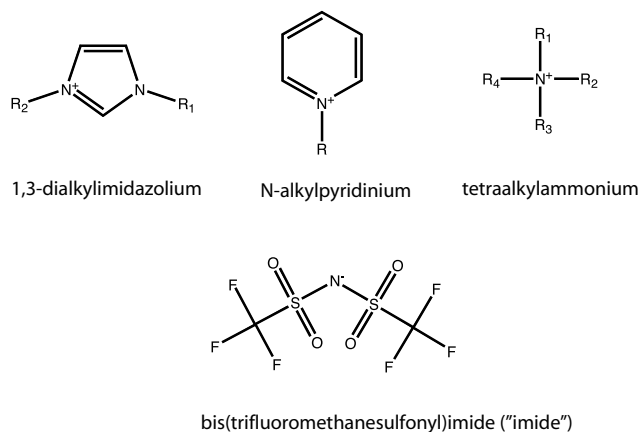bis(trifluoromethanesulfonyl)imide ("imide")

Figure 4.2 — Ions commonly used in room-temperature ionic liquids.

4.1.3 Literature review

As mentioned above, to achieve high effiencies in DSCs, the kinetic competition between desired and unwanted reaction has to be determinant since most of the reactions have a significant driving force. For this reason the kinetics of the different processes shown in figure 4.1 have been widely studied and reviewed several times.[5,6,7] The rate constants differ notably when the combination of dye, semiconductor and electrolyte is modified. Therefore we will focus on systems featuring N3 and derivatives (N719, Z907) (see figure 4.3) anchored on TiO_2 in the presence of the I^-/I_3^- redox couple.

The electron injection rate has been reported for N3 and N719 to be biphasic with a fast sub-100 fs part followed by a smaller slow component (1-100 ps). Numerous studies have been published on the subject and a detailed analysis of these reports is given in the next chapter. However we can already mention that the injection yields have been reported as being near unity for this particular reaction suggesting than no other reaction competes with this process.[8] The back electron transfer reaction has also been largely studied and was found to be slower by several orders of magnitude.[5] The kinetics were found to be mono- or multiexponential, and as strongly dependent upon excitation light intensity. The minimal recombination rates are observed when the average number of electrons injected by nanoparticle was less than one.[9] For N3-derivatives the lifetime of the oxidized dye is found between 0.2 and 1 ms[10,11] Two main reasons are invoked to explain such

(a) N3

(b) N719

(c) Z907
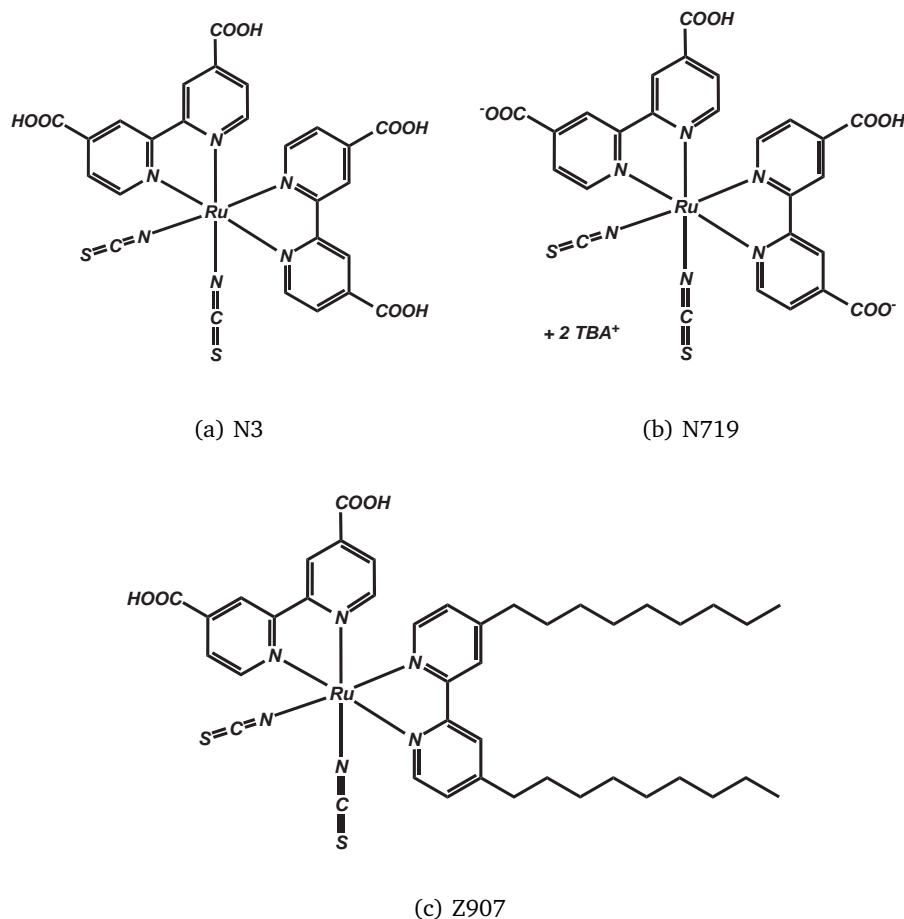
Figure 4.3 — N3 dye sensitizer and derivatives. (TBA$^+$: tetrabutylammonium)

a difference with the forward electron transfer: (a) the high exoergicity of the back transfer make the system lie in the inverted Marcus region and (b) the dynamics of trapping/detrapping of the electrons in the semiconductor control the overall reaction.

Electron transport in nanocrystalline films is also a major issue and is still under debate at the moment. In general the transport is one order of magnitude faster than recombination. Hence, the charge-collection efficiency is usually close to unity.[12] To prevent back electron transfer to the oxidized dye, a redox mediator is added to the electrolyte. Formally, it is oxidized at the working electrode (TiO$_2$) and regenerated at the counter electrode. It acts as an electron shuttle between the two sides of the cell. The most efficient redox couple has so far been the I$^-$/I$_3^-$ system but alternative couples like cobalt complexes[13] or solvent-free SeCN$^-$-based ionic liquids[14] yield

honorable efficiencies. The currently admitted reaction scheme for dye regeneration by the iodide/triiodide couple is described below[15,16]:

$$S^+|SC + 2I^- \quad \rightarrow \quad S|SC + I_2^{\cdot-} \tag{4.1}$$
$$2I_2^{\cdot-} \quad \rightarrow \quad I_2 + 2I^- \tag{4.2}$$
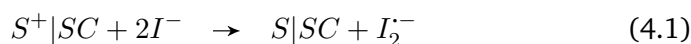
The time needed to regenerate half of the concentration of the dye cation is reduced to $t_{1/2} < 200$ ns when 0.5 M of LiI is added to the electrolyte. The kinetics are strongly dependent upon the concentration of iodide but also on the nature of the counter cation (in this case Li^+). Formation of (I^-,I^-) ion pairs at the surface of TiO_2 was suggested to allow the energetically favorable and faster mechanism involving oxidation of I^- to $I_2^{\cdot-}$ radical to take place.[16] Recombination of the injected electron with the redox couple is also possible. The exact mechanism for this reaction is still under debate. Two schemes have been proposed. In the first one, the electron reduces iodine generated by spontaneous dismutation of I_3^-, and in the second case it reacts with the transient $I_2^{\cdot-}$ ion radical.[12] For some unclear reasons this recombination is exceptionally slow. This is a key figure in the success of this redox couple and the performances of cells based on such systems are so far unequalled.

4.2   Experimental part

4.2.1   Sample preparation

The 8 μm-thick nanocrystalline TiO_2 films were prepared on glass substrates using a previously published procedure.[17,18] Briefly, the colloid paste was spread on a microscope slide by the "doctor blading" technique and, after evaporation of the solvent, placed in a heat gun at 450° for 15 minutes in order to burn the polymer and sinter the nanoparticles. Typically, films prepared by this technique yielded mesoporous interconnected networks consisting of 20 nm-diameter particles with an average rugosity factor of 800 (100/μm).

Dry nanocrystalline films were modified by adsorption of N719[f][19] or the amphiphilic derivative Z907[g][20] from CH_3CN/t-BuOH 1:1 solutions (see figure 4.3). The soaking times and the mother solution concentrations have been varied and will be presented further.

---

[f]$(Bu_4N)_2[Ru^{II}(dcbpyH)_2(NCS)_2]$ (where dcbpy= 4,4'-dicarboxy-2,2'-bipyridyl)
[g]$[Ru^{II}(H_2dcbpy)(dnbpy)(NCS)_2]$ (where dnbpy=4,4'-dinonyl-2,2'-bipyridyl)

A drop of the electrolyte was deposited on the film whereafter it was immediately covered with a thin glass cover slip. The compositions of the different ionic liquids used in this study are given in table 4.1. Mixtures of PMII with MPN, EMITFSI or EMITCM were prepared to modify the concentration of iodide contained in the electrolyte. Films conserved in ionic liquids and in the dark didn't show any degradation for weeks confirming the excellent stability of these assemblies.[20]

The concentration of iodide in pure PMII was calculated from the measured density ($d^{21.5°C}$ (PMII) = 1.531 g/cm^3, MW(PMII) = 252.1 g/mol).

Name	Cation	Anion	Solvent	[I$^-$] / M	Reference
PMII	PMIm^a	I$^-$	-	6.1	MacFarlane et al.[21]
EMITFSI	EMIm^b	imide^c	-	0	Bonhôte et al.[3]
EMITCM	EMIm	TCM^d	-	0	Wang et al.[22]

^{a}1,3-propylmethylimidazolium
^{b}1,3-ethylmethylimidazolium
^{c}bis(trifluoromethanesulfonyl)amide
^{d}tricyanomethanide

Table 4.1 — Compositions of ionic liquids.

4.2.2 Nanosecond spectrometer

Transient absorption measurements were carried out in the experimental setup described in the previous chapter (section 3.2) The excitation laser beam was tuned by the OPO at a wavelength of 540 nm and the intensity reduced to 0.4-1.2 mJ/pulse with neutral density filters. The detection light provided by the Xenon lamp is tuned manually at the indicated wavelengths.

4.2.3 Femtosecond spectrometer

The femtosecond setup was used in the two-color pump-probe configuration. The pump beam was tuned at 530 nm in the first NOPA and the intensity was reduced to < 1 μJ/pulse before the sample. The probe NOPA was used in the NOPA-plus configuration (see 3.1). The first stage was optimized to generate pulses centered at 1100 nm. This infrared beam was then filtered (LL1000, Corion) to remove the shorter wavelength from the

first WLC and focused in a sapphire plate to generate a second continuum. This broadband pulse, now centered around 1100 nm, is much more stable in the region between 800 and 900 nm. The second stage of the NOPA was tuned in order to generate probe pulses at 860 nm. The intensity was reduced to < 0.3 μJ/pulse before hitting the sample. The pump beam proceeds through the 700-ps translation stage and both beams are focused on the sample with one single large size ($\emptyset = 76$ mm) off-axis parabolic mirror. The diameter of the pump laser spot is ~ 400 μm and the sample is constantly rotated to avoid degradation of the dye caused by the heating of the nanocrystalline film.

4.3 Results and Discussion

4.3.1 Transient absorption spectra

N719   The transient spectra of N719- and Z907-sensitized TiO_2 nanocrystalline films in the PMII electrolyte were measured by nanosecond transient absorption. The result for N719 is showed in figure 4.4. Strikingly this result shows significant differences in comparison with the spectrum obtained with the same dye on titania but with a standard electrolyte (fig. 4.5).[16]
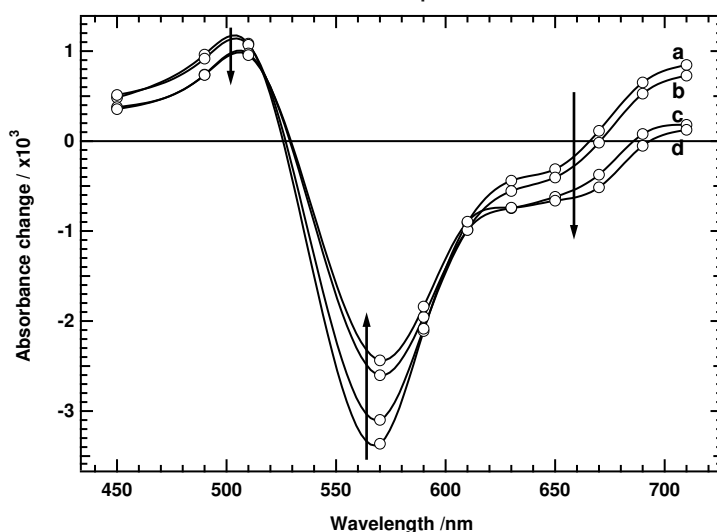
Figure 4.4 — Transient spectrum of N719 on TiO_2 in PMII. Excitation wavelength: 540 nm. Time delay: a) 500 ns; b) $1\mu s$; c) $5\mu s$; d) $10\mu s$.
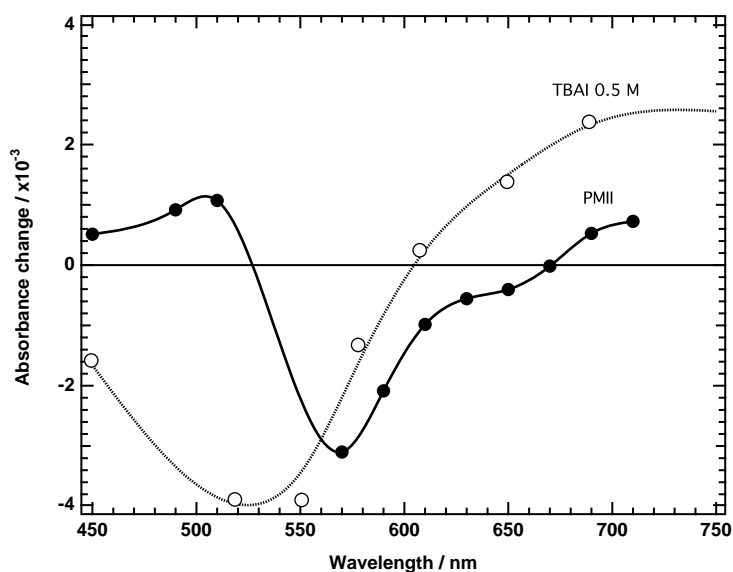
Figure 4.5 — Transient spectra of N719-sensitized TiO_2 after 500 ns in pure PMII (●) and after 200 ns with $Bu_4N^+I^-$ 0.5 M in propylene carbonate (○). [16]

The latter spectrum was unambiguously interpreted as the sum of the bleaching of the fundamental dye, showing a maximum at 530 nm, and the contribution from the oxidized dye. This assumption is consolidated by the difference absorption spectrum calculated from published data obtained for the fundamental and oxidized dyes in solution (figure 4.6). [23,24] Actually, the spectrum for the oxidized dye was obtained with the analogous uncarboxylated dye ($Ru^{II}(bpy)_2NCS_2$) by chemical oxidation with Ce(IV) (10^{-2} M in CH_3CN). This dye was chosen because it is less prone to degradation by oxidation of the thiocyanate ligands, but except for a 20 nm blue shift of the spectrum, its properties are very similar to N719. Therefore, if the spectra have been correctly normalized with respect to the extinction coefficient we can estimate that the isosbestic point has to be near 600 nm. This is in agreement with data obtained for a standard solvent-based electrolyte.

Clearly the situation is different in the presence of PMII. The isosbestic point is shifted for more than 50 nm towards lower energies and a positive absorbance change is observed near 510 nm. Obviously a new species is formed in addition to the oxidized dye. The kinetics corresponding to this transient spectrum are showed at 630 nm in figure 4.7. Interestingly, a small positive peak is observed at very short times. This feature disappears quickly ($t_{1/2}$ = 75 ns) and makes place to a long-lived negative signal which eventually disappears with a half-time of 0.3 ms.
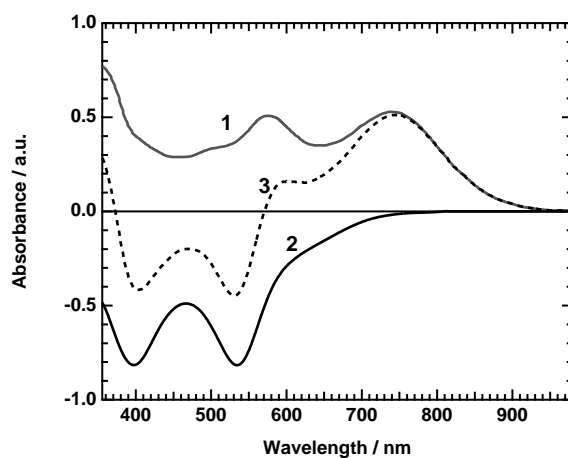
Figure 4.6 — Difference spectrum of N719 (3) calculated from the spectrum of the first oxidation product of the analogous $Ru^{II}(bpy)_2NCS_2$ dye by Ce(IV) in acetonitrile (1) and N719 in ethanolic solution (2). Adapted from Moser et al.[24]

Z907 The spectral properties of Z907 are similar to N719. The benefits of this dye for DSC applications lies in the hydrophobic barrier induced by the long alkyl-chains preventing water and triiodide to reach the surface of TiO_2. This has an influence on the photovoltage because of the reduced concentration of protons adsorbed and also on the photocurrent since dark current (electrons recombining with triiodide) is minimized.[25] Therefore the transient spectrum should be similar to the one obtained with N719 with conventional electrolytes. Again the measured difference spectrum (fig. 4.8) shows singular properties. The positive contribution observed above 600 nm just after the laser pulse disappears and a long-lived bleach is observed. The positive peak observed for N719 at 510 nm is also present but below 490 nm the signal is found to be negative. This spectrum is only understandable if another species with a long (ms) lifetime appears . The fast decay observed at 630 nm is about 100 times slower than for N719.

4.3.2 Identity of the new species

The transient spectra measured for N719- and Z907-sensitized TiO_2 in PMII can not be explained if only the bleaching of the fundamental dye and the absorption by the dye cation, formed upon electron injection, are present. There must be at least one other species present. From the long-lived bleach around 600-650 nm we learn that the dye ground state is not completely regenerated, indicating that the new species is a derived form of the original ruthenium complex. The dye is finally regenerated showing that we can not
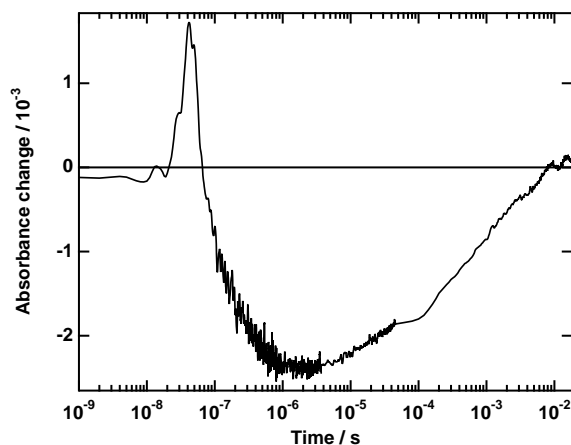
Figure 4.7 — Single kinetic trace at 630 nm for N719-sensitized TiO_2 in PMII.

impute our observation to degradation of the dye. Radical species are not expected to live for such a long time and the excited state formed upon excitation has a lifetime shorter than 50 ns.[19,25] Therefore the only species that could be in agreement with our observations is the reduced dye formed by reductive quenching with iodide.

Unfortunately, no spectral data is available for this compound. We tried to generate the reduced dye with different chemical reductants (tripheny-lamine, EDTA (acid), LiI, Na_2O_4) but the reaction was unsuccessful or the yield too low to show observable modifications. The second approach was to produce the dye anion electrochemically. The experiment was performed in a transparent three-electrode cell. The dye was adsorbed on a TiO_2 layer deposited on a transparent conductive electrode (TCO, $F:SnO_2$) or directly on the TCO, and we used $TBA^+BF_4^-$ 0.1 M in acetronitrile as an electrolyte. The cell was carefully degassed by at least 5 freeze-thaw-pump cycles to remove oxygen that is known to be reduced to peroxide at negative poten-tials.[26,27] When the applied potential is increased towards negative values the spectrum of N719 is red-shifted about 20 nm (fig. 4.9(a)). Below -1.8 V the dye is desorbed. If we wait for some minutes at -1.6 V, the dye is ir-reversibly degraded. The spectrum with the 20-nm shift corresponds to the deprotonated N719 as was observed by others.[19,28] The dye anion formed in our transient absorption experiment is expected to have an excess electron in the LUMO[h] of the initial dye. Calculations and spectroscopic evidences show that this is a π^* orbital located on the dcbpy ligand.[18,29,30,31] Because of the problem of deprotonation for N719 or N3, the ligand-based reduc-

---

[h]LUMO = lowest unoccupied molecular orbital
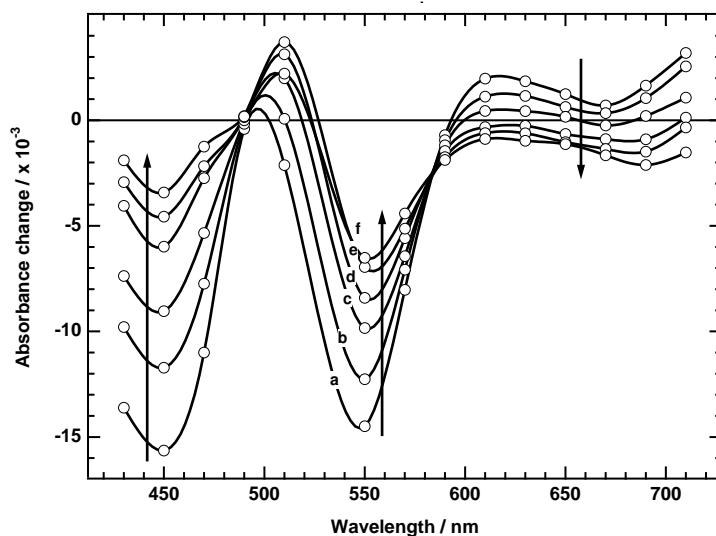
Figure 4.8 — Transient spectra of Z907-sensitized TiO_2 in pure PMII. Exc: 530 nm. Time delay: a) 500ns; b) 1 μs; c) 2 μs; d) 5 μs; e) 10 μs; f) 40 μs.

tion has never been characterized experimentally. However the analogous dye containing the esterified ligand $Ru^{II}(Et_2\text{-}dcbpy)_2NCS_2$ has been studied by Wolfbauer and co-workers.[32] Upon electrochemical reduction, the MLCT bands disappeared whilst new intraligand bands grew in the visible region (figure 4.9(b)). In the case of the dye anion of N719 and Z907, we believe that the spectrum will also be dominated by ligand-based transitions. The band around 510 nm appearing in the transient spectra can therefore be reasonably attributed to the reduced sensitizer.

Reductive quenching of ruthenium bipyridyl complexes at metal oxide interfaces has been observed earlier by several groups.[33,34,35,36] Kamat and coworkers observed reductive quenching of $Ru^{II}(bpy)_2(bpy\text{-}COOH)$ by I^- on SiO_2. More than 50 % of the excited state was quenched when concentrations of iodide as low as 0.4 M were used.[34] Interestingly, they found later that oxidative quenching by I_3^- was also possible.[37] Although no additional I_2 is intentionally added to our ionic liquid, the yellowish colour of PMII shows that some iodine is present and that triiodide may be formed. However this should be a minor contribution and we believe that oxidative quenching is negligible in our experiment. Meyer et al. studied the quenching of ruthenium complexes containing the deeb[i] ligand on TiO_2. In the presence of high concentrations of phenothiazine (PTZ) electron donor, more than 99 % of the excited state was reduced with a bimolecular rate

---

[i]deeb = diethylesterbipyridyl
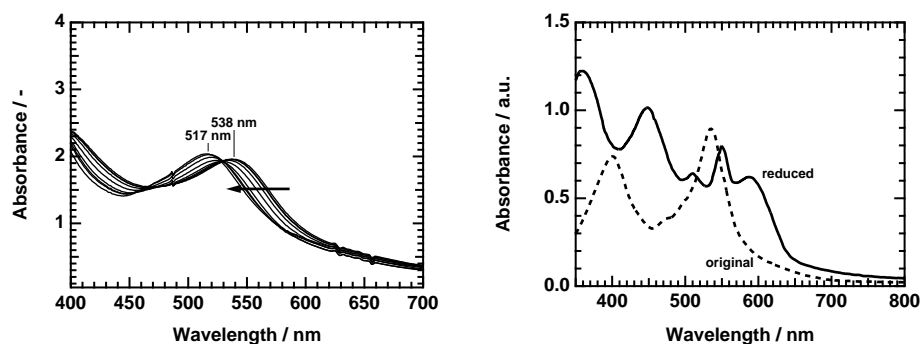
(a) UV-Vis spectra of N719 on TiO$_2$ under negative bias. Applied potentials: 0.0 to -1.6 V vs. Ag/AgCl (steps of 0.2 V).

(b) Ligand-based reduction of Ru^{II}(Et$_2$-dcbpy)$_2$NCS$_2$. Adapted form Wolfbauer et al.[32]

Figure 4.9 — Electrochemical reduction of N719 and Ru^{II}(Et$_2$-dcbpy)$_2$NCS$_2$.

constant up to $8\cdot10^{-9}$ M^{-1}s^{-1}. In that particular case, the dye did not inject electrons directly into TiO$_2$ because the energy of the excited state is lower than the semiconductor's conduction band edge. However in the presence of PTZ, efficient electron injection was observed because of the 300-400 mV energy difference for the dye anion.[33,35] Recently this group showed evidence for the static quenching of the MLCT excited state of the same dye by iodide. The quantum efficiency for this process was 25 % and the reaction was completed within the instrument response time (10 ns). Interestingly, a Stern-Volmer analysis showed the existence of a dye/iodide adduct with an equilibrium constant of K$_{SV}$ = 40 000 M^{-1}.[36] The existence of an interaction between the sulfur atom of the thiocyanate ligands and I$^-$ has been suggested earlier to explain the efficiency of the reduction of the N3$^+$ dye cation in DSCs.[16,38] When adsorbed on the surface of TiO$_2$, the SCN ligands point in the direction of the electrolyte which may facilitate the interaction. Walter et al. suggested on the contrary that an adduct is formed by interaction with the bypyridyl ligands.[39] This observation is based on unequivocal X-ray data obtained for chemically inert cobalt surrogates of the N3$^+$ cation.

In summary, based on spectroscopic evidences and comparison with previous studies we suggest that the ligand-based reduction of the MLCT excited state of N3 derivatives occurs when pure PMII is used as an electrolyte. Despite numerous experimental investigations, the presence of the dye anion has never been reported for N3-sensitized TiO$_2$ nanocrystalline films in the presence of iodide. We think that this is due to the high electron transfer rate to the semiconductor conduction band preventing this reaction to occur and also to the much lower iodide concentration used in conventional

electrolytes ($\sim$ 0.6 M vs. 6.1 M for PMII). In the next sections we will characterize the kinetics and the conditions controlling the reductive quenching and attempt to understand how it can compete with a process as fast as electron injection.

4.3.3 Kinetics and quantum yields for the reductive quenching mechanism

Influence of iodide concentration

As we stated above, the efficiency of the reductive quenching pathway is made possible by the high concentration of iodide present in the ionic liquid. In order to confirm this assumption we prepared a series of binary mixtures of PMII with EMITCM. Increasing the iodide concentration is also expected to cause an acceleration of the regeneration of the dye's oxidized state (S^+). The results are presented in figure 4.10(a). As expected the regeneration rate is accelerated by the increase of the iodide concentration. But more remarkable is the increase of the bleaching remaining at longer times. The kinetics for excited dye reduction are not accessible from these measurements. As it competes with electron injection, we expect this reaction to occur on a sub-ns timescale. If we focus on the absorbance change just after the pump laser pulse in figure 4.10(a) we see that the maximum value decreases with the iodide concentration in agreement with a greater yield for reductive quenching. However it should be noted that some regeneration can also happen during the laser pulse, thus reducing the initial value.

Series of binary mixtures prepared with EMITCM or EMITFSI showed exactly the same behavior. We believe that the observation of reductive quenching is independent of the peculiar properties of ionic liquid and is to be imputed only to the high concentration of iodide. Indeed, using MPN-based electrolytes with concentration of PMII ranging from 0.3 to 2.8 M also revealed the presence of a similar long-lived bleach (fig 4.10(b)).

Since the extinction coefficients of the excited (S^*), oxidized (S^+) and reduced (S^-) states of N719 and Z907 are not measurable independently it is very difficult to get a good estimate of the fraction of excited dyes that undergo reductive quenching instead of direct electron injection. Nevertheless, based on transient absorption data we were able to quantify, at least in a relative fashion this yield. We used the long-lived bleach at 630 nm to evaluate the fraction of excited dyes that are reduced by I^-. We assume
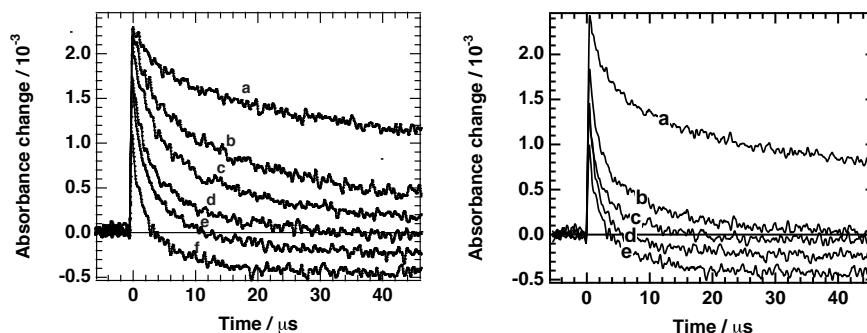
(a) Binary mixtures of PMII and EMITCM (iodide conc: 0-6.1 M). PMII volume percentage (a) 0% ; (b) 5%; (c) 11%; (d) 23%; (e) 45%; (f) 100%.

(b) PMII in MPN, iodide concentration: (a) 0 M ; (b) 0.8 M; (c) 1.5 M; (d) 2.8 M; (e) 6.1 M.

Figure 4.10 — Transient absorbance at 630 nm of Z907-sensitized TiO_2 in the presence of various concentrations of iodide.

here that the absorption of the reduced dye at this wavelength is negligible with respect to the dye in its ground state. If some ligand-based transitions are present at this wavelength it will lessen the absorption change, and our estimations will therefore return lower limits. The maximum value η_{max} is measured in pure PMII. The quantities for lower iodide concentrations are given as fraction of η_{max} in table 4.2. Further estimations based on the approximation of the extinction coefficients by comparisons with similar dyes give a maximum yield of $\eta_{max} \cong 25$ %.[40]

In dye-sensitized solar cells, the iodide concentration usually does not exceed 1 M. As shown in table 4.2, no reductive quenching was measured for Z907 at such concentrations and low yields were observed for N719. This illustrates why this phenomenon has not been recognized earlier in spite of the high number of studies on this topic. Interestingly, the threshold concentration for Z907 is much higher than for N719. These dyes have the same electrochemical and photophysical properties but differ by the long alkyl chains on the non-anchored ligand. Therefore the difference observed here is probably due to steric effects or dissimilar arrangements on the semiconductor's surface. It seems that the nature of the solvent (organic solvent or ionic liquid) has no influence on the production of dye anions. The effect is purely a consequence of the iodide concentration.

[I$^-$] / M	Solvent	N719	Z907
		$\frac{\eta}{\eta_{max}}$ / -	
6.1	-	1	1
2.8	MPN	0.65	0.62
1.5	MPN	0.53	0.29
0.8	MPN	0.38	-
0.3	MPN	0.12	-
2.8	EMITFSI	0.81	0.60
1.4	EMITFSI	0.51	0.26
0.7	EMITFSI	0.32	-
0.3	EMITFSI	-	-
0.0	EMITFSI	-	-

Table 4.2 — Fractions of reductive quenching for various iodide concentrations with respect to pure PMII.

Dye adsorption effects

Usually dye adsorption is achieved by soaking nanocrystalline films overnight in 0.1-0.5 mM dye solutions. We found that the reductive quenching yield was influenced by the adsorption time. Starting with a standard 0.5 mM solution of N719, the adsorption time was varied from 40 min to 48 hours (fig. 4.11(a)). Clearly, the reductive quenching mechanism is favored when the samples are immersed for longer periods. The quenching becomes even unmeasurable when the adsorption time is reduced to 40 minutes.

An experiment complementary to the variation of the soaking time is the modification of the concentration of the dye solutions. This was achieved by using dilutions from the standard solution (0.5 mM), and an additional highly concentrated solution in DMF[j] (9 mM). The dipping time (1 hour) was the same for all samples and chosen in order to maximize the differences. Indeed, appreciable reductive quenching was observed for the film dyed from the 9 mM solution (fig. 4.11(b)) in spite of the relatively short immersion time.

In order to avoid degradation of the dyes, the measurements were generally carried out shortly after sample preparation. We found that storing the samples in the dark for several hours had an influence on the amplitude of the dye reduction. In figure 4.12 this effect is shown for Z907 after only

---

[j]DMF=dimethylformamide
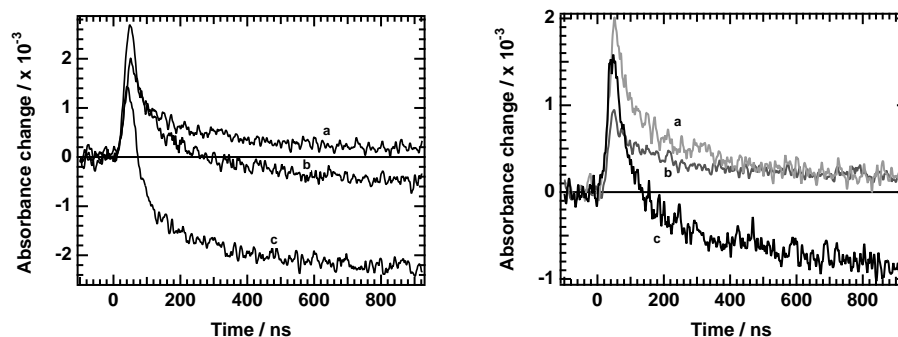
(a) Absorbance change at 630 nm for films dyed for a) 40 min; b) 2.3 hours; c) 2 days.

(b) Absorbance change at 630 nm for films dyed from a) 0.005 mM ; b) 0.05 mM; c) 0.9 mM. dye solutions.

Figure 4.11 — Effects of the dye adsorption for N719-sensitized TiO_2 in pure PMII.

24 hours. The decrease of the yield for reductive quenching was observed for both Z907 and N719 dyes but was difficult to reproduce quantitatively.
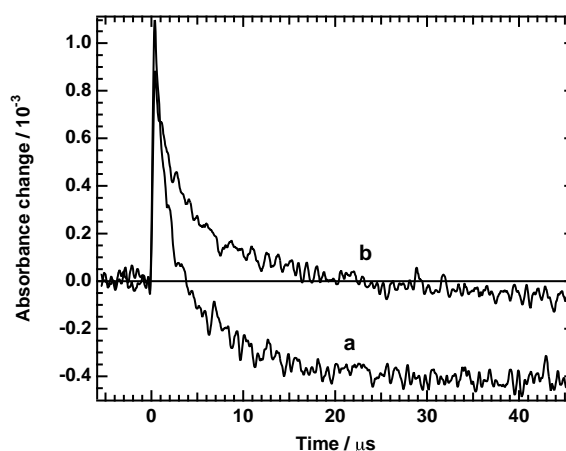
Figure 4.12 — Transient absorption at 630 nm of Z907-sensitized TiO_2 in pure PMII. a) fresh sample; b) aged sample (24 hours).

Kinetics of dye reduction

The nanosecond transient absorption experiments revealed the presence of the dye anion and made it possible to quantify the relative extent of excited dyes that undergo reductive quenching in the presence of a high iodide concentration. Since reductive quenching of the excited state is in competition

with the injection process we performed pump-probe transient absorption measurements in the picosecond time domain. As mentioned previously, various time constants have been reported for electron injection into TiO_2 but none exceeds 100 ps.

The excitation wavelength was set at 530 nm near the maximum absorption of the dyes in their ground states and the samples were probed at 860 nm. This choice is motivated by the observation of several groups showing that, at this wavelength, the contribution of the excited state absorbance is minimized with respect to the oxidized dye absorbance.[41,42] In addition, we do not expect a significant contribution from the dye anion at this wavelength because the LMCT bands responsible for strong absorption for S^+ and S^* are not present in S^-. Films were dyed in 0.5 mM N719 solutions for 1, 2 and 48 hours and an additional sample was prepared from a 0.3 mM solution of N3 (Solaronix, Aubonne) in ethanol (soaking time: 24 h).

Trace	Dye	Soak. time	Time constants and amplitudes
		hours	*ps*
a	N719	48	5.6 (9.1 %), 33.1 (7.8 %)
b	N3	24	2.9 ps (8.8 %)
c	N719	2	8.5 (9.0 %)
d	N719	1	8.4 (6.1 %)

Table 4.3 — Fitting parameters for the transient absorption traces shown in figure 4.13.

All samples showed a fast rise within the pulse duration followed by a slower mono- or biexponential decay (figure 4.13). The traces were fitted with an analytical convolution of a Gaussian instrument response with exponential decays (table 4.3).

Both the excited and the oxidized states absorb at 860 nm. Previous studies showed that a slow component (1-100 ps) for electron injection resulted in a further rise confirming that the excited state has a lower extinction coefficient at this wavelength (for a review see Kallioinen et al.[43]). In our experiment instead of this rise we observed a significant decay. In the absence of iodide such decays have been previously observed and were found to be dependent upon the intensity of the excitation laser pulse.[43] However the decays measured in the presence of PMII are still present when the excitation intensity is reduced. We attribute this decay to the disappearance of the remaining excited dyes by the reductive quenching pathway. The time constants and the relative amplitudes are consistent with the fraction of dyes injecting slowly in the biphasic injection scheme. Therefore we conclude that direct excited dye reduction by iodide competes efficiently with
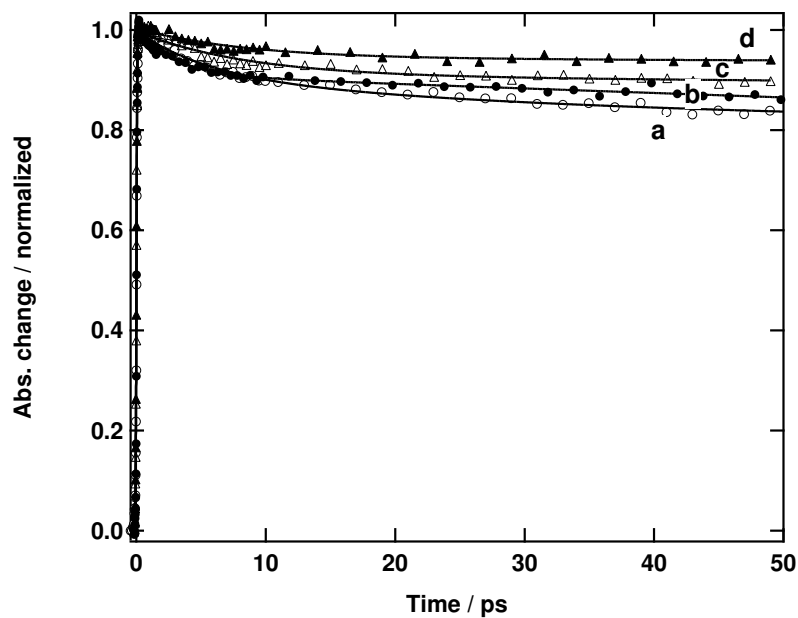
(a) Full timescale.
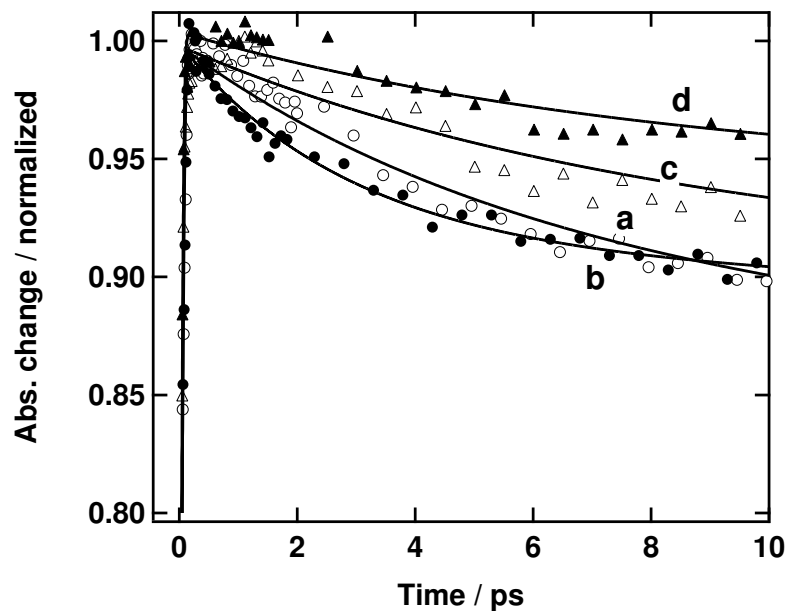
(b) Detail at short times.

Figure 4.13 — Transient absorption traces at 860 nm of dye-sensitized TiO_2 8 μm-thick films. Excitation: 530 nm. Dyes and adsorption time: a) N3 , 24 h; b) N719, 48 h; c) N719, 2h; d) N719, 1h.

the slower phase reported for electron injection. The amplitudes given in table 4.3 are calculated from the amplitudes of the fitted exponential decay divided by the total absorbance change immediately after the excitation pulse. As stated above, this ΔAbs_{max} is a sum of the contribution from both the excited and the oxidized molecules. Since the extinction coefficient of the excited state ($\epsilon_{860}(S^*)$) is smaller than the one of the oxidized dye ($\epsilon_{860}(S^+)$) the amplitudes indicated are slightly smaller than the quantum yields for reductive quenching (see figure 4.14). In brief, this means that the fraction of excited dyes that are reduced is higher than 17 % (N719, 48 hours) in agreement with the estimation obtained from the nanosecond experiments.
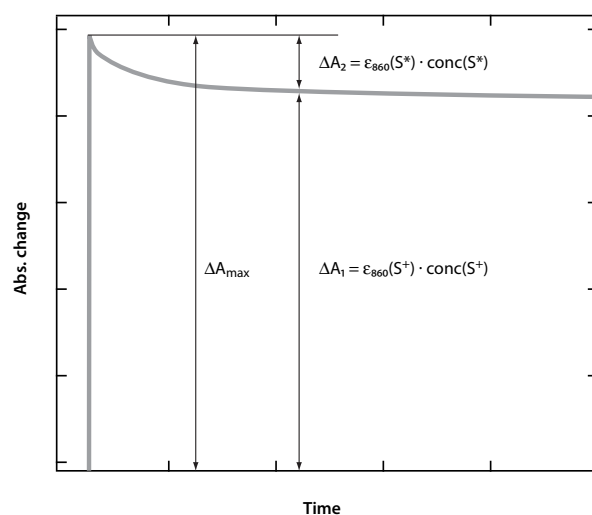
Figure 4.14 — Interpretation of the contributions to the traces shown in figure 4.13. ϵ_{860} is the extinction coefficient at 860 nm of species S^i ($i = *, +$).

As expected from the nanosecond transient absorption measurements, increasing soaking times for N719 lead to higher RQ[k] amplitudes (traces a,c and d). It seems also that the kinetics become more heterogeneous for very long soaking times (trace a). The shape of the trace obtained for N3 is slightly different (trace b). The total amplitude is consistent with the values measured for N719 but the decay constant is reduced to 2.9 ps.

---

[k]RQ = reductive quenching

4.3.4   Discussion - dye aggregation

Evidence for efficient reductive quenching of N3-derivatives excited states at the surface of TiO_2 in the presence of high concentration of iodide is obtained from our time-resolved spectroscopic experiments. The excited state reacts with iodide on a sub-50 ps timescale. Wang et al. measured the apparent diffusion coefficient of iodide in PMII-based electrolytes from steady-state voltammetry.[44] The estimated value ($D_{app} = 3 \cdot 10^{-7}$ cm^2/s) shows that in 50 ps the ionic liquid can be considered as frozen. Therefore some ion pairing must be present before excitation to enable the reaction. The recent observation of a dye/iodide adduct by Clark et al. and the X-ray experiments of Walter and co-workers showing interaction of iodide with a bipyridyl ligand of a N3 surrogate are consistent with our observations (see section 4.3.2).[36,39]

Reductive quenching of ruthenium polypyridyl complexes yield the radical ion $I_2^{\cdot-}$ as a long-lived product.[34,36] The generation of $I_2^{\cdot-}$ is a two step process involving the presence of two I^- ions, $2I^- \rightarrow I_2^{\cdot-} + e^-$. This mechanism is thermodynamically favored with respect to oxidation of I^- leading to the iodine atom ($\phi^0(I^\cdot/I^-) = 1.3$ V and $\phi^0(I_2^{\cdot-}/2I^-) = 1.0$ V vs. SHE).[36,45] Although we could not directly observe the generation of $I_2^{\cdot-}$ in our experiment we believe that this pathway is preferred. Our picosecond data refer to the disappearance of the excited state, thus it is not clear if the generation of $I_2^{\cdot-}$ happens on the same timescale. This would require the presence of a second iodide ion in contact with the reduced dye since ion diffusion is ruled out. The high concentration of iodide could allow this, but the presence of (I^-, I^-) pairs at the surface of TiO_2 provides probably a better explanation. These ion pairs have been previously suggested by Pelet et al. to rationalize the effect of adsorption of potential-determining cations on the semiconductor.[16] Interestingly, we could neither observe reductive quenching on other metal oxide surfaces, such as Al_2O_3, ZrO_2 and Nb_2O_5, nor in solution when using chemical reductants. This indicates that the reaction is specific to TiO_2, in agreement with the previous remarks concerning the presence of ion pairs.

Nevertheless, time constants of 3-30 ps are still slow with respect to the electron injection processes at dye/semiconductor interfaces for sensitizers showing high electronic coupling with the continuum of acceptor states in their excited states. Recent studies involving alizarine dye[46] or bi-isonicotinic acid[47] in conjunction with theoretical investigations of interfacial electron transfer[48,49,50,51] show that electron injection into TiO_2 is expected to occur on a subpicosecond or even more likely on a sub-100 fs timescale. Of particular relevance is the report of Schnadt et al.[47] who showed experimen-

tal evidence for a sub-3 fs charge transfer from bi-isonicotinic acid, which is equivalent to the non-coordinated dicarboxy-bipyridyl ligand present in our complexes. Computational investigations show that the LUMO of N3 is located on the dcbpy ligand attached to the surface. Therefore the coupling should be very similar to the situation with bi-isonicotinic acid and the reaction is expected to be in the same order of magnitude ($<$ 10 fs). However the LUMO+1, located on the free dcpby is also partially occupied upon excitation. The decrease in the electronic coupling should however yield electron transfer rates on the order of 100 fs when originating from that orbital.[31] For these reasons we believe that reductive quenching can not compete with dye molecules directly attached to the surface of the semiconductor.

From the soaking times and concentration of the dye solution dependencies, we learn that the preparation of the films has an influence on the efficiency of the RQ pathway. The dyeing process has obviously no influence on the photophysical properties of the sensitizers. Therefore we conclude that the RQ mechanism is related to the arrangement of the dyes on the TiO_2 surface. For low surface coverage as obtained from diluted dye solution or short soaking times, no reductive quenching is observed. On the opposite, the process becomes more important when the dye concentration on the film is increased. From these observations, in conjunction with the improbability of electron injection as slow as 3-30 ps for dyes directly adsorbed on the surface, we impute the existence of the reductive quenching pathway to the presence of dye *molecular aggregates* in the TiO_2 films.

The role of aggregation on the sensitizing properties of dyes has been of great interest for the photographic industry. Absorption properties and exciton dynamics in cyanine aggregates are crucial parameters for efficient spectral sensitization of silver halides. Formation of H- and J-aggregates of merocyanine dyes has also been studied in a TiO_2 mesoporous network.[52] All these applications were motivated by the change of light absorption properties upon self-assembly of monomers. Unfortunately for N3-derivatives no spectral changes are observed for high-loaded nanocrystalline films where aggregation is expected to take place. This can be explained by the relative insensitivity of the light absorption properties of ruthenium polypyridyl complexes to the environment due to the MLCT character of the dominating transitions. We applied several techniques in order to directly observe aggregates of N3-derivative dyes, but so far no evidence was found. These techniques included ATR-FTIR spectroscopy, transmission IR spectroscopy on CaF_2 substrates, resonant Raman spectroscopy and nanosecond excited state lifetime measurements in solution.

Recently, Neale et al. studied the influence of an adsorbent co-grafted with N3 on dye loading in dye-sensitized solar cells.[53] Their experiments reveal the presence of strongly and weakly adsorbed sensitizers at the surface of TiO$_2$. Although they do not attempt to distinguish between weak binding modes and aggregation, these results reinforce our interpretation.

X-ray structure studies of N3 showed that H-bonding was responsible for molecular packing in the solid state.[54] Similar interactions must be present on the semiconductor's surface. It is so far unclear if the aggregates are pre-exisiting in the dye solutions or if they are formed upon adsorption. It seems that the techniques used to dissolve the solid dyes have an influence on the kinetics for electron injection (see next chapter). This would indicate that dye aggregates are already present before adsorption. Laser light scattering experiments provided also indications that supramolecular particles are found in the dye solutions, although it was not clear if these particles are made of dye molecules or impurities.

The aging effect, i.e. the decrease of the RQ yield several hours after preparation of the sample, can be interpreted as a rearrangement of the dye aggregates. It is recognized that anchoring to the surface is mediated by the carboxylic groups of the dcbpy ligands.[55] Interaction of the ruthenium complexes are expected to be much stronger with TiO$_2$ than intermolecular H-bonding as observed in the solid state. If aggregated dyes penetrate into the mesoporous network it may take some time to reach the equilibrium state where most of the sensitizers are properly adsorbed. Therefore the reductive quenching pathway will become less important as the dyes rearrange towards a better surface coverage.

As discussed above, the injection kinetics are expected to be found on a subpicosecond timescale, but time constants up to 100 ps have been measured for N3-sensitized TiO$_2$ nanoparticles. If aggregation is present on the surface of the semiconductor, it would give an explanation for the origin of the kinetic heterogeneity of electron injection as observed by many different researchers. This topic will be developed in detail in the next chapter. Nevertheless, it is interesting to compare our results to the observation of an aging effect by Lian and co-workers for N3-synthesized TiO$_2$.[56] They found that the amplitude of the slower kinetic phase decreased from 16 % to less than 5 % in aged samples. At that point no explanation was given. We believe that their observations are consistent with a rearrangement of dyes at the surface of the semiconductor thereby increasing the proportion of sensitizers directly anchored to the surface. In that particular experiment the fast kinetic phase was found to occur in less than 50 fs.

The observation of the reductive quenching mechanism has important consequences for the efficiency of dye-sensitized solar cells based on N3 (and derivatives) anchored on TiO_2. DSCs containing electrolytes based on binary mixtures of PMII and EMITCM have shown promising efficiencies (7.4 % at air mass (1.5) full sunlight) with excellent stability. The recorded efficiencies increased concomitantly with the iodide concentration up to a maximum value corresponding to electrolytes containing only 50 % of PMII. Further addition of PMII dropped the total efficiency to less than 6 %. Our results show that above this concentration the reductive quenching pathway is non negligible and leads to lower light-to-electricity energy conversion.[22] In spite of the expected favorable thermodynamic conditions,[33] electron injection from the reduced sensitizer (the so-called *supersensitization* mechanism) is not observed in our experiments. The long lifetime of the dye anion (milliseconds) is in contradiction with an efficient charge transfer to the semiconductor. This is consistent with the assumption that the dyes that undergo reductive quenching are not directly attached to the surface and it shows at the same time that the RQ mechanism is an adverse effect in the sensitization process. The aging effect has also important consequences on the fabrication of DSCs. Although it has been seldom published in the literature, it is very commonly observed that the maximum efficiency of a solar cell is obtained only several hours after the preparation of the device.[20,57] We think that this is related to the time needed for a rearrangement of the aggregates leading to a better surface coverage of the nanoparticles.

From the relative intensities of reductive quenching shown in table 4.2, we found that Z907 is less vulnerable to direct reduction than N719. Two reasons can be invoked to explain these differences. (a) The barrier generated by the hydrophobic moiety of Z907 may hinder the contact with iodide ions, and (b) Z907 is less subject to aggregation because of the steric hindrance induced by the bulky alkyl chains and the lack of H-bonding carboxylic groups on the spectator ligand. If a catalytic effect of TiO_2 is present by the formation of ion pairs, the hydrophobic barrier is likely to be the major cause leading to the difference observed. The observation of slower dye regeneration with this compound is also in agreement with this interpretation.

4.4   Conclusions

Summary   We performed nanosecond transient absorption spectroscopic measurements of nanocrystalline TiO_2 films sensitized by derivatives of the standard N3 ruthenium complex (N719 and Z907) in the presence of high iodide concentrations. For the first time evidence of direct reductive quench-

ing of the sensitizer's excited state by I^- has been observed for this family of dyes. These observations were made possible only by the use of electrolytes based on ionic liquids where iodide concentrations up to 6.1 M are reachable. Although the electrochemical potential of the dye anion is expected to be much higher than the conduction band edge, no electron injection from S^- is observed. Instead the anion showed a lifetime up to several milliseconds. The yield of excited sensitizers that undergo reductive quenching depends strongly on the iodide concentration and is on the order of 25 % for pure PMII.

The presence of the reductive quenching pathway depends also on the preparation of the samples. For short soaking times or adsorption from diluted dye solutions, dye anions were hardly observable. Aging of the samples had also an influence on the extent of the reductive process.

Femtosecond pump-probe experiments were performed in order to measure the kinetics of the excited state's reduction by iodide. The results show that the process is complete in less than 50 ps. This confirms that reductive quenching can compete efficiently with the reported slow phase of the electron injection process.

Our analysis of the kinetics of the reduction process and the effects related to the preparation of the sample made us conclude that reductive quenching was enabled by the presence of dye aggregates at the surface of the semiconductor. In spite of the fact that aggregates could not be observed directly with several experimental approaches, this interpretation gives new insight into adverse effects observed on the photovoltaic properties of ionic liquid based solar cells, and more important in the framework of the present thesis, suggest a new rationale for the kinetic heterogeneity for electron injection from N3 into TiO_2.

Outlook The effect of dye aggregation on the kinetics of electron injection will be discussed in detail in the next chapter. Apart from this aspect, the presence of reductive quenching has important consequences for the DSC scientific community. In spite of the observation of such a mechanism for non-injecting dyes, reductive quenching has never been considered in the discussion of the performance of photovoltaic devices. With the growing use of ionic liquid electrolytes to improve stability of such assemblies, one has to be aware of the presence of the RQ mechanism.

Even more can be learned from the presence of aggregates at the surface of TiO_2. The colligative properties are usually not taken into account in the

design of new dyes for DSC applications. Recently, the presence of coadsorbents facilitating the adsorption of the dye on the surface was shown to increase the performance of cells by up to 10 %, in spite of the slight photocurrent decrease due to lower dye loading.[53,58,59] This improvement was explained partly by the reduction of the dark current, i.e. the recombination of injected electrons with I_3^- ions at the surface of the semiconductor, because of the better surface coverage induced by the presence of the coadsorbents.[59] This illustrates the importance of the optimization of dye self-assembly at the surface and the potential drawback caused by aggregation.

Future experiments will include further characterization of molecular aggregates pre-existing in the dye solutions or formed into the mesoporous network. Direct observation could be obtained from light scattering techniques or infrared spectroscopy. As will be shown in the next chapter the use of dyes unable to form H-bonds is a good alternative for better surface coverage and, furthermore, reduce unwanted phenomena in order to study interfacial charge transfer.

Reductive quenching was so far considered to be an exception and had been observed only for non-injecting dyes. This mechanism could be much more frequent than expected and one should remain aware of this when testing new dyes for photovoltaic applications. Static reductive quenching has been observed recently for the first time by time-resolved photoluminescence experiments.[36] The weak photoluminescence of the dyes studied here (N719 and Z907) precludes the use of a similar technique. However, this technique should be applicable to analogous dyes in the presence of various concentrations of iodide. Using binary mixtures of pmii with another iodide-free ionic liquid will make it possible to perform Stern-Volmer analysis on a much larger window and could lead to the identification of dye/iodide adducts.

4.5   References

1. Wasserscheid, P.; Keim, W. "Ionic liquids - New solutions for transition metal cataly-sis", *Angew. Chem. Int. Ed.* **2000,** *39,* 3773-3789.

2. Angell, C. A. Origin and control of low-melting behaviour in salts, polysalts, salt sol-vates, and glassformers. In *Proc. of the May 2001 NATO-ASI on Molten Salts*; Gaune-Escard, M., Ed.; Kluwer Scientific Pub.: 2002.

3. Bonhôte, P.; Dias, A. P.; Papageorgiou, N.; Kalyanasundaram, K.; Grätzel, M. "Hy-drophobic, highly conductive ambient-temperature molten salts", *Inorg. Chem.* **1996,** *35,* 1168-1178.

4. Papageorgiou, N.; Athanassov, Y.; Armand, M.; Bonhôte, P.; Pettersson, H.; Azam, A.; Grätzel, M. "The performance and stability of ambient temperature molten salts for solar cell applications", *J. Electrochem. Soc.* **1996,** *143,* 3099-3108.

5. Grätzel, M.; Moser, J. E. Electron Transfer in Chemistry. In , Vol. 5; Balzani, V., Ed.; Wiley-VCH: 2001; Chapter "Solar Energy Conversion", pages 589–641.

6. Qu, P.; Meyer, G. J. Electron Transfer in Chemistry. In , Vol. 4; Balzani, V., Ed.; Wiley-VCH: 2001; Chapter "Dye Sensitization of Electrodes", pages 353–406.

7. Durrant, J. R.; Haque, S. A.; Palomares, E. "Towards optimisation of electron transfer processes in dye sensitised solar cells", *Coord. Chem. Rev.* **2004,** *248,* 1247-1257.

8. Katoh, R.; Furube, A.; Yoshihara, T.; Hara, K.; Fujihashi, G.; Takano, S.; Mu-rata, S.; Arakawa, H.; Tachiya, M. "Efficiencies of electron injection from excited N3 dye into nanocrystalline semiconductor (ZrO_2, TiO_2, ZnO, Nb_2O_5, SnO_2, In2O3) films", *J. Phys. Chem. B* **2004,** *108,* 4818-4822.

9. Nusbaumer, H.; Moser, J. E.; Zakeeruddin, S. M.; Nazeeruddin, M. K.; Grätzel, M. "Co-II(dbbiP)$_2^{2+}$ complex rivals tri-iodide/iodide redox mediator in dye-sensitized photovoltaic cells", *J. Phys. Chem. B* **2001,** *105,* 10461-10464.

10. Haque, S. A.; Tachibana, Y.; Willis, R. L.; Moser, J. E.; Grätzel, M.; Klug, D. R.; Durrant, J. R. "Parameters influencing charge recombination kinetics in dye-sensitized nanocrystalline titanium dioxide films", *J. Phys. Chem. B* **2000,** *104,* 538-547.

11. Wang, P.; Zakeeruddin, S. M.; Moser, J. E.; Grätzel, M. "A new ionic liquid electrolyte enhances the conversion efficiency of dye-sensitized solar cells", *J. Phys. Chem. B* **2003,** *107,* 13280-13285.

12. Frank, A. J.; Kopidakis, N.; van de Lagemaat, J. "Electrons in nanostructured TiO_2 solar cells: transport, recombination and photovoltaic properties", *Coord. Chem. Rev.* **2004,** *248,* 1165-1179.

13. Nusbaumer, H.; Zakeeruddin, S. M.; Moser, J. E.; Grätzel, M. "An alternative efficient redox couple for the dye-sensitized solar cell system", *Chem. Eur. J.* **2003,** *9,* 3756-3763.

14. Wang, P.; Zakeeruddin, S. M.; Moser, J. E.; Humphry-Baker, R.; Grätzel, M. "A solvent-free, SeCN-/(SeCN)$_3^-$ based ionic liquid electrolyte for high-efficiency dye-sensitized nanocrystalline solar cells", *J. Am. Chem. Soc.* **2004,** *126,* 7164-7165.

15. Montanari, I.; Nelson, J.; Durrant, J. R. "Iodide electron transfer kinetics in dye-sensitized nanocrystalline TiO$_2$ films", *J. Phys. Chem. B* **2002,** *106,* 12203-12210.

16. Pelet, S.; Moser, J. E.; Grätzel, M. "Cooperative effect of adsorbed cations and iodide on the interception of back electron transfer in the dye sensitization of nanocrystalline TiO$_2$", *J. Phys. Chem. B* **2000,** *104,* 1791-1795.

17. Barbe, C. J.; Arendse, F.; Comte, P.; Jirousek, M.; Lenzmann, F.; Shklover, V.; Grätzel, M. "Nanocrystalline titanium oxide electrodes for photovoltaic applications", *J. Am. Ceram. Soc.* **1997,** *80,* 3157-3171.

18. Nazeeruddin, M. K.; Kay, A.; Rodicio, I.; Humphry-Baker, R.; Müller, E.; Liska, P.; Vlachopoulos, N.; Grätzel, M. "Conversion of Light to Electricity by Cis-X$_2$bis(2,2'-Bipyridyl-4,4'-Dicarboxylate)Ruthenium(II) Charge-Transfer Sensitizers (X = Cl$^-$, Br$^-$, I$^-$, CN$^-$, and SCN$^-$) on Nanocrystalline TiO$_2$ Electrodes", *J. Am. Chem. Soc.* **1993,** *115,* 6382-6390.

19. Nazeeruddin, M. K.; Zakeeruddin, S. M.; Humphry-Baker, R.; Jirousek, M.; Liska, P.; Vlachopoulos, N.; Shklover, V.; Fischer, C. H.; Grätzel, M. "Acid-base equilibria of (2,2'-bipyridyl-4,4'-dicarboxylic acid)ruthenium(II) complexes and the effect of protonation on charge-transfer sensitization of nanocrystalline titania", *Inorg. Chem.* **1999,** *38,* 6298-6305.

20. Wang, P.; Zakeeruddin, S. M.; Moser, J. E.; Nazeeruddin, M. K.; Sekiguchi, T.; Grätzel, M. "A stable quasi-solid-state dye-sensitized solar cell with an amphiphilic ruthenium sensitizer and polymer gel electrolyte", *Nat. Mater.* **2003,** *2,* 402-407.

21. MacFarlane, D. R.; Golding, J.; Forsyth, S.; Forsyth, M.; Deacon, G. B. "Low viscosity ionic liquids based on organic salts of the dicyanamide anion", *Chem. Commun.* **2001,** 1430-1431.

22. Wang, P.; Wenger, B.; Humphry-Baker, R.; Moser, J. E.; Teuscher, J.; Kantlehner, W.; Mezger, J.; Stoyanov, E. V.; Zakeeruddin, S. M.; Grätzel, M. "Charge separation and efficient light energy conversion in sensitized mesoscopic solar cells based on binary ionic liquids", *J. Am. Chem. Soc.* **2005,** *127,* 6850-6856.

23. Das, S.; Kamat, P. V. "Spectral characterization of the one-electron oxidation product of cis-bis(isothiocyanato)bis(4,4'-dicarboxylato-2,2'-bipyridyl) ruthenium(II) complex using pulse radiolysis", *J. Phys. Chem. B* **1998,** *102,* 8954-8957.

24. Moser, J. E.; Noukakis, D.; Bach, U.; Tachibana, Y.; Klug, D. R.; Durrant, J. R.; Humphry-Baker, R.; Grätzel, M. "Comment on measurement of ultrafast photoinduced electron transfer from chemically anchored Ru-dye molecules into empty electronic states in a colloidal anatase TiO$_2$ film", *J. Phys. Chem. B* **1998,** *102,* 3649-3650.

25. Zakeeruddin, S. M.; Nazeeruddin, M. K.; Humphry-Baker, R.; Pechy, P.; Quagliotto, P.; Barolo, C.; Viscardi, G.; Grätzel, M. "Design, synthesis, and application of amphiphilic ruthenium polypyridyl photosensitizers in solar cells based on nanocrystalline TiO$_2$ films", *Langmuir* **2002,** *18,* 952-954.

26. Mentus, S. "Oxygen reduction on anodically formed titanium dioxide", *Electrochim. Acta* **2004,** *50,* 27-32.

27. Tsujiko, A.; Itoh, H.; Kisumi, T.; Murakoshi, K.; Nakato, Y. "Observation of Cathodic Photocurrents at Nanocrystalline TiO_2 Film Electrodes, Caused by Enhanced Oxygen Reduction in Alkaline Solutions", *J. Phys. Chem. B* **2002,** *106,* 5878-5885.

28. Wolfbauer, G.; Bond, A. M.; Deacon, G. B.; MacFarlane, D. R.; Spiccia, L. "Experimental and theoretical investigations of the effect of deprotonation on electronic spectra and reversible potentials of photovoltaic sensitizers: Deprotonation of cis-L_2RuX_2 (L=2,2 '-bipyridine-4,4 '-dicarboxylic acid; X = CN^-, NCS^-) by electrochemical reduction at platinum electrodes", *J. Am. Chem. Soc.* **2000,** *122,* 130-142.

29. Fantacci, S.; De Angelis, F.; Selloni, A. "Absorption spectrum and solvatochromism of the [Ru(4,4 '-COOH-2,2 '-bpy)$_2$(NCS)$_2$] molecular dye by time dependent density functional theory", *J. Am. Chem. Soc.* **2003,** *125,* 4381-4387.

30. Monat, J. E.; Rodriguez, J. H.; McCusker, J. K. "Ground- and excited-state electronic structures of the solar cell sensitizer bis(4,4'-dicarboxylato-2,2'-bipyridine)bis(isothiocyanato)ruthenium(II)", *J. Phys. Chem. A* **2002,** *106,* 7399-7406.

31. Persson, P.; Lundqvist, M. J. "Calculated structural and electronic interactions of the ruthenium dye N3 with a titanium dioxide nanocrystal", *J. Phys. Chem. B* **2005,** *109,* 11918-11924.

32. Wolfbauer, G.; Bond, A. M.; MacFarlane, D. R. "Electrochemical and spectroscopic studies on the reduction of the cis-(Et$_2$dcbpy)$_2$RuX$_2$ series of photovoltaic sensitizer precursor complexes (Et$_2$dcbpy = diethyl 2,2'-bipyridine-4,4'-dicarboxylate, X = Cl^-, I^-, NCS^-, CN^-)", *J. Chem. Soc., Dalton Trans.* **1999,** 4363-4372.

33. Bergeron, B. V.; Meyer, G. J. "Reductive electron transfer quenching of MLCT excited states bound to nanostructured metal oxide thin films", *J. Phys. Chem. B* **2003,** *107,* 245-254.

34. Nasr, C.; Hotchandani, S.; Kamat, P. V. "Role of iodide in photoelectrochemical solar cells. Electron transfer between iodide ions and ruthenium polypyridyl complex anchored on nanocrystalline SiO_2 and SnO_2 films", *J. Phys. Chem. B* **1998,** *102,* 4944-4951.

35. Thompson, D. W.; Kelly, C. A.; Farzad, F.; Meyer, G. J. "Sensitization of nanocrystalline TiO_2 initiated by reductive quenching of molecular excited states", *Langmuir* **1999,** *15,* 650-653.

36. Clark, C.; Marton, A.; Meyer, G. "Evidence for static quenching of MLCT excited states by iodide", *Inorg. Chem.* **2005,** *44,* 3383–3385.

37. Kamat, P.; Haria, M.; Hotchandani, S. "C-60 cluster as an electron shuttle in a Ru(II)-polypyridyl sensitizer-based photochemical solar cell", *J. Phys. Chem. B* **2004,** *108,* 5166–5170.

38. Hagfeldt, A.; Grätzel, M. "Molecular photovoltaics", *Acc. Chem. Res.* **2000,** *33,* 269-277.

39. Walter, B.; Elliott, C. "Interaction of I^- and I_3^- with a redox-stable Cr(III)-based structural surrogate for photo-oxidized "N3 dye"", *Inorg. Chem.* **2001,** *40,* 5924–5927.

40. Teuscher, J. "Investigation de l'agrégation de complexes polypyridyles de ruthénium (II) à la surface d'oxydes nanocristallins par photolyse par éclair laser", Master's thesis, Ecole Polytechnique Fédérale de Lausanne, 2002.

41. Kallioinen, J.; Benkö, G.; Sundström, V.; Korppi-Tommola, J. E. I.; Yartsev, A. P. "Electron transfer from the singlet and triplet excited states of $Ru(dcbpy)_2(NCS)_2$ into nanocrystalline TiO_2 thin films", *J. Phys. Chem. B* **2002,** *106,* 4396-4404.

42. Tachibana, Y.; Moser, J. E.; Grätzel, M.; Klug, D. R.; Durrant, J. R. "Subpicosecond interfacial charge separation in dye-sensitized nanocrystalline titanium dioxide films", *J. Phys. Chem.* **1996,** *100,* 20056-20062.

43. Kallioinen, J.; Benkö, G.; Myllyperkiö, P.; Khriachtchev, L.; Skårman, B.; Wallenberg, R.; Tuomikoski, M.; Korppi-Tommola, J.; Sundström, V.; Yartsev, A. P. "Photoinduced ultrafast dynamics of $Ru(dcbpy)_2(NCS)_2$- sensitized nanocrystalline TiO_2 films: The influence of sample preparation and experimental conditions", *J. Phys. Chem. B* **2004,** *108,* 6365-6373.

44. Wang, P.; Zakeeruddin, S. M.; Comte, P.; Exnar, I.; Grätzel, M. "Gelation of ionic liquid-based electrolytes with silica nanoparticles for quasi-solid-state dye-sensitized solar cells", *J. Am. Chem. Soc.* **2003,** *125,* 1166-1167.

45. Henglein, A. "Energetics of Reactions of O_{aq}^- and of O^--transfer Reactions between Radicals", *Radiat. Phys. Chem.* **1980,** *15,* 151-158.

46. Huber, R.; Moser, J. E.; Grätzel, M.; Wachtveitl, J. "Real-time observation of photoinduced adiabatic electron transfer in strongly coupled dye/semiconductor colloidal systems with a 6 fs time constant", *J. Phys. Chem. B* **2002,** *106,* 6494-6499.

47. Schnadt, J.; Brühwiler, P. A.; Patthey, L.; O'Shea, J. N.; Södergren, S.; Odelius, M.; Ahuja, R.; Karis, O.; Bässler, M.; Persson, P.; Siegbahn, H.; Lunell, S.; Mårtensson, N. "Experimental evidence for sub-3-fs charge transfer from an aromatic adsorbate to a semiconductor", *Nature* **2002,** *418,* 620-623.

48. Duncan, W. R.; Stier, W. M.; Prezhdo, O. V. "Ab initio nonadiabatic molecular dynamics of the ultrafast electron injection across the alizarin-TiO_2 interface", *J. Am. Chem. Soc.* **2005,** *127,* 7941-7951.

49. Ramakrishna, S.; Willig, F.; May, V.; Knorr, A. "Femtosecond spectroscopy of heterogeneous electron transfer: Extraction of excited-state population dynamics from pump-probe signals", *J. Phys. Chem. B* **2003,** *107,* 607-611.

50. Thoss, M.; Kondov, I.; Wang, H. B. "Theoretical study of ultrafast heterogeneous electron transfer reactions at dye-semiconductor interfaces", *Chem. Phys.* **2004,** *304,* 169-181.

51. Lanzafame, J. M.; Palese, S.; Wang, D.; Miller, R. J. D.; Muenter, A. A. "Ultrafast Nonlinear-Optical Studies of Surface-Reaction Dynamics - Mapping the Electron Trajectory", *J. Phys. Chem.* **1994,** *98,* 11020-11033.

52. Nuesch, F.; Moser, J. E.; Shklover, V.; Grätzel, M. "Merocyanine aggregation in mesoporous networks", *J. Am. Chem. Soc.* **1996,** *118,* 5420-5431.

53. Neale, N. R.; Kopidakis, N.; van de Lagemaat, J.; Grätzel, M.; Frank, A. J. "Effect of a Coadsorbent on the Performance of Dye-Sensitized TiO_2 Solar Cells: Shielding versus Band-Edge Movement", *J. Phys. Chem. B* **2005,** *109,* ASAP.

54. Shklover, V.; Ovchinnikov, Y. E.; Braginsky, L. S.; Zakeeruddin, S. M.; Grätzel, M. "Structure of organic/inorganic interface in assembled materials comprising molecular components. Crystal structure of the sensitizer bis[(4,4 '-carboxy-2,2 '-bipyridine)(thiocyanato)]ruthenium(II)", *Chem. Mater.* **1998,** *10,* 2533-2541.

55. Nazeeruddin, M. K.; Humphry-Baker, R.; Liska, P.; Grätzel, M. "Investigation of sensitizer adsorption and the influence of protons on current and voltage of a dye-sensitized nanocrystalline TiO$_2$ solar cell", *J. Phys. Chem. B* **2003,** *107,* 8981-8987.

56. Asbury, J. B.; Ellingson, R. J.; Ghosh, H. N.; Ferrere, S.; Nozik, A. J.; Lian, T. Q. "Femtosecond IR study of excited-state relaxation and electron-injection dynamics of Ru(dcbpy)$_2$(NCS)$_2$ in solution and on nanocrystalline TiO$_2$ and Al$_2$O$_3$ thin films", *J. Phys. Chem. B* **1999,** *103,* 3110-3119.

57. Kubo, W.; Kitamura, T.; Hanabusa, K.; Wada, Y.; Yanagida, S. "Quasi-solid-state dye-sensitized solar cells using room temperature molten salts and a low molecular weight gelator", *Chem. Commun.* **2002,** 374-375.

58. Wang, P.; Klein, C.; Humphry-Baker, R.; Zakeeruddin, S.; Grätzel, M.and Frank, A. J. "Stable >= 8% efficient nanocrystalline dye-sensitized solar cell based on an electrolyte of low volatility", *Appl. Phys. Lett.* **2005,** *86,.*

59. Zhang, Z.; Zakeeruddin, S.; O'Regan, B.; Humphry-Baker, R.; Grätzel, M. "Influence of 4-Guanidinobutyric Acid as Coadsorbent in Reducing Recombination in Dye-Sensitized Solar Cells", *J. Phys. Chem. B* **2005,** *109,* ASAP.

Origin of the kinetic heterogeneity in N3-sensitized TiO$_2$

Summary

N3 adsorbed on nanocrystalline TiO$_2$ films has been regarded as a model system for the study of the ultrafast electron injection process. Most recent studies have reported charge injection kinetics to take place with a fast (< 100 fs) phase, followed by a slower (0.7-100 ps) component. This complex behavior has prevented the development of a satisfying kinetic model and has often led to contradicting conclusions. Here we show that the observed kinetic heterogeneity is actually due to the aggregation of dye molecules on the surface rather than to a dual excited state mechanism as previously suggested. Controlled deposition of dye molecules onto titania made it possible to obtain monophasic injection dynamics (τ < 20 fs). This result suggests the process is beyond the scope of vibration-mediated electron transfer models and is controlled by the electron dephasing in the solid.

5.1   Introduction

The primary step in light-to-electricity conversion in a dye-sensitized so-
lar cell (DSC) is the electron injection into the semiconductor's conduction
band.[1] The overall efficiency of the cell relies on a fast, efficient electron
transfer process and this issue has naturally been tackled since the very be-
ginning of DSC development. Since the breakthrough-paper in 1991[2] pre-
senting DSCs based on mesoscopic TiO_2 electrodes with an overall efficiency
of 7.1 %, the attention has been focused on the Ru(II) polypyridyl com-
plexes and more particularly *cis*-[bis(4,4'-dicarboxy-2,2'-bipyridyl)-bis(thio-
cyanato)]ruthenium(II) ($\equiv$ *cis*-[Ru^{II}(dcbpy)$_2$(NCS)$_2$]) hereafter called *N3*
since it was the third of a long series of dyes synthesized by M.K. Nazerud-
din. Optimization of solar cells based on this dye soon yielded efficiencies
of 10 %.[3] These successes led to the commercialization of the compound
(by Solaronix, Aubonne) and its use in the majority of studies concerned
with dye-sensitized solar cells for the last decade. Naturally, the injection
kinetics relevant to these devices have also been investigated principally in
N3-sensitized TiO_2.
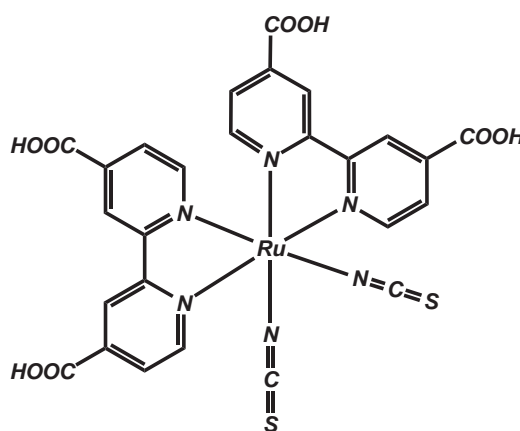
Figure 5.1 — Structure of the N3 dye (*cis*-[Ru^{II}(dcbpyH$_2$)$_2$(NCS)$_2$]).

While earlier studies used indirect techniques (nanosecond transient absorp-
tion and measurement of fluorescence lifetime)[4] to estimate the rate con-
stant for charge injection into TiO_2, it was soon recognized that femtosecond
transient absorption spectroscopy was the most appropriate tool for direct
proofing of the formation of the oxidized dye or the appearance of an in-
jected electron in the semiconductor's conduction band. The first recorded
femtosecond-resolved experiment involving N3 on TiO_2 was performed by
Tachibana et al. in 1996.[5] They found biphasic injection kinetics consisting
of a fast unresolved part (< 150 fs) and a slower component (1.2 ps). Not

long after, this system was explored by Hannappel et al. under high-vacuum conditions.[6] The 25 fs monophasic time constant found here was however strongly questioned due to the evident dye degradation that took place in their experiment.[7,8] The group of Lian at Emory University then began to apply mid-infrared fs transient absorption spectroscopy to this system. In their first contribution, a single < 50 fs component was observed.[9] In 2000, the same technique was applied by Heimer et al. and yielded a < 350 fs upper limit.[10] Beginning one year later the group of Sundström in Lund produced a series of remarked papers that has been recurrently cited by the DSC scientific community.[11,12,13,14,15] These reports, with addition of the later contributions of the groups of Durrant[16,17,18,19] and Lian,[20,21,22,23] make a total of 12 publications in peer-reviewed journals for the sensitization of TiO_2 by the N3 dye. The different time constants and experimental conditions of all these studies are reported in table 5.1.

5.1.1   Energetics

All the publications cited in table 5.1 gave different interpretations to their observations. Before going into the details of these analyses one would like to define the thermodynamics of the possible processes. To achieve electron injection, the oxidation potential of the excited dye $\phi^0(S^+/S^*)$ needs to be more negative than the conduction band flatband potential of the semiconductor ($\phi_{fb} \cong \phi_{cb}$ for nanometer-sized particles). This condition can be rewritten with the experimentally available quantities as:

$$\phi^0(S^+/S) < \phi_{cb} + \frac{\Delta E_{0,0}}{F} \tag{5.1}$$

where $\phi^0(S^+/S)$ is the oxidation potential of the dye in its ground state and $\Delta E_{0,0}$ the excitation energy. The presence of energy states lying below the conceptual conduction bottom edge considerably complicates this picture. In fact, due to the presence of these trapping sites, the band edge is more a continuous distribution of states than it is a Fermi-like function. These sites correspond to imperfectly coordinated atoms or impurities inserted in the lattice. They can be present in the bulk but are obviously more often encountered at the surface of the particles. The high surface-to-volume ratio for nanometer-sized particles presents a critical role for surface defects. The distribution of the low-lying states has been the topic of numerous recent studies.[24,25,26,27,28] They agree in general with an exponential distribution of states but much uncertainties remain about the exact density and the nature of the trap states.

Wavelengths [nm]		Time constants and amplitudes		Environment and references	
Pump	Probe	fs	ps	Environment	Reference
605	750	<150 (50%)	1.2 (50%)	EC/PC[a]	Tachibana et al.[5]
550	1100	<25		UHV[b]	Hannappel et al.[6]
400	4630	<50		air	Ellingson et al.[9]
400	4730	<50 (84%)	1.7 (16%)	air	Asbury et al.[20]
520,560,600	760	<100 (35%)	1.3 (22%), 13 (43%)	EC/PC,air	Durrant et al.[16]
560	760	<100 (29%)	1.0 (25%), 13 (46%)	EC/PC[a]	Tachibana et al.[17]
590	5400	<350		DCM[c]	Heimer et al.[10]
540	810	<150 (44%)	1.1 (20%), 12 (23%), 100 (13%)	N_2	Kallioinen et al.[15]
530	860	28 (50%)	1.0 (11%), 9.5 (12%), 50 (7%)	CH_3CN	Benkö et al.[12]
455	810	<20 (70%)	1.8 (20%), 10 (3%), 50 (12%)		
595	760	<150 (30%)	0.7 (25%), 17 (45%)	EC/PC[a]	Tachibana et al.[19]
400	3–10 μm	<100 (75%)	20 (25%) ($\alpha = 0.5$)[d]	Water, pH=2	Asbury et al.[22]
540	720	<200[e]	13[e]	CH_3CN	Kuciauskas et al.[23]

[a] ethylene carbonate / propylene carbonate 1:1
[b] ultrahigh vacuum
[c] dicholoromethane
[d] fitted with a stretched exponential
[d] the amplitude was not estimated because of the unknown contribution from the excited state absorption at 720 nm

Table 5.1 — Reported time constants for N3-sensitized TiO_2 (adapted from Kallioinen et al.[11]).

The potential of the electron in the dye before injection is also subject to some complications. First, the oxidation potential of the dye in its ground state is expected to vary due to the contribution of the environment. Here we can use Gerischer's picture for electron transfer (see section 2.7). In this model the environment induces harmonic fluctuations giving rise to a Gaussian-shape distribution function for the potential characterized by the reorganization energy λ. In addition several orbitals can be populated upon excitation of N3 by visible light. *Ab initio* calculations show that MLCT and LBCT (ligand-based charge transfer) excited states are present and hardly discernable.[29,30] Still the donating orbital is always located on a single dcbpy ligand. Another parameter is the evolution of the excited state before electron transfer. For ruthenium complexes, high spin-orbit coupling enables efficient intersystem crossing. But internal conversion, vibrational relaxation and interligand electron transfer (ILET) is also expected. The time constants for these processes have been reported to be as low as 43 fs, but depending on the conditions they are found in a range between tens of femtosecond up to nanoseconds.[12,31,32] Therefore the excited dye, prepared in a Franck-Condon state, can undergo relaxation or inject directly from the *hot state*. A diagram showing the energetics of interfactial electron transfer from N3 to TiO_2 is depicted in figure 5.2.
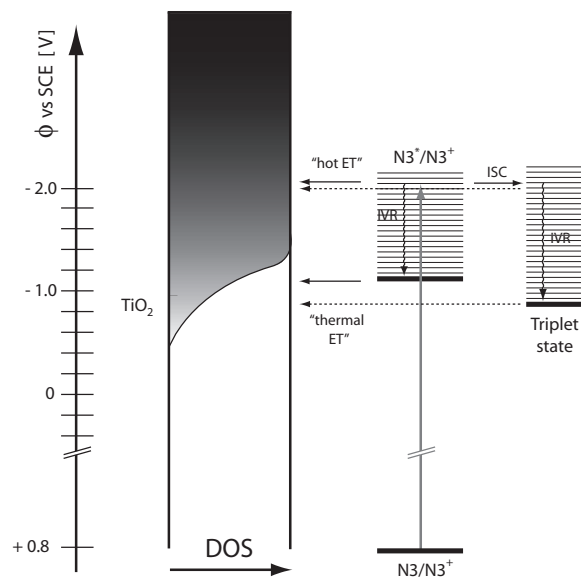
Figure 5.2 — Energy diagram for the charge injection from N3 to TiO_2. DOS: density of states, ISC: intersystem crossing, IVR: internal vibrational relaxation. The interligand electron transfer and the fluctuations of the redox potential due to the environment are not shown. The dye redox potentials are adopted from Sauvé et al.[33]

5.1.2   Interpretations

As shown in table 5.1 the data available in the literature display a vast heterogeneity. The observed time constants range from less than 20 fs to 100 ps and the amplitudes for the slow components are found between 0 and 71 %. Unsurprisingly, various explanations have been given to rationalize these results. In the years between 1996 and 2000, most of the studies showed monophasic injection and a few revealed a slower part but the origin of this feature remained unclear.[5,6,8,9,10,20] After 2000, all measurements featured a slower component and a model evolved gradually. Tachibana et al. were the first to suggest that the origin of the multiexponential kinetics was to be inputed to the semiconductor.[17] At that point they suspected various dye-semiconductor interactions to yield different kinetics. Later, a comparative study of N3 and its deprotonated derivative N719 led to the attribution of the multiexponential behavior to the varying density of states in TiO_2.[19] This interpretation has since then been constantly refined. The Lund group developed a model by including competition between electron injection from the single excited state and intersystem crossing (ISC).[12] In this picture, the dye molecules going through the ISC pathway are subject to electron thermalization and see a lower density of states in the acceptor than the molecules injecting directly from the singlet state. The reason why thermalization was efficient in the triplet state was later credited to an interligand electron transfer locating the electron to be transferred on the ligand that is not attached directly to the surface. The increased separation between the donor and the acceptor thus reduces the electronic coupling.[14] The group of Lian also adopted the two-state model with slower injection from the triplet state, and this has been more largely accepted by the dye solar cells community.[34]

5.1.3   Motivation

Why would one like to add another contribution to this overstudied topic? In fact the initial goal of this thesis was not to feed the controversy about electron injection from N3 to TiO_2 but rather to use other dyes and other semiconductors in order to probe the nuclear and electronic factors governing the kinetics. Nevertheless, after the discovery of the reductive quenching pathway in the presence of high iodide concentration (chapter 4), a new perspective was given. To explain why dye reduction could compete with a process as fast as electron injection into TiO_2, we suggested that some aggregation of the dye molecules was present on the surface. In that case the separation between the donor and the semiconductor's acceptor

states would not be constant, but rather look like a distribution of distances. Since electronic coupling is expected to fall off exponentially with distance, the rate constant for electron injection would be dramatically reduced, and competition with dye reduction would be possible.

If we now apply this suggestion to electron injection in the absence of iodide or any other reductive agent, it would give a reasonable explanation for the observation of multiexponential kinetics. Our work was then motivated by this hypothesis and some elements confirming this idea are given below.

## 5.2   Experimental part

5.2.1   Sample preparation

Transparent 8 μm-thick nanocrystalline films of TiO$_2$ nanocrystalline films were prepared using the same technique as for dye-sensitized solar cells.[35] Films were soaked overnight in a dye solution. Three different dye solutions were used:

- Commercial **N3** (Solaronix), 0.3 mM in ethanol

- Home-synthesized **N3**, 0.3 mM in ethanol

- Home-synthesized **N719**, 0.5 mM in CH$_3$CN/t-BuOH 1:1

The home-synthesized N3 and N719 dye solutions were prepared by dissolving ca. 10 mg of dye powder into 50 mL of solvent. The complete dissolution was obtained after stirring vigorously for > 3 hours at room temperature. N3 powder from Solaronix (Ru535) was dissolved in ethanol by sonication. After about 5 minutes no visible particles were remaining.

N719 is the doubly deprotonated derivative of N3 available with tetrabutyl-ammonium counter ions (N719 = (Bu$_4$N)$_2$[Ru^{II}(dcbpyH)$_2$(NCS)$_2$]). Anchoring of N3 and N719 sensitizer molecules is known to take place through the two carboxylic groups that are in trans position to the NCS ligands. For N3, this anchoring is associated with the deprotonation of the involved carboxylic groups. Therefore, species adsorbed on the TiO$_2$ surface are expected to be identical for both forms of the dye. Films derivatized with N3 and N719 indeed displayed similar spectra with a broad maximum at 532 nm, corresponding to a metal-to-ligand charge transfer transition (MLCT)

of the complexes[36] (figure 5.3). A redox inactive ionic liquid (1-ethyl-2-methylimidazolium bis(trifluoromethylsulfonyl) imide) was used as a reaction medium in all samples.[37]. The absorption spectra were measured in a Cary 1E spectrophotometer (Varian).
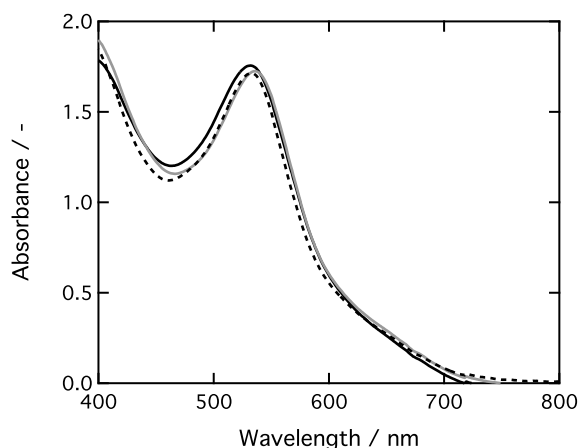

Figure 5.3 — Absorption spectra of 8 μm-thick sensitized TiO_2 films. Home-synthesized N3 (solid black line), Solaronix N3 (solid grey line) and N719 (dashed line).

5.2.2   Time-resolved spectrometer

These experiments were carried out in the two-color pump-probe scheme in order to obtain the best time resolution. The pump beam was tuned by the NOPA to excite the dye at 535 nm in the vicinity of the absorption maximum. The probe wavelength was set at 860 nm. Since this wavelength is close to the central wavelength of the fundamental beam from the CPA laser (778 nm) the second NOPA was used in the NOPA-plus configuration (see 3.1). The first stage was optimized to generate pulses centered at 1100 nm. This infrared beam was then filtered (LL1000, Corion) to remove the shorter wavelength from the first WLC and focused in a sapphire plate to generate a second continuum. This broadband pulse, now centered around 1100 nm, is much more stable in the region between 800 and 900 nm. Amplification in the second stage of the NOPA yields pulses with intensitites of 4-5 μJ with a duration of ca. 30 fs after compression. The pump beam proceeds through the 700-ps translation stage and both beams are focused on the sample with one single large size (ø= 76 mm) off-axis parabolic mirror. The sample is constantly rotated to avoid degradation of the dye caused by the heating of the nanocrystalline film.

5.3 Results and Discussion

N3 from Solaronix For a direct comparison with data reported in a majority of earlier studies, we begin with the commercially available N3 dye. The time evolution of the formation of the oxidized dye following ultrashort laser pulse excitation was measured. The probe wavelength was set at 860 nm where it was established by different groups that the dye oxidized state has a much higher extinction coefficient than the excited state.[15,17] As depicted in fig. 5.4, the absorption change due to the dye oxidized state was observed to rise with a first sub-100 fs phase followed by a slower kinetic component. Data were fitted with a sum of two analytical convolutions of a Gaussian instrument response (cross-correlation time of ca. 57 fs) with exponential growths with $\tau_1 = 76$ fs (84 %) and $\tau_2 = 45$ ps (16 %). In comparison with available data from the literature, the amplitude of the second kinetic compartment was found to be rather small.[15] However, the reproducibility of this amplitude was poor. Depending on the film preparation (adsorption time, dye solution concentration, ...), relative amplitudes varied considerably, while the kinetics were found to remain practically identical.
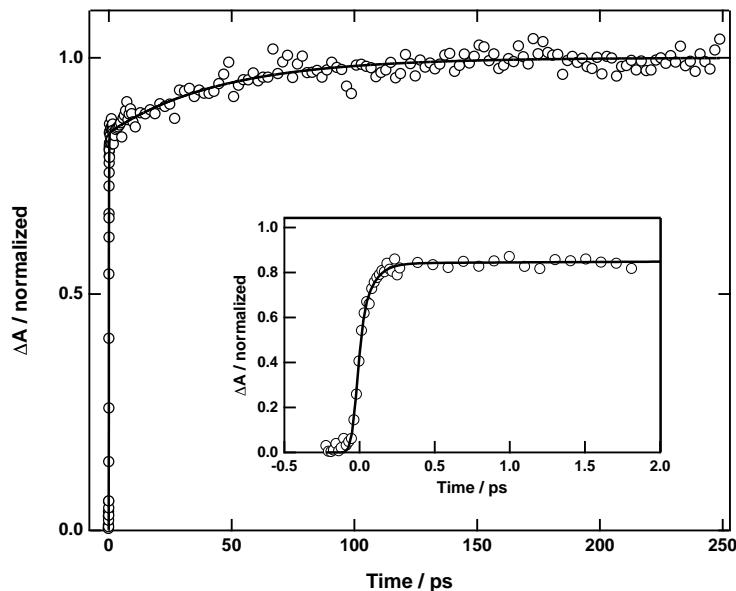
Figure 5.4 — Transient absorption signal obtained upon femtosecond pulse excitation of N3 (Solaronix) complex dye adsorbed on nanocrystalline TiO_2 films. The inset shows the same trace on an extended timescale. Excitation pulse wavelength: 535 nm, probe wavelength: 860 nm. The observed growth of the signal corresponds to the appearance of the dye oxidized state produced by the charge injection process.

Home-synthesized N3 and N719   This study was extended to the use of homemade N3 and N719. The observed amplitude of the slow part was considerably reduced by using our own preparation of N3 and disappeared totally when the deprotonated variant of the dye was used (figure 5.5). For homemade N3, the slow part accounted for only 4 % of the total rise with a time constant of 24 ps.
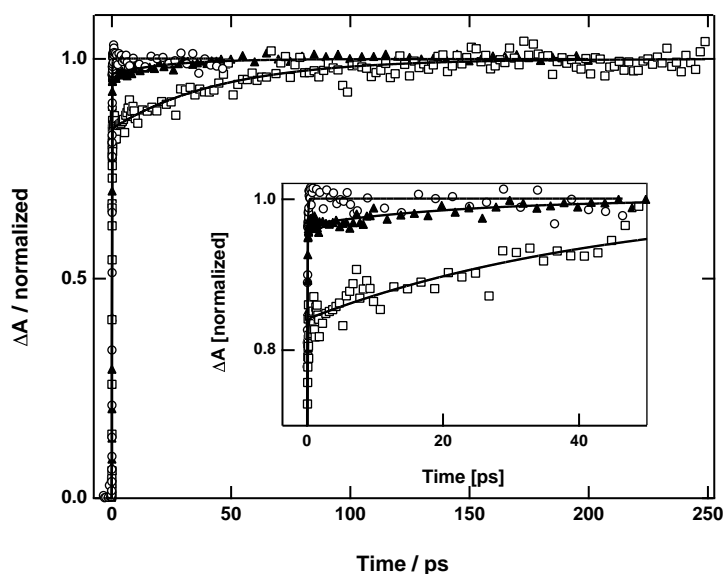
Figure 5.5 — Transient absorbance measured at 860 nm upon ultrashort laser pulse excitation at 535 nm of commercial N3 (□), homemade N3 (▲), and N719 (○). The insert displays the same data at a shorter timescale.

The variability of the amplitude of the ps phase and, furthermore, the total disappearance of this component for N719 indicate that the origin of the biphasic kinetic behavior is not to be found in the photophysical properties of the dyes but rather in their colligative properties. This observation is consistent with our initial hypothesis which assigns the slow kinetics to aggregated dyes. Contrary to the cases of dye molecules such as cynanines or xanthenes, aggregation does not cause any observable change in the absorption spectrum of N3 and N719. Aggregation of the dye on the surface provides an obvious rationale for the kinetic heterogeneity of interfacial electron transfer. Electron tunneling theory predicts an exponential dependence of the electron transfer rate with the distance separating the donor and the acceptor. Assuming a damping factor $\beta = 1.2$ Å^{-1}, the distance increase required to explain the observed slowing down of the injection is estimated to 3-7 Å. This figure is consistent with the geometric separation induced by dye aggregation. Diffusion of excitons within dye aggregates and intermolecular electron transfer mechanisms could also account for a spreading

of interfacial reaction rates. The main difference between the N3 and the N719 form of the sensitizer lies in the solubility of these two compounds. N719 is more soluble in polar solvents and, because of electrostatic repulsion, dianions of the deprotonated dye are less prone to aggregate. The commercial N3 powder (Solaronix), constituted of large crystals, appeared to be more difficult to solubilize. Sonication of this compound in ethanol, as often reported in the literature, tend to produce a colloidal suspension of the dye, thus favoring the deposition of pre-existing aggregates onto the oxide surface. The poor reproducibility of the amplitude of the slow kinetic component in our experiments and in the literature is compatible with various degree of aggregation, depending on the adsorption time and history of the dye solution.

The reductive quenching pathway observed by laser transient absorption spectroscopy in the nanosecond time domain (see chapter 4) was found to be suppressed when the dye was adsorbed from very dilute solutions. On the basis of this observation, dye-loaded films were prepared from an ethanolic solution of the commercial N3 sensitizer diluted 20 times (1.5 $\cdot 10^{-5}$ M). Strikingly, under these conditions, no slow growth component was observed anymore (figure 5.6), suggesting that the dye uptake from the dilute solution resulted in lower surface coverage preventing aggregation. Films dyed in the dilute solution displayed an optical density of only 0.35 at 534 nm, instead of 1.5 for those prepared using the higher sensitizer concentration.

Previous X-ray analysis of a single crystal of N3 showed the interaction between the sensitizer molecules to be due to hydrogen bonding.[38] Similarly, H-bonding induces dye aggregation in solution and in the adsorbed state. However, due to the deprotonation of two carboxylic groups, N719 is less prone to undergo aggregation. Based on these observations we repeated the transient absorption measurements with Z105, a dye containing a phosphonic acid group as an anchoring function (more information about this dye will be given in chapter 7). Since aggregation is likely to involve H-bonding from the carboxylic groups and considering that the adsorption constant was found to be 80 times higher than for the dcbpy complex, this dye is expected to be adsorbed on the TiO_2 surface as a monomer.[39] Indeed, the electron injection kinetics for Z105 is found to be monophasic, and again the time constant, faster than 20 fs, could not be resolved with our experimental setup (figure 5.7).

Monophasic electron transfer time constant   The complete disappearance of the slow phase in the case of N719 and N3 adsorbed from diluted
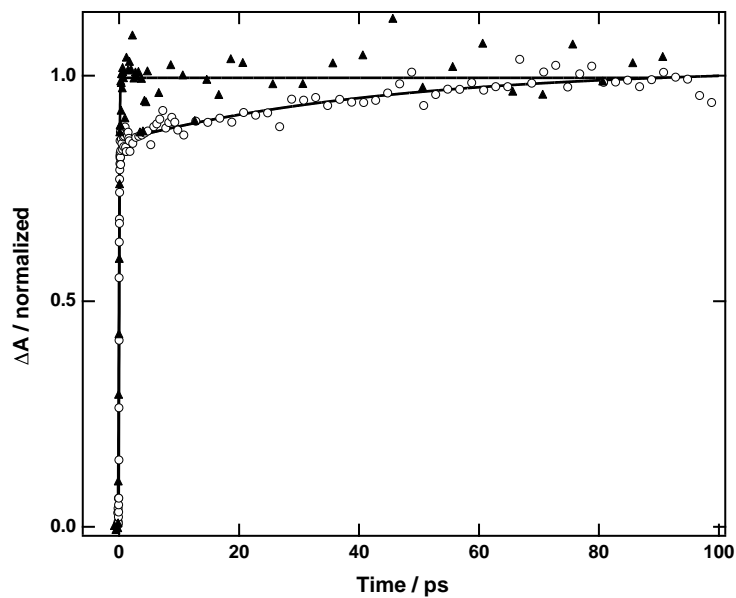
Figure 5.6 — Transient absorbance measured at 860 nm upon ultrashort laser pulse excitation at 535 nm of commercial N3 (○), and the same dye adsorbed from a 20x diluted solution ($1.5 \cdot 10^{-5}$ M) (▲).
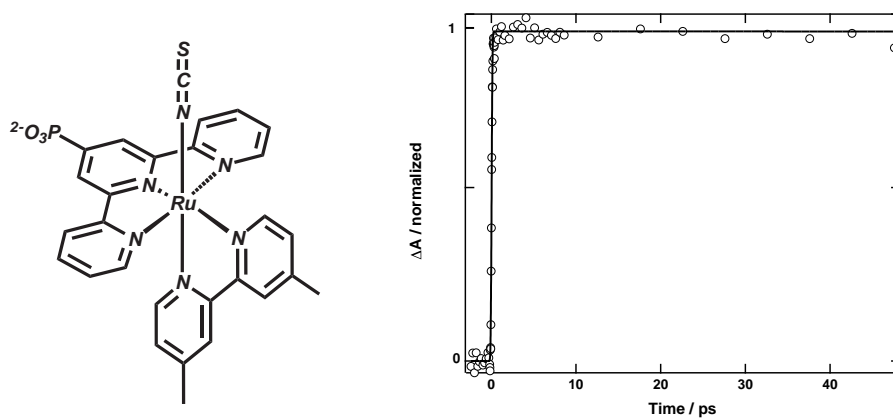

(a) Structure of the Z105 sensitizer dye.

(b) Transient absorbance at 600 nm upon laser excitation at 530 nm of Z105.

**Figure 5.7** — Electron injection from Z105 into nanocrystalline TiO$_2$

solutions of the dye suggests that the sensitizer is adsorbed as a monomer on the surface. These conditions facilitate the determination of the electron injection rate freed of artifacts due to dye aggregation. The fast part of the rise of the oxidized dye in the experiments with homemade N3 as well as for N719 could not be resolved with our experimental setup. However an upper limit for the time constant can be estimated by simulating the effect of an exponential rise with a time constant of 20 fs or 50 fs with the same instrument response. It is clear from figure 5.8 that with the cross-correlation time for this experiment (57 fs), a process occurring with a time constant of 20 fs would be detectable. Therefore we are quite confident to establish an upper limit for the time constant for electron injection from N719 to TiO_2 $\tau_{inj} < 20 \ fs$. An electron transfer rate constant of this magnitude implies the electronic coupling of the excited dye with the quasi-continuum of acceptor states constituting the conduction band of the solid is quite strong. In the normal Marcus approach to model the dynamics of electron transfer processes, the rate determining step is constituted by the relaxation of intramolecular and solvent nuclear degrees of freedom. For most species the time required for this vibrational reorganization is limited to a lower value of 100 fs. In our case, electron transfer is significantly faster than typical nuclear relaxation and is believed to be controlled only by the electron dephasing time of the semiconductor.
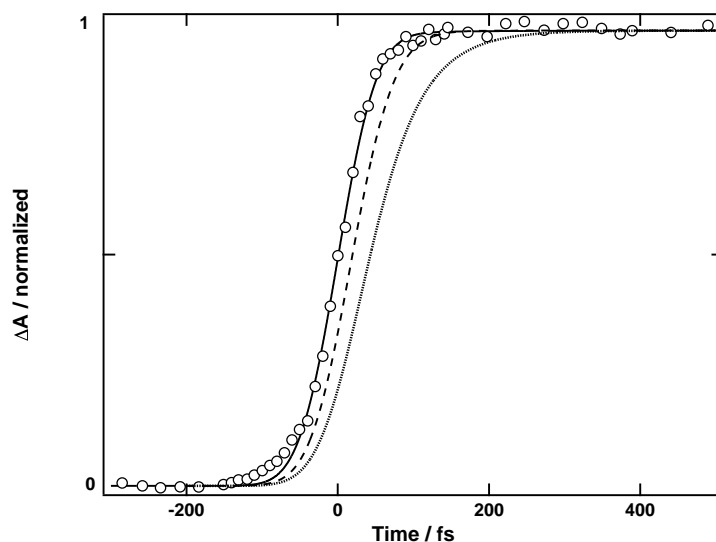
Figure 5.8 — Transient absorbance measured at 860 nm upon ultrashort laser pulse excitation at 535 nm of homemade N719 (∘). The simulated traces are obtained from the convolution of an exponential rise with a time constant of 20 fs (dashed line) or 50 fs (dotted line) and the fitted gaussian instrument response (solid line, FWHM = 57 fs).

To understand our results, we apply the model developed by Lanzafame and coworkers (see chapter 2, page 25)[40]. The main point here is that the huge number of acceptor semiconductor states creates the possibility of localizing the charge in the acceptor space without any need to invoke nuclear relaxation. After excitation, if the electronic coupling is strong, the electron tunnels resonantly to a single semiconductor state which is mixed with the entire quasi-continuum of conduction band states (figure 5.9). The wave function propagation remains coherent unless some relaxation process is present. Because of the probability of being located on the donor is now much smaller and the very fast relaxation processes for the electron in the conduction band phase, the electron is efficiently localized in the semiconductor. In this delocalization/relaxation model, the charge separation is now controlled by the dephasing time (as fast as 10 fs) and no more by nuclear relaxation in the molecular donor and environment as stated in the Marcus theory. This picture is compatible with our observation where the transfer is complete within a timescale where atoms may be considered as "frozen". It is interesting to note that the critical parameters for the electron injection rate are still electronic coupling and the density of states as predicted by Golden Rule-based theories. However, this model authorizes time constants much shorter than the limits given by the traditional theory. Unfortunately, we could not find any study reporting electron dephasing times in TiO_2. Terahertz spectroscopy however revealed, that carriers equilibrate thermally with the lattice in 300 fs.[41] Since electron dephasing is obviously much faster than thermal equilibration, a time constant lower than 20 fs, as found in our experiment, is not surprising.

Comparison with other studies A new reading of the previously published results can be carried out in the light of these new results. The slow electron injection kinetics (1-100 ps) observed in numbers of recent publications, and the large disparity of the estimated time constants and amplitude of these components are easily explained if we consider aggregation on the surface. As mentioned above, aggregation induces an increase in the distance separating the donor from the surface. This effect causes the exponential decay of the electronic coupling to reduce the injection rates from sub-100 fs to picoseconds. We showed that N3 was much more subject to aggregation than other derivatives because of the high number of carboxylic groups giving rise to efficient H-bonding. Yet, the attention has been concentrated on this dye. It is interesting to note that most of the studies featured the commercial dye which in our study showed the highest amplitude for the slow processes.
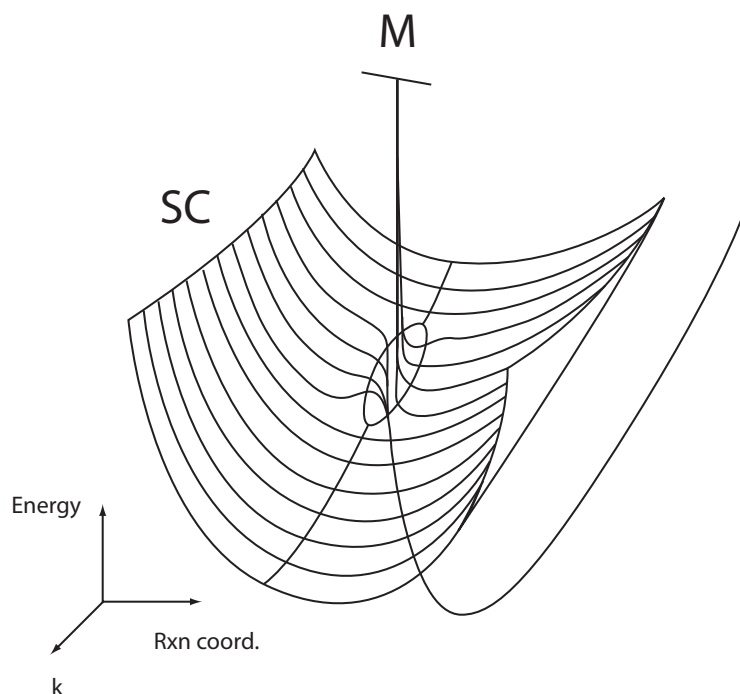
Figure 5.9 — Potential energy diagram for a charge transfer between a molecular state (M) and a semiconductor (SC) showing the interaction of the reaction coordinate with the manifold of k states of the semiconductor. For an electron injection process M is the reactant surface and SC is the product surface. In this case the large number of electronic levels coupled to the product surface assists the development of a charge-separated state. (Adapted from Lanzafame et al.[40])

Discussion of the validity of electron transfer theories in the case of interfacial dye-to-semiconductor electron transfer has been conducted essentially about the slow dynamics. However, an analysis of the predicted comportment would be much more pertinent for well-defined interfaces, i. e. monolayers adsorbed on the surface. Therefore, fast kinetics are more appropriate for testing models. Regrettably, the debate about the slow components has obscured this topic. A notable exception is the observation of a sub-3 fs electron injection from bi-isonicotinic acid anchored to a TiO_2 surface by Schnadt and coworkers.[42] In that case the donor is nothing else but the dicarboxy-bipyridyl ligand of N3. Since electron injection in N3 occurs from a MLCT state located on the dcpby ligand the situation is very likely to be the same in terms of electronic coupling and relaxation processes. Interestingly, they also invoked the model described by Lanzafame and coworkers to rationalize their observations.

5.4 Conclusions

Femtosecond transient absorption spectroscopy has been applied to measure the electron injection kinetics from the N3 dye to the conduction band of TiO$_2$. Depending on the preparation of the dyed mesoporous films and the degree of protonation of the sensitizers, the kinetics evolved from a single sub-20 fs time constant to a biphasic comportment with a slower phase characterized by time constants up to 45 ps. We impute the slower injection kinetics to dye molecules distant from the surface because of aggregation. The widely accepted interpretations based only on the excited state properties are found to be insufficient since the slow phase can be completely removed just by changing the preparation of the samples. Our result show that electron injection from N3 into TiO$_2$ is very similar to the case of bi-isonicotinic acid adsorbed on the same material and for which a sub-3 fs charge transfer has been observed. In these conditions Marcus-type theories for electron transfer are no more valid since injection is completed on a timescale much shorter than any nuclear relaxation process. Therefore we propose that the electron injection kinetics for N3 on TiO$_2$ obeys a delocalization/relaxation model where the limiting step is given by electron dephasing in the semiconductor's conduction band.

These findings provide a new perspective for the discussion of the electron injection processes relevant to dye-sensitized solar cells. Selecting dyes less prone to aggregate like Z105, the way is open for further investigations without the bias induced by the poor arrangement of the sensitizers on the surface. Under such conditions the effects of electronic coupling using different dyes or the importance of the distribution of acceptor states in the semiconductor can be tackled on a much clearer basis. As mentioned in the previous chapter aggregation has also an importance in the performance of DSCs since molecules injecting with a slower rate can undergo reductive quenching in the presence of iodide.

The present results bring the importance of the control of self-assembly of adsorbates on surfaces into focus. This problem has been known for years in the scientific community concerned with silver halide photography. Unfortunately, this issue has been widely neglected by groups working on the kinetics of dye/semiconductor interfacial processes. Our work underlines the role of dye aggregation and puts it back at the center of the discussion.

5.5 References

1. Grätzel, M. "Photoelectrochemical cells", *Nature* **2001,** *414,* 338-344.

2. O'Regan, B.; Grätzel, M. "A Low-Cost, High-Efficiency Solar-Cell Based on Dye-Sensitized Colloidal TiO_2 Films", *Nature* **1991,** *353,* 737-740.

3. Nazeeruddin, M. K.; Kay, A.; Rodicio, I.; Humphry-Baker, R.; Müller, E.; Liska, P.; Vlachopoulos, N.; Grätzel, M. "Conversion of Light to Electricity by Cis-X_2bis(2,2'-Bipyridyl-4,4'-Dicarboxylate)Ruthenium(II) Charge-Transfer Sensitizers (X = Cl^-, Br^-, I^-, CN^-, and SCN^-) on Nanocrystalline TiO_2 Electrodes", *J. Am. Chem. Soc.* **1993,** *115,* 6382-6390.

4. Grätzel, M.; Moser, J. E. Electron Transfer in Chemistry. In , Vol. 5; Balzani, V., Ed.; Wiley-VCH: 2001; Chapter "Solar Energy Conversion", pages 589–641.

5. Tachibana, Y.; Moser, J. E.; Grätzel, M.; Klug, D. R.; Durrant, J. R. "Subpicosecond interfacial charge separation in dye-sensitized nanocrystalline titanium dioxide films", *J. Phys. Chem.* **1996,** *100,* 20056-20062.

6. Hannappel, T.; Burfeindt, B.; Storck, W.; Willig, F. "Measurement of ultrafast photoinduced electron transfer from chemically anchored Ru-dye molecules into empty electronic states in a colloidal anatase TiO_2 film", *J. Phys. Chem. B* **1997,** *101,* 6799-6802.

7. Das, S.; Kamat, P. V. "Spectral characterization of the one-electron oxidation product of cis-bis(isothiocyanato)bis(4,4 '-dicarboxylato-2,2 '-bipyridyl) ruthenium(II) complex using pulse radiolysis", *J. Phys. Chem. B* **1998,** *102,* 8954-8957.

8. Moser, J. E.; Noukakis, D.; Bach, U.; Tachibana, Y.; Klug, D. R.; Durrant, J. R.; Humphry-Baker, R.; Grätzel, M. "Comment on measurement of ultrafast photoinduced electron transfer from chemically anchored Ru-dye molecules into empty electronic states in a colloidal anatase TiO_2 film", *J. Phys. Chem. B* **1998,** *102,* 3649-3650.

9. Ellingson, R. J.; Asbury, J. B.; Ferrere, S.; Ghosh, H. N.; Sprague, J. R.; Lian, T. Q.; Nozik, A. J. "Dynamics of electron injection in nanocrystalline titanium dioxide films sensitized with [Ru(4,4'-dicarboxy-2,2'-bipyridine)$_2$(NCS)$_2$] by infrared transient absorption", *J. Phys. Chem. B* **1998,** *102,* 6455-6458.

10. Heimer, T. A.; Heilweil, E. J.; Bignozzi, C. A.; Meyer, G. J. "Electron injection, recombination, and halide oxidation dynamics at dye-sensitized metal oxide interfaces", *J. Phys. Chem. A* **2000,** *104,* 4256-4262.

11. Kallioinen, J.; Benkö, G.; Myllyperkiö, P.; Khriachtchev, L.; Skårman, B.; Wallenberg, R.; Tuomikoski, M.; Korppi-Tommola, J.; Sundström, V.; Yartsev, A. P. "Photoinduced ultrafast dynamics of Ru(dcbpy)$_2$(NCS)$_2$- sensitized nanocrystalline TiO_2 films: The influence of sample preparation and experimental conditions", *J. Phys. Chem. B* **2004,** *108,* 6365-6373.

12. Benkö, G.; Kallioinen, J.; Korppi-Tommola, J. E. I.; Yartsev, A. P.; Sundström, V. "Photoinduced ultrafast dye-to-semiconductor electron injection from nonthermalized and thermalized donor states", *J. Am. Chem. Soc.* **2002,** *124,* 489-493.

13. Benkö, G.; Myllyperkiö, P.; Pan, J.; Yartsev, A. P.; Sundström, V. "Photoinduced electron injection from $Ru(dcbpy)_2(NCS)_2$ to SnO_2 and TiO_2 nanocrystalline films", *J. Am. Chem. Soc.* **2003,** *125,* 1118-1119.

14. Benkö, G.; Kallioinen, J.; Myllyperkiö, P.; Trif, F.; Korppi-Tommola, J. E. I.; Yartsev, A. P.; Sundström, V. "Interligand electron transfer determines triplet excited state electron injection in RuN3-sensitized TiO_2 films", *J. Phys. Chem. B* **2004,** *108,* 2862-2867.

15. Kallioinen, J.; Benkö, G.; Sundström, V.; Korppi-Tommola, J. E. I.; Yartsev, A. P. "Electron transfer from the singlet and triplet excited states of $Ru(dcbpy)_2(NCS)_2$ into nanocrystalline TiO_2 thin films", *J. Phys. Chem. B* **2002,** *106,* 4396-4404.

16. Durrant, J. R.; Tachibana, Y.; Mercer, I.; Moser, J. E.; Grätzel, M.; Klug, D. R. "The excitation wavelength and solvent dependance of the kinetics of electron injection in $Ru(dcbpy)_2(NCS)_2$ sensitized nanocrystalline TiO_2 films", *Z. Phys. Chem.* **1999,** *212,* 93-98.

17. Tachibana, Y.; Haque, S. A.; Mercer, I. P.; Durrant, J. R.; Klug, D. R. "Electron injection and recombination in dye sensitized nanocrystalline titanium dioxide films: A comparison of ruthenium bipyridyl and porphyrin sensitizer dyes", *J. Phys. Chem. B* **2000,** *104,* 1198-1205.

18. Tachibana, Y.; Haque, S. A.; Mercer, I. P.; Moser, J. E.; Klug, D. R.; Durrant, J. R. "Modulation of the rate of electron injection in dye-sensitized nanocrystalline TiO_2 films by externally applied bias", *J. Phys. Chem. B* **2001,** *105,* 7424-7431.

19. Tachibana, Y.; Nazeeruddin, M. K.; Grätzel, M.; Klug, D. R.; Durrant, J. R. "Electron injection kinetics for the nanocrystalline TiO_2 films sensitised with the dye $(Bu_4N)_2Ru(dcbpyH)_2(NCS)_2$", *Chem. Phys.* **2002,** *285,* 127-132.

20. Asbury, J. B.; Ellingson, R. J.; Ghosh, H. N.; Ferrere, S.; Nozik, A. J.; Lian, T. Q. "Femtosecond IR study of excited-state relaxation and electron-injection dynamics of $Ru(dcbpy)_2(NCS)_2$ in solution and on nanocrystalline TiO_2 and Al_2O_3 thin films", *J. Phys. Chem. B* **1999,** *103,* 3110-3119.

21. Asbury, J. B.; Hao, E.; Wang, Y. Q.; Ghosh, H. N.; Lian, T. Q. "Ultrafast electron transfer dynamics from molecular adsorbates to semiconductor nanocrystalline thin films", *J. Phys. Chem. B* **2001,** *105,* 4545-4557.

22. Asbury, J. B.; Anderson, N. A.; Hao, E. C.; Ai, X.; Lian, T. Q. "Parameters affecting electron injection dynamics from ruthenium dyes to titanium dioxide nanocrystalline thin film", *J. Phys. Chem. B* **2003,** *107,* 7376-7386.

23. Kuciauskas, D.; Monat, J. E.; Villahermosa, R.; Gray, H. B.; Lewis, N. S.; McCusker, J. K. "Transient absorption spectroscopy of ruthenium and osmium polypyridyl complexes adsorbed onto nanocrystalline TiO_2 photoelectrodes", *J. Phys. Chem. B* **2002,** *106,* 9347-9358.

24. Bailes, M.; Cameron, P.; Lobato, K.; Peter, L. "Determination of the density and energetic distribution of electron traps in dye-sensitized nanocrystalline solar cells", *J. Phys. Chem. B* **2005,** *109,* 15429–15435.

25. Bisquert, J.; Zaban, A.; Greenshtein, M.; Mora-Sero, I. "Determination of rate constants for charge transfer and the distribution of semiconductor and electrolyte electronic energy levels in dye-sensitized solar cells by open-circuit photovoltage decay method", *J. Am. Chem. Soc.* **2004,** *126,* 13550-13559.

26. Fabregat-Santiago, F.; Mora-Sero, I.; Garcia-Belmonte, G.; Bisquert, J. "Cyclic voltammetry studies of nanoporous semiconductors. Capacitive and reactive properties of nanocrystalline TiO_2 electrodes in aqueous electrolyte", *J. Phys. Chem. B* **2003,** *107,* 758-768.

27. Rothenberger, G.; Fitzmaurice, D.; Grätzel, M. "Optical Electrochemistry - 3. Spectroscopy of Conduction-Band Electrons in Transparent Metal-Oxide Semiconductor-Films - Optical Determination of the Flat-Band Potential of Colloidal Titanium-Dioxide Films", *J. Phys. Chem.* **1992,** *96,* 5983-5986.

28. Willis, R. L.; Olson, C.; O'Regan, B.; Lutz, T.; Nelson, J.; Durrant, J. R. "Electron dynamics in nanocrystalline ZnO and TiO_2 films probed by potential step chronoamperometry and transient absorption spectroscopy", *J. Phys. Chem. B* **2002,** *106,* 7605-7613.

29. De Angelis, F.; Fantacci, S.; Selloni, A. "Time-dependent density functional theory study of the absorption spectrum of Ru(4,4 '-COOH-2,2 '-bpy)$_2$(NCS)$_2$ in water solution: influence of the pH", *Chem. Phys. Letters* **2004,** *389,* 204-208.

30. Monat, J. E.; Rodriguez, J. H.; McCusker, J. K. "Ground- and excited-state electronic structures of the solar cell sensitizer bis(4,4'-dicarboxylato-2,2'-bipyridine)bis(isothiocyanato)ruthenium(II)", *J. Phys. Chem. A* **2002,** *106,* 7399-7406.

31. Bhasikuttan, A. C.; Okada, T. "Excited-state relaxation dynamics of Ru(dcbpy)$_2$(NCS)$_2$, studied by fluorescence upconversion spectroscopy", *J. Phys. Chem. B* **2004,** *108,* 12629-12632.

32. Waterland, M. R.; Kelley, D. F. "Photophysics and relaxation dynamics of Ru(4,4 ' dicarboxy-2,2 '-bipyridine)$_2$cis(NCS)$_2$ in solution", *J. Phys. Chem. A* **2001,** *105,* 4019-4028.

33. Sauve, G.; Cass, M.; Coia, G.; Doig, S.; Lauermann, I.; Pomykal, K.; Lewis, N. "Dye sensitization of nanocrystalline titanium dioxide with osmium and ruthenium polypyridyl complexes", *J. Phys. Chem. B* **2000,** *104,* 6821–6836.

34. Anderson, N. A.; Lian, T. "Ultrafast electron injection from metal polypyridyl complexes to metal-oxide nanocrystalline thin films", *Coord. Chem. Rev.* **2004,** *248,* 1231-1246.

35. Barbe, C. J.; Arendse, F.; Comte, P.; Jirousek, M.; Lenzmann, F.; Shklover, V.; Grätzel, M. "Nanocrystalline titanium oxide electrodes for photovoltaic applications", *J. Am. Ceram. Soc.* **1997,** *80,* 3157-3171.

36. Nazeeruddin, M. K.; Humphry-Baker, R.; Liska, P.; Grätzel, M. "Investigation of sensitizer adsorption and the influence of protons on current and voltage of a dye-sensitized nanocrystalline TiO_2 solar cell", *J. Phys. Chem. B* **2003,** *107,* 8981-8987.

37. Bonhôte, P.; Dias, A. P.; Papageorgiou, N.; Kalyanasundaram, K.; Grätzel, M. "Hydrophobic, highly conductive ambient-temperature molten salts", *Inorg. Chem.* **1996,** *35,* 1168-1178.

38. Shklover, V.; Ovchinnikov, Y. E.; Braginsky, L. S.; Zakeeruddin, S. M.; Grätzel, M. "Structure of organic/inorganic interface in assembled materials comprising molecular components. Crystal structure of the sensitizer bis[(4,4 '-carboxy-2,2 '-bipyridine)(thiocyanato)]ruthenium(II)", *Chem. Mater.* **1998,** *10,* 2533-2541.

39. Zakeeruddin, S. M.; Nazeeruddin, M. K.; Pechy, P.; Rotzinger, F. P.; Humphry-Baker, R.; Kalyanasundaram, K.; Grätzel, M.; Shklover, V.; Haibach, T. "Molecular engineering of photosensitizers for nanocrystalline solar cells: Synthesis and characterization of Ru dyes based on phosphonated terpyridines", *Inorg. Chem.* **1997,** *36,* 5937-5946.

40. Lanzafame, J. M.; Palese, S.; Wang, D.; Miller, R. J. D.; Muenter, A. A. "Ultrafast Nonlinear-Optical Studies of Surface-Reaction Dynamics - Mapping the Electron Trajectory", *J. Phys. Chem.* **1994,** *98,* 11020-11033.

41. Turner, G. M.; Beard, M. C.; Schmuttenmaer, C. A. "Carrier localization and cooling in dye-sensitized nanocrystalline titanium dioxide", *J. Phys. Chem. B* **2002,** *106,* 11716-11719.

42. Schnadt, J.; Brühwiler, P. A.; Patthey, L.; O'Shea, J. N.; Södergren, S.; Odelius, M.; Ahuja, R.; Karis, O.; Bässler, M.; Persson, P.; Siegbahn, H.; Lunell, S.; Mårtensson, N. "Experimental evidence for sub-3-fs charge transfer from an aromatic adsorbate to a semiconductor", *Nature* **2002,** *418,* 620-623.

Distance dependence of interfacial electron transfer kinetics

Summary

The influence of the distance on the kinetics of electron transfer at dye/semi-conductor interfaces have been studied by two different approaches. In the first part we use a series of bridged sensitizers containing p-phenylene spacer groups. The rate constants for forward and back ET are found to fall off exponentially with distance but the associated damping factor are significantly different ($\beta_{\text{inj.}}$ = 0.19 Å^{-1} vs. $\beta_{\text{rec.}}$ = 0.5 Å^{-1}). In the second part, the dye was adsorbed onto core-shell nanocrystalline films made of TiO$_2$ covered with Al$_2$O$_3$ layers of controlled thickness. In this case, weak distance-dependence was observed for both electron transfers. Different reasons are invoked to explain the rather low damping factors obtained from our experiments. Although the mechanisms leading to the weak influence of the distance are not the same in the two experimental parts, these results demonstrate that charge transport over substantial distances is possible at heterogeneous interfaces.

6.1   Introduction

The distance dependence of electron transfer kinetics is a key issue in several different research fields. Long range ET (> 5 Å), especially in proteins, plays a crucial role in biochemistry, including photosynthesis and metabolism.[1] It is also at the center of current investigations in the field of molecular electronics, where the conductance in a metal-molecule-metal assembly can be regarded as an electron transfer process.[2] Interfacial electron transfer in electrochemistry, charge injection and transport through electron- or hole-transporting layers in organic light-emitting diodes (OLED), and charge separation in dye-sensitized solar cells are all strongly dependent upon the distance over which charge transfer occurs.[3]

Because of the variety of research fields concerned with this topic, various approaches have been adopted to tune the distance. In molecular electronics, electron transport accross metal-molecule-metal junction has been studied, often at a single-molecule level, by scanning probe methodologies (STM[a], AFM[b]). In these experiments, the separation between the electrodes is simply defined by the length of the molecule. Self-assembled monolayers (SAMs) of, for example thioalkanes, at metallic electrodes were widely characterized by electrochemical techniques. However, the most intense effort has been exerted on the analysis of photoinduced electron transfer in molecular, or supramolecular, donor-bridge-acceptor systems (fig. 6.1). These systems generally feature organic or inorganic donor and acceptor pairs separated by a bridge containing repeated units (CH_2, phenyl, peptides, . . .). The control of the distance is then defined by the number of units separating the photoactive species. The effect of the conjugation has been widely studied and several theoretical contributions are available.[4,5,6]

Figure 6.1 — Donor-Bridge-Acceptor system.

In dye-sensitized solar cells, the system can be regarded as a D/A system where the donor is the sensitizer and the conduction band of the semicon-

---

[a]Scanning Tunneling Microscopy
[b]Atomic Force Microscopy

ductor acts as an acceptor. As discussed earlier, the kinetic control of the forward and back electron transfer is a central issue in the development of efficient devices. In particular, the back electron transfer to the oxidized sensitizer has to be very slow in order to guarantee efficient electron collection. One way to reduce the rate of this transfer is to increase the distance between the donor and the acceptor. Attempts to control the charge separation distance will be discussed below.

In addition to the number of applications concerned by this issue, modifying the distance is an excellent way to study the electronic factors controlling electron transfer kinetics. In this chapter, we will report on the influence of distance on the electron transfer from ruthenium polypyridyl complex sensitizers to TiO_2 nanoparticles by two different approaches: a) the use of bridged-sensitizers containing phenyl spacer groups, and b) core-shell nanoparticles featuring an insulating barrier of controlled thickness.

6.1.1 Theory

Standard electron transfer theory   In the weak-coupling limit, the starting point is generally the golden-rule approach:

$$k_{ET} = \frac{2\pi}{\hbar}|H_{DA}|^2(FCWD) \tag{6.1}$$

where H_{DA} is the electronic coupling matrix element between the donor and the acceptor and FCWD are the thermally averaged Franck-Condon factors. Electron transport through a bridge is a tunnelling effect, therefore the electronic factor (H_{DA}) is expected to fall off exponentially with distance because of the exponential radial character of the electronic wavefunctions of the donor and the acceptor:

$$|H_{DA}|^2 \propto \exp\left[-\beta(r-r_0)\right] \tag{6.2}$$

where r_0 is the Van der Waals separation and β is a constant that determines the falloff rate of with distance. For chemical reactions where the FCWD changes negligibly with distance, the rate constant can be expressed as:

$$k_{ET} = k_0 \exp\left[-\beta(r-r_0)\right] \tag{6.3}$$

This is only true if the reorganization energy is very small since this parameter is also expected to change with distance. However, many chemical systems have shown an exponential falloff of k_{ET} with distance. The damping factor β has generally been found in the range 0.8-1.2 Å^{-1}, but can be as low as 0.2 Å^{-1} for π-conjugated molecules (see table 6.1).

Bridge	$\beta\,/\,\text{Å}^{-1}$
Sat. hydrocarbon	~1.0
Unsat. hydrocarbon	~0.2
DNA	0.1-1.5
Alkane	0.9-1.3
Oligophenylene	0.4-0.5
C_{60}	0.11

Table 6.1 — Typical damping factors for Donor-Bridge-Acceptor systems.[3,5,7]

The above discussion is based on the assumption that the transfer is a coherent tunneling process. This model, called *superexchange model* (see figure 6.2), is valid when the bridge contains high-lying orbitals that are never populated during the electron transfer. In these conditions, the damping factor can be calculated from:

$$\beta = 2\ln(H_{BB}/\Delta E_B) \qquad (6.4)$$

where H_{BB} is the internal coupling energy between the bridge units and ΔE_B is the energy of the mediating state above the ground state.

Another model is proposed when the electron has the possibility to reduce (or oxidize in case of hole transfer) bridge units. In this *hopping model* the charge can reside on a single unit or be delocalized over the entire bridge and diffuse by hopping between the bridge sites. If diffuse hopping becomes rate limiting, the distance dependence of the electron transfer is inversely proportional to the D/A separation:

$$k_{ET} \propto 1/N \qquad (6.5)$$

where N is the number of bridge units.

As introduced in chapter 2, golden-rule based approaches are not valid in the strong coupling limit. Therefore an exponential electron transfer rate distance dependence might be broken as one reduces the bridge length, causing a transition towards an adiabatic ET regime.

Conductance To characterize metal-molecule-metal junctions, one generally uses the Landauer equation giving the conductance g at zero Volt and zero Kelvin through a 1D conductor:

$$g = \frac{2e^2}{h}T \qquad (6.6)$$
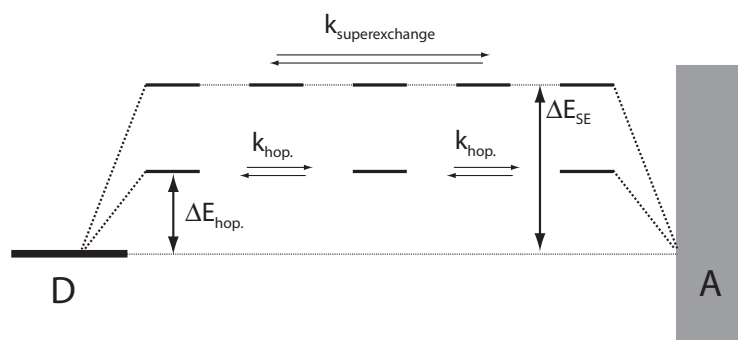
Figure 6.2 — Superexchange and hopping models for the distance dependence of the electron transfer rate constant k_{ET} between a molecular donor and a continuum of acceptor states.

where T is the transmission function containing electronic coupling strengths at the contacts and inside the molecule. Nitzan derived a relationship between the conductance and the rate constant obtained from standard ET theories.[8] This approach leads also to the estimation of the traversal time through a molecular bridge. This *tunneling time* is given by:

$$\tau = \frac{\hbar N}{\Delta E_B} \qquad (6.7)$$

where N is the number of bridge states. One should mention here that the transfer in Landauer's approach is purely a coherent electronic process. It has recently been extended in order to include incoherent processes (dephasing, relaxation)[9] but it still doesn't include nuclear factors like reorganization energy as in the standard Marcus theory. For tunneling through a molecular spacer of width ~ 10 Å, (N=2-3) and a barrier height $\Delta E_B = 1$ eV the tunneling time is about $\tau \cong 2$ fs.[2,3]

6.1.2   Literature review

Most studies of distance-dependent electron transfer kinetics at interfaces have been performed by electrochemical techniques on SAM-modified electrodes (see Smalley et al.[10] and references therein). These techniques are excellent for long-bridge electron transfer, but for shorter bridges the results are more ambiguous. Therefore, ultrafast laser techniques have been applied to study these systems. Oligophenylenevinylene bridges have been studied by the indirect laser-induced temperature jump technique. Unlike other bridges studied so far, the rate constants were not limited by electronic coupling for bridges up to 28 Å long, and the damping factor was extremely low (β=0.06 Å).[11]

Direct measurements of bridge-assisted electron transfer was investigated by transient absorption spectroscopic techniques. Lian and co-workers synthesized and studied a series of Re complexes containing 0-5 methylene bridging groups inserted between the metallic complex and the anchoring group. They applied mid-IR femtosecond spectroscopy to measure the electron injection kinetics of these complexes adsorbed on TiO_2[12] and SnO_2.[13] An exponential distance dependence was found for long bridges (3-5 methylene) with β=0.79 Å on SnO_2. For shorter bridges, a deviation from the exponential behavior was observed. It was suggested that a transition towards adiabatic ET due to strong coupling was responsible for this breakdown. Galoppini et al. synthesized a family of rigid-rod and tripodal linkers to anchor sensitizers to the surface of semiconductors.[14] These assemblies are made of a chromophore (Ru polypyridyl complex, pyrene, ...) covalently attached to a rigid spacer made of p-phenyleneethynylene units and anchored to the semiconductor by rigid tripodal or simply two COOR groups. An astonishing subpicosecond injection rate was observed over a distance of 24 Å, indicating important delocalization of the excited state over the rigid spacer arm.[15] Most of these sensitizers were studied in the nanosecond time domain and injection was found to happen within the pulse rise ($k_{inj} > 10^8$ s^{-1}). More recently, the perylene-based tripodal sensitizer was used in conjunction with other perylene sensitizers by the group of Willig who performed femtosecond spectroscopic measurements in ultra-high vacuum.[16,17] They measured time constants ranging from 13 fs (Pe'-COOH) to 4 ps (Pe'-tripod) and found an exponential dependence upon distance with $\beta = 1$ Å^{-1}.

More reports are available for back electron transfer from the semiconductor to the oxidized sensitizer. The tripodal sensitizers were extensively studied in a series of papers by nanosecond spectroscopy.[18,19,20,21] Surprisingly, no clear dependence on the distance was observed. The authors suggested that the relatively constant kinetics were governed by the trapping/detrapping processes in the semiconductor. The lengthening of the bridge does not lead in all instances to slower kinetics, especially if the linker is too flexible as it is the case for alkyl spacers,[22] or when bending is easy as observed for one-carboxyl anchoring groups.[23] Interestingly, distance sensitivity was observed for back electron transfer from SnO_2 nanoparticles to weakly (electrostatically) bound metal complexes, suggesting the kinetics as controlled by electronic coupling rather than nuclear motion.[24] Here, a mechanism involving deep trap states was proposed to explain the results. Comparison of a series of ruthenium bipyridyl and Zn-porphyrins showed a strong dependence when the distance varied over only 3 Å ($\beta = 0.95$ Å^{-1}).[25]

Another approach to slow down back transfer without altering the injection rate is achieved by the so-called *molecular dyads*. This stategy was first applied by Bonhôte et al. who grafted a triarylamine moiety on ruthenium

terpyridyl complexes. In theses assemblies, ultrafast (< 1 ns) electron injection is followed by fast (10-20 ns) hole transfer to the triarylamine. The charge separated state had a half-lifetime of 3 - 300 μs, depending on the distance between the surface of TiO_2 and the oxidized amine. The distance dependence was lower than expected and it was suggested that the dyads adopted a tilted orientation on the surface.[26] Other dyads have been synthesized and very long-lived (4 s) charge separation has been achieved by this strategy.[27,28]

Alternatively, insulating layers of large band gap metal oxides have been used as barriers for back electron transfer in DSCs.[29,30,31,32,33,34] In this approach, both electron transfers (forward and back ET) should be retarded. As the injection rate is more than 1000 times faster than the lifetime of the excited state, it is expected that high charge separation yields will still be achieved while retardation of back transfer will improve electron collection. Indeed, a slightly better performance is attained in such devices. The origin of the back ET retardation has been imputed primarily to two effects: a) the passivation of the TiO_2 surface reducing the number of surface traps and b) the decrease of electronic coupling due to the increased distance.[35] So far no systematic study of the distance effect has been carried out on this type of interfaces.

In this chapter, we report on the distance dependence of interfacial electron transfer by two different approaches. First, bridged sensitizers, featuring ruthenium terpyridyl complexes separated from the surface by 0-2 phenyl units have been studied with various time-resolved techniques in order to characterize both the forward and the back transfer. In a second phase, we used Al_2O_3/TiO_2 core-shell nanoparticles with insulating layers of controlled thickness to investigate the retardation of both charge transfers.

6.2   Experimental part

6.2.1   Materials

The dyes P0, P1 and P2 (also known as Z235, N773 and N790) were synthesized by Drs. Zakeeruddin and Nazeeruddin in our institute. The design of these dyes is based on the well-known "black dye".[36] TiO_2 nanocrystalline films (8 μm-thick) were soaked overnight in the dye solutions ($\sim$ 0.3 mM in EtOH). After dyeing they were rinsed with ethanol and left to dry. No solvent was added.

(a) P0 (Z235)   (b) P1 (N773)   (c) P2 (N790)
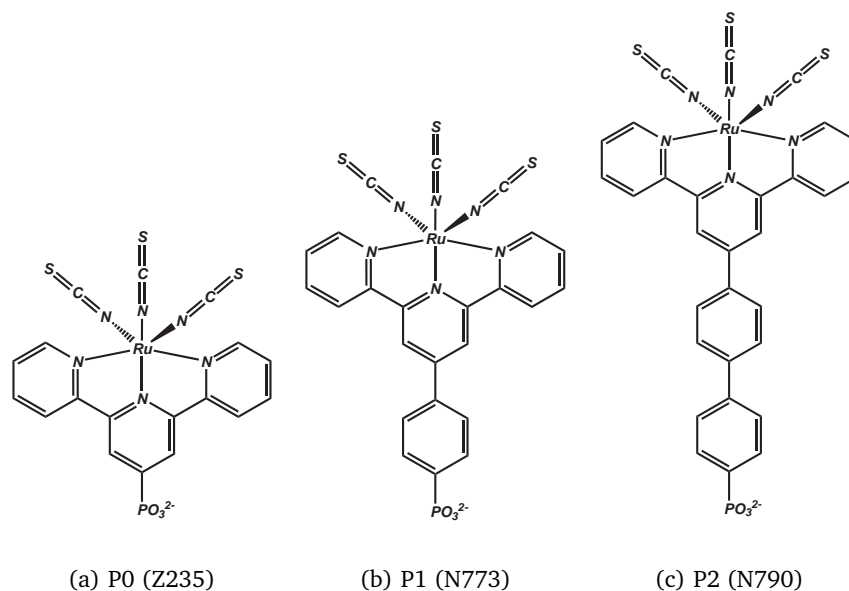
Figure 6.3 — Dye sensitizers used in this study.
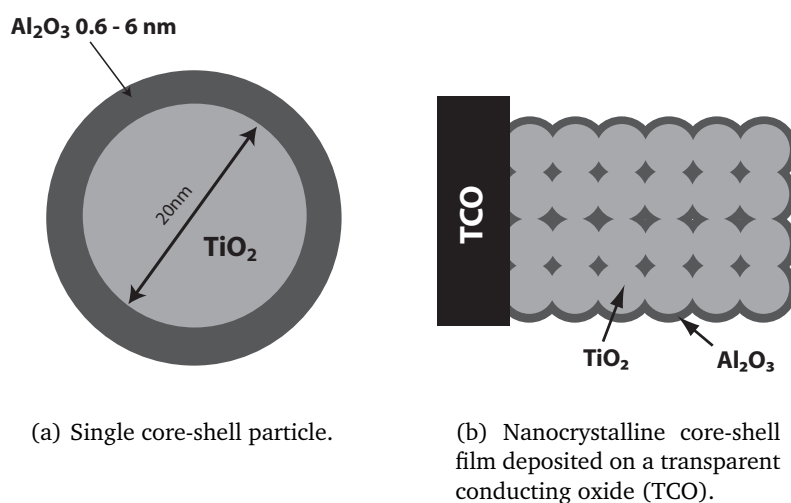
Films made of core-shell nanoparticles were prepared by the group of Prof. Schoonman at ECN, Delft (Netherlands). Al_2O_3 was deposited on TiO_2 nanocrystalline films prepared as described earlier, except that the substrate was made of conductive glass. The atomic layer deposition (ALD) technique allowed the control of the insulating layer thickness. ALD is a modification of CVD[c] with the major difference that, in ALD, the gas reactants are introduced sequentially into the reaction chamber. A deposition cycle consists typically of a) the exposure of the film to a precursor (containing aluminum) followed by b) the oxidation of the precursor to form alumina. Five cycles are needed to form a complete monolayer (3 Å). Films modified by 0, 10, 20, 25, 30, 40, 50 and 100 cycles (resp. 0.6, 1.2, 1.5, 1.9, 2.4, 3.0 and 6.0 nm thicknesses) were available. Regrettably, the entire process and the details of the films characterization could not be obtained. The films were dipped overnight in 0.3 mM ethanolic solutions of P0 (Z235).

6.2.2   Methods

Ultrafast kinetics were measured in the two-colors pump-probe scheme (see chapter 3). The pump (535 nm) and probe wavelength (570 nm) were

---

[c]Chemical Vapour Deposition

(a) Single core-shell particle.

(b) Nanocrystalline core-shell film deposited on a transparent conducting oxide (TCO).

Figure 6.4 — Al_2O_3/TiO_2 core-shell nanocrystalline films.

tuned by the two NOPAs. The intensities of both pulses were reduced to less than 1 μJ. The samples were constantly translated in order to avoid degradation mainly due to heat. The pump beam proceeded through the 700 ps translation stage. Both beams were focused on the sample by a single large size (ø= 76 mm) off-axis parabolic mirror.

Transient absorption measurements were carried out in the experimental setup described previously (section 3.2). The excitation laser beam was tuned by the OPO at a wavelength of 535 nm. The detection light provided by the Xenon lamp is tuned manually at the indicated wavelengths. Steady-state absorption was measured by a HP-8353 spectrophotometer (Hewlett-Packard).

6.3 Results

6.3.1 Bridged sensitizers

Steady-state absorption

All three dyes show the same spectral signature in ethanolic solutions. The spectrum is dominated in the visible range by two MLCT bands at 570 and 530 nm. In comparison with the black dye,[36] which has three carboxylic

groups on the terpyridyl ligand, the spectrum is considerably blue-shifted. In fact it resembles strongly the analogous [Ru$^{\text{II}}$(terpy)(NCS)$_3$] dye[36] showing that the phosphonate group has a weak influence on the absorption properties. As expected, the phenyl units of the bridge do not participate in the MLCT transitions. When the dyes are adsorbed onto the surface of TiO$_2$ no particular change is observed. In contrast to carboxylated dyes, deprotonation upon attachment to the surface has no influence on the photophysics.
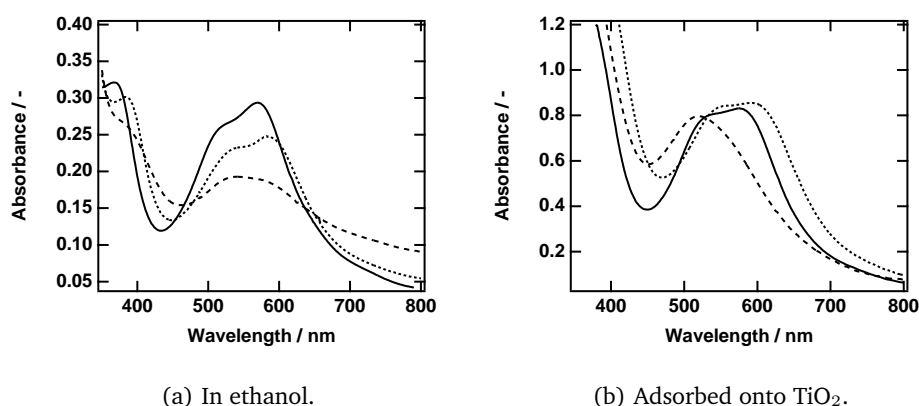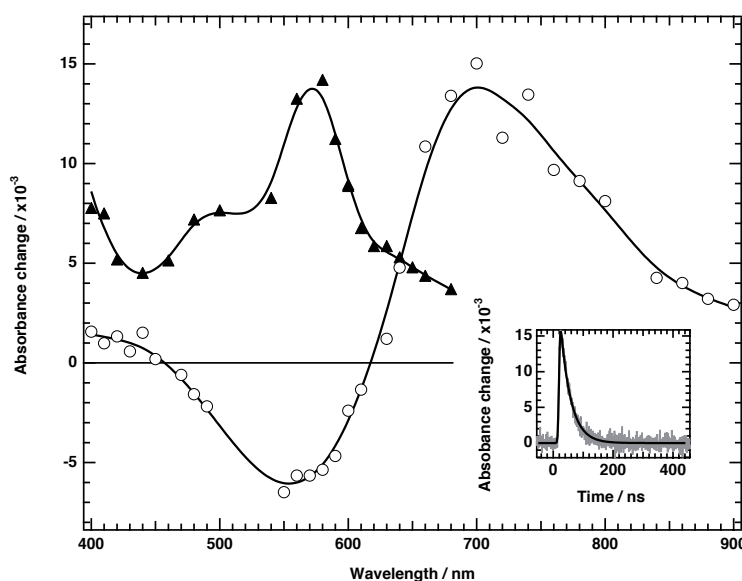

(a) In ethanol.   (b) Adsorbed onto TiO$_2$.

Figure 6.5 — Absorption spectra of P0 (full), P1(dotted) and P2 (dashed).

Transient absorption spectra

The transient absorption spectra of P0 in ethanol and adsorbed on the surface of TiO$_2$ have been measured in the ns-μs time domain. The results are shown in figure 6.6. Strikingly, no bleaching is observed in solution. This means that the excited state has a bigger extinction coefficient than the ground state in the entire the visible range. The spectrum of the excited state is probably dominated in its red part by LMCT transitions from the triplet state usually formed in a few hundreds of femtoseconds in this type of complexes.[37] For shorter wavelengths (500-600 nm), we attribute the strong absorption to ligand-centered transitions of the terpyridyl anion.[38]. A lifetime of 34 ns was measured after fitting the decay trace at 570 nm with a single exponential convoluted with a Gaussian instrument response (FWHM = 7.1 ns).

The difference spectrum on TiO$_2$ is significantly modified in comparison with the one obtained in solution. The bleaching of the ground state is this time noticeable with a minimum corresponding roughly to the MLCT peak. For longer wavelengths, the spectrum shows a broad positive peak centered around 700 nm that we attribute to the oxidized state of the dye.

Figure 6.6 — Transient absorption spectrum of P0 dye in ethanol (▲, after 30 ns), and adsorbed on TiO$_2$ (○, after 1μs). The inset shows the decay of the excited state observed at 570 nm in MPN (lifetime : 34 ns).

As for N3 derivatives (see chapter 4), the absorption of the dye cation is dominated by LMCT bands originating from the thiocyanate ligands. This transient is long-lived and decays on a microsecond timescale.

Electron transfer kinetics

Electron injection   From the transient spectral signatures of the excited and oxidized states presented above, we chose to probe the samples at 570 nm. At this wavelength the excited state yields a positive signal, whereas the bleaching of the ground state dominates when the excited state is formed. The transient traces recorded for P0, P1 and P2 are shown in figure 6.7. All three dyes show the formation of a positive signal corresponding to absorption of the excited state followed by a fast, multiexponential decay that we attribute to the formation of the dye cation by electron transfer to the semiconductor's conduction band. Interestingly, a negative signal was observed after less than 1 ps for P0 and $\sim$ 500 ps for P1 but was not visible for P2 within the duration of the measurement (700 ps). This shows that the excited dyes are still present for P1 and P2 after a considerable delay, suggesting that the injection quantum yield is much less than unity in contrast to the observations made for non-bridged dyes. The data were satisfactorily fitted with biexponential decays convoluted with a Gaussian instrument re-

sponse. The time constants and the relative amplitudes of both exponential decays are given in table 6.2.
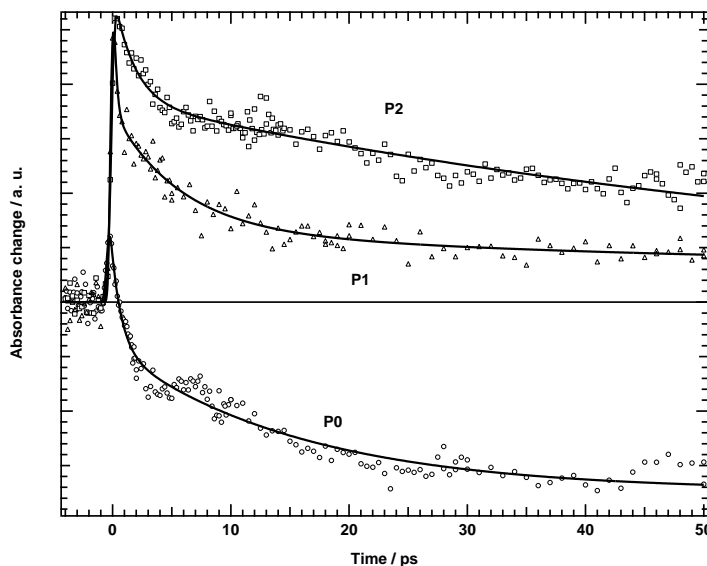
Figure 6.7 — Transient absorption dynamics of P0 (O), P1($\triangle$) and P2 ($\square$) dyes adsorbed on TiO$_2$. Pump: 535 nm, probe: 570 nm.

Dye	Time constants and amplitudes	
	fs	*ps*
P0	850 (48 %)	16 (52 %)
P1	1750 (39 %)	73 (61 %)
P2	5760 (75 %)	51 (25 %)

Table 6.2 — Biexponential fitting parameters for the transient absorption traces shown in figure 6.7.

Assuming the distance dependence of the kinetics is mainly controlled by the change in the electronic coupling between the donor and the acceptor, the rate constant should decay exponentially with the distance:

$$k_{ET} \cong k_0 \exp\left[-\beta(r - r_0)\right] \tag{6.8}$$

where r$_0$ is the van der Waals separation. The damping factor β can be estimated from the semi-logarithmic plot of the rate constants with respect to distance as shown in figure 6.8. The distance corresponds to the separation between the ruthenium atom of the sensitizer and the nearest titanium atom of the TiO$_2$ surface. These parameters were calculated from semi-empirical geometry optimizations (ZINDO) carried out with the CAChe software package. The rate constants of the fast part of the decays followed an almost perfect linear trend leading to $\beta = 0.19 \pm 0.01$ Å^{-1}, while no trend is observed for the slow part.
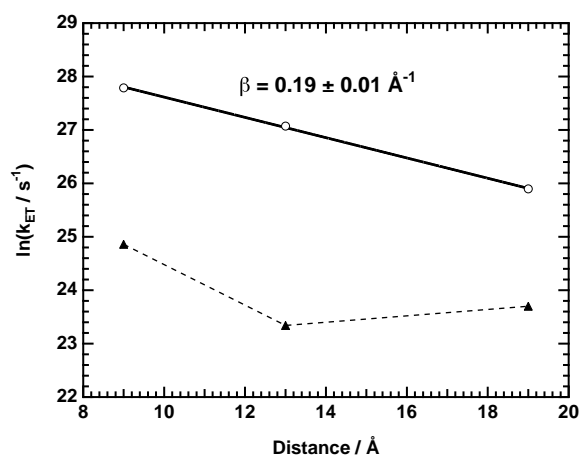
Figure 6.8 — Semi-log plot of the rate constant for the fast part (O), and the slow part (▲) of the biexponential fits of figure 6.7. The slope of the linear fit for the fast rate constants is -0.19 ± 0.01 Å.

Back electron transfer The kinetics of the recombination reaction between the injected electrons in the semiconductor and the oxidized dye have been studied by nanosecond transient absorption spectroscopy. At low light intensity, the transient traces recorded at 600 nm could be fitted with a single exponential decay. Again, the fitted time constants are plotted versus the distance in order to estimate the damping factor β (figure 6.9). Although the linear trend is less obvious than for the injection reaction, we find $\beta = 0.5 \pm 0.1 \text{ Å}^{-1}$.
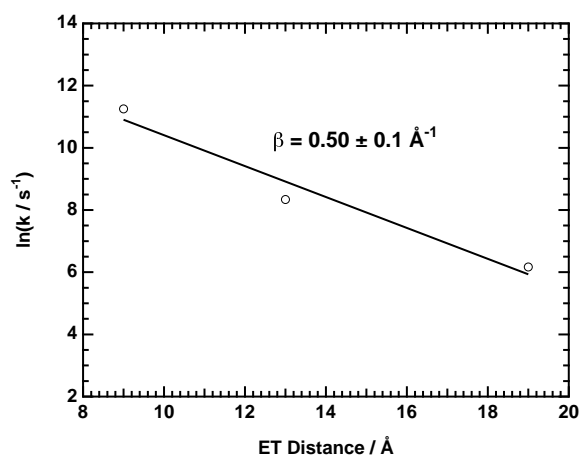

Figure 6.9 — Back electron transfer time constants with respect to the charge separation distance for bridged sensitizers.

6.3.2   Core-shell nanocrystalline films

Steady-state absorption

All core-shell nanocrystalline films were dyed with P0 (Z235) sensitizer. Figure 6.10 shows the steady-state absorption spectra of this dye on Al_2O_3, TiO_2 and Al_2O_3/TiO_2 core-shell nanocrystalline films. Again, no spectral change is observed when adsorbed on the different substrates. The differences in the intensities are not indicative of the coverage of the surface but rather of the different porosity and thicknesses of the different materials.
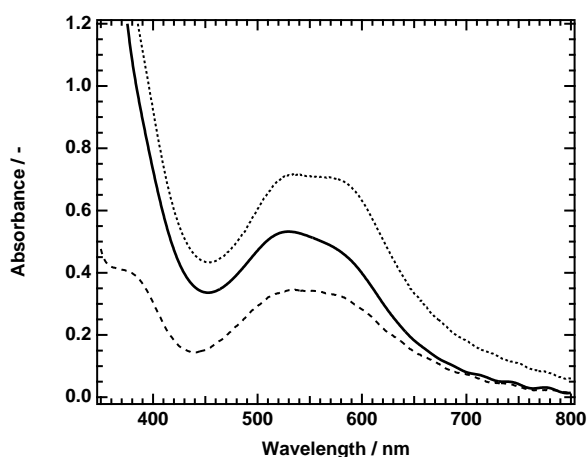

Figure 6.10 — Steady-state absorption of P0 adsorbed on Al_2O_3/TiO_2 1.2 nm-thick core-shell film (full), Al_2O_3 (dashed) and TiO_2 (dotted).

Back electron transfer kinetics

Nanosecond transient absorption measurements have been performed on core-shell films containing alumina layers of 0, 6, 12, 15, 18, 24, 30 and 60 Å thicknesses. The excitation laser beam (535 nm) was intentionally kept at a low intensity ($< 80~\mu J/cm^2$) to ensure that, on average, less than one e_{cb}^-/S^+ charge-separated pair was produced per nanocrystalline particle upon pulsed irradiation. Under such conditions, first-order kinetics have been reported for charge recombination at Ru complexes/TiO_2 interfaces.[39] Here, the kinetics were still strongly multiexponential although no intensity dependence was observed at such low fluences. The lifetime of the oxidized state formed upon electron injection to the semiconductor was monitored at 650 nm. In order to compare the samples we measured the half-lifetime ($t_{1/2}$) of the oxidized state to quanitify the recombination rate. Selected

traces, shown in figure 6.11, illustrate that the recombination rate varies over several orders of magnitude, spanning from $t_{1/2} = 6$ μs for bare TiO_2 to $t_{1/2} = 0.06$ s for 60 Å-thick alumina layers. Obviously, the presence of dyes in their excited state can be ruled out owing to the transients observed, which are significantly longer than the lifetime of the excited state (34 ns).
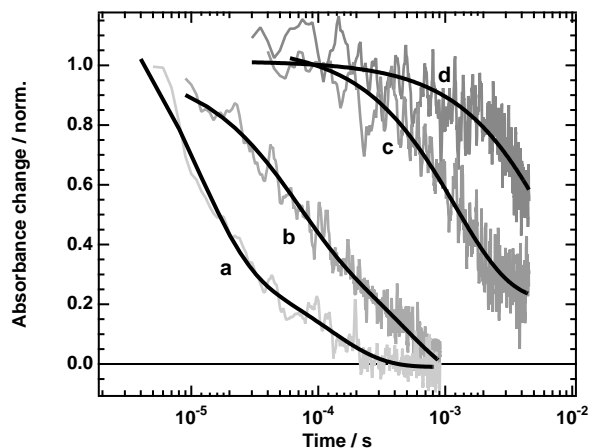
Figure 6.11 — Transient absorption traces of P0-sensitized core-shell films. Pump: 535 nm, probe: 650 nm. Al_2O_3 layer thickness: a) 0 nm, b) 1.8 nm, c) 3.0 nm, d) 6.0 nm.

Figure 6.12 depicts the dependence of the half-lifetimes with respect to the thickness of the alumina barrier. Again, an exponential relation was found, and the damping parameter obtained from the slope of the semi-logarithmic plot is $\beta = 0.15 \pm 0.01$ Å^{-1}.
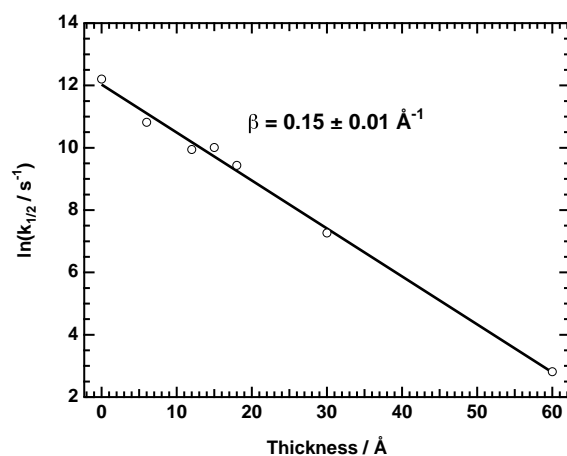
Figure 6.12 — Semi-log plot of $k_{1/2}$ versus Al_2O_3 layer thickness for P0-sensitized core-shell nanoparticles. The slope of the linear fit is -0.15 $\pm$ 0.01 Å.

Electron injection kinetics

The forward electron transfer from P0 sensitizer to core-shell nanocrystalline films was measured by femtosecond pump-probe spectroscopy. The pump pulse (530 nm) prepared the dye in a state from where it can inject an electron into the semiconductor either directly from its vibrationally excited state ("hot state") or after vibrational relaxation. As shown earlier, at 570 nm the excited state shows a positive absorption change whereas the formation of the dye cation, upon electron transfer to the semiconductor, yields a negative signal, indicative of a bleach of the ground state. The transient absorption traces obtained on core-shell substrates with various alumina thicknesses are depicted in figure 6.13. Vibrational relaxation for this type of complexes is expected to happen in a few picoseconds.[37] The trace observed for the 60 Å layer (trace d of fig. 6.13) clearly indicates that cooling of the molecule does not lead to spectral changes at the selected wavelength. Therefore we assume that the excited state dynamics observed only reflect two processes: 1) deactivation of the excited state, and 2) electron transfer to the semiconductor. Back electron transfer is not expected to take place on this timescale as discussed in the previous section.

The injection rate of P0 into TiO_2 was previously reported to be multiexponential with time constants of 820 fs (49 %) and 17.5 ps (51 %).[40] However, a faster component could not be resolved due to the limited instrument response (200 fs). Here, with the noticeable exception of the 60 Å-thick sample, all traces show an ultrafast decay with a sub-100 fs time constant. This component is then followed by a slower part that has been fitted with two additional exponential decays convoluted with the same Gaussian instrument response. In addition to the traces shown in figure 6.13, measurements with core-shell films with 6, 15 and 18 Å-thick Al_2O_3 layers were performed. All showed strongly heterogeneous kinetics with time constants between tens of fs and tens of ps.

Trace	Al_2O_3 thickness	Time constants and amplitudes
	nm	*fs/ps*
a	1.2	71 fs (8 %), 1.1 ps (28 %), 16 ps (64 %)
b	2.4	44 fs (0.3 %), 4.7 ps (53 %), 71 ps (45 %)
c	3.0	76 fs (15 %), 900 fs (20 %), 41 ps (31 %)
d	6.0	240 ps (93 %)

Table 6.3 — Fitting parameters for the transient absorption traces shown in figure 6.13.

Due to the high number of time constants needed to describe each kinetic trace, we could not reasonably build a semi-logarithmic plot of the rate
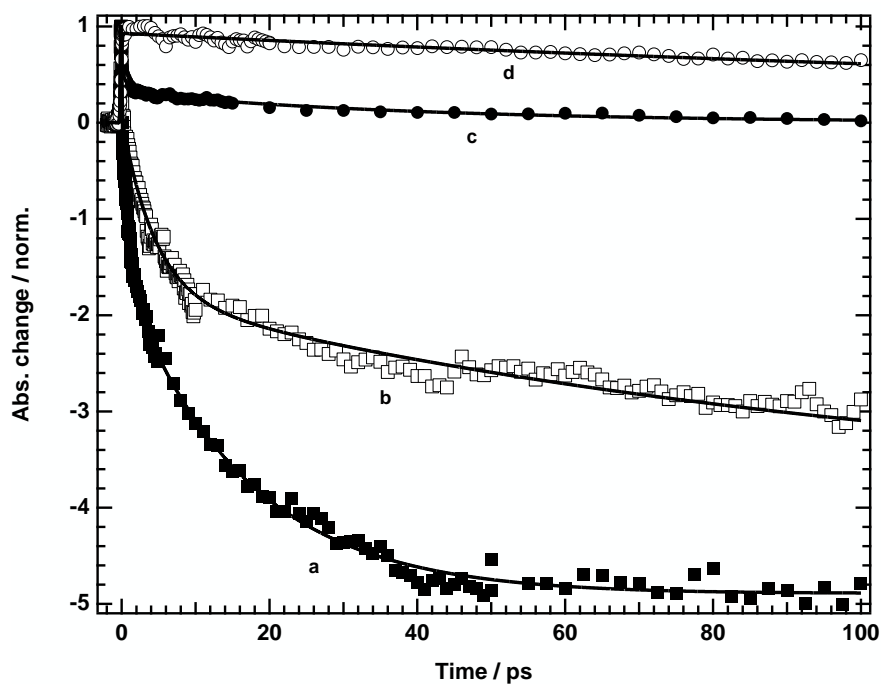
(a) Full timescale
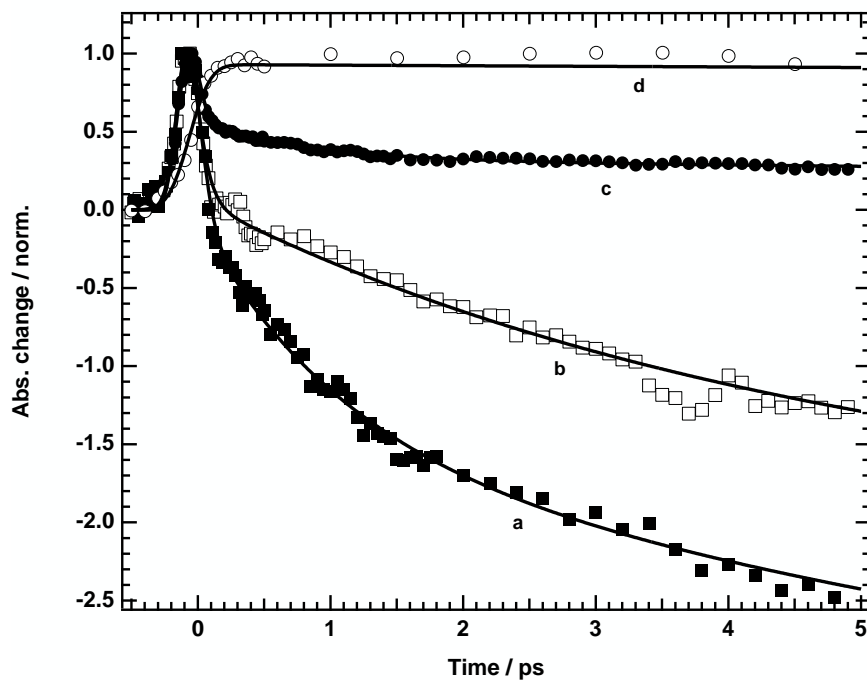
(b) Detail

Figure 6.13 — Transient absorbance of Z235-sensitized Al_2O_3/TiO_2 core-shell films. Pump: 530 nm, probe: 560 nm. Alumina layer thickness: a) 1.2 nm; b) 2.4 nm; c) 3.0 nm; d) 6.0 nm.

constants with respect to distance. Therefore, an exponential dependence upon distance as observed for bridged sensitizers or for the back electron transfer in core-shell assemblies, can not be validated in this case. However, qualitative examination of figure 6.13 indicates that the alumina layer has a strong influence on the formation of the oxidized state. For relatively thin layers (12 Å), the reaction is complete in less than 100 ps. In contrast, almost nothing is observed for very thick layers (60 Å) during the same time. It is not clear from these experiments if the small decay observed for the latter trace is due to electron injection or simply excited state relaxation. The fit yields a time constant of 240 ps which is much shorter than the lifetime of the excited state in solution (34 ns), but significant errors can still arise because the fit only covers a small part of the complete decay. However, the nanosecond data showed that electrons are injected into these films suggesting that the 240 ps time constant actually corresponds to the electron transfer process.

We simulated the effect of different values of the decay parameter β on the kinetics of electron transfer with the insulating barrier thicknesses available in this study (figure 6.14). We used equation 6.8, where k_0 was set to $1/820$ fs^{-1}, corresponding to the injection rate into bare TiO$_2$, and (r - r_0) is equal to the thickness of the alumina layer. Our experimental results clearly show that electron injection occurs with a relatively high quantum yield for barriers as thick as 20-30 Å. Since this process is in competition with the relaxation of the excited state, the time constant has to be lower than 10^{-9} s. From our plot we see that this condition is achieved only for β < 0.3 Å^{-1}. More likely, in comparison with the time constants measured experimentally (tens of picoseconds), β should be around 0.1-0.2 Å^{-1}. These values are consistent with those obtained for back electron transfer and also for bridged sensitizers.

6.4   Discussion

The distance dependence of the electron transfer kinetics at dye/semiconductor interfaces have been studied by two different approaches: a) the use of bridged sensitizers, and b) the application of an insulating shell on TiO$_2$ core nanoparticles. Transient absorption spectroscopy in the fs-ps and μs-s time domains made it possible to quantify the electron transfer rates for both forward and back electron transfers. The results are in good agreement with an exponential dependence of the rate constant upon distance as predicted for electron tunneling processes. The damping parameter β estimated from
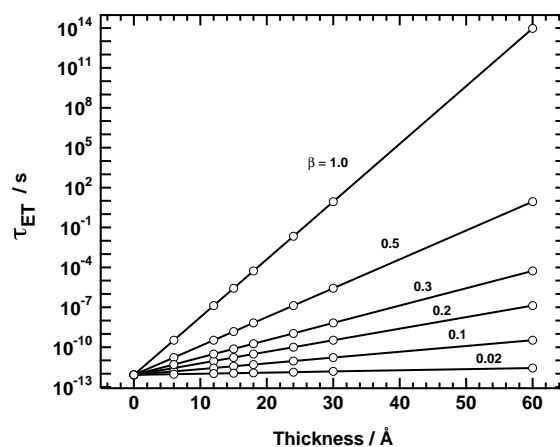
Figure 6.14 — Simulation of the dependence of the time constant for electron transfer from P0 to TiO_2 versus the thickness of an insulating layer. The damping parameter β is varied from 0.02 to 1 Å^{-1}.

the different experiments is close to constant, around 0.1-0.2 Å^{-1}, indicative of a weak distance dependence.

Bridged sensitizers

Biphasic kinetics were observed for the forward electron transfer by femtosecond spectroscopy. Strikingly, the rate of the first component follows a nearly perfect exponential law, while no such trend is found for the second component. In the light of the results presented in the previous chapters, we presume that the second component is representative of electron transfer occuring from aggregated dyes. This would explain the rate difference between the two components (3 orders of magnitude), and also the lack of a uniform trend since the orientation of the dyes in a second adsorption sphere is not likely to be homogeneous. For these reasons, we will only discuss the first component, characteristic of strongly adsorbed sensitizers.

Interestingly, the distance parameter β estimated from the fit of the rate constants is significantly different for the forward and the back electron transfers. While the value of $\beta = 0.5$ Å^{-1} observed for the recombination reaction is consistent with those reported for self-assembled monolayers (SAMs) containing p-phenylene spacer groups ($\beta = 0.35 - 0.5$ Å^{-1}),[41,42,43] the distance dependence of the fast phase of the injection process is surprisingly low. Different reasons can be invoked to understand this difference. First, an error could arise from the estimation of the distance used in the "beta

plot". As mentioned, we measured the distance between the metal center of the sensitizer and the nearest titanium atom of the semiconductor from semi-empirical geometry optimizations. This distance is certainly overestimated since we know that the electron to be transferred is located on the terpyridyl ligand in the excited state. However, if the shape of the LUMO is the same for all three dyes this should not have an influence on the magnitude of β because it depends on the distance change $(r - r_0)$ and not on the absolute value. If the LUMO is delocalized over the bridge the charge separation distance may be reduced for up to 2 Å for P1 (respectively 4 Å for P2). In such conditions, β would come up to ~ 0.3 Å. This argument was namely invoked Piotrowiak et al.[15] to explain subpicosecond electron injection into TiO_2 over a distance of 24 Å for tripodal sensitizers containing a phenylethynyl bridge. Although our simplistic estimation does not explain the totality of the difference between forward and back transfer it may contribute to some extent. Another parameter that we have to consider is the orientation of the dyes on the surface. Even if a dye monolayer is present at the surface, the optimal arrangement of the molecules may yield a tilted orientation. The reduction of the distance would be proportional to the length of the bridge and therefore would result in a bigger damping parameter. However, this factor should be the same for both transfers and can not explain the difference observed.

In the preceding discussion, we considered implicitly that the reorganization energy of the complex was negligible, and thus the influence of the distance was completely imputed to electronic factors. While nuclear factors are likely to have a weak influence on electron injection due to the relative immobility of the molecules on this timescale, the situation might be completely different for electron transfer. Computational simulations of the distance-dependence of the electrical transmission (see eq. 6.6) of oligo(p-phenylene) SAMs revealed damping factors in the range 0.17 - 0.28 Å^{-1}.[44] Although the authors claim good agreement with experimental results, we find that the theoretical values, obtained from purely electronic factors, exactly predict the value obtained for electron injection. Since the reorganization energy is expected to increase with the length of the bridge, the back ET rate will decrease accordingly, and thus the distance parameter will be overestimated. We believe that the influence of nuclear factors for back ET, conjugated with the effect of charge delocalization in the excited state for electron injection, can reasonably explain the significant difference observed for the distance dependence of both interfacial charge transfers.

Core-shell nanoparticles

Retardation of the back electron transfer over several order of magnitudes is achieved by inserting an insulating layer between TiO_2 and the sensitizer while efficient electron injection is still observed. This result is consistent with the increase of the overall efficiency of dye-sensitized solar cells featuring core-shell nanocrystalline films.[30,31,32,33] More surprising is the weak dependence of the kinetics upon the thickness of the layer. The magnitude of the estimated β distance parameters are similar to π-conjugated systems or C_{60} films.[3,5,7] In other words the conductance of these "insulating" layers is similar to molecular wires or electron transport layers (ETL).

In contrast to bridged sensitizers, the modification of the ET kinetics with distance is here purely an electronic factor. Indeed, the nuclear parameters controlling the charge transfer (inner-sphere and outer-sphere reorganization energies) are unchanged since the same sensitizer is used for all experiments. Therefore, we expect a clear exponential dependence for both forward and back transfers. However, because of the important kinetic heterogeneity, this could not be verified for electron injection. Different reasons can be invoked to rationalize this behavior. First, the arrangement of the molecules on the surface can lead to a distribution of distances. The dye may adopt a tilted orientation when adsorbed on the surface. Yet, taking into account the strong adsorption energy for phosphonic acid[45] and the short distance separating the LUMO from the semiconductor, the distance may vary over 1-2 Å only.[d] Multilayer adsorption or formation of molecular aggregates on the surface of the semiconductor has been discussed in the previous chapters. Owing to the size of the dye (> 13 Å), the presence of a second layer could lead to dramatic changes in the kinetics since the distance can be lenghtened for more than 12 Å, i.e. approximately 2 times the radius of P0 sensitizer. Typically, such an increment (12 Å) would multiply the time constant from 11 times (if $\beta = 0.2$ Å^{-1}) to more than 400 times (if $\beta = 0.5$ Å^{-1}). These rough calculations clearly illustrate that the kinetic heterogeneity may arise from aggregation only. However, although it could not be quantified, a significant trend is observed when the layer thickness is increased (figure 6.13). Since molecular arrangement on the surface is not expected to be influenced by the width of the alumina barrier, it does not provide a sufficient explanation to describe the results. Up to now, the Al_2O_3 film has been considered as homogeneous. Although no characterization of the morphology of the film is available, the layer is likely to contain pinholes, that could account for the fast part (sub-100 fs) observed for almost

---

[d]This distance, as well as the following estimations, are based on the geometry of P0 obtained from semi-empirical calculations (ZINDO).

each sample. In addition, variable thickness could arise from the deposition technique if the reactants do not penetrate homogeneously into the mesoporous network.

In agreement with the previous remarks concerning the variable thickness or the arrangement of molecules on the surface, kinetic heterogeneity is also observed for back electron transfer. Unlike for ultrafast measurements, a single parameter (the half-lifetime) can be used to describe the kinetics despite the multiexponential character. From the excellent agreement with an exponential dependence of the rate constant upon distance (fig. 6.12), we believe that $k_{1/2}$ is a reliable parameter to describe the effect of the alumina layer on the recombination kinetics. Although the injection quantum yield was not quantified for these measurements, significant formation of the oxidized dye was observed for all samples. This is in contradiction with the argument that for thick layers (40-60 Å) charge separation is mediated by dyes located in pinholes or cracks in the barrier.

As mentioned above, the damping parameter estimated from these experiments is extremely low ($\beta = 0.15$ Å^{-1}). The tunneling probability T between two metallic electrodes separated by a potential barrier can be estimated from basic quantum mechanics:[46]

$$T = T_0 \exp(-2\kappa\Delta x)$$
$$\text{where} \quad \kappa = \left[\frac{2m_e E_B}{\hbar^2}\right] \tag{6.9}$$

Here, T_0 is a pre-factor close to unity, E_B is the height of the barrier potential, m_e the electron mass, Δx is the thickness of the barrier and 2κ is a decay length that has a meaning similar to β. Bulk, stoichiometric Al$_2$O$_3$ (sapphire) has a band gap of 8.8 eV.[47] This means that the position of the conduction band edge is at least 3 eV above the dye excited state.[33] From equation 6.9, we estimate (with $E_B = 3$ eV) $\beta \cong 2\kappa = 1.8$ Å^{-1}. As stated earlier, the superexchange model for bridge-assisted electron transfer is equivalent to coherent tunneling through virtual states that are not populated during the process. Therefore, the reasoning followed above should be valid for our systems. Obviously, the parameter β obtained from eq. 6.9 is disproportionate. Indeed, with such a distance dependence, no electron transfer would be observed for a distance more than 7 Å wide.[e] From these considerations, we conclude that there must be some lower lying states in the alumina layer that can mediate electron transfer efficiently. Recently it was reported that in ultrathin tunnel barriers made of amorphous aluminum oxide, the barrier height (with respect to metallic aluminum) was only 1.2

---

[e]from eq. 6.8: $\beta = 1.8$ Å^{-1}, $k_0 = 10^{13}$, k(7 Å) = 1/30 ns^{-1}

eV.[48] This shows that the electronic structure of alumina/titania core-shell nanoparticles can not be derived directly from the bulk properties. The electron work function in metallic aluminum is 4.2 eV,[49] therefore with such a barrier, the absolute value of the empty states in amorphous aluminum oxide would be around -1.5 eV vs. SHE. In comparison, the potential of the unrelaxed excited dye can be estimated from the value of the Ru(III)/Ru(II) oxidation potential of the analogous "black dye", which is 0.58 V vs. SHE. Thus, when excited at 530 nm the potential of the excited state is about -1.7 eV. Surprisingly, the sensitizer should be able to inject into amorphous alumina at this excitation wavelength. Despite the lack of information concerning the crystallinity of the films used in this study, we believe that a superexchange mechanism involving virtual bridge states from amorphous aluminum oxide can satisfactorily explain the weak distance dependence observed in our experiments.

The benefits of a thin Al_2O_3 layer on TiO_2 nanocrystalline films were interpreted in terms of retardation of the tunneling back electron transfer to the oxidized dye or to the redox electrolyte $(I_3^-)^f$.[30,31,32,33] More recently it was suggested that in addition to the distance effect, the retardation is imputed to the passivation of the surface trap states of TiO_2 that are able to transfer electrons to acceptor species.[35] Although no evidence for surface passivation is observed here, our results are in agreement with these studies.

6.5   Conclusions

The distance dependence of interfacial electron transfer at dye/semiconductor interfaces has been studied by two different approaches. First we used a series of bridged sensitizers containing p-phenylene spacers adsorbed on TiO_2. The kinetics of both forward and back ET were recorded by time-resolved spectroscopy in the fs-ps and μs-s time domains. The ultrafast electron injection was found to be biphasic with a clear exponential distance-dependence of the fast part, but no obvious trend for the slower phase. From the plot of the rate constants with respect to the distance over which the transfer takes place, we could estimate the damping parameter β. While the value for back ET is in agreement with other experimental data ($\beta = 0.5$ Å^{-1}), the influence of the distance is much weaker for electron injection ($\beta = 0.19$ Å^{-1}). The difference between the two interfacial electron transfers is attributed to the delocalization of the LUMO in the excited state, added

---

^{f}see chapter 4

to the influence of nuclear factors (reorganization energy) for back electron transfer.

In the second part of this study, we investigated the kinetics of interfacial ET across a thin layer of Al_2O_3 deposited onto TiO_2 nanocrystalline films. In this case, efficient electron transfer was observed over distances up to 60 Å. As for bridged sensitizer, substantial kinetic heterogeneity was observed for electron injection, and an exponential dependence of the rate constant upon the distance could not be verified. However, from the magnitude of the time constants observed for thick barriers (20 - 60 Å), we estimate an upper limit for the distance parameter $\beta = 0.3$ Å^{-1}. In contrast, the half-lifetime for back ET decreased clearly with an exponential decay ($\beta = 0.15$ Å^{-1}). The weak influence of the distance on both ET rates is surprising if we consider the large potential barrier theoretically present for electron tunneling. However, taking into consideration the reduction of the potential barrier due to the amorphous character of thin alumina layers, such low β are not unconceivable.

It is clear from the heterogeneity observed in the kinetic data and the reduced number of points available for the fit,[g] that the estimations for β must be taken with care. The adsorption of chemical species onto nanoparticles is far from the ideal picture representing dye monolayers adsorbed perpendicularly to the surface. Heterogeneity is certainly present in the orientation of the molecules on the surface, the thickness of insulating layers, aggregation of the dyes, etc.. In spite of that, clear exponential dependence of interfacial ET rate upon distance is found in most of the situations studied here, indicating that the heterogeneity is somehow averaged.

Although the mechanism leading to the weak influence of distance for interfacial ET are not the same for core-shell particles as for bridged sensitizers, our experiments demonstrate that efficient charge transport over significant distances can be achieved at dye/semiconductor interfaces. These results encourage the use of various strategies to control electron transfer kinetics for the development of devices such as dye-sensitized solar cells but also in the emerging field of molecular electronics.

Obviously, the effort should be prolonged in order to get more details about the factors that enable fast charge transport over significant distances. Apart from the synthesis of new samples (dyes and core-shell nanocrystalline films), attention should be paid to the arrangement of the molecules on the sur-

---

[g]for bridged sensitizers, each point corresponds to a new chemical synthesis !

faces. Further experiments could also include the control of the crystallinity of the insulating barriers in order to assess our hypotheses.

The present study was made possible by the conjunction of different skills, represented by the synthetic chemists who prepared the dyes, the materials scientists that made the core-shell films and, of course, laser spectroscopists. We think that this multi-disciplinar aspect is not only a interesting characteristic of this type of investigations, but also a key requirement to get data of adequate quality.

6.6 References

1. Gray, H. B.; Winkler, J. R. "Electron transfer in proteins", *Annu. Rev. Biochem.* **1996,** *65,* 537-561.

2. Nitzan, A. "Electron transmission through molecules and molecular interfaces", *Annu. Rev. Phys. Chem.* **2001,** *52,* 681–750.

3. Zhu, X. Y. "Charge Transport at Metal-Molecule Interfaces: A Spectroscopic View", *J. Phys. Chem. B* **2004,** *108,* 8778-8793.

4. Newton, M. D. "Quantum Chemical Probes of Electron-Transfer Kinetics - the Nature of Donor-Acceptor Interactions", *Chem. Rev.* **1991,** *91,* 767-792.

5. Adams, D. M. *et al.* "Charge transfer on the nanoscale: Current status", *J. Phys. Chem. B* **2003,** *107,* 6668-6697.

6. Winkler, J. R. "Electron tunneling pathways in proteins", *Curr. Opin. Chem. Biol.* **2000,** *4,* 192-198.

7. Barbara, P. F.; Meyer, T. J.; Ratner, M. A. "Contemporary issues in electron transfer research", *J. Phys. Chem.* **1996,** *100,* 13148-13168.

8. Nitzan, A. "A relationship between electron-transfer rates and molecular conduction", *J. Phys. Chem. A* **2001,** *105,* 2677–2679.

9. Segal, D.; Nitzan, A.; Davis, W. B.; Wasielewski, M. R.; Ratner, M. A. "Electron transfer rates in bridged molecular systems 2. A steady-state analysis of coherent tunneling and thermal transitions", *J. Phys. Chem. B* **2000,** *104,* 3817-3829.

10. Smalley, J. F.; Finklea, H. O.; Chidsey, C. E. D.; Linford, M. R.; Creager, S. E.; Ferraris, J. P.; Chalfant, K.; Zawodzinsk, T.; Feldberg, S. W.; Newton, M. D. "Heterogeneous electron-transfer kinetics for ruthenium and ferrocene redox moieties through alkanethiol monolayers on gold", *J. Am. Chem. Soc.* **2003,** *125,* 2004-2013.

11. Sikes, H. D.; Smalley, J. F.; Dudek, S. P.; Cook, A. R.; Newton, M. D.; Chidsey, C. E. D.; Feldberg, S. W. "Rapid electron tunneling through oligophenylenevinylene bridges", *Science* **2001,** *291,* 1519-1523.

12. Asbury, J. B.; Hao, E. C.; Wang, Y. Q.; Lian, T. Q. "Bridge length-dependent ultrafast electron transfer from Re polypyridyl complexes to nanocrystalline TiO_2 thin films studied by femtosecond infrared spectroscopy", *J. Phys. Chem. B* **2000,** *104,* 11957-11964.

13. Anderson, N. A.; Ai, X.; Chen, D. T.; Mohler, D. L.; Lian, T. Q. "Bridge-assisted ultrafast interfacial electron transfer to nanocrystalline SnO_2 thin films", *J. Phys. Chem. B* **2003,** *107,* 14231-14239.

14. Galoppini, E. "Linkers for anchoring sensitizers to semiconductor nanoparticles", *Coord. Chem. Rev.* **2004,** *248,* 1283–1297.

15. Piotrowiak, P.; Galoppini, E.; Wei, Q.; Meyer, G. J.; Wiewior, R. "Subpicosecond photoinduced charge injection from Molecular tripods into mesoporous TiO_2 over the distance of 24 angstroms", *J. Am. Chem. Soc.* **2003,** *125,* 5278-5279.

16. Ernstorfer, R.; Felber, S.; Storck, W.; Galoppini, E.; Wei, Q.; Willig, F. "Distance dependence of heterogeneous electron transfer probed in ultra-high vacuum with femtosecond transient absorption", *Res. Chem. Intermed.* **2005,** *31,* 643–647.

17. Gundlach, L.; Felber, S.; Storck, W.; Galoppini, E.; Wei, Q.; Willig, F. "Femtosecond two-photon photoemission probing electron injection from the excited singlet state of perylene attached to a long rigid tripod anchor-cum-spacer on rutile $TiO_2(110)$", *Res. Chem. Intermed.* **2005,** *31,* 39–46.

18. Galoppini, E.; Guo, W. Z.; Zhang, W.; Hoertz, P. G.; Qu, P.; Meyer, G. J. "Long-range electron transfer across molecule-nanocrystalline semiconductor interfaces using tripodal sensitizers", *J. Am. Chem. Soc.* **2002,** *124,* 7801-7811.

19. Galoppini, E.; Guo, W.; Qu, P.; Meyer, G. "Long-distance electron transfer across molecule-nanocrystalline semiconductor interfaces", *J. Am. Chem. Soc.* **2001,** *123,* 4342–4343.

20. Hoertz, P.; Carlisle, R.; Meyer, G.; Wang, D.; Piotrowiak, P.; Galoppini, E. "Organic rigid-rod linkers for coupling chromophores to metal oxide nanoparticles", *Nano Lett.* **2003,** *3,* 325–330.

21. Wang, D.; Mendelsohn, R.; Galoppini, E.; Hoertz, P. G.; Carlisle, R. A.; Meyer, G. J. "Excited state electron transfer from Ru(II) polypyridyl complexes anchored to nanocrystalline TiO_2 through rigid-rod linkers", *J. Phys. Chem. B* **2004,** *108,* 16642-16653.

22. Beek, W.; Janssen, R. "Spacer length dependence of photoinduced electron transfer in heterosupramolecular assemblies of TiO_2 nanoparticles and terthiophene", *J. Mater. Chem.* **2004,** *14,* 2795–2800.

23. Kilsa, K.; Mayo, E. I.; Kuciauskas, D.; Villahermosa, R.; Lewis, N. S.; Winkler, J. R.; Gray, H. B. "Effects of Bridging ligands on the current-potential behavior and interfacial kinetics of ruthenium-sensitized nanocrystalline TiO_2 photoelectrodes", *J. Phys. Chem. A* **2003,** *107,* 3379-3383.

24. Gaal, D.; Mcgarrah, J.; Liu, F.; Cook, J.; Hupp, J. "Nonadiabatic electron transfer at the nanoscale tin-oxide semiconductor/aqueous solution interface", *Photochem. Photobiol. Sci.* **2004,** *3,* 240–245.

25. Clifford, J.; Palomares, E.; Nazeeruddin, M.; Grätzel, M.; Nelson, J.; Li, X.; Long, N.; Durrant, J. "Molecular control of recombination dynamics in dye-sensitized nanocrystalline TiO_2 films: Free energy vs distance dependence", *J. Am. Chem. Soc.* **2004,** *126,* 5225–5233.

26. Bonhôte, P.; Moser, J. E.; Humphry-Baker, R.; Vlachopoulos, N.; Zakeeruddin, S. M.; Walder, L.; Grätzel, M. "Long-lived photoinduced charge separation and redox-type photochromism on mesoporous oxide films sensitized by molecular dyads", *J. Am. Chem. Soc.* **1999,** *121,* 1324-1336.

27. Haque, S.; Handa, S.; Peter, K.; Palomares, E.; Thelakkat, M.; Durrant, J. "Supermolecular control of charge transfer in dye-sensitized nanocrystalline TiO_2 films: Towards a quantitative structure-function relationship", *Angew. Chem. Int. Ed.* **2005,** *44,* 5740–5744.

28. Hirata, N.; Lagref, J.; Palomares, E.; Durrant, J.; Nazeeruddin, M.; Grätzel, M.; Di Censo, D. "Supramolecular control of charge-transfer dynamics on dye-sensitized nanocrystalline TiO$_2$ films", *Chem. Eur. J.* **2004,** *10,* 595–602.

29. Diamant, Y.; Chen, S. G.; Melamed, O.; Zaban, A. "Core-shell nanoporous electrode for dye sensitized solar cells: the effect of the SrTiO$_3$ shell on the electronic properties of the TiO$_2$ core", *J. Phys. Chem. B* **2003,** *107,* 1977-1981.

30. Kay, A.; Grätzel, M. "Dye-sensitized core-shell nanocrystals: Improved efficiency of mesoporous tin oxide electrodes coated with a thin layer of an insulating oxide", *Chem. Mater.* **2002,** *14,* 2930-2935.

31. Kumara, G. R. R. A.; Tennakone, K.; Perera, V. P. S.; Konno, A.; Kaneko, S.; Okuya, M. "Suppression of recombinations in a dye-sensitized photoelectrochemical cell made from a film of tin IV oxide crystallites coated with a thin layer of aluminium oxide", *J. Phys. D: Appl. Phys.* **2001,** *34,* 868-873.

32. Palomares, E.; Clifford, J. N.; Haque, S. A.; Lutz, T.; Durrant, J. R. "Slow charge recombination in dye-sensitised solar cells (DSSC) using Al$_2$O$_3$ coated nanoporous TiO$_2$ films", *Chem. Commun.* **2002,** 1464-1465.

33. Palomares, E.; Clifford, J. N.; Haque, S. A.; Lutz, T.; Durrant, J. R. "Control of charge recombination dynamics in dye sensitized solar cells by the use of conformally deposited metal oxide blocking layers", *J. Am. Chem. Soc.* **2003,** *125,* 475-482.

34. O'Regan, B.; Scully, S.; Mayer, A.; Palomares, E.; Durrant, J. "The effect of Al$_2$O$_3$ barrier layers in TiO$_2$/Dye/CuSCN photovoltaic cells explored by recombination and DOS characterization using transient photovoltage measurements", *J. Phys. Chem. B* **2005,** *109,* 4616–4623.

35. Fabregat-Santiago, F.; Garcia-Canadas, J.; Palomares, E.; Clifford, J.; Haque, S.; Durrant, J.; Garcia-Belmonte, G.; Bisquert, J. "The origin of slow electron recombination processes in dye-sensitized solar cells with alumina barrier coatings", *J. Appl. Phys.* **2004,** *96,* 6903–6907.

36. Nazeeruddin, M. K.; Pechy, P.; Renouard, T.; Zakeeruddin, S. M.; Humphry-Baker, R.; Comte, P.; Liska, P.; Cevey, L.; Costa, E.; Shklover, V.; Spiccia, L.; Deacon, G. B.; Bignozzi, C. A.; Grätzel, M. "Engineering of efficient panchromatic sensitizers for nanocrystalline TiO$_2$-based solar cells", *J. Am. Chem. Soc.* **2001,** *123,* 1613-1624.

37. Bhasikuttan, A. C.; Suzuki, M.; Nakashima, S.; Okada, T. "Ultrafast fluorescence detection in tris(2,2 '-bipyridine)ruthenium(II) complex in solution: Relaxation dynamics involving higher excited states", *J. Am. Chem. Soc.* **2002,** *124,* 8398-8405.

38. Amouyal, E.; Mouallem-Bahout, M.; Calzaferri, G. "Excited States of M(II,d^6)-4'-Phenylterpyridine Complexes: Electron Localization", *J. Phys. Chem.* **1991,** *95,* 7641-7649.

39. Nusbaumer, H.; Moser, J. E.; Zakeeruddin, S. M.; Nazeeruddin, M. K.; Grätzel, M. "Co-II(dbbiP)$_2^{2+}$ complex rivals tri-iodide/iodide redox mediator in dye-sensitized photovoltaic cells", *J. Phys. Chem. B* **2001,** *105,* 10461-10464.

40. Pelet, S. *Femtosecond Dynamics of Electron Transfer in the Photosensitization of Wide Band Gap Semiconductors,* Thesis, Ecole Polytechnique Fédérale de Lausanne, 2002.

41. Bumm, L.; Arnold, J.; Dunbar, T.; Allara, D.; Weiss, P. "Electron transfer through organic molecules", *J. Phys. Chem. B* **1999,** *103,* 8122–8127.

42. Ishida, T.; Mizutani, W.; Aya, Y.; Ogiso, H.; Sasaki, S.; Tokumoto, H. "Electrical conduction of conjugated molecular SAMs studied by conductive atomic force microscopy", *J. Phys. Chem. B* **2002,** *106,* 5886–5892.

43. Wold, D.; Haag, R.; Rampi, M.; Frisbie, C. "Distance dependence of electron tunneling through self-assembled monolayers measured by conducting probe atomic force microscopy: Unsaturated versus saturated molecular junctions", *J. Phys. Chem. B* **2002,** *106,* 2813–2816.

44. Kondo, M.; Tada, T.; Yoshizawa, K. "Wire-length dependence of the conductance of oligo(p-phenylene) dithiolate wires: A consideration from molecular orbitals", *J. Phys. Chem. A* **2004,** *108,* 9143–9149.

45. Nilsing, M.; Lunell, S.; Persson, P.; Ojamae, L. "Phosphonic acid adsorption at the TiO_2 anatase (101) surface investigated by periodic hybrid HF-DFT computations", *Surf. Sci.* **2005,** *582,* 49–60.

46. Vanmaekelbergh, D. Electron Transfer in Chemistry. In , Vol. 1; Balzani, V., Ed.; Wiley-VCH: 2001; Chapter "Electron Transfer at Electrodes and Interfaces", pages 126–188.

47. French, R. "Electronic Band-Structure of Al_2O_3, With Comparison To Aion And Ain", *J. Am. Ceram. Soc.* **1990,** *73,* 477–489.

48. Rippard, W.; Perrella, A.; Albert, F.; Buhrman, R. "Ultrathin aluminum oxide tunnel barriers", *Phys. Rev. Lett.* **2002,** *88,* 046805.

49. *CRC Handbook of Chemistry and Physics, 85th Edition;* CRC Press: 2004-2005.

Dependence of electron injection kinetics upon the density of states

Summary

The influence of the density of acceptor states on the kinetics of electron injection at dye/semiconductor interfaces is investigated. Postulating electron injection from unrelaxed excited states, we propose to probe the bottom of the conduction band edge of nanocrystalline Nb_2O_5 by the variation of the excitation wavelength. In the first part, thorough characterization of the static and dynamic properties of Z105 dye sensitizer is carried out. Then the dynamics of electron transfer to niobia is investigated at several excitation wavelengths by transient absorption spectroscopy. When excited at 600 nm, electron transfer is slightly retarded (2-3 times). This rather weak effect is interpreted as a consequence of the poor spectral resolution inherent to the use of femtosecond light pulses.

129

7.1 Introduction

In the previous chapters, we mainly discussed the influence of the electronic coupling on the kinetics of dye-to-semiconductor electron transfer. When the distance is changed, intentionally by inserting bridges or barriers between the chromophore and the acceptor, or inadvertently as observed when the dyes do not form a perfect monolayer, the electron transfer rate decreases predominantly because of the reduced overlap between the donors' and the acceptors' electronic orbitals. Standard electron transfer theory generally separates the nuclear from the electronic factors. This separation is a direct consequence of the Born-Oppenheimer approximation in the adiabatic electron transfer picture. For non-adiabatic models, despite the breakdown of the BOA, the use of a diabatic basis allows one to neglect Born-Oppenheimer couplings, leading to the standard golden rule expression:[1,2]

$$k_{ET} = \frac{2\pi}{\hbar}|H_{DA}|^2 (FCWD) \tag{7.1}$$

where H_{DA}, the electronic coupling matrix element, accounts for the electronic factor and the Franck-Condon weighted density of states (FCWD) represents the nuclear factor. Without approximation the FCWD is calculated from the quantum-mechanical overlap of all nuclear modes (Franck-Condon factors) weighted by the actual population of theses modes obtained from Boltzmann statistics. The level of approximation of this factor (classical, mixed quantal-classical, full quantal) leads to the standard equations of electron transfer theory (see chapter 2).

Due to the very high density of states in the acceptor phase, the nuclear overlap is large and the FCWD is considered to approach unity. However, this condition is not true when the energy of the donor state is situated close to the bottom of the conduction band where the DOS[a] drops dramatically. In such a configuration, nuclear *and* electronic coupling are significantly reduced and a decrease of the transfer rate and efficiency is predicted.[3]

The reduced density of states of TiO_2 below the conduction band edge has often been invoked to rationalize biphasic electron transfer kinetics observed for TiO_2 sensitized by ruthenium complexes (see 5.1.2 and references therein). Briefly, the fast phase is attributed to electron injection occurring from a vibrationally unrelaxed singlet state, while the slower component arises from a triplet or any other relaxed state with a lower energy. In this two-state model the relaxed dye samples a lower density of acceptor states in the semiconductor and therefore electron transfer is much slower since

---

[a]Density of states

both electronic and nuclear overlaps decline. Our own results (presented in chapter 5) suggest that the origin of the kinetic heterogeneity lies in the variation of the electronic coupling due to a distribution of distances separating the dye from the semiconductor surface, rather than a consequence of a two-state mechanism. So far, with the donors properly adsorbed on the nanoparticles, our experiments show no influence of the density of states of TiO_2 for the standard N3 and analogous dyes. This suggests that for each photon absorbed an electron is readily transferred into the conduction band of TiO_2. This is in agreement with the photocurrent action spectra found to almost coincide with the light absorption spectrum, for photovoltaic devices made with this type of Ru complexes.[4]

Here we propose a new approach to study the effect of the density of states on the kinetics of electron injection at dye/semiconductor interfaces. The experiment is based on the postulate that electron transfer occurs from a thermally unrelaxed state ("hot state"). If the transfer arises directly from the vibronic state prepared upon light absorption, the excited dye will "feel" different densities of states as the excitation wavelength is varied (see figure 7.1). Let's assume that the relaxed electronic state (corresponding to the 0-0 excitation) is energetically lower than the conduction band edge of the semiconductor. If we excite the dye at this particular transition, no electron injection will be observed. If now the excitation wavelength is systematically increased we will probe different densities of states until the donor state is well above the band edge.

One difficulty in this approach is to find a dye/semiconductor couple with matching energy levels. The dye's lower excited state has to lie below the band edge while its absorption spectrum must be large enough to cover the energy area where the density of states drops. Here we suggest to replace TiO_2 with Nb_2O_5 nanocrystalline films. The conduction band of niobia is known to be slightly shifted ($\sim$0.1-0.4 eV) towards higher energies with respect to titania.[5,6,7] On this material, the LUMO of the N3 sensitizer is lower than the conduction band edge but remarkable photovoltaic performance has still been observed by several groups.[5,8,9,10] This was explained by the existence of "hot" electron transfer as mentioned above.[6,7]

The starting point for our experiments will be a study by Moser et al.[6] They reported excitation-wavelength dependence of charge separation quantum yields in the sensitization of various semiconductors by N3 dye. A near-unity quantum yield was observed for TiO_2 over the complete absorption spectrum of the dye, while no injection was observed for zirconia. Interestingly, with Nb_2O_5 the yield dropped dramatically when the excitation wavelength exceeded 600 nm. This was interpreted as an indication that the vibronic states populated with such excitation energies lie underneath the
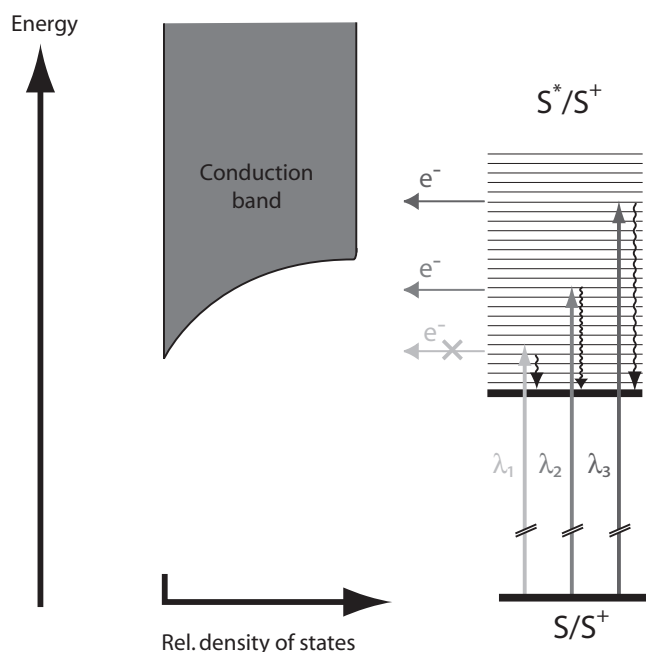
Figure 7.1 — Principle of the experiment proposed to explore the effect of the density of states on the kinetics of electron injection. In the presence of "hot" electron transfer, it is postulated that the variation of the excitation wavelength enables one to probe the DOS at the conduction band edge. In this picture we expect the following behavior: a) no injection for λ_1, b) fast and monophasic rate for λ_3 and c) slower injection for λ_2.

conduction band edge of the semiconductor, providing evidence for "hot" electron transfer at shorter wavelengths. This interpretation was further consolidated by surface photovoltage spectroscopy experiments.[7] As mentioned, these experiments featured N3 dye sensitizer. In the light of our own results indicating multilayer adsorption or aggregation of this dye in mesoporous networks, we suggest to use [Ru(HP-terpy)Me$_2$-bpy)NCS] (Z105) as an alternative sensitizer.[11] This choice is motivated by the similarities of this complex with the standard N3 dye (oxidation potential, E_{0-0} transition energy), while the absence of slow components for electron injection indicates excellent adsorption on the semiconductor's surface (see 5.3)

Direct, time-resolved observation of electron injection from Ru polypyridyl complexes into Nb$_2$O$_5$ has been reported recently for the first time by Ai et al.[12] They measured the injection dynamics of a series of dyes (including N3) and found biphasic kinetics similar to what is observed on TiO$_2$. The first phase (< 100 fs, $\sim$ 35 % of the total rise) was followed by a slower, multiexponential component with time constants in the range 30 ps - 3 ns.
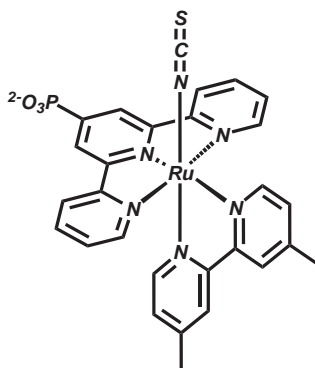
Figure 7.2 — Structure of the [Ru(HP-terpy)Me$_2$-bpy)NCS] sensitizer dye (Z105).

The decreasing rates were attributed to the reduced density of states in the semiconductor at energy levels corresponding to the relaxed excited states. The excitation wavelength was kept constant at 400 nm, thereby generating unrelaxed excited states far above the conduction band edge. Apart from the aforementioned studies by Moser and co-workers,[6,7,13] dye-sensitized Nb$_2$O$_5$ has only been investigated for photovoltaic devices.[5,9,14,15,16,17,18] Although overall solar-to-electricity conversion efficiencies up to 8.1 % have been reported at low light intensities, low attention is nowadays paid to Nb$_2$O$_5$-based DSCs. Zaban and co-workers showed that DSCs featuring bi-layer films made of TiO$_2$ covered by a thin niobia layer (2-3 nm) displayed increased overall efficiencies.[19,20] This effect was interpreted as a consequence of the potential barrier formed by the niobia layer, hindering back electron transfer. The quantum yields for electron injection from N3 into various semiconductors including Nb$_2$O$_5$ have been estimated recently from nanosecond transient absorption measurements.[8] The quantum yield was found to be near unity for all materials investigated except ZrO$_2$ where no injection could be observed at all. Again the excitation wavelength used (532 nm), prepared excited states significantly above the conduction band edges.

The effect of the density of states on the injection dynamics at dye/semi-conductor interfaces was first studied by comparison of different materials. Lian et al. reviewed the injection rates for TiO$_2$, SnO$_2$, Nb$_2$O$_5$ and ZnO nanocrystalline films.[12,21] Even though no consensus was reached for dye-sensitized SnO$_2$ and ZnO films, the trend seems to yield biphasic injection on all substrates. A fast unresolved part (< 100 fs) is always present, but the kinetics and the amplitudes of slower components have been subject to many discussions. This component probably shows a superposition of effects due to the density of acceptor states and inhomogeneous adsorption on the

surface. It is therefore very sensitive to the preparation of the samples and the experimental conditions.

Several other approaches have been proposed to investigate the properties of the acceptor phase. Tachibana et al. observed a 25-fold retardation of $t_{50\%}$ by applying an external -0.7 V bias, in agreement with a reduced density of acceptor states.[22] Cation adsorption (Li$^+$, H$^+$, ...) is another technique known to positively shift the potential of the conduction band of TiO$_2$. As expected, the general trend is that cation adsorption leads to faster injection.[23,24,25,26] However, one should mention here that most of these conclusions have been drawn on the behavior of the slower component and again some uncertainties about dye adsorption remain.

7.2 Experimental part

7.2.1 Materials

Titanium dioxide (8 μm thick) nanocrystalline films have been prepared following the standard procedure described earlier in this report (see 4.2.1). A published procedure was also used to produce transparent Al$_2$O$_3$ films (thickness: 7 μm, average particle diameter: 6.5 nm, porosity: 0.71, roughness factor: 112/μm).[27] The method developed by Lenzmann in acidic medium has been adopted for the synthesis of Nb$_2$O$_5$ films.[9,28] While alumina and titania films were prepared on standard microscope slides, nanocrystalline niobia films were deposited on fluorine-doped SnO$_2$ conducting glass to avoid bending of the substrate during the firing step. The thickness after sintering at 575 °C was about 7 μm. Referring to Lenzmann's studies, the niobia films are crystalline when sintered at this temperature.

All films were dyed by soaking them overnight in a 0.3 mM solution of [Ru(HP-terpy)Me$_2$-bpy)NCS] (Z105) in a mixture of EtOH and DMSO (90:10 % v/v). After dye uptake the films were quickly rinsed with ethanol and dried. Then a drop of an inert ionic liquid (EMITFSI)[29] was added and the film covered with a thin glass cover slip (Menzel-Gläser, thickness: 0.13-0.16 mm). The films conserved in this medium and in the absence of light did not show degradation for weeks. However, the experiments were usually carried out shortly after sample preparation.

7.2.2   Methods

Time-resolved spectroscopy

Transient absorption spectra were obtained in the pump-supercontinuum probe scheme presented in chapter 3. The pump beam was tuned to the indicated wavelengths by the two-stage NOPA and reduced to less than 0.4 μJ per pulse before being focused on the sample with a fused silica lens (f = 250 mm). The spot size on the sample was 240 μm, corresponding to a fluence of 0.9 mJ/cm^2 ($< 3 \cdot 10^{15}$ photons/cm^2, 9 sun). The broadband probe pulse (< 0.2 μJ) has approximately the same diameter as the pump. Signal and reference beams were recorded in the double-diode array detector after travelling through the spectrograph. For each measurement cycle (pump on/off), 5 scans (time exposure: 100 ms) were averaged and smoothed. Up to 25 cycles were recorded for each time delay, corresponding to a total average of over 12000 pulses. The time delay was controlled by the 700-ps translation stage in the pump path.

Complementary nanosecond transient absorption data were obtained with the setup described in chapter 3. The intensity of the excitation light (520 nm) was maintained at a low level to ensure fluence-independent kinetics. Unless otherwise specified, the samples were probed at 600 nm.

Computational details

Full geometry optimization and electronic structure calculations of the Z105 complex dye were performed employing density functional theory (DFT). The basis sets of Stevens, Basch, Krauss and Jasien (SBKJ)[30] were used for the Ru, S and P atoms where the inner shells are represented by relativistic effective core potentials (ECP's). For C, O, N and H, 6-31G(d) basis sets were used. A starting geometry was first obtained from Hartree-Fock (HF) calculations performed using the same basis set in Cs symmetry. This geometry was then optimized using the B3LYP functional and the hessian was calculated analytically. All calculations were performed using the GAMESS programs[31] on a standard personal computer (Intel P4, 2.8 GHz) under Linux OS or a dual-processor G5 Power Macintosh (Apple) under Mac OS X.

7.3   Results and Discussion

7.3.1   Dye characterization

We have found previously that injection into TiO_2 from the Z105 dye sensitizer was fast ($k > 1/20$ fs^{-1}) and monophasic, indicating that a dye monolayer was present at the semiconductor's surface. Therefore to minimize the effects due to improper dye adsorption, we chose to use this compound for all experiments. The steady-state absorption spectra, measured on Al_2O_3, TiO_2 and Nb_2O_5 (figure 7.3) showed no significant difference with the published spectrum measured in solution.[11] This spectrum is dominated by a broad absorption peak centered at 493 nm that was attributed to a MLCT transition. In contrast to carboxylic groups, the phosphonate group has a weak influence on the electronic properties of the polypyridyl ligands, and the lack of spectral changes upon adsorption is an illustration of this property.
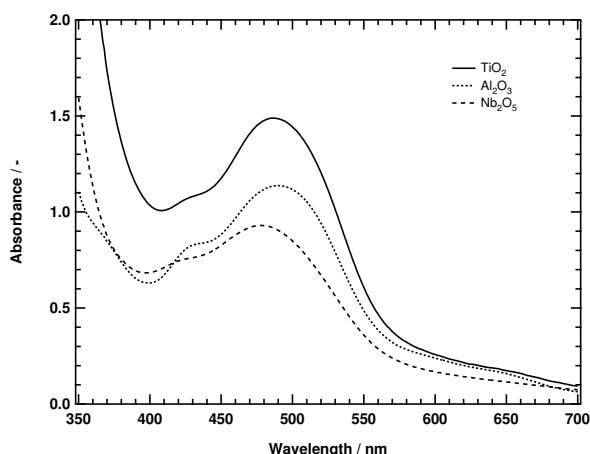
Figure 7.3 — Steady-state absorption spectra of Z105 adsorbed on TiO_2 (full), Al_2O_3 (dotted) and Nb_2O_5 (dashed) in a pure inert ionic liquid (EMITFSI).

Strong anchoring is expected through the phosphonate group. The adsorption constants measured experimentally are found about one order of magnitude higher than for analogous carboxylated dyes.[11,32] Recently, a computational study of the adsorption of phosphonic acid onto anatase, confirmed the increased anchoring strength (60 % with respect to formic acid) and showed that a monodendate binding mode stabilized by hydrogen bonds (fig. 7.4 left), and various bidentate modes were the most probable adsorption configurations.[33] Experimental investigations, in contrast, favored bidentate and tridentate modes.[34,35]
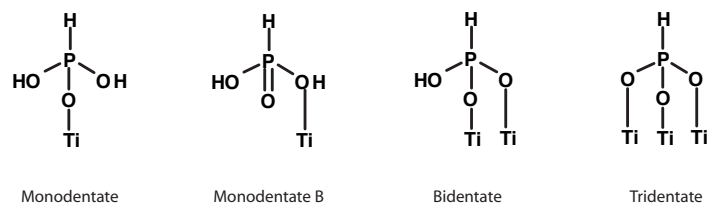
Figure 7.4 — Phosphonate binding modes on TiO_2.

For N3 and derivative dyes (N719, Z907, ...), both anchoring and spectator ligands are likely to be populated upon visible light excitation as indicated by DFT calculations.[36] In the case of Z105, it is not clear whether significant energetic differences are to be found between the terpyridyl anchoring ligand and the methylated bipyridyl spectator ligand. Therefore we calculated an optimized geometry and the corresponding electronic configuration using DFT. A complete computational study of this complex adsorbed on a semiconductor is beyond the scope of this work, however, we think that some interesting features are still available at this level of theory. The optimized geometry is globally in good agreement with the crystal structure obtained from X-ray diffraction.[11] Though it should be noted that the Ru-N bonds are slightly longer (< 5 %) in the calculated structure. This can have a significant impact on the energy levels, thus the absolute values should be taken with caution. It seems that all Ru-N bonds are lengthened in a similar way indicating that the relative energy levels of the bipyridyl- and terpyridyl-based molecular orbitals is respected.

The electronic structure of Z105 and some representative molecular orbitals are given in figures 7.5 and 7.6. As for N3, the highest occupied molecular levels are Ru(4d) orbitals that are delocalized over the NCS ligand.[36,37,38] Ru(II) dyes typically have six electrons occupying three nearly degenerate t_{2g} orbitals. For NCS containing dyes, additional contribution from occupied orbitals of the ligand so that the HOMOs are mixed Ru-NCS orbitals. The lowest few unoccupied levels are formed by orbitals located in both bipyridyl and terpyridyl ligands. Although it seems that the LUMO is clearly located on the anchoring ligand, the next empty levels have contribution from both ligands. As expected the antibonding (d^*) orbitals of the metal center are found well above the LUMOs. Although the excited states have not been computed here, the electronic configuration is in agreement with attribution of the absorption bands to MLCT transitions. As an indication, the HOMO-LUMO gap (2.0 eV, 620 nm) is consistent with the E_{0-0} estimated from the experimental spectrum. From our calculations we expect both ligands to be populated upon light excitation, and therefore be involved in electron transfer reactions. Recently, electronic coupling of N3 adsorbed on a TiO_2

(a) DFT geometry

(b) Calculated frontier orbitals
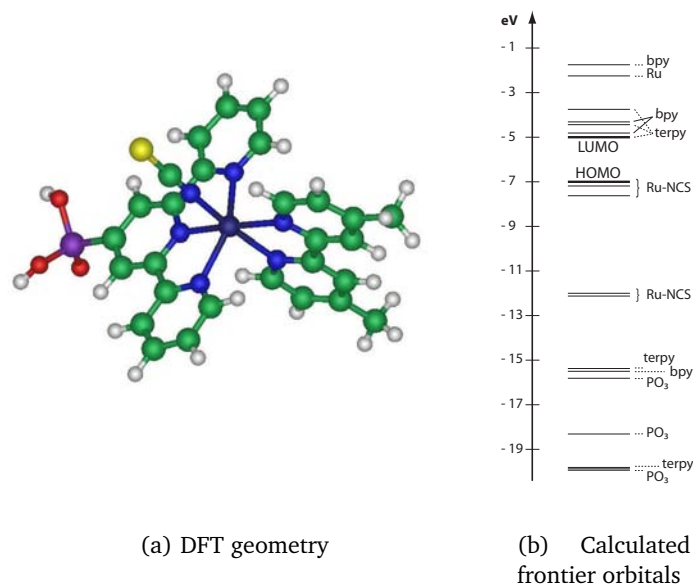
Figure 7.5 — Computational study of Z105

cluster has been computed revealing that the transfer rate could decrease for one order of magnitude (10 fs → 100 fs) depending on whether the initial electron density was located on the anchoring or the spectator ligand[36]

7.3.2 Excited state dynamics on TiO_2 and Al_2O_3

The transient absorption spectra of Z105 adsorbed on TiO_2 and Al_2O_3 have been measured in the fs/ps time domain. The results obtained on TiO_2 are depicted in figure 7.7. As predicted by photovoltaic performance[11] and our own measurements (see 5.3) efficient electron transfer is observed for Z105-sensitized TiO_2. Therefore the transient data presented in figure 7.7 contain the spectral signature of the oxidized dye. Since we expect to observe both the excited and the oxidized state simultaneously for retarded electron injection on Nb_2O_5, it is important to get a precise knowledge of the transient spectral properties of these species.

In order to get the best resolution for the time and spectral behavior, we perform a singular value decomposition (SVD) of the data matrix, which rows and columns correspond to the single wavelengths and time position vectors, respectively. This purely mathematical technique decomposes the initial matrix into linearly independent information (base vectors) and as-

(a) HOMO   (b) LUMO

(c) LUMO+1   (d) LUMO+2

(e) LUMO+6   (f) LUMO+8
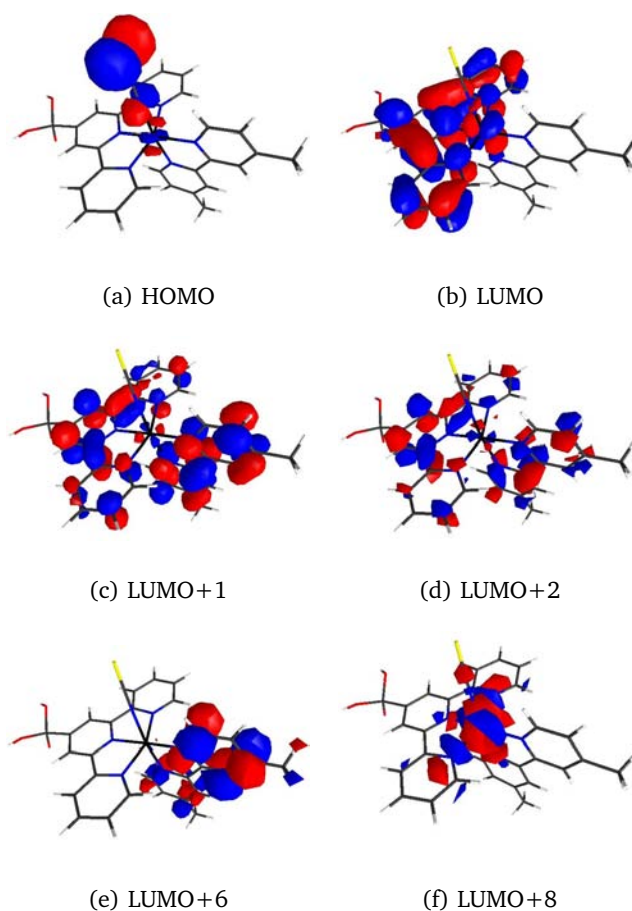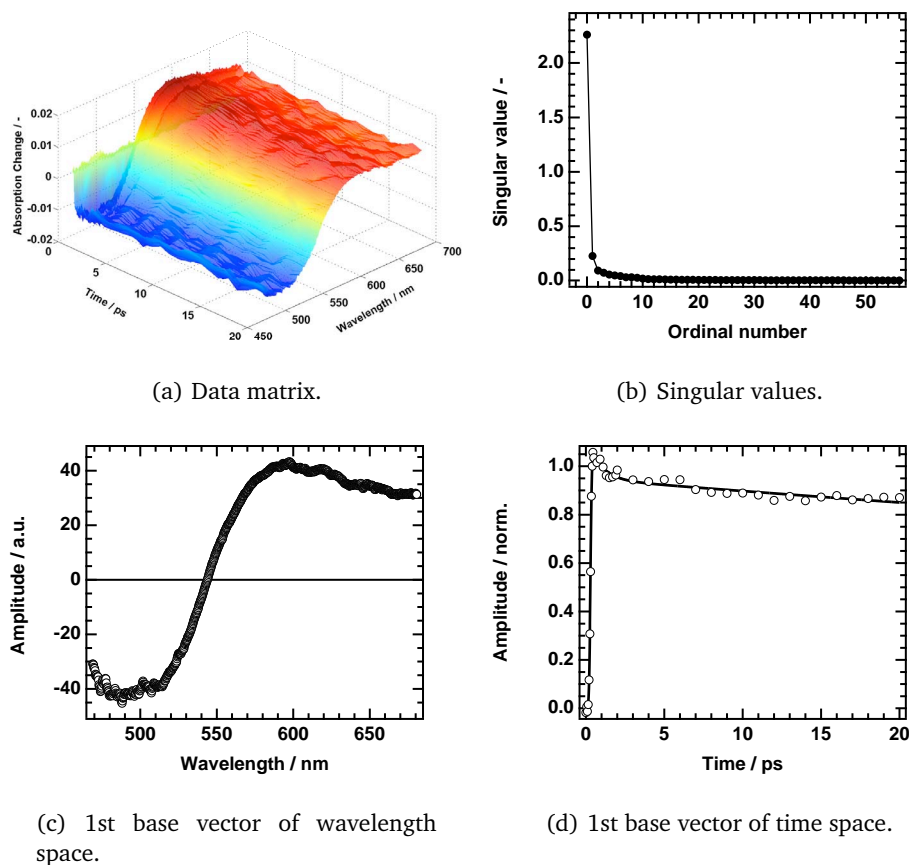
Figure 7.6 — Selected molecular orbitals

signs a singular value to each of these components. The number of non-zero singular values gives the rank of the matrix, i.e. in our case the number of transient chemical species.[39] The SVD of the measured transient data clearly shows one dominating singular value suggesting that a single chemical species is present (see figure 7.8(b)). The row vector associated with this value gives the spectral shape of this species, and its time evolution is given by the base vector shown in figure 7.8(d). All the following components, associated with much smaller singular values, show no consistent time or spectral characteristics, and are therefore imputed to experimental noise.

The transient spectrum obtained after data reduction by SVD, is a combination of bleaching of the ground state and absorption by the dye cation formed upon electron injection. A minimum is observed around 490 nm in accordance with the absorption peak of the ground state. In analogy with other dye complexes, the positive absorption band is attributed to a LMCT
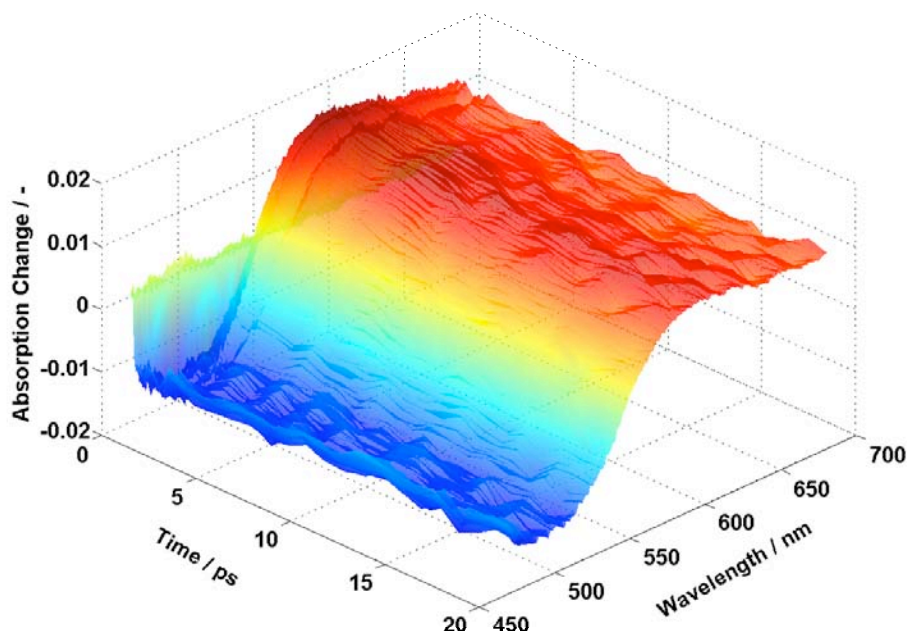
Figure 7.7 — Transient absorbance change after photoexcitation of Z105 on TiO$_2$. Excitation wavelength: 520 nm.

transition where electron density is transferred from the thiocyanate ligand to the Ru(III) center.[40] Interestingly, no other species is identified, indicating that electron injection is complete within the pulse duration. Repetition of this experiment on a longer timescale (up to 700 ps) did not reveal the presence of another species in agreement with our assignements. In contrast to our previous two-color pump-probe experiments (see 5.3), the time profile associated with this spectrum shows a significant multiexponential decay. Since the decay is not associated with the rise of another spectral component, the disappearance of the dye cation is expected to take place by back transfer or degradation. From nanosecond transient absorption measurement, we find that the kinetics for back electron transfer at low light intensity ($< 50~\mu J/cm^2$) was well described by a single exponential with time constant $\tau = 28~\mu s$, which is incompatible with the decay observed in the ultrafast data However, it is known that at higher fluences the rate becomes much faster and multiexponential.[41,42] Up to one average electron injected per nanoparticle the kinetics are independent of the light intensity. Above, it seems that both deviation from first-order kinetics and trap-filling effects lead to an acceleration of the recombination rate. Fast, fluence-dependent decays have also been observed in the picosecond time domain by Kallioinen et al. for N3-sensitized TiO$_2$.[43] In that particular case, the decay was imputed to both degradation and fast recombination. In our
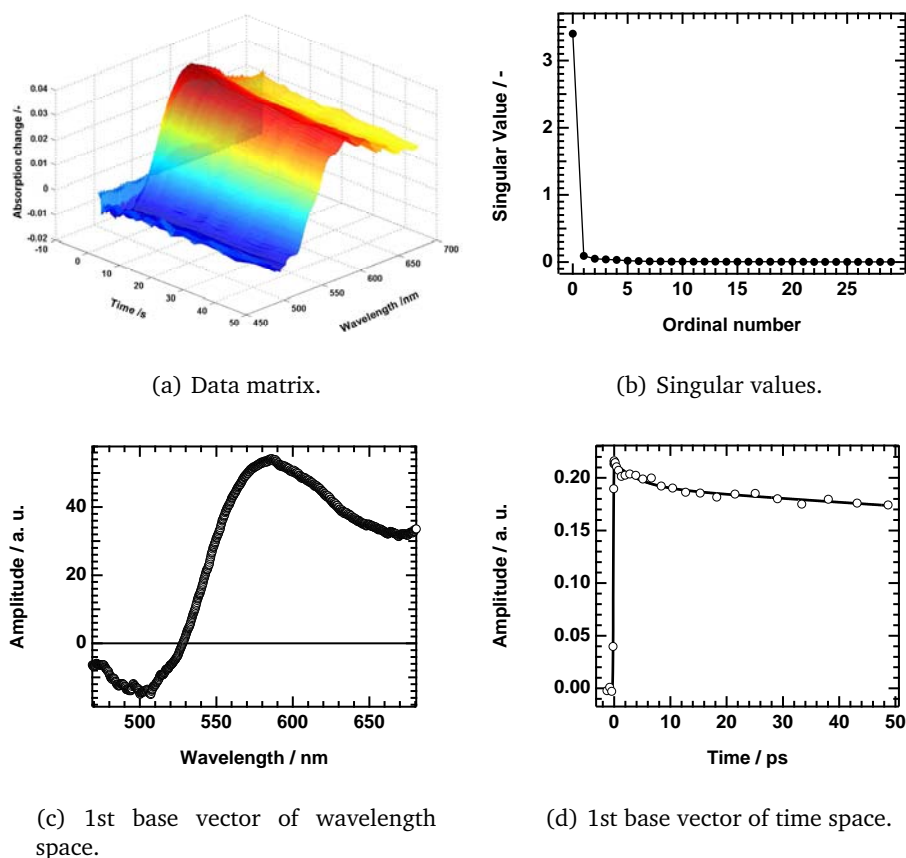
(a) Data matrix.

(b) Singular values.

(c) 1st base vector of wavelength space.

(d) 1st base vector of time space.

Figure 7.8 — Singular value decomposition of the data matrix obtained for Z105 on TiO_2.

experiment, the sample could not be rotated because light scattering by the film contributed to increase noise. Therefore we think that dye destruction is the main reason for the decay shown in figure 7.8(d). Further support is given by the fact that the time evolution was completely different when the experiment was carried out on a different timescale (for example 0-700 ps with the same number of time steps). However, due to the high fluence in this kind of experiments (900 $\mu J/cm^2$, $\sim$ 9 sun), fast recombination can not be excluded.

The same procedure was applied to the transient absorption data obtained on Al_2O_3 (figure 7.9). Again, one single component was observed over the timescale of our experiment (0 -700 ps). The position of the conduction band of alumina precludes electron transfer to the semiconductor. There-fore, we deduce that the recorded spectrum displays the spectral signature of the excited state of Z105. The time evolution of this component is charac-

terized by a fast part (τ_1 = 4.5 ps (11 %)) followed by a slower component (τ_2 = 490 ps (89 %)). Nanosecond transient absorption measurements reveal that the excited-state lifetime is well described by a biexponential decay (τa = 440 ps (56 %), τb = 14.3 ns (44 %), data not shown). In contrast to the data obtained on TiO_2, the time constants are easily reproduced, independent of the time range of the experiments. Although dye degradation can not be excluded, this indicates that the decays indeed correspond to excited state relaxation. It has been reported that ruthenium polypyridyl complexes undergo ultrafast intersystem crossing (τ_{ISC} = 40 - 160 fs), followed by vibrational cooling (τ_{IC} = 0.6 - 5 ps).[44,45,46] The lack of spectral evolution of the 4.5 ps component suggest that it not associated with a significant change in the electronic configuration.[46] This decay is therefore imputed to vibrational cooling of the excited dye. The following decays are assigned to relaxation to the ground state.

(a) Data matrix.

(b) Singular values.

(c) 1st base vector of wavelength space.

(d) 1st base vector of time space.

Figure 7.9 — Singular value decomposition of the data matrix obtained for Z105 on Al_2O_3.

A faster component, indicative of intersystem crossing, could not be observed even whith much shorter time steps (25 fs). After correction of the chirp (see chapter 3 for chirp analysis) and SVD data reduction, the same 4.5 ps component was still observed. Interestingly, with this time resolution oscillatory features could be observed (figure 7.10). The frequencies associated with these oscillations were estimated using the fast Fourier transform (FFT) algorithm. The resulting spectrum is dominated by a peak at $\omega = 143$ cm^{-1}. Our ab initio calculations indicate that several low frequency bending modes of the terpyridyl and thiocyanate ligands are present in this area but the accuracy of the calculations is not good enough to assign this feature to a particular mode. No lattice modes of Al_2O_3, that could be involved in a fast ballistic process, are found in this region.[47] At this level, it is not reasonable to try to extract more information from the frequencies associated with these oscillations. Whether it is representative of vibrational modes of the ground or excited state is beyond the resolution of our experiment. However it is interesting to note that the time constant assigned to vibrational cooling is in agreement with the presence of oscillations. Although the situation might be slightly different on TiO_2, these observations support our previous conclusions, stating that sub-100 fs electron injection at dye/TiO_2 interfaces was beyond the scope of vibration-mediated ET kinetic models.
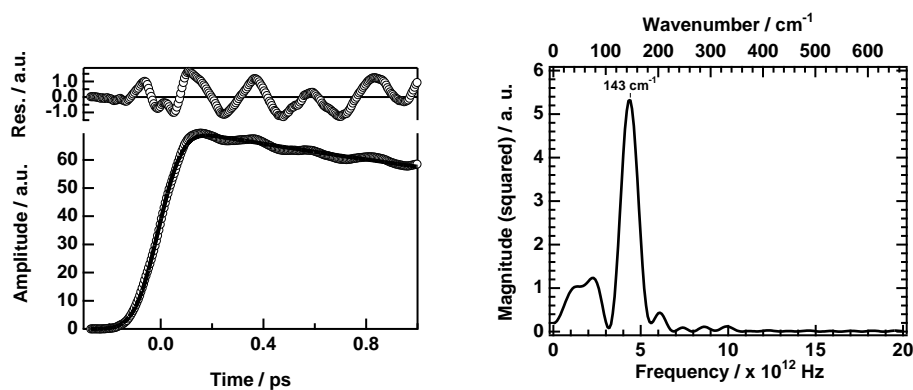

(a) Time base vector and residuals of the fit.

(b) FFT analysis of the residuals.

Figure 7.10 — Analysis of the oscillations observed for Z105 adsorbed on Al_2O_3. The time vector is obtained after SVD data reduction and is corrected for chirp.

In the next paragraph we compare the transient spectrum obtained on titania, illustrating the presence of the dye cation, with the spectrum containing the contribution of the excited state, measured on alumina (figure 7.11). Two features are remarkable. First, the ratio between the positive absorption peak and the negative well, assigned to the bleaching of the ground

state, is much bigger on alumina. This indicate that the excited state shows strong light absorption over the whole spectral range probed in this experiment. Similar conclusions have been drawn for the P0 complex in the previous chapter (6.3.1). At that point we assigned these absorption properties to the terpyridyl anion formed upon excitation.[48] This seems also to be valid in the case of Z105. A second interesting feature is shown by the shape of the peak centered around 580 nm. In contrast to the spectrum observed on TiO_2, this peak is much more pronounced. Again such features are common in ruthenium complexes containing thiocyanate ligands. The maximum of the oxidized state's absorption, assigned to a LMCT transition from the SCN ligand to the metal center, is often significantly red-shifted with respect to the charge transfer from the bi- or terpyridyl ligand to the empty d orbitals of the ruthenium atom as observed in the excited state.[40] In conclusion, the spectral signatures of the two main transient species formed upon light excitation of dye/semiconductor assemblies have been characterized. In the following section, theses differences will be used to discuss the retarded electron injection into niobium oxide films.
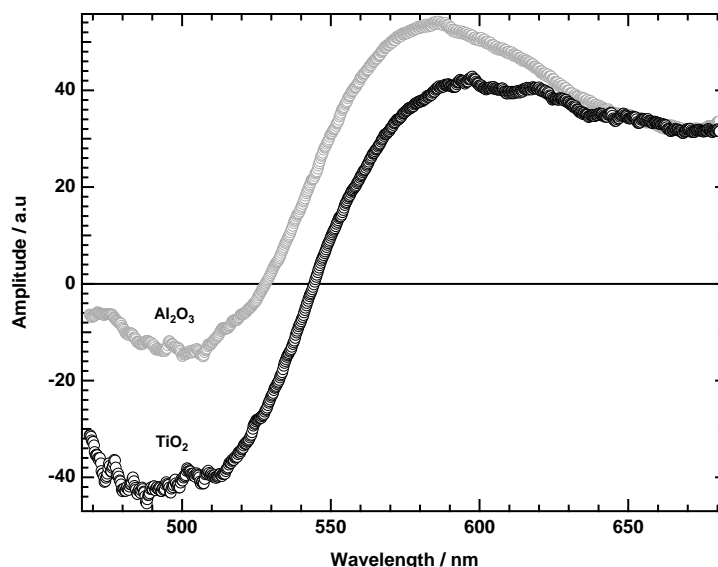
Figure 7.11 — Comparison of the transient spectra obtained after SVD for Z105 on TiO_2 (black circles) and Al_2O_3 (grey circles).

7.3.3 Excitation-wavelength dependence of electron injection into Nb_2O_5

Transient absorption data of Z105 adsorbed onto nanocrystalline niobium oxide have been measured after excitation by ultrashort light pulses cen-
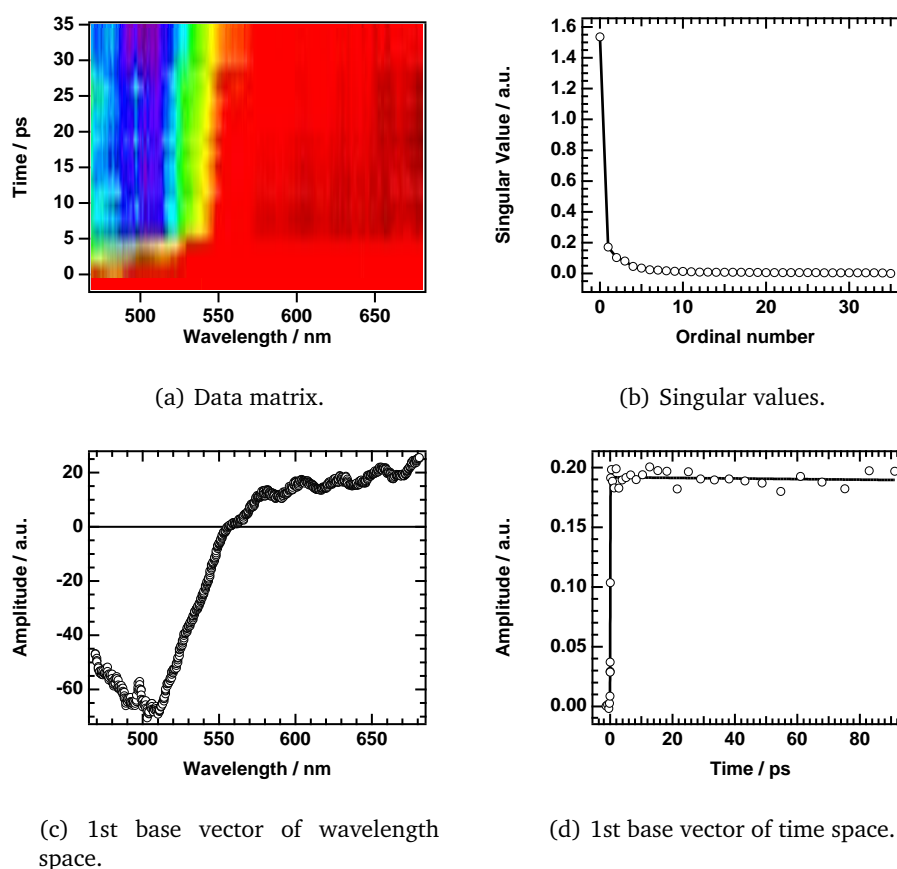
tered at 520, 560, 600, 630 and 670 nm. To predict if electron transfer from Z105 to Nb_2O_5 is possible, we have to estimate the energetic levels involved in the reaction. Previous electrochemical studies of Z105 in DMSO indicated oxidation and reduction potentials at +1.10 and -1.13 V vs. SHE.[11] The minimum energy between the ground and the excited state (E_{0-0}) can be estimated from the intersection between the absorption and the emission spectra. The redox potential of the excited state can then be approximated by the following equation:

$$\phi^0(S^+/S^*) = \phi^0(S^+/S) - E_{0-0}/F \qquad (7.2)$$

where F is the Faraday constant. With E_{0-0} = 1.9 eV, the formal redox potential of the excited state is -0.8 V vs. SHE. This value is slightly higher than the potential estimated for N3 (-0.71 V), and somewhat more positive than the deprotonated form (N719, -0.99 V).[49] The absolute position of the conduction band edge (ϕ_{cb}) of nanocrystalline Nb_2O_5 is much more difficult to estimate. As for other metal oxides, the potential is expected to vary significantly upon adsorption of charged species on the surface.[50] For example, a Nernstian 59 mV/pH shift is often observed in aqueous medium. In addition, ϕ_{cb} also depends on the crystallinity of the material.[28] As a consequence, ϕ_{cb} for nanocrystalline niobia has generally been given relative to TiO_2 and was found to be shifted negatively for ~0.1-0.4 V.[5,6,7] Here we will refer to the values given in the study by Moser et al.[6] since the films were prepared following the same procedure. As small differences are found between the formal redox potential of Z105's excited state and the dye used in their experiments (N3), we expect to reach the conduction band edge when exciting Z105 in the wavelength range 570-620 nm.

Excitation wavelength: 520 nm The data obtained upon excitation of Z105 on Nb_2O_5 at 520 nm (figure 7.12) show many similarities with those observed on TiO_2. As for the previous samples, data reduction was performed by singular value decomposition (SVD). Again a single component is identified. Because of considerable light scattering by the niobia films and also lower optical densities, the results contain much more experimental noise as those obtained on TiO_2 and Al_2O_3. This is illustrated by the increased number of non-negligible singular values as shown in figure 7.12(b). The first ten components have been carefully scrutinized, but only the first component was kept since all the following vectors displayed random time evolution. The spectrum associated with the first singular value is assigned to the product of electron injection into Nb_2O_5 in analogy with that observed on titania. As for TiO_2, the reaction is completed within the instrument response (FWHM=140 fs). This result is in agreement with the observations of Ai et al. of a sub-100 fs component in the electron injection

kinetics of N3 into Nb_2O_5 films. However, no slower phase was observed in our case, indicating that a single mechanism was responsible for excited state quenching. Again, this observation is supported by the idea of aggregation or weak adsorption for N3 and derivative dyes on the surface of metal oxides, developed in the previous chapters. However, even if the slow phase observed in the cited report is due to dyes kept at some distance of the surface, the decrease of the rate constants with the oxidation potential of the excited states might well be a consequence of the reduced density of states near the bottom edge of the conduction band of the semiconductor.

(a) Data matrix.

(b) Singular values.

(c) 1st base vector of wavelength space.

(d) 1st base vector of time space.

Figure 7.12 — Singular value decomposition of the data matrix obtained for Z105 on Nb_2O_5. Excitation wavelength: 520 nm.

Excitation wavelength: 600 nm Except for a decreased signal-to-noise ratio due to lower light absorption, the data measured with a 560 nm excitation reveal similar characteristics as with a 520 nm pump wavelength, i. e. monophasic electron injection within the instrument response. At 600 nm, the noise is further increased and the response is more complex, pre-
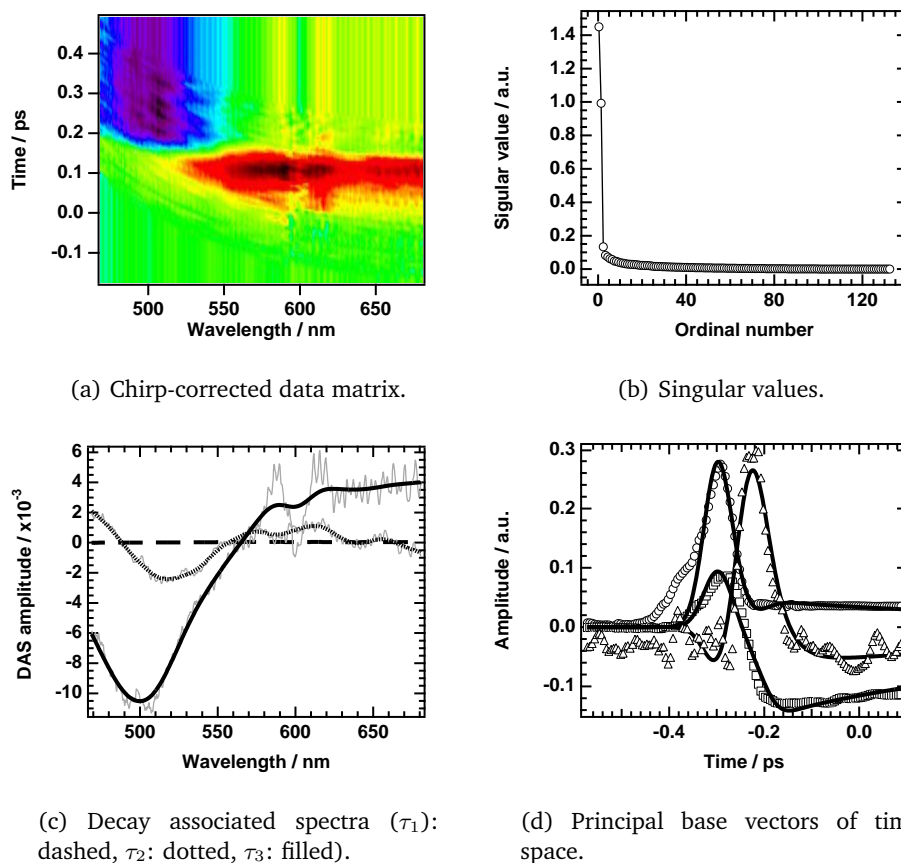
venting interpretation without data reduction. After correction for the chirp, SVD of data obtained with short time steps was performed. From the singular values' plot (fig. 7.13(b)) we deduce that the rank of the inital matrix, corresponding roughly to the number of transient species, is at least two. The analysis of the base vectors associated with the first ten singular values reveals that only the first three components have a non-random time evolution. Since we have more than one significant component, assignment of the base vectors in the wavelength space to transient species is not straightforward as in the previous cases. To extract this information we perform a global analysis of the three orthogonal time vectors and rebuild the decay associated spectra (DAS) from the respective fitted coefficients. Here, the time vectors are fitted with the sum of three exponential decays convoluted with a Gaussian instrument response. The parameters of the Gaussian (μ, σ) and the time constants (τ_1, τ_2 and τ_3) are optimized globally, while the amplitudes vary for each time vector. Finally, the DAS are obtained by the following equation:

$$\text{DAS}_k = \sum_{i=1}^{3} s_i a_{i,k} U_i \qquad (7.3)$$

where index k refers to the convoluted functions, index i to the vectors obtained from the SVD, s_i are the singular values, $a_{i,k}$ the fitted amplitudes and U_i the base vectors in the wavelength space.[51,52] This treatment leads to the DAS showed in figure 7.13, where $\tau_1 = 14$ fs, $\tau_2 = 28$ fs and $\tau_3 = 784$ fs. Obviously, the spectrum associated with τ_1 has a minor contribution and is neglected hereafter. The DAS associated with the longer time constant (τ_3) is almost identical to the one observed on niobia when the same sample is excited at 520 nm. It is therefore assigned to the formation of the oxidized state following electron transfer from Z105 to the conduction band of Nb_2O_5. The remaining spectrum (associated to τ_2) can neither be imputed to the sole contribution of the excited state nor to the dye cation. In contrast, it is consistent with the spectrum obtained when the spectral signature obtained on TiO_2 is subtracted from the one measured on Al_2O_3 (see fig, 7.11). Therefore, we assign this DAS to a mixture of both the excited and the oxidized states. Within this assumption, $\tau_2 = 28$ fs corresponds to the time constant for electron transfer.

In order to refine the analysis, a global fit of the unreduced data matrix was performed in parallel to the procedure using SVD. The model used to fit the matrix consists of an analytical convolution of a Gaussian instrument response with two exponential decays (see 3.4). The amplitudes and the parameters for the Gaussian (μ and σ) have been optimized for each wavelength, while the time constants were optimized globally. To facilitate convergence, the raw data matrix was first interpolated to contain only 30 wavelengths. From the fitted parameters of the instrument response,we

(a) Chirp-corrected data matrix.

(b) Singular values.

(c) Decay associated spectra (τ_1: dashed, τ_2: dotted, τ_3: filled).

(d) Principal base vectors of time space.

Figure 7.13 — Singular value decomposition of the data matrix obtained for Z105 on Nb_2O_5. Excitation wavelength: 600 nm.

could reproduce the chirp and cross-correlation observed by the Kerr gating technique presented in chapter 3. Two decays, with time constants $\tau_1 = 28$ fs and $\tau_2 = 5.4$ ps, gave a satisfying fit in the time range investigated. The decay associated spectra (DAS), containing the optimized amplitudes, are depicted in figure 7.14. The DAS corresponding to the fastest component is very noisy and is therefore difficult to impute to a specific transient species. Interestingly, the time constant found for the fast decay (28 fs) is the same as the one obtained from the previous analysis. In contrast, the spectrum associated with the second decay can clearly be imputed to the oxidized state formed upon electron injection. The value of the time constant is subject to considerable error due to the limited time range and will not be discussed here.

With the application of both the SVD and the global fitting procedures to our measurements, we can build the following, consistent picture. In contrast
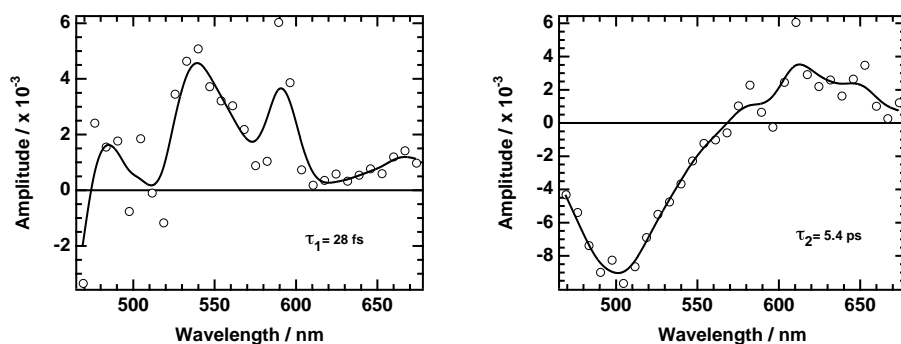
(a) DAS for $\tau_1 = 28$ fs.   (b) DAS for $\tau_1 = 5.4$ ps.

Figure 7.14 — Decay associated spectra (DAS) obtained from a global fit of the chirp-corrected data matrix measured for Z105 on Nb_2O_5. Excitation wavelength: 600 nm.

to data recorded on TiO_2 or on Nb_2O_5 with a shorter excitation wavelength, evidence for the presence of excited dyes surviving the pump laser pulse is observed. Electron transfer follows rapidly with a time constant on the order of 30 fs. From the amplitudes of the time vector associated with the excited state of the dye, it seems that a fraction of the dyes does not inject at all, or at least with a reduced rate.

Excitation wavelength > 600 nm   Unfortunately, the quality of the data obtained with excitation wavelengths of 630 and 670 nm was not good enough to draw reasonable conclusions. As mentioned before, Z105 absorbs weakly above 600 nm and the signal-to-noise ratio is decreased accordingly. As an example, in figure 7.15 we show a plot of the singular values corresponding to the transient data obtained at an excitation wavelength of 670 nm. The number of non-negligible components increases drastically with noise. The component associated with the largest singular value still contains a bleaching below ~ 550 nm and a positive part above, but the poor quality of the data does not allow unequivocal assignment.

Discussion

Electron injection from Z105 to the conduction band of TiO_2 and Nb_2O_5 is found to occur with time constants lower than 30 fs. This is in agreement with the interpretation of Moser and co-workers, who assigned the excitation-wavelength dependence of electron injection yields into various
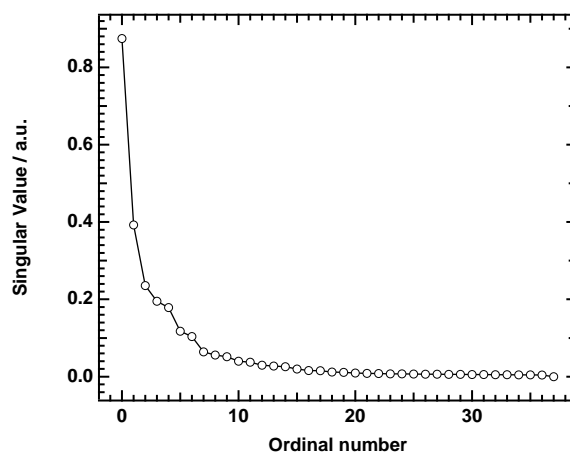
Figure 7.15 — Singular values obtained from the decomposition of data measured for Z105 on Nb_2O_5. Excitation wavelength: 670 nm.

metal oxides semiconductors, to "hot" electron transfer.[6] To our knowledge, the aforementioned study by Ai et al.[12] was the first to report time-resolved measurements of electron injection from Ru complexes to niobium oxide. As for TiO_2, our observations confirm the existence of a fast component but no slower injection phase was noticed, indicating that Z105 is also adsorbed in a uniform way on Nb_2O_5.

Reduction of the electron injection rate due to a lower density of acceptor states in the semiconductor can hardly be detected on Nb_2O_5 expect when the dye is excited at 600 nm. In that particular case, the rate is decreased for $\sim$ 2-3 times if we assume injection times on the order of 10 fs as observed for a bipyridyl ligand alone[53] or from theoretical contributions.[36,54,55] Assuming that the density of states drops exponentially below the conduction band edge, and a linear dependence of the reaction rate with the density of states, we would expect a much larger effect. However, at least two reasons can be invoked to rationalize our observations.

First, one should remark that the femtosecond light pulses produced in our NOPA generally have a spectral width of about 30 nm, approaching the Fourier limit.[56] If we report this width on the potential scale used to discuss the energetics relevant to electron transfer we find that this parameter is no more negligible (figure 7.16). For example, a laser pulse centered at 600 nm with FWHM = 30 nm, covers a range of about 200 meV. If we add thermal disorder in the ground state at room temperature ($\sim$3 kT), the energy distribution of the unrelaxed excited states might well cover the potential range corresponding to the exponential breakdown of the density of states in the semiconductor.
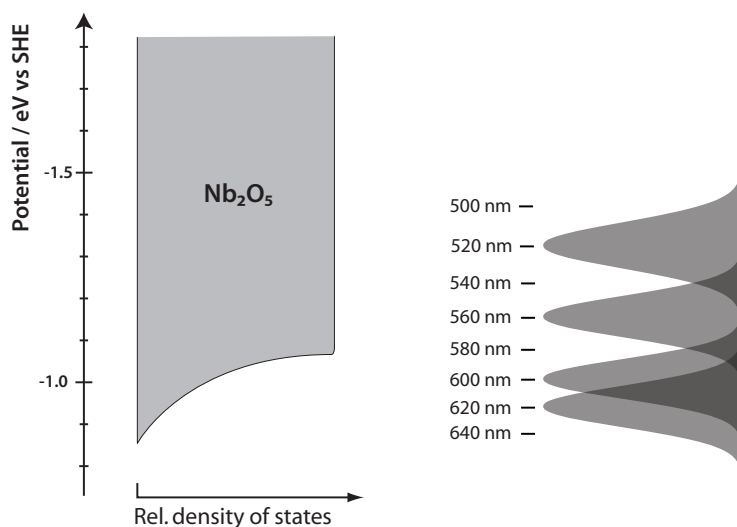
Figure 7.16 — Energy diagram representing the energy bandwidth of femtosecond pulses relative to the conduction band of Nb_2O_5. The flat-band potential of the semiconductor is adopted from Moser et al.[6] and the level of the fs pulse levels are calculated from the oxidation potential of Z105 in DMSO ($\phi^0(S^+/S) = + 1.1$ V vs. SHE).

To refine this picture, some knowledge of the extent of the falloff region is essential. This topic is currently under intense debate for TiO_2 due to its influence on the open-circuit potential (V_{oc}) of dye-sensitized solar cells. Unfortunately, little is know about these properties in Nb_2O_5 nanocrystalline films. From the slope of the light absorption spectrum around the bandgap region and also from photovoltammetry measurements, one can roughly estimate that the density of states grows over $\sim$300 mV.[7,9,28] Like many other oxide semiconductors, niobia tends to be oxygen deficient. Therefore, comparison with titania is useful to understand how surface defect states can influence the profile of the conduction band edge. From various photoelectrochemical techniques, the energy distribution of trap states $g(E)$ has been found to have an exponential form:

$$g(E) = g_0 \exp\left(\alpha \frac{E - E_{cb}}{kT}\right) \tag{7.4}$$

where E is the trap energy, E_{cb} the conduction band edge energy and the parameter g_0 is a constant. The parameter α which describes the steepness of the trap-state distribution, is related to the average trap depth m_c by the equality: $\alpha = kT/m_c$.[57] Typical experimental values are found in the range $m_c = 60\text{-}100$ meV.[58,59,60,61,62,63] The profiles of the densities of states calculated from equation 7.4 for typical m_c values are depicted in figure 7.17. These estimations indicate that the energy range corresponding to trap

states below the conduction band edge, extends over 300-400 meV. This is in agreement with the rough approximation made for Nb_2O_5. Taking now the trap distribution and the width of the laser pulses into consideration, we understand that we almost probe the totality of the depletion zone with an excitation pulse centered close to an optimal wavelength. This may explain why we could observe effects related to the varying density of states only at a single wavelength (i.e. 600 nm). With the technique used in this study, we were not able to probe the very bottom of the states distribution where the DOS should drop for orders of magnitude, revealing proportional effects on the kinetics of electron transfer.
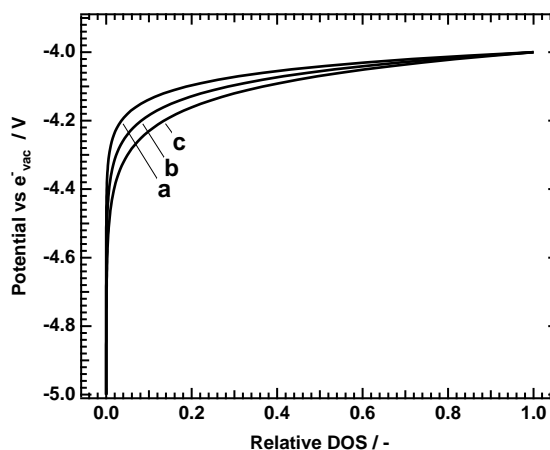
Figure 7.17 — Energy distribution of trap states calculated from equation 7.4. The value of α is obtained from the average trap depth m_c equal to a) 60 meV b) 80 meV and c) 100 meV.

The preceding remarks about the distribution of states in the semiconductor were based on the assumption that these states are actually empty in the course of the experiments. Due to the high fluence (up to 9 sun) necessary to measure weak absorption differences, the Fermi level in the semiconductor may increase dramatically under illumination. The kinetics of back electron transfer of an injected electron to the oxidized dye for Z105 on TiO_2, was found to be significantly shorter than the interval between two pulses (1 ms). Thus, except for deep traps, we do not expect charge accumulation. However within pulse rise, we expect the density of acceptor states to be considerably reduced by the number of electrons injected. Trapping of electrons in the conduction band of nanocrystalline metal oxides can occur in less than 500 fs.[64,65,66] Therefore, after a short time delay, the profile of the empty acceptor states distribution can be considerably altered by trap-filling upon illumination. This effect could explain why we were not able to record the DOS effect on a longer timescale.

7.4   Conclusions

Summary   Based on a study by Moser and co-workers, we tackled the question of the effect of the density of acceptor states on the kinetics of electron transfer at dye/semiconductor interfaces, by varying the wavelength of the excitation laser pulse. Since electron transfer is expected to occur from a "hot", thermally unrelaxed state, isoenergetic levels in the semiconductor will be probed. After a thorough review of the characteristics of the Z105 dye sensitizer and additional *ab initio* computation of the dye's electronic configuration, we performed femtosecond transient absorption measurements by the pump-supercontinuum probe technique. Excited state dynamics of Z105 adsorbed on nanocrystalline films of TiO_2 and Al_2O_3 revealed the spectral signatures of the excited and oxidized state of Z105. On alumina, the observation of oscillations attributed to some low frequency vibrational mode of the dye, surviving for several picoseconds supports the idea that electron transfer on TiO_2 is achieved before thermal relaxation.

Because of a negative shift of the conduction band edge potential of niobia with respect to titania, nanocrystalline Nb_2O_5 films were used to investigate electron injection from an excited state in the vicinity of the bottom of the accepting band. When excited with a laser pulse centered at 520 nm, the excited state of Z105 lies above the conduction band edge of Nb_2O_5. In these conditions, ultrafast electron injection was observed within the pulse duration. In contradiction with a recent study of the kinetics of the sensitization of niobia by different ruthenium polypyridyl complexes, no slow phase was observed.[12] As for N3-sensitized TiO_2, we attribute the slower phase to injection from weakly adsorbed or aggregated dyes kept at some distance from the semiconductor's surface.

When the sample is excited at 600 nm, we observed a slight retardation of the electron injection ($\tau_{ET} = 28$ fs) that we assign to an effect of the density of states. In addition we observed that some excited dyes remain after the fast injection phase, indicating that one part of the excited population could not inject. Unfortunately, for longer wavelengths, no trustable data could be obtained because of the low signal-to-noise ratio of the experimental response.

The decrease of the electron transfer rate due to the reduced density of states at the bottom of the conduction band of Nb_2O_5, is much smaller than expected if we consider that the profile of the trap state distribution follows an exponential falloff. After careful examination of the reported distribution of accepting states and of the energy range associated with the spectral width of the excitation pulses, we find that the spectral resolution is not

good enough to obtain an accurate description of the problem with this technique.

Outlook The distribution of acceptor states in the conduction band of semiconductors is often invoked to discuss the kinetics of electron transfer at dye/semiconductor interfaces. Our result indicate that due to the inherent spectral width of femtosecond laser pulsed, it is very difficult to investigate the dependence upon the density of states for hot electron injection. In terms of standard electron transfer theory, we remark that the electronic factors dominate the variations of injection kinetics, namely by the effect of distance. Nuclear factors certainly play an important role in this type of reaction but the weak dependence upon the DOS indicate that a near-unity FCWD is present in most cases.

As mentioned above, in the case of biphasic electron injection, effects related to the density of states are observed. However, it should be mentioned that these observations concern thermally relaxed dyes. Although it has not yet been clearly established, electron transfer might not happen in the same regime in the fast and the slow phase. In other words, a transition between a barrierless regime and an activation regime can take place. Under these conditions, nuclear factors are expected to play an important role.

Despite the weak effects observed so far, we think that this approach deserves further attention. The main drawbacks of the samples used in this study consisted in excessive light scattering and low light absorption above 600 nm. New films have recently been prepared in our group with better optical properties and also higher roughness factors. In conjunction with the use of dyes with an extended extinction coefficient in the red part of the spectrum, without forming aggregates, it should be possible to refine the results presented here.

7.5 References

1. Newton, M. D.; Sutin, N. "Electron-Transfer Reactions In Condensed Phases", *Annu. Rev. Phys. Chem.* **1984,** *35,* 437-480.

2. Sumi, H. Electron Transfer in Chemistry. In , Vol. 1; Balzani, V., Ed.; Wiley-VCH: 2001; Chapter "Adiabatic versus Non-Adiabatic Electron Transfer", pages 64–108.

3. Thoss, M.; Kondov, I.; Wang, H. B. "Theoretical study of ultrafast heterogeneous electron transfer reactions at dye-semiconductor interfaces", *Chem. Phys.* **2004,** *304,* 169-181.

4. Grätzel, M. "Conversion of sunlight to electric power by nanocrystalline dye-sensitized solar cells", *J. Photochem. Photobiol. A* **2004,** *164,* 3-14.

5. Sayama, K.; Sugihara, H.; Arakawa, H. "Photoelectrochemical properties of a porous Nb_2O_5 electrode sensitized by a ruthenium dye", *Chem. Mater.* **1998,** *10,* 3825-3832.

6. Moser, J. E.; Wolf, M.; Lenzmann, F.; Grätzel, M. "Photoinduced charge injection from vibronically hot excited molecules of a dye sensitizer into acceptor states of wide-bandgap oxide semiconductors", *Z. Phys. Chem.* **1999,** *212,* 85-92.

7. Lenzmann, F.; Krueger, J.; Burnside, S.; Brooks, K.; Grätzel, M.; Gal, D.; Ruhle, S.; Cahen, D. "Surface photovoltage spectroscopy of dye-sensitized solar cells with TiO_2, Nb_2O_5, and $SrTiO_3$ nanocrystalline photoanodes: Indication for electron injection from higher excited dye states", *J. Phys. Chem. B* **2001,** *105,* 6347-6352.

8. Katoh, R.; Furube, A.; Yoshihara, T.; Hara, K.; Fujihashi, G.; Takano, S.; Murata, S.; Arakawa, H.; Tachiya, M. "Efficiencies of electron injection from excited N3 dye into nanocrystalline semiconductor (ZrO_2, TiO_2, ZnO, Nb_2O_5, SnO_2, In2O3) films", *J. Phys. Chem. B* **2004,** *108,* 4818-4822.

9. Lenzmann, F. *Mesoporous, Nanoparticulate Films of Nb_2O_5 and ZrO_2. Preparation and Characterization.,* Thesis, Ecole Polytechnique Fédérale de Lausanne, 2000.

10. Filho, D. D. B.; Franco, D. W.; Filho, P. P. A.; Alves, O. L. "Niobia films: surface morphology, surface analysis, photoelectrochemical properties and crystallization process", *J. Mater. Sci.* **1998,** *33,* 2607-2616.

11. Zakeeruddin, S. M.; Nazeeruddin, M. K.; Pechy, P.; Rotzinger, F. P.; Humphry-Baker, R.; Kalyanasundaram, K.; Grätzel, M.; Shklover, V.; Haibach, T. "Molecular engineering of photosensitizers for nanocrystalline solar cells: Synthesis and characterization of Ru dyes based on phosphonated terpyridines", *Inorg. Chem.* **1997,** *36,* 5937-5946.

12. Ai, X.; Guo, J. C.; Anderson, N. A.; Lian, T. Q. "Ultrafast electron transfer from Ru polypyridyl complexes to Nb_2O_5 nanoporous thin films", *J. Phys. Chem. B* **2004,** *108,* 12795-12803.

13. Moser, J. E.; Grätzel, M. "Excitation-wavelength dependence of photoinduced charge injection at the semiconductor-dye interface: Evidence for electron transfer from vibrationally hot excited states", *Chimia* **1998,** *52,* 160-162.

14. Aegerter, M. A. "Sol-gel niobium pentoxide: A promising material for electrochromic coatings, batteries, nanocrystalline solar cells and catalysis", *Sol. Energy Mater. Sol. Cells* **2001,** *68,* 401-422.

15. Barros, D. D.; Abreu, P. P.; Alves, O. L.; Franco, D. W. "Sensitization of niobium pentoxide thin films by cis-dithiocyanate (2,2-bipyridyl-4,4 ' dicarboxylic acid) ruthenium(II) complex", *J. Sol-Gel. Sci. Technol.* **2000,** *18,* 259-267.

16. Barros, D.; Abreu, P.; Werner, U.; Aegerter, M. "Photoelectrochemical properties of sol-gel Nb_2O_5 films", *J. Sol-Gel. Sci. Technol.* **1997,** *8,* 735–742.

17. Guo, P.; Aegerter, M. "Ru(II) sensitized Nb_2O_5 solar cell made by the sol-gel process", *Thin Solid Films* **1999,** *351,* 290–294.

18. Hara, K.; Horiguchi, T.; Kinoshita, T.; Sayama, K.; Sugihara, H.; Arakawa, H. "Highly efficient photon-to-electron conversion with mercurochrome-sensitized nanoporous oxide semiconductor solar cells", *Sol. Energy Mater. Sol. Cells* **2000,** *64,* 115–134.

19. Chen, S. G.; Chappel, S.; Diamant, Y.; Zaban, A. "Preparation of Nb_2O_5 coated TiO_2 nanoporous electrodes and their application in dye-sensitized solar cells", *Chem. Mater.* **2001,** *13,* 4629-4634.

20. Zaban, A.; Chen, S. G.; Chappel, S.; Gregg, B. A. "Bilayer nanoporous electrodes for dye sensitized solar cells", *Chem. Commun.* **2000,** 2231-2232.

21. Anderson, N. A.; Lian, T. "Ultrafast electron injection from metal polypyridyl complexes to metal-oxide nanocrystalline thin films", *Coord. Chem. Rev.* **2004,** *248,* 1231-1246.

22. Tachibana, Y.; Haque, S. A.; Mercer, I. P.; Moser, J. E.; Klug, D. R.; Durrant, J. R. "Modulation of the rate of electron injection in dye-sensitized nanocrystalline TiO_2 films by externally applied bias", *J. Phys. Chem. B* **2001,** *105,* 7424-7431.

23. Asbury, J. B.; Anderson, N. A.; Hao, E. C.; Ai, X.; Lian, T. Q. "Parameters affecting electron injection dynamics from ruthenium dyes to titanium dioxide nanocrystalline thin film", *J. Phys. Chem. B* **2003,** *107,* 7376-7386.

24. Furube, A.; Katoh, R.; Hara, K.; Sato, T.; Murata, S.; Arakawa, H.; Tachiya, M. "Lithium ion effect on electron injection from a photoexcited coumarin derivative into a TiO_2 nanocrystalline film investigated by visible-to-IR ultrafast spectroscopy", *J. Phys. Chem. B* **2005,** *109,* 16406–16414.

25. Kelly, C. A.; Farzad, F.; Thompson, D. W.; Stipkala, J. M.; Meyer, G. J. "Cation-controlled interfacial charge injection in sensitized nanocrystalline TiO_2", *Langmuir* **1999,** *15,* 7047-7054.

26. She, C.; Anderson, N.; Guo, J.; Liu, F.; Goh, W.; Chen, D.; Mohler, D.; Tian, Z.; Hupp, J.; Lian, T. "pH-dependent electron transfer from Re-bipyridyl complexes to metal oxide nanocrystalline thin films", *J. Phys. Chem. B* **2005,** *109,* 19345–19355.

27. Nuesch, F.; Moser, J. E.; Shklover, V.; Grätzel, M. "Merocyanine aggregation in mesoporous networks", *J. Am. Chem. Soc.* **1996,** *118,* 5420-5431.

28. Lenzmann, F.; Shklover, V.; Brooks, K.; Grätzel, M. "Mesoporous Nb_2O_5 films: Influence of degree of crystallinity on properties", *J. Sol-Gel. Sci. Technol.* **2000,** *19,* 175-180.

29. Bonhôte, P.; Dias, A. P.; Papageorgiou, N.; Kalyanasundaram, K.; Grätzel, M. "Hydrophobic, highly conductive ambient-temperature molten salts", *Inorg. Chem.* **1996,** *35,* 1168-1178.

30. Stevens, W.; Krauss, M.; Basch, H.; Jasien, P. "Relativistic Compact Effective Potentials And Efficient, Shared-Exponent Basis-Sets For The 3rd-Row, 4th-Row, And 5th-Row Atoms", *Can. J. Chem.* **1992,** *70,* 612–630.

31. Schmidt, M.; Baldridge, K.; Boatz, J.; Elbert, S.; Gordon, M.; Jensen, J.; Koseki, S.; Matsunaga, N.; Nguyen, K.; SU, S.; Windus, T.; Dupuis, M.; Montgomery, J. "General Atomic And Molecular Electronic-Structure System", *J. Comput. Chem.* **1993,** *14,* 1347–1363.

32. Gillaizeau-Gauthier, I.; Odobel, F.; Alebbi, M.; Argazzi, R.; Costa, E.; Bignozzi, C.; Qu, P.; Meyer, G. "Phosphonate-based bipyridine dyes for stable photovoltaic devices", *Inorg. Chem.* **2001,** *40,* 6073–6079.

33. Nilsing, M.; Lunell, S.; Persson, P.; Ojamae, L. "Phosphonic acid adsorption at the TiO_2 anatase (101) surface investigated by periodic hybrid HF-DFT computations", *Surf. Sci.* **2005,** *582,* 49–60.

34. Bae, E.; Choi, W.; Park, J.; Shin, H.; Kim, S.; Lee, J. "Effects of surface anchoring groups (Carboxylate vs phosphonate) in ruthenium-complex-sensitized TiO_2 on visible light reactivity in aqueous suspensions", *J. Phys. Chem. B* **2004,** *108,* 14093–14101.

35. Guerrero, G.; Mutin, P.; Vioux, A. "Anchoring of phosphonate and phosphinate coupling molecules on titania particles", *Chem. Mater.* **2001,** *13,* 4367–4373.

36. Persson, P.; Lundqvist, M. J. "Calculated structural and electronic interactions of the ruthenium dye N3 with a titanium dioxide nanocrystal", *J. Phys. Chem. B* **2005,** *109,* 11918-11924.

37. Fantacci, S.; De Angelis, F.; Selloni, A. "Absorption spectrum and solvatochromism of the $[Ru(4,4'-COOH-2,2'-bpy)_2(NCS)_2]$ molecular dye by time dependent density functional theory", *J. Am. Chem. Soc.* **2003,** *125,* 4381-4387.

38. Monat, J. E.; Rodriguez, J. H.; McCusker, J. K. "Ground- and excited-state electronic structures of the solar cell sensitizer bis(4,4'-dicarboxylato-2,2'-bipyridine)bis(isothiocyanato)ruthenium(II)", *J. Phys. Chem. A* **2002,** *106,* 7399-7406.

39. Satzger, H.; Zinth, W. "Visualization of transient absorption dynamics - towards a qualitative view of complex reaction kinetics", *Chem. Phys.* **2003,** *295,* 287-295.

40. Moser, J. E.; Noukakis, D.; Bach, U.; Tachibana, Y.; Klug, D. R.; Durrant, J. R.; Humphry-Baker, R.; Grätzel, M. "Comment on measurement of ultrafast photoinduced electron transfer from chemically anchored Ru-dye molecules into empty electronic states in a colloidal anatase TiO_2 film", *J. Phys. Chem. B* **1998,** *102,* 3649-3650.

41. Haque, S. A.; Tachibana, Y.; Willis, R. L.; Moser, J. E.; Grätzel, M.; Klug, D. R.; Durrant, J. R. "Parameters influencing charge recombination kinetics in dye-sensitized nanocrystalline titanium dioxide films", *J. Phys. Chem. B* **2000,** *104,* 538-547.

42. Nusbaumer, H.; Moser, J. E.; Zakeeruddin, S. M.; Nazeeruddin, M. K.; Grätzel, M. "Co-II(dbbiP)$_2^{2+}$ complex rivals tri-iodide/iodide redox mediator in dye-sensitized photovoltaic cells", *J. Phys. Chem. B* **2001,** *105,* 10461-10464.

43. Kallioinen, J.; Benkö, G.; Myllyperkiö, P.; Khriachtchev, L.; Skårman, B.; Wallenberg, R.; Tuomikoski, M.; Korppi-Tommola, J.; Sundström, V.; Yartsev, A. P. "Photoinduced ultrafast dynamics of Ru(dcbpy)$_2$(NCS)$_2$- sensitized nanocrystalline TiO$_2$ films: The influence of sample preparation and experimental conditions", *J. Phys. Chem. B* **2004,** *108,* 6365-6373.

44. Bhasikuttan, A. C.; Suzuki, M.; Nakashima, S.; Okada, T. "Ultrafast fluorescence detection in tris(2,2 '-bipyridine)ruthenium(II) complex in solution: Relaxation dynamics involving higher excited states", *J. Am. Chem. Soc.* **2002,** *124,* 8398-8405.

45. Bhasikuttan, A. C.; Okada, T. "Excited-state relaxation dynamics of Ru(dcbpy)$_2$(NCS)$_2$, studied by fluorescence upconversion spectroscopy", *J. Phys. Chem. B* **2004,** *108,* 12629-12632.

46. McCusker, J. K. "Femtosecond absorption spectroscopy of transition metal charge-transfer complexes", *Acc. Chem. Res.* **2003,** *36,* 876-887.

47. Ruan, H.; Frost, R.; Kloprogge, J.; Duong, L. "Far-infrared spectroscopy of alumina phases", *Spectrochim. Acta, Part A* **2002,** *58,* 265–272.

48. Amouyal, E.; Mouallem-Bahout, M.; Calzaferri, G. "Excited States of M(II,d^6)-4'-Phenylterpyridine Complexes: Electron Localization", *J. Phys. Chem.* **1991,** *95,* 7641-7649.

49. Nazeeruddin, M. K.; Zakeeruddin, S. M.; Humphry-Baker, R.; Jirousek, M.; Liska, P.; Vlachopoulos, N.; Shklover, V.; Fischer, C. H.; Grätzel, M. "Acid-base equilibria of (2,2 '-bipyridyl-4,4 '-dicarboxylic acid)ruthenium(II) complexes and the effect of protonation on charge-transfer sensitization of nanocrystalline titania", *Inorg. Chem.* **1999,** *38,* 6298-6305.

50. Watson, D.; Meyer, G. "Electron injection at dye-sensitized semiconductor electrodes", *Annu. Rev. Phys. Chem.* **2005,** *56,* 119–156.

51. van Stokkum, I.; Larsen, D.; van Grondelle, R. "Global and target analysis of time-resolved spectra", *Biochimica Et Biophysica Acta-Bioenergetics* **2004,** *1657,* 82–104.

52. Bonacina, L. *Ultrafast Structural Dynamics in Electronically Excited Many-Body Systems,* Thesis, Ecole Polytechnique Fédérale de Lausanne, 2004.

53. Schnadt, J.; Brühwiler, P. A.; Patthey, L.; O'Shea, J. N.; Södergren, S.; Odelius, M.; Ahuja, R.; Karis, O.; Bässler, M.; Persson, P.; Siegbahn, H.; Lunell, S.; Mårtensson, N. "Experimental evidence for sub-3-fs charge transfer from an aromatic adsorbate to a semiconductor", *Nature* **2002,** *418,* 620-623.

54. Ramakrishna, S.; Willig, F.; May, V.; Knorr, A. "Femtosecond spectroscopy of heterogeneous electron transfer: Extraction of excited-state population dynamics from pump-probe signals", *J. Phys. Chem. B* **2003,** *107,* 607-611.

55. Stier, W.; Prezhdo, O. V. "Nonadiabatic molecular dynamics simulation of light-induced, electron transfer from an anchored molecular electron donor to a semiconductor acceptor", *J. Phys. Chem. B* **2002,** *106,* 8047-8054.

56. Diels, J.-C.; Rudolph, W. *Ultrashort Laser Pulse Phenomena;* Academic Press, Inc.: 1996.

57. Frank, A. J.; Kopidakis, N.; van de Lagemaat, J. "Electrons in nanostructured TiO$_2$ solar cells: transport, recombination and photovoltaic properties", *Coord. Chem. Rev.* **2004,** *248,* 1165-1179.

58. Durrant, J. R.; Haque, S. A.; Palomares, E. "Towards optimisation of electron transfer processes in dye sensitised solar cells", *Coord. Chem. Rev.* **2004,** *248,* 1247-1257.

59. Fabregat-Santiago, F.; Mora-Sero, I.; Garcia-Belmonte, G.; Bisquert, J. "Cyclic voltammetry studies of nanoporous semiconductors. Capacitive and reactive properties of nanocrystalline TiO_2 electrodes in aqueous electrolyte", *J. Phys. Chem. B* **2003,** *107,* 758-768.

60. van de Lagemaat, J.; Frank, A. J. "Effect of the surface-state distribution on electron transport in dye-sensitized TiO_2 solar cells: Nonlinear electron-transport kinetics", *J. Phys. Chem. B* **2000,** *104,* 4292-4294.

61. van de Lagemaat, J.; Frank, A. J. "Nonthermalized electron transport in dye-sensitized nanocrystalline TiO_2 films: Transient photocurrent and random-walk modeling studies", *J. Phys. Chem. B* **2001,** *105,* 11194-11205.

62. Neale, N. R.; Kopidakis, N.; van de Lagemaat, J.; Grätzel, M.; Frank, A. J. "Effect of a Coadsorbent on the Performance of Dye-Sensitized TiO_2 Solar Cells: Shielding versus Band-Edge Movement", *J. Phys. Chem. B* **2005,** *109,* ASAP.

63. Zhang, Z.; Zakeeruddin, S.; O'Regan, B.; Humphry-Baker, R.; Grätzel, M. "Influence of 4-Guanidinobutyric Acid as Coadsorbent in Reducing Recombination in Dye-Sensitized Solar Cells", *J. Phys. Chem. B* **2005,** *109,* ASAP.

64. Cavaleri, J. J.; Colombo, D. P.; Bowman, R. M. "Ultrafast charge carrier dynamics of SnO_2 nanoclusters: A refined-interpretation of the electron-hole kinetics in metal oxides", *J. Phys. Chem. B* **1998,** *102,* 1341-1346.

65. Colombo, D. P.; Roussel, K. A.; Saeh, J.; Skinner, D. E.; Cavaleri, J. J.; Bowman, R. M. "Femtosecond Study of the Intensity Dependence of Electron-Hole Dynamics in TiO_2 Nanoclusters", *Chem. Phys. Letters* **1995,** *232,* 207-214.

66. Turner, G. M.; Beard, M. C.; Schmuttenmaer, C. A. "Carrier localization and cooling in dye-sensitized nanocrystalline titanium dioxide", *J. Phys. Chem. B* **2002,** *106,* 11716-11719.

CHAPTER 8

Summary and outlook

Summary

In this work, we studied the influence of the electronic and nuclear factors controlling the dynamics of electron transfer at dye/semiconductor interfaces. Although the principal experimental tool was a versatile femtosecond spectrometer, valuable results were also obtained by time-resolved spectroscopy in the ns-ms time domain. The improvements of the experimental setup, especially to optimize the quality of data acquisition in the pump-supercontinuum probe scheme, was an important part of the work.

In the first part, we reported the observation of a reductive quenching mechanism when high iodide concentrations are present in the electrolyte. Here, the system studied consisted of derivatives of the standard N3 dye [Ru^{II}-(dcbpyH$_2$)$_2$(NCS)$_2$] adsorbed on nanocrystalline TiO$_2$ films. This alternative deactivation pathway, made possible by the use of ionic liquids, has been characterized by nanosecond and femtosecond measurements. It has namely been found that excited state interception by iodide ions occurs on

a sub-50 ps timescale, excluding diffusion of the reactants. From these experiments, we conclude that the dyes that undergo reductive quenching by iodide are not directly adsorbed at the surface of the semiconductor. Instead, these results suggest that dye aggregation is present in the mesoporous film.

In the light of the previous results, we investigated the effect of the sample preparation on the injection dynamics of N3 (and its deprotonated analog N719) into TiO_2. Strikingly, when the conditions are optimized to reduce aggregation, the slow kinetic component was reduced, and even disappeared completely for N719. These results strongly question the previous two-state mechanism adopted by several research groups. In addition, the rate of monophasic electron transfer ($\tau < 20$ fs), indicates that vibration-mediated ET, as predicted by standard models, can not be applied in this case. These observations rather suggest that the injection is controlled by electron dephasing in the solid.

In the following chapters, deliberate strategies are adopted to examine the influence of electronic coupling and nuclear factors on the charge injection process. First, the distance between the chromophore and the semiconductor acceptor states is systematically increased by two different approaches: a) the use of bridged sensitizers containing phenyl groups between the chromophore and the anchoring group and b) coating the TiO_2 film with thin layers of Al_2O_3 of various thicknesses. For bridged sensitizers, both forward and back electron transfers show an exponential dependence upon distance, in agreement with a process governed by electron tunneling. However, the damping factors estimated from our results are not identical for both transfers, indicating that nuclear reorganization plays a role in the back ET reaction. Because of heterogeneous injection kinetics, no verification of an exponential dependence could be achieved for the samples featuring thin alumina layers. However, qualitative analysis of the data indicate that the influence of the distance for electron injection is similar to that observed for back ET, i.e. an exponential dependence with $\beta = 0.15\,\text{Å}^{-1}$. This value is extremely low as indicated by comparisons with basic calculations of electron tunneling across a potential barrier. Referring to studies reporting efficient tunneling through amorphous aluminum oxide barriers, we suggest that the poor crystallinity of the alumina layer results in the presence of low-lying empty states prone to be involved in a superexchange mechanism.

A second strategy, more likely to reveal effects imputed to nuclear factors, is to examine the density of acceptor states in the semiconductor, by a systematic variation of the excitation wavelength. The idea is that since electron transfer occurs prior to vibrational relaxation of the excited dye, isoenergic states of the conduction band will be probed. Since the density of states is expected to fall off exponentially at the bottom of the conduction band,

it is essential that the energies of the excited states match with the band edge. According to a previous study, this condition is fulfilled for Nb_2O_5 films sensitized by a ruthenium polypyridyl complex. Surprisingly, a very weak retardation was observed (2-3 times). After careful analysis, we conclude that the spectral width inherent to femtosecond laser pulses is too broad to accurately probe the variations of the density of states.

Outlook

The sum of the results obtained in this work provides an improved perception of the intimate mechanisms governing electron transfer at dye/semiconductor interfaces. Several findings have direct implications for the scientific community concerned with dye-sensitized solar cells. First, the presence of the reductive quenching mechanism has previously only been taken into consideration for dyes that do not inject directly in their excited state.[1,2] With the systematic use of ionic liquids to improve the stability of DSCs, this issue can no longer be neglected.[3,4,5,6,7,8,9,10] The possibility of reductive quenching also indicates that ultrafast electron transfer is essential for optimal performance, suggesting that the concept of "kinetic redundancy" introduced by Durrant and co-workers has to be refined.[11,12]

The influence of dye aggregation on the dynamics of electron injection is relevant to both DSC performance and to the general interpretation of ultrafast kinetics at semiconductor interfaces. While the role of aggregation has recently been illustrated in the effect of adsorbents cografted with a sensitizer on TiO_2,[13] our results show that this parameter has to be considered in any process involving adsorption of dyes at heterogeneous interfaces. In particular, the previous interpretations of N3-sensitized TiO_2 have to be revisited with this issue kept in mind. The parameters influencing the dynamics of interfacial ET for ruthenium polypyridyl complexes have essentially been discussed on the basis of effects observed on the slower kinetic components.[12,14,15,16,17,18] While the conclusions drawn from these experiments are probably correct for weakly adsorbed species, they may reveal erroneous for molecules directly adsorbed on the surface. This opinion is reinforced by the magnitude of the rate constants obtained for strongly adsorbed dyes, which suggest a transition from a vibration-mediated model towards a regime where the transfer is governed by electron dephasing in the solid.[19,20,21]

Globally, the picture that arises from this work is that electronic factors mostly govern injection dynamics. As mentioned, exponential distance-dependencies and the dramatic effects related to dye aggregation (3 orders

of magnitude retardation) are consistent with electron tunneling mechanisms. Even when the density of states is reduced, it seem that the nuclear factors tend to unity for dye sensitization of metal oxide semiconductors.

From these considerations, one can envisage further work in the following directions. First, the study of the influence of the density of states should be continued. Since visible light pulses seem to be too broad to resolve the acceptor's DOS at the bottom of the conduction band, one could think of using infrared radiation to excite the dyes. The difficulty of this approach is naturally to find a dye/semiconductor couple with matching energy levels. For direct infrared excitation, the HOMO has to lie slightly below the conduction band. This approach may be difficult to concretize since the highest occupied levels of organic and inorganic dyes are usually found several eV below. Another strategy could be to first prepare the dye in a non-injecting relaxed excited state by a visible pulse and further populate higher states with a delayed infrared laser pulse. Refinement of the injection kinetics across insulating layers could also be performed by the use of a dye presenting monophasic injection. The control of the crystallinity of the metal oxide layer is also required to assess the results presented in this thesis.

8.1 References

1. Bergeron, B. V.; Meyer, G. J. "Reductive electron transfer quenching of MLCT excited states bound to nanostructured metal oxide thin films", *J. Phys. Chem. B* **2003,** *107,* 245-254.

2. Thompson, D. W.; Kelly, C. A.; Farzad, F.; Meyer, G. J. "Sensitization of nanocrystalline TiO$_2$ initiated by reductive quenching of molecular excited states", *Langmuir* **1999,** *15,* 650-653.

3. Papageorgiou, N.; Athanassov, Y.; Armand, M.; Bonhôte, P.; Pettersson, H.; Azam, A.; Grätzel, M. "The performance and stability of ambient temperature molten salts for solar cell applications", *J. Electrochem. Soc.* **1996,** *143,* 3099-3108.

4. Wang, P.; Zakeeruddin, S. M.; Moser, J. E.; Humphry-Baker, R.; Grätzel, M. "A solvent-free, SeCN-/(SeCN)$_3^-$ based ionic liquid electrolyte for high-efficiency dye-sensitized nanocrystalline solar cells", *J. Am. Chem. Soc.* **2004,** *126,* 7164-7165.

5. Wang, P.; Zakeeruddin, S. M.; Moser, J. E.; Nazeeruddin, M. K.; Sekiguchi, T.; Grätzel, M. "A stable quasi-solid-state dye-sensitized solar cell with an amphiphilic ruthenium sensitizer and polymer gel electrolyte", *Nat. Mater.* **2003,** *2,* 402-407.

6. Wang, P.; Wenger, B.; Humphry-Baker, R.; Moser, J. E.; Teuscher, J.; Kantlehner, W.; Mezger, J.; Stoyanov, E. V.; Zakeeruddin, S. M.; Grätzel, M. "Charge separation and efficient light energy conversion in sensitized mesoscopic solar cells based on binary ionic liquids", *J. Am. Chem. Soc.* **2005,** *127,* 6850-6856.

7. Wang, P.; Zakeeruddin, S. M.; Comte, P.; Exnar, I.; Grätzel, M. "Gelation of ionic liquid-based electrolytes with silica nanoparticles for quasi-solid-state dye-sensitized solar cells", *J. Am. Chem. Soc.* **2003,** *125,* 1166-1167.

8. Kubo, W.; Kitamura, T.; Hanabusa, K.; Wada, Y.; Yanagida, S. "Quasi-solid-state dye-sensitized solar cells using room temperature molten salts and a low molecular weight gelator", *Chem. Commun.* **2002,** 374-375.

9. Kubo, W.; Kambe, S.; Nakade, S.; Kitamura, T.; Hanabusa, K.; Wada, Y.; Yanagida, S. "Photocurrent-determining processes in quasi-solid-state dye-sensitized solar cells using ionic gel electrolytes", *J. Phys. Chem. B* **2003,** *107,* 4374-4381.

10. Paulsson, H.; Hagfeldt, A.; Kloo, L. "Molten and solid trialkylsulfonium iodides and their polyiodides as electrolytes in dye-sensitized nanocrystalline solar cells", *J. Phys. Chem. B* **2003,** *107,* 13665-13670.

11. Haque, S.; Palomares, E.; Cho, B.; Green, A.; Hirata, N.; Klug, D.; Durrant, J. "Charge separation versus recombination in dye-sensitized nanocrystalline solar cells: the minimization of kinetic redundancy", *J. Am. Chem. Soc.* **2005,** *127,* 3456–3462.

12. Durrant, J. R.; Haque, S. A.; Palomares, E. "Towards optimisation of electron transfer processes in dye sensitised solar cells", *Coord. Chem. Rev.* **2004,** *248,* 1247-1257.

13. Neale, N. R.; Kopidakis, N.; van de Lagemaat, J.; Grätzel, M.; Frank, A. J. "Effect of a Coadsorbent on the Performance of Dye-Sensitized TiO$_2$ Solar Cells: Shielding versus Band-Edge Movement", *J. Phys. Chem. B* **2005,** *109,* ASAP.

14. Anderson, N.; Lian, T. "Ultrafast electron transfer at the molecule-semiconductor nanoparticle interface", *Annu. Rev. Phys. Chem.* **2005,** *56,* 491–519.

15. Benkö, G.; Kallioinen, J.; Korppi-Tommola, J. E. I.; Yartsev, A. P.; Sundström, V. "Photoinduced ultrafast dye-to-semiconductor electron injection from nonthermalized and thermalized donor states", *J. Am. Chem. Soc.* **2002,** *124,* 489-493.

16. Benkö, G.; Myllyperkiö, P.; Pan, J.; Yartsev, A. P.; Sundström, V. "Photoinduced electron injection from $Ru(dcbpy)_2(NCS)_2$ to SnO_2 and TiO_2 nanocrystalline films", *J. Am. Chem. Soc.* **2003,** *125,* 1118-1119.

17. Kallioinen, J.; Benkö, G.; Myllyperkiö, P.; Khriachtchev, L.; Skårman, B.; Wallenberg, R.; Tuomikoski, M.; Korppi-Tommola, J.; Sundström, V.; Yartsev, A. P. "Photoinduced ultrafast dynamics of $Ru(dcbpy)_2(NCS)_2$- sensitized nanocrystalline TiO_2 films: The influence of sample preparation and experimental conditions", *J. Phys. Chem. B* **2004,** *108,* 6365-6373.

18. Watson, D.; Meyer, G. "Electron injection at dye-sensitized semiconductor electrodes", *Annu. Rev. Phys. Chem.* **2005,** *56,* 119–156.

19. Lanzafame, J. M.; Miller, R. J. D.; Muenter, A. A.; Parkinson, B. A. "Ultrafast Charge-Transfer Dynamics at SnS_2 Surfaces", *J. Phys. Chem.* **1992,** *96,* 2820-2826.

20. Lanzafame, J. M.; Palese, S.; Wang, D.; Miller, R. J. D.; Muenter, A. A. "Ultrafast Nonlinear-Optical Studies of Surface-Reaction Dynamics - Mapping the Electron Trajectory", *J. Phys. Chem.* **1994,** *98,* 11020-11033.

21. Schnadt, J.; Brühwiler, P. A.; Patthey, L.; O'Shea, J. N.; Södergren, S.; Odelius, M.; Ahuja, R.; Karis, O.; Bässler, M.; Persson, P.; Siegbahn, H.; Lunell, S.; Mårtensson, N. "Experimental evidence for sub-3-fs charge transfer from an aromatic adsorbate to a semiconductor", *Nature* **2002,** *418,* 620-623.

Remerciements

Pro ainsi que François Rotzinger pour m'avoir initié au calcul de propriétés moléculaires. Merci également à Gaby et Nono de l'atelier d'électronique.

D'une manière générale je remercie tout les membres du LPI qui m'ont accompagné au cours ce travail. Je pense tout particulièrement à Robert, Isabelle et Hervé avec qui j'ai partagé bien plus que problèmes scientifiques. Mes pensées vont également à ceux qui ont rendu mon quotidien à l'EPFL aussi agréable (Sébastien, Keyvan, Emmanuel, Antoine, ...).

Finalement je profite de cette occasion pour remercier mes parents qui m'ont soutenu et encouragé sans cesse depuis le début de mes études. Ce travail est dédié à Eve-Marie et à nos enfants Mara et Tristan. Malgré les longues journée passées loin de la maison, les inévitables périodes de doutes, leur soutien à été constant et inconditionnel. Pour finir je tiens à assurer à Mara que maintenant que cette thèse est terminée je ne vais pas en recommencer une nouvelle !

Curriculum Vitae

Name:	*Bernard Wenger*
Date, place of birth:	*21.4.1976, Neuchâtel*
Nationality:	*Swiss*
Address:	*Laboratoire de photonique et interfaces*
	Institut de chimie et ingéniérie chimique
	Ecole Polytechnique Fédérale de Lausanne
	Station 6, CH-1015 Lausanne
	Tel: +41 21 693 31 73
	Fax: +41 21 693 41 11
	e-mail: bernard.wenger@epfl.ch

Education

2001-2005:	PhD Thesis. " Effect of Electronic and Nuclear Factors on the Dynamics of Dye-to-Semiconductor Electron Transfer", under the supervision of Prof. J.-E. Moser in the group of Prof. M. Grätzel. EPFL.
1999-2000:	Diploma work on "Dynamics of charge separation in the sensitization of mesoporous TiO_2 films by molecular dyads", under the supervision of Prof. J.-E. Moser.
1995-2000:	Chemical engineering studies at EPFL.
1991-1995:	Gymnase cantonal de Neuchâtel. Scientific maturity (cum laude).

Teaching and working experience

2001-2005:   Teaching assistant for the course of "Chemical Thermodynamics" (Prof. M. Grätzel, EPFL).

Teaching assistant for the 3rd year laboratory for chemical engineering students. (EPFL).

2000-2001:   Chemist at the Center of Hydrogeology of the University of Neuchâtel (civilian service).

Publications

Wenger, B.; Grätzel, M.; Moser, J. "Rationale for kinetic heterogeneity of ultrafast light-induced electron transfer from Ru(II) complex sensitizers to nanocrystalline TiO_2", *J. Am. Chem. Soc.* **2005,** *127,* 12150–12151.

Wang, P.; Wenger, B.; Humphry-Baker, R.; Moser, J. E.; Teuscher, J.; Kantlehner, W.; Mezger, J.; Stoyanov, E. V.; Zakeeruddin, S. M.; Grätzel, M. "Charge separation and efficient light energy conversion in sensitized mesoscopic solar cells based on binary ionic liquids", *J. Am. Chem. Soc.* **2005,** *127,* 6850-6856.

Wenger, B.; Grätzel, M.; Moser, J. E. "Origin of the kinetic heterogeneity of ultrafast light-induced electron transfer from Ru(II)-complex dyes to nanocrystalline semiconducting particles", *Chimia* **2005,** *59,* 123-125.

Kuang, D.; Ito, S.; Wenger, B.; Klein, C.; Moser, J. E.; Humphry-Baker, R.; Zakeeruddin, S.; Grätzel, M. "High Molar Extinction Coefficient Ruthenium Sensitizers for Dye-Sensitized Solar Cells", *J. Am. Chem. Soc.* submitted.

Bauer, C.; Wenger, B.; Pelet, S.; Grätzel, M.; Moser, J. E. "Ultrafast distance-dependent electron transfer in dye/semiconductor systems", *J. Phys. Chem. B* in preparation.

Wenger, B.; Teuscher, J.; Grätzel, M.; Moser, J. E. "Reductive quenching of excited states in dye-sensitized mesoporous TiO_2 films", *J. Am. Chem. Soc.* in preparation.

Presentations

– Swiss Group of Photochemistry and Photobiology, Graduate Student Symposium 2003, Fribourg (Switzerland), Apr. 11-12, 2003, **(poster)**.

– European Science Foundation - Summer School, Molecular Basis of Fast and Ultrafast Processes, Vilamoura (Portugal), Jun. 12-15, 2003, **(poster)**.

– Femtochemistry VI (Int. Conference on Femtochemistry), Paris (France), Jul. 6-10, 2003, **(poster)**.

– Swiss Chemical Society, Fall Meeting, Lausanne (Switzerland), Oct. 9, 2003, **(poster)**

– European Science Foundation, Femtochemistry and Femtobiology (ULTRA) Program Final Conference, Pécs (Hungary), Mar. 25-28, 2004, **(short talk + poster)**.

– Swiss Chemical Society, Fall Meeting, Zürich (Switzerland), Oct. 7, 2004, **(poster)**, *SCS prize for the best poster presentation in the section Physical Chemistry*.

– Swiss Chemical Society, Fall Meeting, Lausanne (Switzerland), Oct. 13, 2005, **(poster)**.